THE NON-LINEAR VORTEX-EXCITED VIBRATION OF A VERTICAL CYLINDER IN WAVES

by

Kenjirou Hayashi

Thesis submitted in accordance with the requirements of the University of Liverpool for the Degree of Doctor in Philosophy.

December 1984

ABSTRACT

This study deals with some of the non-linear phenomena of the vortex-excited vibration of a cylinder in waves. Laboratory experiments have been performed to study comprehensively the dynamic transverse response of a vertical cylinder in regular waves. The test cylinder was pivoted at its base and supported by spring at the top. The movement of the test cylinder in the direction of the inline force was restricted in most of the experiments.

The relationship between the vortex-excited vibration of the test cylinder and the following important parameters, have been observed; the lift coefficient, the ratio of wave frequency to natural frequency of test cylinder, the Keulegan-Carpenter number, the wave depth parameter, the damping factor, and the cylinder mass parameter. In some ways the characteristics of the vortex-excited vibration of the cylinder in waves are similar to those observed in steady flow. However, the following important differences have been obtained:

(1) In the case of steady flow, perfect resonance appears in the range of lock-on, but in waves, it appears only near to f_W/f_{nW} = 1/2, 1/3, 1/4 ... (multi appearance), elsewhere vortex-coupling may occur for right damping in which the oscillation frequency is not simply a multiple of the wave frequency.

(2) The existence of the amplification of the lift force acting on the vortex-excited cylinder in comparison with the stiffly mounted cylinder is a function of the frequency ratio of the wave frequency to natural frequency and Keulegan-Carpenter number.

A wake oscillator model has been developed for the unsteady vortex-excited vibration of a vertical cylinder in waves. Although this cannot explain the general phenomena of the vortex-excited vibration in waves observed in the present work, it reproduces roughly the amplification of the lift force around perfect resonance.

ACKNOWLEDGEMENTS

I would like to express my thanks to the academic and tecnical staff of the Department of Civil Engineering of the University of Liverpool for their advice and help through this study.

In particular, I would like to express my thanks and appreciation to Dr. J. R. Chaplin for the patient supervision and helpful advice he provided throughout my work contained in this thesis.

I also would like to thank Miss D. Girling who typed efficiently this thesis and Mrs. B. Cotgreave for the skilful tracing.

I wish to express my thanks and gratitude to the National Defence Academy in Japan, which has given me a chance to study at Liverpool University, and my teachers, colleagues and friends who also encouraged my study.

Finally I am grateful to my wife and family.

CONTENTS

SYMBOLS

a	$\rho D^2 L/(8\pi^2.S^2.M)$
b	numerical constant (interaction parameter)
B	magnetic flux density
b_1, b_2	dimension of the magnet pole
C_{ar}	added mass coefficient at perfect resonance
C_{as}	added mass coefficient in the condition of free vibration in still water
C_{Lm}	mean value of the effective coefficient of the lift force acting on the observed vortex-excited cylinder
C_{Lma}	lift coefficient calculated by using ζ_{ta}
C_{Lmw}	lift coefficient calculated by using ζ_{tw}
C_{Lmv}	lift coefficient calculated by using ζ_{tv}
C'_{La}	$dC_{La}/d\tau$
C''_{La}	$d^2C_{La}/d\tau^2$
C_{La}	instantaneous effective lift coefficient
C_L	lift coefficient
C	total linear damping coefficient (see Fig. 2.1)
C_{LC}	fluctuating lift coefficient
C_{Lo}	representative value of the lift coefficient for a cylinder stiffly mounted
C_a	added mass coefficient
C_{mt}	total damping matrix
C_s	damping coefficient of the springs
C_e	damping coefficient of electro-magnetic damper
C_w	damping coefficient of the fluid
C_{Le}	effective lift coefficient

$C_{Le}(n)$	lift coefficient for the n-th harmonic
C_{mo}	value of C_{mt} at $\eta = 0$
C_{Bm}	variability of C_{mt}
C_D	drag coefficient
$\overline{C}_{Le}$	mean effective lift coefficient
C_{VL}	coefficient of variation
rms.C_L	root-mean-square values of the lift coefficient
C_{VY}	coefficient of vibration of the half peak-to-peak amplitude of the vortex-excited vibration
D	diameter of the cylinder
d	mean water depth
$dF\ell$	lift force acting on the elemental length dz
E_{df}	energy dissipated in one cycle of vibration by the fluid damping force
E_{dfi}	energy dissipated in one cycle of vibration by the fluid damping force
fv	vortex shedding frequency
f_n	natural frequency of the cylinder
$F_{m\ell}$	total lift force moment matrix (moment produced by the lift force acting on the cylinder)
f_w	wave frequency
F_c	force produced on the conducting plate
f_{na}	natural frequency of the test cylinder in air
f_{nw}	natural frequency of the test cylinder in water
$f_{ym'}$	mean value of the frequency of the vortex-excited vibration of the test cylinder
f_{so}	maximum instantaneous vortex-shedding frequency experienced by the test cylinder when stiffly mounted in waves
H	wave height

I_e	current
I_c	A.C. current
K	total stiffness (see Fig. 2.1)
kd	wave depth parameter
K_{mt}	stiffness matrix
k_s	stiffness of the springs
k	wave number $2\pi/L_w$
K_{mo}	value of K_{mt} at $\eta = 0$
K_{mt}	stiffness matrix
K_{Bm}	variability of K_{mt}
K_{mta}	stiffness of the test cylinder in air
K_{mtw}	stiffness of the test cylinder in water
L	length of a cylinder
L_w	wave length
ℓ_e	length of the coil
m	cylinder mass per unit length
M_a	added mass
M_{mt}	total mass matrix
m_a	added mass of water per unit length
M_{mo}	mass matrix at $\eta = 0$
M_{mt}	mass matrix
M_{Bm}	variability of M_{mt}
m_e	effective mass per unit length of the test cylinder
$m_e/\rho D^2$	mass ratio
$2m_e(2\pi\ \zeta_t)/\rho D^2$	normalised damping (reduced)
M_{mta}	mass matrix in air
M_{mtw}	mass matrix in water
M	magnifications factor of lift force (lift coefficient acting on a stiffly mounted cylinder)
N_e	number of turns of the coil

N	number of waves
R_e	Reynolds number
R_p	$m\zeta/(\rho D^2\ C_{L_0})$
R_c	resistance of the eddy current circuit in the conducting plate
rms.C_L	root-mean-square values of the lift coefficient
S	Strouhal number
SKC	surface Keulegan-Carpenter number
T	wave period
t	time
U_m	maximum velocity in a cycle of oscillating flow
u_m	maximum horizontal wave particle velocity at z
u	horizontal water particle velocity in waves
u_{m0}	maximum horizontal particle velocity at still water level
U_c	moving velocity of a conducting plate
v	velocity of the ambient flow
V_r	reduced velocity
V_w	volume of water displaced by the structure
V_{emf}	electro-magnetic potential
x	transverse displacement of cylinder (see Fig. 2.1)
x_r	x/D
y_h	transverse displacement of the cylinder at the still water level
$\dot{y}_h$	dy_h/dt
$\ddot{y}_h$	d^2y_h/dt^2
Y_{hi}	amplitude of the i-th oscillation of the test cylinder at the still water level
Y_{hi}/D	non-dimensional test cylinder displacement
Y_{hi-2}	amplitude of the test cylinder at the (i-2)-th period

Y_{hi+3}	amplitude of the test cylinder at the (i+3)-th period
Y_{hm}	mean value of the half peak-to-peak amplitude of the vortex-excited vibration at mean water level
y_r	y_h/D
$\dot{y}_r$	$dy_r/d\tau$
$\ddot{y}_r$	$d^2y_r/d\tau^2$
z	vertical distance, with origin in bottom of frame
dz	elemental length
α	numerical constant (Van der Pol coefficient)
β	R_e/KC
γ	numerical constant (Van der Pol coefficient)
δ_r	normalised (stability or reduced) damping ($2m_e$ $2\pi\zeta/\rho D^2$)
ζ	damping factor of the cylinder $C/(2M\ \omega_n)$
ζ_t	total damping factor of the test cylinder
ζ_s	damping factor of the spring
ζ_m	damping factor of the electro-magnetic damper
ζ_f	damping factor of the fluid
ζ_w	fluid damping factor of the test cylinder in still water
ζ_{ta}	total damping factor in air (at $Y_{hi}/D = 0.1$)
ζ_{tw}	total damping factor in water (at $Y_{hi}/D \cong 0.1$)
ζ_{tai}	total damping factor in air
ζ_{twi}	total damping factor in water
ζ_{fi}	fluid damping
ζ_{tv}	damping factor in still water at $Y_{hi}/D = Y_{hm}/D$
η	water surface displacement of wave
κ	numerical constant
μ_e	magnetic permeability
ν	kinematic viscosity of the fluid

ρ	density of fluid (water)
τ	$\omega_{nt} = 2\pi\, f_n.t$
$\phi(n)$	phase lag between the n-th harmonic lift coefficient, $C_{Le}(n)$, and the surface elevation of wave, η
$\phi_A(n)$	phase angle between the vibration of the test cylinder, y_h, and lift force
$\phi_B(n)$	phase angle between the displacement of the test cylinder, y_h, and the water surface elevation, η
$\phi_A(2)$	theoretical values of the phase angle
ω_o	$f_v/f_n = S\, v/f_nD$ or f_{so}/f_n (in 6.2)
ω_w	circular wave frequency $= 2\pi.f_w = 2\pi/T$
ω_n	circular natural frequency of the cylinder $2\pi\, f_n = \sqrt{K_{mo}/M_{mo}}$

LIST OF FIGURES

LIST OF TABLES

LIST OF PLATES

CHAPTER 1

1-1 Introduction

The dynamic response of offshore structures to the wave forces acting on them is one of the most important factors in their design. There have been many instances reported where the failure of a structure is believed to have been caused by its response at frequencies of acting wave forces acting on it. The increasing demands of offshore development have led to the construction of platforms in deeper waters, such as part of the North Sea. In this case, much more attention has to be given to the dynamic response of the structure to wave forces, because its natural frequency decreases with increasing size and may approach those of the wave forces.

Wave forces are usually resolved into two components, an inline force and a transverse force (a lift force). The inline force, acting along the direction of wave propagation, is usually expressed by using Morison's equation, and acts predominantly at a frequency equal to the wave frequency. The lift force, acting normally to the direction of wave propagation, is caused by vortex shedding. The lift forces act predominantly at frequencies which are multiples of the wave frequency and mainly depend on the Keulegan-Carpenter number (KC).

Some structural failures are considered to be caused by resonance of the natural frequency of the offshore structure with the frequency of the lift force, since offshore structures are designed so that their natural frequencies are higher than the frequency of the inline force.

Therefore, the structure's dynamic response to the lift forces must be considered most important, and this has received considerable attention in recent years.

A great deal of research has been done to understand the process of vortex shedding oscillation in steady flow. In this case, if the vortex shedding frequency approaches the natural frequency of a lightly damped cylinder, the vibration of the cylinder becomes larger and this large vibration can drive the eddies to be shed with a frequency ranging between the natural frequency of the cylinder and the Strouhal frequency.

This phenomena is usually called "vortex-excited vibration", or "lock-on" between the frequency of vortex shedding and the frequency of the vibrating cylinder. Under "lock-on" conditions, large resonant vibrations usually occur, and the lift forces are amplified both by the increase of vortex strength and by the improved correlation in the phase of vortex shedding along the cylinder axis.

A similar phenomenon may occur, if an elastically mounted vertical cylinder is placed in waves. However, the incident flow acting on a vertical cylinder in waves is oscillatory, varies with depth, and possesses a vertical component, because the water particle paths in waves are orbital and their displacements diminish with increasing depth. The vortices produced by an incident flow passing a cylinder, are subsequently swept back, passing the cylinder in the opposite direction. Therefore, the process of vortex shedding and the vortex excited vibration of the cylinder in waves may be different from the case of steady flow.

However, few people have studied the vortex excited vibrations of a cylinder in waves and in harmonic flow. This process is not understood as well as the case of steady current flow. A lot of experimental work remains to be done in this area.

It is very difficult to solve the fluid dynamic problem of vortex excited vibration with an exact solution because of the complexity of the non-linear fluid and structure interaction. Therefore, several mathematical models have been proposed and developed to describe this interaction.

One of the most interesting and useful of these models is "the wake oscillator model". This was first introduced by Hartlen and Currie (1970) and further developed to account for increased vortex strength. The idea of this model, which was based on the works of Birkhoff and Zarantonello (1957), and Bishop and Hassan (1964), is that the transverse vibration of the cylinder in the lock-on condition might be modelled by using the equation of motion of a non-linear oscillator. In this model, the non-linear behaviour of the lift coefficient under lock-on conditions is assumed to satisfy a form of the Van der Pol equation, and is coupled to the equation of motion of the cylinder by means of a forcing term. Another model is the "correlation model" introduced by Blevins and Burton (1976). This model was created to account for the increased spanwise correlation of the wake under lock-on conditions. Its theoretical framework is based on a representative spanwise correlation and cylinder amplitude determining the vortex forces.

These two models are only approximations of the fluid-structure interaction, and a large amount of experimental data is required to fix the model parameters. Nevertheless, it is important and useful for engineers that such models can explain the well-known lock-on effect of the cylinder in steady flow.

The modelling of the vortex-excited vibration of a cylinder in harmonic flow or in waves is not so advanced as in the case of steady current flow, because these phenomena are still more complicated and are not understood as well as in the latter case.

In addition, there are some ambiguities in the definition of the added mass and the damping coefficient which are used in the dynamic equations of motions in these models. The added mass is of importance when calculating the natural frequency of the cylinder. The damping factor is of crucial importance when estimating the dynamic displacement of a cylinder. These values should be defined and measured in conditions where there is vortex-excited vibration. However, it is very difficult to define and measure them in these conditions. Therefore, the values presently used are those measured when a cylinder is set in air or in still water. More experimental and theoretical work should be undertaken to define properly the added mass and the damping factor in both conditions.

1-2 Outline of Thesis

The purpose of the present work is to study the vortex-excited vibration of a cylinder in waves. Laboratory experiments have been performed to study comprehensively the dynamic transverse response of a vertical cylinder in regular waves. The test cylinder was pivoted at its base and supported by springs at the top. The movement of the test cylinder in the direction of the inline force was restricted in most of the experiments.

The relationships between the vortex-excited vibration of the test cylinder and the following quantities have been observed: the ratio of wave frequency to natural frequency, the Keulegan-Carpenter number, the wave depth parameter (wave number), damping coefficient, and a cylinder mass parameter (mass ratio). The damping coefficient was adjusted by using an electro-magnetic damper to increase the range of experimental conditions. The characteristics of the damping coefficient in still water were measured and for small amplitudes coupled with the theoretical results of Stokes (1901) and Wang (1968).

The lift forces acting on a vortex-excited, vibrating cylinder were estimated from the transverse displacement of the cylinder measured at its top. The lift forces acting on a stiffly mounted cylinder were also estimated from the moments about its bottom measured in the same wave conditions, in order to find the amplification of lift forces acting on a vortex-excited, vibrating cylinder.

Modelling work for the non-linear vortex-excited vibration of the test cylinder in waves was also carried out, by means of a development of the wake oscillator model.

CHAPTER 2

LITERATURE REVIEW

2-1 Introduction

The aim of this chapter is to provide a description of previous research concerning the vortex-excited vibration of a cylinder in waves, as a background to the work to be described in later chapters.

The subject of vortex-excited vibration in steady flow is introduced in the first section. The general characteristics of the lift forces acting on a stiffly mounted cylinder in steady flow will be outlined. Secondly, the characteristics of the vortex-excited vibration of the cylinder in steady flow will be described. Finally, modelling work will be described with emphasis on the wake oscillator model. The understanding of this work will be useful in the study of the vortex-excited vibration in waves. The origin of the vibration in both cases, steady flow and waves, is due to vortex-shedding from the surface of the cylinder.

The second section is concerned with the characteristics of lift forces acting on a stiffly mounted cylinder in oscillating flow (two dimensional harmonic flow and waves). Secondly, previous work on the vortex-excited vibration in oscillating flow will be introduced. There will be many similarities between the characteristics of the vortex-excited vibrations of the cylinder in two dimensional harmonic flow and in waves.

In the third section, the characteristics of the added mass and the damping are described. These two parameters take a very important role among the features of vortex-excited vibration.

2-2 Vibration Induced by Steady Flow

2-2-1 The lift force on a stiffly mounted cylinder in steady flow

A great deal of research has been done to understand the phenomenon of vortex shedding from a stiffly mounted cylinder in steady flow. The relationship between the vortex shedding frequency, f_V, and the velocity of the ambient flow, v, was first found by Strouhal (1878). This relationship is shown as follows

$$f_V = S \frac{V}{D} \qquad (2\text{-}1)$$

where S = the dimensionless Strouhal number

D = the diameter of the cylinder.

The relationship between the Strouhal number, S and the Reynolds number ($R_e = vD/\nu$, ν = kinematic viscosity of the fluid) was revealed by Rayleigh (1896). The phenomenon of vortex shedding was also examined in a pioneering work by Karman (1912). The following behaviour has been confirmed by a number of researchers, (Morkovin (1964), Roshko (1954), Bishop and Hassan, (1964), after King et al. (1973), Leinhard (1966), after Blevins (1977) and Bearman (1969).

(1) In the range of Subcritical Reynolds number ($10^2 < R_e < 10^5$), the value of S is stable and is about 0.2 for smooth circular cylinders.

(2) In the range of R_e between 10^5 and 10^6, the scatter in S is large and it has a maximum of about 0.4.

(3) At high supercritical R_e range ($R_e > 2 \times 10^6$), the scatter in S is small and it increases slightly with increasing R_e.

The effect of the aspect ratio L/D (L: length of a cylinder) and the effect of sizes of end plates on the vortex-shedding frequency were shown by Gouda (1975) (see King (1977)).

The measurement of the lift force caused by the vortex shedding has been done by many researchers. However, a dominant feature of it is that it is much more sensitive to flow than the drag force. The relationship between the Reynolds number, R_e, and the lift coefficient, C_L, obtained by the several researchers has been summarised by Morkovin (1964) and Sarpkaya and Isaacson (1981). The fluctuation of the lift force is larger than that of the drag force, especially in the subcritical range. This shows the sensitivity of the lift force to the stream turbulence. The effect of the gaps has been pointed out experimentally by Humphreys (1960), see Sarpkaya and Isaacson (1981). The effect of small amplitude oscillations about 0.05.D has been reported by Koopmann (1967), see Blevins (1977). The effect of the turbulence of the ambient flow has been reported by Surry (1969), see King et al. (1973). His results show that the lift force increases with increasing turbulent level. The effect of various disturbances is shown clearly in Fig. 3.4 of Sarpkaya and Isaacson (1981).

2-2-2 The vortex-excited vibration of cylinders in steady flow

A great number of experiments have been done in order to study the phenomenon of vortex-excited vibration of cylinders in steady flow. Summaries have been made by Mair and Maull (1971), Parkinson (1974), Blevins (1977), King (1977) and Sarpkaya (1979).

An important characteristic of this vortex-excited vibration is that of 'lock-on' or 'synchronization' between the vortex-shedding frequency and the vibration frequency of the cylinder. When vortex-excited vibration occurs;

(1) the vortex strength is increased

(2) the correlation in the phase of the vortex-shedding along the cylinder axis is increased

(3) the cylinder oscillates at or near its natural frequency and the vortex-shedding is locked to this frequency, which may differ from the vortex-shedding frequency for stationary cylinders (Strouhal frequency).

This lock-on effect was probably first recognised and documented by Meier-Windhorst (1939), (see King et al. (1973)) and Bishop and Hassan (1964).

The characteristics of the vibration frequency, amplitude, phase angle, and fluctuating pressure on the surface of a circular cylinder at subcritical Reynolds numbers were measured in detail by Feng (1968), Ferguson and Parkinson (1967) and Bearman (1978) see (Griffin (1979)).

The relationship between the vortex-excited vibration and the reduced velocity, for several values of damping (sometimes expressed as a normalised (stability or reduced) damping parameter, δ_r) has been measured by Feng (1968), Unemara (1971) (see King et al. (1973), and King (1977)). The range of reduced velocity in which the vortex-excited vibration occurs, becomes wider with decreasing δ_r. The value of the reduced velocity at which the peak amplitude occurs, increases with decreasing δ_r. The normalised damping δ_r and reduced velocity V_r are defined as follows

$$\delta_r = \frac{2m.2\pi\zeta}{\rho D^2}$$

$$V_r = \frac{v}{f_n D} \tag{2-2}$$

where m = the mass per unit length of cylinder

ζ = the damping factor of the cylinder

f_n = the natural frequency of the cylinder

ρ = the density of fluid.

From the stationary cylinder, vortices may be shed in cells. The length of each cell is related to the correlation length which is a characteristic length associated with the average size of the vortices being shed from the cylinder (see El Baroudi (1960)). Its values vary with Reynolds number, turbulence, aspect ratio (L/D), and surface roughness. Typical values are summarised as follows by King (1977).

Reynolds Number	Correlation Length	Source
$40<R_e<150$	15D-20D	Gerlach and Dodge (1970)
$150<R_e<10^5$	2D-3D	Gerlach and Dodge (1970)
$1.1x10^4<R_e<4.5x10^4$	3D-6D	El.Baroudi (1969)
$10^5<R_e$	0.5D	Gerlach and Dodge (1970)
$R_e = 2x10^5$	1.56D	Humphreys (1960)

When a cylinder is resonantly excited due to vortex-shedding, its vibration may be accompanied by increased correlation length of the vortices being shed along the cylinder. Therefore, the lift force acting on the vortex-excited cylinder may be increased. The visual observations of the spanwise organisation of the vortex wake have been made by Koopmann (1967). The increased correlation length has been measured by Toebes (1969) and Ramberg and Griffin (1976).

The fluctuating lift forces on vibrating cylinders have been measured, among others, by Griffin and Koopmann (1977) using freely oscillating cylinders in air flow, and Mercier (1973) (see Griffin (1979)) and Sarpkaya (1978), using cylinders forced to oscillate in water. Bearman (1978) has measured the fluctuating pressures on a vibrating cylinder in water, and has found good agreement between measurements of the phase angle between the pressure and displacement on a cylinder forced to oscillate, and the comparable phase measurements on a freely oscillating cylinder at resonance (see Griffin (1979)).

2-2-3 Modelling of vortex-excited vibrations

It is very difficult to solve the Navier-Stokes equations for flow about a vortex-excited vibrating cylinder, and no satisfactory solution to the non-linear fluid-structure interaction problem has yet been found. Therefore several mathematical models have been proposed to explain the experimental observations. A general review of the models in existence has been given by Parkinson (1974) and Sarpkaya and Isaacson (1981).

The variation of the wake width as a consequence of the transverse vibration may be one of the most important features of the vortex-excited vibration related to Karman vortex-shedding (see Di Silvio (1969)). This phenomenon was taken account of, in order to explain the lock-on phenomenon, in the models of Landweber (1942) (see Di Silvio (1969)), Di Silvio (1969) and Sawamoto et al. (1979). However, the phenomenon of the vortex-excited vibration is generally not well explained by their models. The assumptions used are not generally valid and, for the characteristics of vortex-shedding, should be considered in more detail.

On the other hand, the idea that the nature of vortex-excited vibration might be modelled by a simple non-linear oscillator equation was suggested by Birkhoff and Zarantonello (1957) and reinforced by Bishop and Hassan (1964) through their observation of an oscillating cylinder in uniform flow.

This idea was pursued by Hartlen and Currie (1970). In their models, the vibration of the cylinder, which is mounted flexibly on springs with total stiffness K, the total linear damping coefficient C (see Fig. 2.1 after Hartlen and Currie (1970)), is expressed by the following equations.

$$\ddot{x}_r + 2\zeta\dot{x}_r + x_r = a\omega_0^2 C_{LC} \tag{2-3}$$

$$\ddot{C}_{LC} - \alpha\omega_0 \dot{C}_{LC} + \frac{\gamma}{\omega_0}(\dot{C}_{LC})^3 + \omega_0^2 C_{LC} = b\dot{x}_r \tag{2-4}$$

where

$x_r = \frac{x}{D}$

$\dot{x}_r = dx_r/d\tau$

$\ddot{x}_r = d^2x_r/d\tau^2$

$\tau = \omega_n t$

$\zeta = C/(2.M.\omega_n)$

$a = \rho D^2 L/(8\pi^2.S^2.M)$

$$\omega_0 = f_v/f_n = S\frac{v}{f_n D} \tag{2-5}$$

C_{LC} = the fluctuating lift coefficient

$$= \frac{\text{Lift force acting on the cylinder}}{(\frac{1}{2}.\ \rho.v^2.DL)}$$

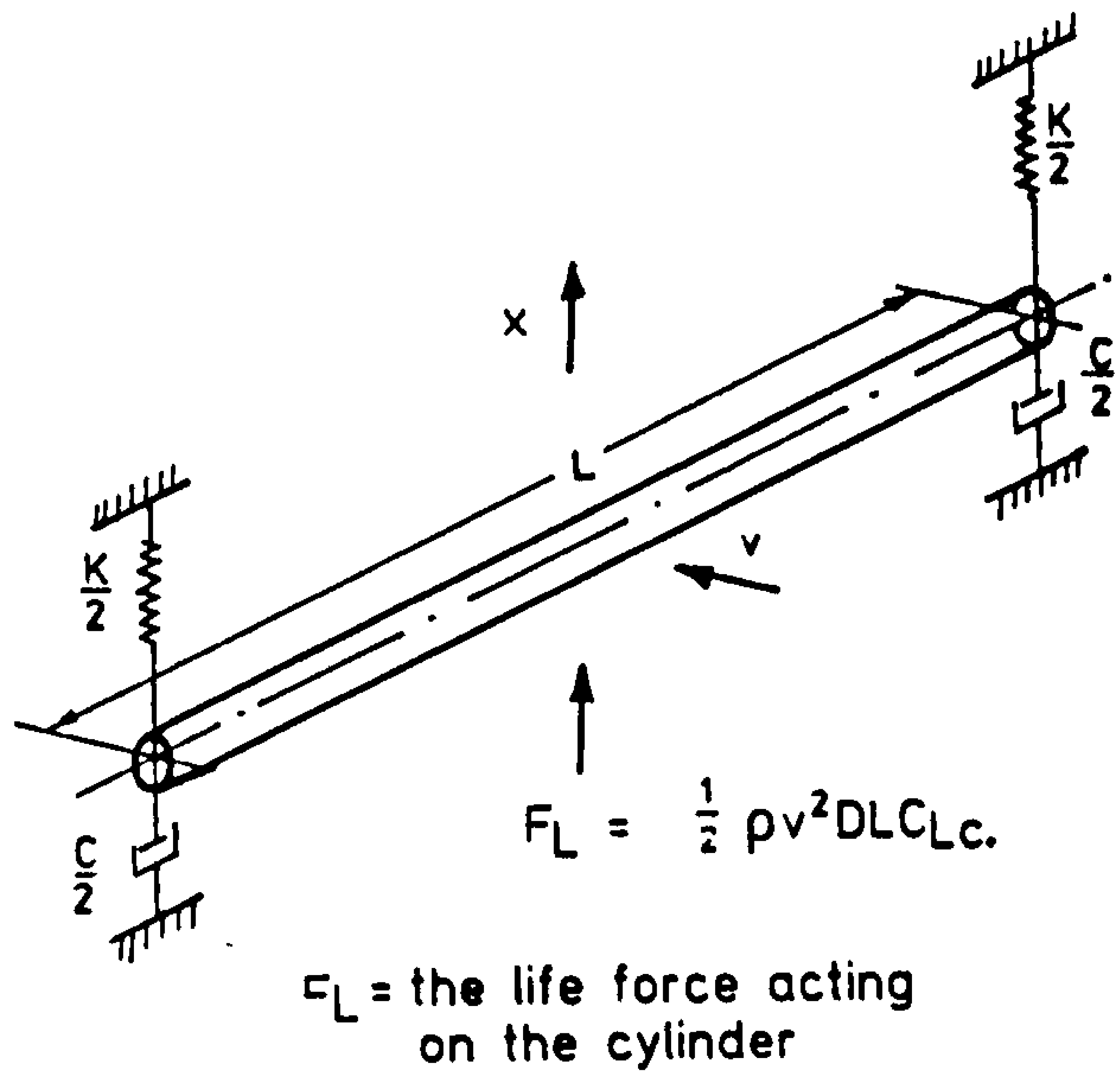

Fig. 2.1 Model of Structure for Analysis (after Hartlen and Currie(1970))

Eq.(2-3) is the equation of dynamic equilibrium of the cylinder, Eq.(2-4) shows that the fluctuating lift coefficient, C_{LC}, is made to satisfy is a Van der Pol equation. The dimensionless parameters α and γ are the Van der Pol coefficients and b is the interaction parameter. In Eq.(2-4), the first and fourth terms can express a generating harmonic oscillation of C_{LC} in which the normalised frequency of C_{LC} is ω_0. The third and fourth terms in Eq.(2-4) comprise the damping. A small value of C_{LC} is amplified by the second term and when the amplitude of C_{LC} arrives at a larger value, it is restricted by the third term. Therefore the amplitude of C_{LC} is "self-limited". The fifth term, $b\dot{x}_r$, is the forcing term. This is introduced to couple the oscillation of C_{LC} to the vibration of the cylinder. When the interaction parameter b is 0, the fluid and structure oscillations are decoupled.

Therefore, when the cylinder is mounted stiffly, C_{LC} is determined by the solution of Eq.(2-4) with $b = 0$. In this case, the amplitude of fluctuating lift coefficient is as follows

$$C_{LC} = \left(\frac{4\alpha}{3\gamma}\right)^{1/2} \tag{2-6}$$

The lock-on phenomenon is qualitatively reproduced by the Hartlen-Currie model. In order to make this model more useful, the relationship between the constant values (α, γ, b), which probably vary in each experimental condition, and the physical constants of the flexibly supported cylinders has to be found from experimental measurements. However this relationship has not been obtained for the Hartlen-Currie model.

In order to pursue the purpose described above, a modified Van der Pol equation was introduced as the governing equation for the fluctuating lift on the vortex-excited cylinder by Skop and Griffin (1973). They obtained good quantitative agreement with some of the experimental results of Koopmann (1967) and Parkinson et al. (1968). They also obtained a set of relations between the empirical parameter, used in their modified Van der Pol equation for the fluctuating lift, and the physical mass and damping parameters of the equation of the dynamic equilibrium of the cylinder.

In these two wake oscillator models, no systematic attempt was made to base the model on known fluid dynamic properties. The model behaviour cannot generally be explained in terms of fluid phenomena. In order to consider this point, Iwan and Blevins (1974) have proposed a non-linear oscillator formation in which a "hidden flow variable" was introduced to describe the effect of the vortex-shedding; the force on the vortex-excited cylinder was evaluated from the momentum equation in the transverse direction. The resulting mathematical equation form of this model is non-linear and was very similar to that for Skop and Griffin model (see Iwan (1975)).

It is implicitly assumed that the vortex-shedding is completely correlated along the length of the cylinder in the wake oscillator model described above. However, in a practical case as described in 2-2-2, the variation of the correlation length with the amplitude of the vibration has a large effect on the lift force acting on the vortex-excited cylinder.

In order to account for this, the correlation model has been introduced by Blevins and Burton (1976). The theoretical framework is based on a representative spanwise correlation and vortex force depending on the cylinder amplitude. The vibration is self-exciting and self-limiting. These phenomena show good agreement with independently obtained experimental evidence.

2-3 Vibration Induced by Oscillating Flow

2-3-1 The lift force on a stiffly mounted cylinder in oscillating flow

The forces acting on a stiffly mounted cylinder in oscillating flow (harmonic oscillating flows or waves) are usually resolved into two components. One is called the inline force which acts in the direction of the oscillating flow and the other is called the transverse force (or lift force) which acts normal to the direction of the oscillating flow. The inline force is usually calculated by Morison's equation (Morison et al. (1950)) in which it is assumed to be the sum of an inertial force and a drag force. The predominant frequency of the inline force equals to the wave frequency. The lift force is caused by the vortex-shedding and its predominant frequency is a multiple of the wave frequency and mainly depends on the Keulegan-Carpenter number (KC). Therefore, the structure's dynamic response to lift forces is probably more important than to inline force. The lift force is usually expressed in terms of a lift coefficient, C_L.

Many investigations have been done in order to understand the characteristics of the inline forces and the transverse forces. Summaries for these have been made by several researchers (for example, CIRIA Report UR 8 (1978), Sarpkaya and Isaacson (1981), Holmes (1981)). There have been few investigations in the field, or in the range of high Reynolds number, compared with the laboratory studies.

Apart from inline forces on cylinders in oscillating flow, many studies of the lift forces have been done. Keulegan and Carpenter (1958) observed the vortex-shedding pattern from submerged horizontal cylinders placed in the node of a standing wave. They found a close relationship between the vortex-shedding frequency and a period parameter (called Keulegan-Carpenter number) defined as follows

$$KC = \frac{U_m T}{D} \tag{2-7}$$

in which U_m = the maximum velocity in a cycle of oscillating flow

T = the wave period

D = the tube diameter

Bidde (1971) carried out measurements of both inline and lift forces on a vertical cylinder in waves. He found that the lift force was not negligible and that there was a close relationship, which was similar to that described above, between the characteristics of lift force and the flow pattern around the cylinder.

Sarpkaya (1976) measured the lift force acting on smooth and rough cylinders for a wide range of Reynolds numbers, Keulegan-Carpenter numbers, and relative roughness. He obtained a clear relationship between the lift coefficient, C_L, and KC as a function of the dimensionless value β defined as $\beta = R_e/KC$.

Isaacson and Maull (1976) have studied the total lift forces on a stiffly mounted vertical cylinder in waves. They obtained a relationship between C_L and surface KC number as a function of the wave depth parameter, kd, defined as

$$kd = \frac{2\pi d}{L_w} \tag{2-8}$$

where d = the mean water depth

L_w = the wave length

Chakrabarti et al. (1976) have measured the lift forces acting on sectional parts of a stiffly mounted vertical cylinder in waves. They also obtained the relationship between C_L and KC number. The influence of the sectional position was not clear in their results. The lift forces acting on an inclined cylinder have been measured by Shigemura (1980) and Cotter et al. (1984).

The dependence of the lift force on the KC number has been confirmed by these researchers described above and other researchers. However, the scatter of the lift coefficients is large. This may be due to the irregularity of the lift force with time acting on the cylinder in oscillating flow. The characteristics of this have been reported by Sawaragi and Nakamura (1975), Maull and Milliner (1978), Sawamoto and Kikuchi (1979), and Ikeda and Yamamoto (1981).

2-3-2 Vortex excited vibration of cylinders in oscillating flow

The characteristics of the dynamic response of flexible or flexibly mounted cylinders in oscillating flow are not sufficiently understood. This is mainly due to the complexity of the phenomena, because the incident flow is oscillatory and in waves varies with depth and possesses a vertical velocity component. The number of investigations on the vortex-excited vibration of the cylinder in oscillating flow (both two dimensional flow and in waves) is small.

Rajabi (1979) and Sarpkaya and Rajabi (1979) studied the vortex-excited vibration of the cylinder in two dimensional oscillating flow (harmonic flow) in a U-shaped water tunnel. Their results indicate the following interesting results:

(1) A flexibly-mounted cylinder may undergo synchronized oscillations when the reduced velocity V_r, defined $V_r = U_m/f_nD$; U_m = the maximum velocity in a cycle of oscillating flow, is in the range of 5 to 7.5.

(2) Perfect resonance, at which the dynamic response of the cylinder is maximum, occurs at $V_r \simeq 5.6$. At perfect resonance, the ratio of lift force frequency to the natural frequency remains nearly equal to unity and the lift forces are amplified nearly two times compared to that of a stationary cylinder in the same flow.

(3) The relative amplitude of oscillation is a unique function of $R_p = m\zeta/(\rho D^2 C_{LO})$, m = the cylinder mass per unit length, C_{LO} = the representative value of the lift coefficient for a corresponding cylinder stiffly mounted in the same flow.

It should be noted that their results are of limited value because their data were obtained in the range of high Keulegan-Carpenter number (about 30 < KC < 130) and relatively high damping (about 0.03 ~ 0.06).

Sawaragi et al. (1977) have investigated the inline and transverse dynamic response of a cantilevered circular cylinder in regular waves in the range of Reynolds number between 1500 to 6200, with Keulegan-Carpenter numbers between 2 and about 20. They have reported that the perfect resonance appears when $f_w = 1/2\ f_n$ and $1/3\ f_n$, a multiple appearance of the resonant frequency, in the range of Keulegan-Carpenter number over 4.

In an analytical model, they represented the time variation of the lift force by using the formulae which were proposed by Sawaragi et al. (1976) to express the time variation of the lift force for a stiffly mounted cylinder. The total lift force was then expressed as the superposition of each of its harmonic frequency components. In their model, the effect of the fluid damping, in proportion to the moving velocity of the cylinder, was considered.

Zedan et al. (1980) have investigated experimentally the dynamic response of a cantilevered cylinder in both the inline and transverse directions. The experiment were carried in regular waves in two cases, representing wave depth parameters of kd = 1.63 (intermediate water depth) and kd = 2.6 (deep water depth), in a Keulegan-Carpenter range of 10 to 14.5 and a Reynolds number range of 4×10^4 to 7×10^4. They obtained the following results:

(1) The vortex shedding frequency is twice the wave frequency for most test cases.

(2) Most pile response energy in the transverse direction occurs at the cylinder natural frequency f_n, and twice the wave frequency $2f_w$.

(3) When lock on appears, the response in both directions becomes mono-harmonic with a frequency of $2f_w$.

(4) Vortex-excited vibration is shown to produce substantial dynamic amplification of deflection not only in the transverse direction but also in the inline direction.

(5) The transverse top deflection plotted against the reduced velocity, V_r, for kd = 2.6, shows two distinct peaks at V_r = 5.75 and V_r = 7.3. In the case of kd = 1.63, a sharp peak appears at V_r = 5.5 and second less defined peak appears at V_r = 6.2.

Zedan and Rajabi (1981) have evaluated the lift force acting on the vortex-excited cylinder by using the experimental data obtained by Zedan et al. (1980) described above. They obtained the effective lift coefficient as a function of time from transverse bottom and top acceleration measurements, and compared them with those evaluated in two dimensional harmonic flow obtained by Sarpkaya and Rajabi (1979). The following results were obtained:

(1) The maximum response correlates reasonably well with the result of a flexibly mounted cylinder in two dimensional harmonic flow.

(2) The correlation of the lift coefficient with Keulegan-Carpenter number alone is poor because it depends strongly on V_r.

(3) At perfect resonance, the maximum effective lift coefficients are amplified between 1.6 and 1.93 times compared to those of a stiffly mounted cylinder in two dimensional harmonic flow at the same value of the Keulegan-Carpenter number.

Isaacson and Maull (1981) have investigated the dynamic response of a vertical cylinder in regular waves. The cylinder was pin-jointed at its base and spring mounted above the water surface to be left free to vibrate in any direction. The relationships between the dynamic response of the cylinder and other important parameters, which were indicated by dimensional analysis, have been obtained. The important parameters of the problems consist of the ratio of cylinder natural frequency to wave frequency, f_w/f_n, the Keulegan-Carpenter number, KC, the wave depth parameter, kd, and a mass ratio. The experimental data have been obtained for the following ranges or approximate values of the main parameters.

kd ≅ 1,2,3,4

f_n/f_w ≅ 1.0 - 4.0

KC ≅ 5 - 20

mass ratio ≅ 3, 4, 6, 7, 10.4, 13.0

The application of available data obtained from stiffly mounted cylinders to the prediction of vortex-excited vibration was considered in their study.

Angrilli and Cossalter (1982) have investigated the vortex-excited vibration of a cantilevered pile, flexible only in the transverse direction, in regular waves. The main results obtained are as follows:

(1) The range of substantial transverse oscillations of the cylinder was increased by the appearance of a lock-on effect in the range of f_w between $0.9.f_n$ and $1.1.f_n$.

(2) Perfect resonance occurs at V_r = 17.5 for $f_w = f_n$ and SKC = 17.5, at Vr = 5.75 for $f_w = f_n/2$ and KC = 11.5, at V_r = 5.93 for $f_w = f_n/3$ and KC = 17.8, and at V_r = 8.98 for $f_w = f_n/4$ and KC 35.92.

Those values of the reduced velocity $V_r = 5.75$ and 5.93 are very close to those obtained by Sarpkaya and Rajabi (1979) for two dimensional harmonic flows and Zedan et al. (1980) for waves. However, the appearance of perfect resonance at $V_r = 8.98$ and 35.92 should be considered more significantly.

2-4 The Added Mass and the Damping Factor

2-4-1 The added mass

When a structure is vibrating in still water or in the vortex-excited condition, a certain amount of water can be considered to become entrained and move with the vibration of the structure. (Milne-Thomson, 1968). This mass of water is called the added mass, M_a, and is given by

$$M_a = C_a . \rho . V_w \qquad (2\text{-}10)$$

where V_w is the volume of water displaced by the structure, ρ is the density of water and C_a is the added mass coefficient.

In inviscid flow, the value of the added mass is determined mathematically by potential flow theory and depends on the shape of the structure. The theoretical value of the added mass coefficient, C_a, for a circular cylinder in inviscid flow is 1.0 (Lamb, 1975). However, in real flow, the value of the added mass is influenced by the flow conditions around the structure, such as vortex-shedding and free surface effects. Therefore, it is difficult to estimate the added mass theoretically.

The added mass has a considerable influence on the natural frequency of the structure in a fluid. It must be taken account of properly in a study of the vortex-excited vibration of the structure.

Sarpkaya (1976) obtained the experimental result that the added mass coefficient of a circular cylinder, vibrating in still fluid, was slightly less than unity. King (1971) reported that the added mass in still water and the added mass in the vortex-excited condition were nearly equal. This result followed from the comparison of the natural frequency in still water and frequency of the inline vibrations excited by vortex shedding in steady flow. Sarpkaya (1978) measured the lift force acting on a rigid circular cylinder undergoing forced transverse oscillations in a uniform flow. From his results, he obtained a relationship between the added mass coefficient and the reduced velocity, V_r, that the added mass coefficient decreases rapidly with increasing V_r, becomes nearly equal to unity at perfect synchronization, and then becomes negative at V_r increases further.

2-4-2 <u>The damping</u>

Damping is defined as the energy dissipation due to the vibration of a structure. (Haberman, 1968). The dynamic response of the structure to the force acting on it is restricted by the damping. Therefore the damping must be considered significantly in the study of vortex-excited vibration of a structure in a fluid. When a structure is vibrating in a fluid, the damping may be composed of the structural material damping and the fluid damping. The structural material damping can be measured in the free vibration test of the structure in air. However, the definition and the measurement of the fluid damping are very difficult because the mechanism which generates it is very complex. The fluid damping may be considered to be composed of viscous drag, which is produced by shearing between the free stream and the surface of the structure, and the pressure drag, which is produced by flow separating from the structure and forming a wake (Blevins, 1977).

The fluid damping measured in the free vibration test of a structure in still water is often used in the design of the dynamic response of the structure in the vortex-excited condition. However, the relationship between the fluid damping in still water and the fluid damping in the vortex-excited condition of the structure is not clear. In order to overcome this ambiguity, Sarpkaya and Isaacson (1981) suggested that if we were able to express all the fluid forces resulting from the fluid-structure interaction in the forcing term of the structure, there would be no need for the fluid damping to be considered separately.

Bramley (1969) tested a section of a rigid cylinder and concluded that the damping was composed of viscous at low amplitudes of the oscillation of the cylinder, and it became amplitude dependent at the large amplitudes (see King (1972)).

King (1972) investigated the fluid damping of circular cylinders in various depths of still water. He obtained the result that the fluid damping coefficient is approximately constant and independent of amplitude effect for initial amplitudes of up to 0.5 diameters, and that the damping coefficient increases very rapidly for $d/L \gtrsim 0.5$. (d = water depth, L = length of the cylinder).

Verley (1978) measured the damping of oscillations in still water and various currents. His results show that for lower amplitude of oscillation the damping is a function of flow velocity, but for larger amplitude of oscillation it becomes independent of flow velocity.

The fluid damping may be related to the drag force caused by the movement of the cylinder. The characteristics of the drag force in the range of small Keulegan-Carpenter number have been studied by several investigators (for example Bearman et al. (1984)).

2-5 Conclusion

The main conclusion, arising from this brief review of the literature concerning vortex-excited vibration of a cylinder in waves, is that there have been very few relevant investigations and that the understanding of it is very poor compared with that for the vortex-excited vibration of a cylinder in steady flow. The following points should be noted:

(1) There is very little data on vortex-excited vibrations of a cylinder in two dimensional harmonic flow in the range of low Keulegan-Carpenter number.

(2) The lock-on phenomenon for the vortex-excited vibration of the cylinder in oscillating flow is not understood so well as in the case of steady flow.

(3) The relationships between the dynamic response of the cylinder in waves and important parameters such as f_w/f_n, KC, kd, damping factor and a mass ratio are not understood well. In most studies on vortex-excited vibration of cylinders in waves,

the important parameters have been held constant or varied over restricted ranges in different combinations. Therefore, a study such as Isaacson and Maull (1981), in which the main parameters have covered wider ranges and have been changed in different combinations, is very important and valuable.

(4) The influences of the damping and added mass on the vortex-excited vibration of cylinder both in steady flow and in waves have not been considered very fully.

(5) There is no model able to explain or reproduce properly the vortex-excited vibration of a cylinder in oscillating flow.

In view of the above, laboratory experiments have been performed, in the present work to study more closely the relationship between the dynamic response and the important parameter described above. The final purpose of the present study is to work towards establishing a model which can explain the phenomena of the vortex-excited vibration of a cylinder in oscillating flow. The application of the wake oscillator model developed for steady flow is also considered for oscillating flow.

CHAPTER 3

LINEARISED MODEL OF THE VIBRATION OF THE TEST CYLINDER

3-1 Introduction

The vortex-excited vibration of the test cylinder which was used in the experimental work of the present study is described in detail in Chapter 4. Its response in waves is simulated by the linearised model described in this chapter. The purpose of this modelling work is to identify the important parameters of the vortex-excited vibration of the test cylinder in waves. The non-linear fluid structure interaction is not considered in this model. However, the simple solution of the linearised model is quite helpful in finding the important parameters which control the vortex-excited vibration of the test cylinder in waves. The relationship between the vortex-excited vibration and these parameters above was examined in the experimental work described in Chapter 4. The solution of the linearised model will be used in the analysis of these experimental data.

The free vibration of the test cylinder in still water is also simulated by the linearised model. The purpose of this work is to understand the change of the damping factor with amplitude for its test cylinder vibrating in still water. In this model, the drag force, which is proportional to the square of the velocity of the cylinder, is considered as the fluid damping. The solution is used to analyse the experimental data which was obtained in the experiments described in Chapter 4.

3-2 Linearised Model for the Transverse Vibration of the Cylinder in Waves

3-2-1 The equation of motion

The definition sketch of the test cylinder is shown in Fig. 3-1. The explanation of symbols used is also described in Fig. 3-1. The cylinder is pivoted on the bottom of the flume and supported laterally by springs at the top. The damping of the cylinder is adjusted by using an electro-magnetic eddy-current damper.

The dynamic response of the test cylinder to the lift forces may be described by using the equation of motion as follows.

$$M_{mt} \cdot \ddot{y}_h + C_{mt} \cdot \dot{y}_h + K_{mt} \cdot y_h = F_{m\ell} \tag{3-1}$$

where y_h = the transverse displacement of the cylinder at the still water level (d = 80cm)

$\dot{y}_h$ = dy_h/dt

$\ddot{y}_h$ = d^2y_h/dt^2

M_{mt} = total mass matrix

C_{mt} = total damping matrix

K_{mt} = stiffness matrix

$F_{m\ell}$ = total lift force moment matrix (3-2)

The equation above shows the equivalence of the following moments taken about the pivot of the base.

(1) The value of $N_{mt} \cdot y_h$ is the total moment of the inertia force of the cylinder including the added mass effect and is given as Eq.(3-3).

$$M_{mt}.y_h = [\int_0^{\ell_3} m.(\frac{z}{\ell}).z.dz + \int_0^{r} m_q.(\frac{z}{\ell}).z.dz. + \int_r^{\ell_7} m_c.(\frac{z}{\ell}).z.dz$$

$$+ \int_{\ell_2}^{\ell_1} m_f.(\frac{z}{\ell}).z.dz + \int_{\ell_4}^{\ell_3} m_h.(\frac{z}{\ell}).z.dz + \int_{\ell_5}^{\ell_6} m_s.(\frac{z}{\ell}).z.dz$$

$$+ \int_0^{d} m_I.(\frac{z}{\ell}).z.dz + \int_0^{d+\eta} m_a.(\frac{z}{\ell}).z.dz]y_h \qquad (3\text{-}3)$$

In which the added mass of water per unit length is given as Eq.(3-4).

$$m_a = \frac{1}{4}.C_a.\rho.\pi.D^2.dz \qquad (3\text{-}4)$$

where D = the diameter of the test cylinder

ρ = the fluid density

C_a = added mass coefficient

The added mass coefficient, C_a, is an unknown value as described in Chapter 2. Therefore, in the analysis of the experimental data described in Chapter 4, the mass matrix of the test cylinder is estimated from the stiffness matrix defined Eq.(3-7), and the natural frequency of the test cylinder in still water.

The water surface displacement of wave is shown as Eq.(3-5) by linear wave theory.

$$\eta = \frac{H}{2}. \sin(\frac{2\pi t}{T}) \qquad (3\text{-}5)$$

(2) $C_{mt}.y_h$ is the total moment produced by the structural damping, the electro-magnetic damping and unknown fluid damping, and it is given by Eq.(3-6).

$$C_{mt}.\dot{y}_h = \{\frac{r^2}{\ell} C_s + \frac{\ell_8{}^2}{\ell} C_e + \int_0^{d+\eta} C_w.(\frac{z}{\ell}).z.dz\}\dot{y}_h \qquad (3\text{-}6)$$

where C_s = the damping coefficient of the springs

C_e = the damping coefficient of electro-magnetic damper

C_w = the damping coefficient of the fluid

The fluid damping is unknown. There are two ways of treating it in the analysis of the experimental data.

(a) As suggested by Sarpkaya and Isaacson (1981), the fluid damping may be considered as a part of loading term. Then

$C_w = 0$

or (b) Fluid damping is considered to be equivalent to the fluid damping of the test cylinder in still water.

(3) $K_{mt}.y_h$ is the moment produced by the stiffness of the structure and it is given by

$$K_{mt}.y_h = [K_s \frac{r^2}{\ell}$$

$$- \{ \int_0^{\ell_3} m.g.(\frac{z}{\ell}).dz + \int_0^{r} m_q.g.(\frac{z}{\ell}).dz + \int_r^{\ell_7} m_c.g.(\frac{z}{\ell}).dz$$

$$+ \int_{\ell_2}^{\ell_1} m_f.g.(\frac{z}{\ell}).dz + \int_{\ell_4}^{\ell_3} m_h.g.(\frac{z}{\ell}).dz + \int_{\ell_5}^{\ell_6} m_s.g.(\frac{z}{\ell}).dz$$

$$+ \int_0^{d} m_I.(\frac{z}{\ell}).dz\} + \int_0^{d+\eta} \rho_w.g.\frac{\pi.D^2}{4}.(\frac{z}{\ell}).dz]y_h \qquad (3\text{-}7)$$

where K_s is the stiffness of the springs.

The first term of the right hand side of Eq.(3-7) shows the moment due to the spring force. The second one shows the moment due to the distributed weight of the test cylinder when it is in a deflected position from the vertical. The third one shows the moment due to the buoyancy of the test cylinder when it is in a deflected position from the vertical.

(4) $F_{m\ell}$ is the moment produced by the lift force acting on the cylinder. The estimation of the lift force will be described in detail in the next section.

3-2-2. <u>The estimation of the lift force</u>

The lift force acting on the elemental length dz of the cylinder in waves, dF_ℓ, is commonly calculated by Eq.(3-8).

$$dF_\ell = \frac{1}{2} C_L \rho D u^2 dz \tag{3-8}$$

where C_L = the lift coefficient

u = the horizontal water particle velocity in waves.

Therefore, the total bending moment produced by the lift force, Fm_ℓ, can be expressed by Eq.(3-9)

$$F_{m\ell} = \frac{1}{2} \rho . D . \int_0^{d+\eta} C_L . u^2 . z . dz \tag{3-9}$$

However, as described in Chapter 2, the characteristics of C_L with the position, z, in waves are not known well. In order to overcome this problem, the effective lift coefficient is defined by Eq.(3-10). This definition is proposed by Zedan and Rajabi (1981).

$$C_{Le} = \int_0^{d+\eta} C_L.u^2.z.dz / \int_0^{d+H/2} u_m^2.z.dz \qquad (3\text{-}10)$$

$$C_{Le} \doteq \int_0^{d+\eta} C_L.u^2.z.dz / \int_0^{d} u_m^2.z.dz \qquad d >> H \qquad (3\text{-}11)$$

where u_m is the maximum horizontal wave particle velocity at z.

Taking Eq.(3-10) into account, $F_{m\ell}$ is described as Eq.(3-12).

$$F_{m\ell} = \frac{1}{2}.\rho.D.C_{Le}. \int_0^{d} u_m^2.z.dz, \qquad (3\text{-}12)$$

and is given as follows by linear wave theory

$$u_m = \frac{\pi H}{T} \cosh(k.z)/\sinh(kd) \qquad (3\text{-}13)$$

where k = the wave number, $\frac{2\pi}{L_W}$

kd = the wave depth parameter = k.d

L_W = the wave length

T = the period of wave

H = the wave height

By substituting Eq.(3-13) into Eq.(3-12), $F_{m\ell}$ is given as

$$F_{m\ell} = \frac{1}{2}\,\rho . D . C_{Le} . u_{ms}^{2} . d^{2} . F_{s}(kd) \tag{3-14}$$

where u_{ms} is the maximum horizontal particle velocity at still water level and is given as

$$u_{ms} = \frac{2\pi H}{T}\,\coth(kd); \tag{3-15}$$

$F_s(kd)$ is an index which describes the characteristics of the distribution of u^2 with z. $F_s(kd)$ is given as

$$F_s(kd) = \frac{1}{4(k.d)^2}\,\{kd.\sinh(2kd)-0.5.\cosh(2kd) + (kd)^2+0.5\}/\cosh^2(kd) \tag{3-16}$$

Now, the effective lift coefficient, C_{Le}, may be expressed in a series form as follows

$$C_{Le} = \sum_{n=1}^{N} C_{Le}(n)\sin(n.\omega_W.t+\phi(n)) \tag{3-17}$$

where $C_{Le}(n)$ = the lift coefficient for the n-th harmonic

ω_W = circular wave frequency (= $2\pi.f_W$ = $2\pi/T$)

f_W = the wave frequency

$\phi(n)$ = phase lag between the n-th harmonic lift coefficient, $C_{Le}(n)$, and the surface elevation of wave.

The above expression is commonly used to describe the time-variation of the lift coefficient (for example, Chakrabarti et al. (1976)).

3-2-3 The solution of the equation of motion

The equation of motion, Eq.(3-1), is a non-linear equation since the values of M_{mt}, C_{mt} and K_{mt} are the function of a water surface elevation, η. In order to obtain a simple solution, it is linearised as follows. Let M_{mt}, C_{mt} and K_{mt} be expressed

$$\begin{aligned} M_{mt} &= M_{Bm}\, M_{mo} \\ C_{mt} &= C_{Bm}\, C_{mo} \\ K_{mt} &= K_{Bm}\, K_{mo} \end{aligned} \tag{3-18}$$

where M_{mo}, C_{mo} and K_{mo} are the values of M_{mt}, C_{mt} and K_{mt} at $\eta = 0$.

Therefore, M_{Bm}, C_{Bm} and K_{Bm} show the variability of these values with t/T. Then Eq.(3-1) is written as follows.

$$M_{Bm}\, M_{mo}\, \ddot{y}_h + C_{Bm}\, C_{mo}\, \dot{y}_h + K_{Bm}\, K_{mo}\, y_h = F_{m\ell} \tag{3-19}$$

If the wave height, H, is small, the values of M_{Bm}, C_{Bm} and K_{Bm} may be approximated as $M_{Bm} = C_{Bm} = K_{Bm} = 1$ and in this case Eq.(3-19) may be described by Eq.(3-20)

$$M_{mo}\, \ddot{y}_h + C_{mo}\, \dot{y}_h + K_{mo}\, y_h = F_{m\ell}$$

$$\ddot{y}_h + 2\zeta_t\, \omega_n\, \dot{y}_h + \omega_n^2\, y_h = F_{m\ell}/M_{mo} \tag{3-20}$$

where ω_n is the circular natural frequency of the cylinder and defined as

$$\omega_n = 2\pi\, f_n = \sqrt{K_{mo}/M_{mo}}$$

f_n = natural frequency of the cylinder (3-21)

And ζ_t is the total damping factor of the test cylinder, defined as

$$\zeta_t = \frac{C_{mo}}{2\omega_n M_{mo}} = \zeta_s + \zeta_m + \zeta_f \tag{3-22}$$

where ζ_s is the damping factor of the spring and is given as

$$\zeta_s = \frac{r^2}{d} C_s/(2\omega_n M_{mo}) \tag{3-22-A}$$

ζ_m is a damping factor of the electro-magnetic damper and is given as

$$\zeta_m = \frac{\ell_s^{\,2}}{d} C_e/(2\omega_n M_{mo}) \tag{3-22-B}$$

ζ_f is the damping factor of the fluid and is given by

$$\zeta_f = \int_0^{d+\eta} C_w.(\frac{z}{\ell}).z.dz/(2\omega_n M_{mo}) \tag{3-22-C}$$

In the present study of the vortex-excited vibration of the test cylinder in waves, the fluid damping factor, ζ_f, is shown as follows by the definition of the fluid damping described in 3-2-1.

(a) $\zeta_f = 0$

(b) $\zeta_f = \zeta_w$ (3-22-D)

where ζ_w is the fluid damping factor of the test cylinder in still water.

When the value of $F_{m\ell}$ is expressed by Eq.(3-14) and C_{Le} is expressed by Eq.(3-17), the equation of motion of the cylinder, described by Eq.(3-20), becomes a linear differential equation.

Then, the solution of it is given as follows

$$\frac{y_h}{D} = \frac{3F_s(kd).SKC^2.(\frac{f_w}{f_n})^2 d^2}{8\pi^2(\frac{m_e}{\rho D^2})\ell^2} \sum_{n=1}^{n=N} \left[\frac{C_{Le}(n).\sin(2\pi n\, f_n t+\phi_A(n))}{\sqrt{(1-(n\,\frac{f_w}{f_n})^2)^2+(2\zeta_t.n\,\frac{f_w}{f_n})^2}}\right] \tag{3-23}$$

now $\ell = d$, it is given as

$$\frac{y_h}{D} = \frac{3F_s(kd).SKC^2.(\frac{f_w}{f_n})^2}{8\pi^2(\frac{m_e}{\rho D^2})} \sum_{n=1}^{n=N} \left[\frac{C_{Le}(n).\sin(2\pi n\, f_n t+\phi_A(n)}{\sqrt{(1-(n\,\frac{f_w}{f_n})^2)^2+(2\zeta_t.n\,\frac{f_w}{f_n})^2}}\right] \tag{3-23-A}$$

where SKC is a surface Keulegan-Carpenter number defined as follows.

$$SKC = \frac{u_{mo}.T}{D} \tag{3-24}$$

in which U_{mo} is the maximum horizontal particle velocity at still water level. It is given as follows by linear wave theory.

$$U_{mo} = \frac{\pi H}{T} \tanh(kd) \tag{3-25}$$

$\phi_A(n)$ is a phase angle between the vibration of the test cylinder, y_h, and lift force, and is given as

$$\phi_A(n) = \tan^{-1}\{\frac{2\zeta_t . n . \frac{f_w}{f_n}}{1-(n.\frac{f_w}{f_n})^2}\} \tag{3-26}$$

where m_e is the effective mass per unit length of the test cylinder given by

$$m_e = \frac{M_{mo}}{\int_0^d (\frac{z}{\ell}).z.dz} = \frac{3M_{mo}}{(\frac{d^3}{\ell})} = \frac{3M_{mo}}{d^2} \qquad d = \ell \tag{3-27}$$

If f_w nearly equals the value of f_n/n ($n = 1,2,3...$), y_h/D is approximated as

$$\frac{y_h}{D} = \frac{3F_s.(kd).SKC^2.(\frac{f_w}{f_n})^2}{8\pi^2(\frac{m_e}{\rho D^2})}$$

$$\times [\frac{C_{Le}(n)}{\sqrt{\{1-(n\frac{f_w}{f_n})^2\}^2+(2\zeta_t.n.\frac{f_w}{f_n})^2}} \sin\{2\pi n.f_n.t+\phi_A(n)\}] \tag{3-28}$$

and when $f_w/f_n = n$, $(n=1,2,3,...)$, at resonance, the vibration, y_{hr}, of the test cylinder is given as

$$\frac{y_h}{D} = \frac{3F_s(kd).SKC^2.(\frac{f_w}{f_n})^2}{8\pi^2(\frac{m_e}{\rho D^2}).2\zeta_t} . C_{Le}(n).\sin\{2\pi f_w t+\phi_A(n)\}$$

$$= \frac{3F_s(kd).SKC^2.(\frac{f_w}{f_n})^2}{4\pi\ 2m_e(\frac{2\pi\ \zeta_t}{\rho D^2})} . C_{Le}(n)\sin\{2\pi f_w t+\phi_A(n)\} \qquad (3\text{-}29)$$

where

$$\phi_A(n) = \frac{\pi}{2} \qquad (3\text{-}30)$$

Eq.(3-23) shows that the vortex-excited vibration of the test cylinder is related to the following parameters:

kd, SKC, f_w/f_n, $m_e/\rho D^2$, C_{Le}, ζ_t

In which $m_e/\rho D^2$ is a mass ratio.

Eq.(3-29) shows that the amplitude of the test cylinder at resonance is related to the following parameters.

kd, SKC, C_{Le}, $2m_e.(2\pi\ \zeta_t)/\rho D^2$, f_w/f_n

In which $2m_e(2\pi\ \zeta_t)/\rho D^2$ is a normalised (reduced) damping.

On the other hand, the lift force acting on the observed vortex-excited cylinder can be estimated from Eq.(3-23) or (3-29).

Eq.(3-26) shows that phase angle between the vibration of the cylinder and the lift force acting on it is related to the frequency ratio, $n.f_w/f_n$, and total damping coefficient, ζ_t.

The relationships between these parameters and the vortex-excited vibration of the test cylinder were examined experimentally in Chapter 4, and the data was analysed by using these equations above. In this case, it should be noted that fluid damping, ζ_f, is defined in two ways as shown Eq.(3-22-D). When ζ_f is defined as 0, ζ_t only includes the damping factor of spring, ζ_s, and the damping factor of electro-magnetic damper, ζ_m.

3-3 Damping in Still Water

The free vibration of the test cylinder in still water is also described by the equation of motion described in Section 3-2. In this case, there is no exciting force to the cylinder, and its vibration decays due to the damping force in the springs, the damping force of electro-magnetic damper and the fluid damping force.

If the fluid damping force is associated with a drag force which is proportional to the square of the velocity of the cylinder, the fluid damping factor, ζ_f, is described by Eq.(3-31), by the definition of the damping factor shown in Eq.(3-22-A).

$$\zeta_f = \frac{\rho D |\dot{y}_h| \int_0^d C_D (\frac{z}{\ell})^2 \, z.dz}{4\omega_n M_{mo}} \tag{3-31}$$

where C_D = drag coefficient

ω_n = circular natural frequency of cylinder in still water

The energy, dissipated in one cycle of vibration by the fluid damping force, E_{df}, is given as

$$E_{df} = \int_{\text{one cycle}} F_{df} = \int_{t_i}^{t_i+T} F_{df}\, \dot{y}_h\, dt \tag{3-32}$$

where F_{df} is written as follows

$$F_{df} = 2M_{mo}\, \omega_n\, \zeta_f$$

$$= \frac{1}{2}\, \rho D |\dot{y}_h| y_h \int_0^d C_D(\frac{z}{\ell}) dz \tag{3-33}$$

The fluid damping coefficient defined by Eq.(3-31) is a function of $|\dot{y}_h|$. Therefore it changes with t.

Now we assume that ζ_f defined by Eq.(3-31) is substituted by a constant value ζ_{fi} over one period ($t = t_i$ to $t = t_i + T_n$, see Fig. 3.2),

$$\zeta_{fi} = \frac{\rho . D . \kappa . y_{hi} . \int_0^d C_D(\frac{z}{\ell})^2\, z . dz}{4M_{mo}} \tag{3-34}$$

where κ = numerical constant

The energy, E_{dfi}, dissipated in one cycle of vibration by this fluid damping force, E_{dfi}, is given as

$$E_{dfi} = \int_{\text{one cycle}} F_{dfi}.dy = \int_{t_i}^{t_i+T_n} F_{dfi}.\dot{y}_h.dt \qquad (3\text{-}35)$$

where F_{dfi} is given as

$$F_{dfi} = 2M_o.\omega_n.\zeta_{fi}.\dot{y}_h$$

$$= \frac{\kappa}{2}\,\rho.D|\dot{y}_{hi}|y_{hi}.\omega_n \int_0^d C_D.(\frac{z}{\ell})dz \qquad (3\text{-}36)$$

Putting E_{dfi} equal to E_{df},

$$\int_{t_i}^{t_i+T} F_{df}.\dot{y}_h.dt = \int_{t_i}^{t_i+T} F_{dfi}.\dot{y}_h\, dt \qquad (3\text{-}37)$$

We assume that the drag coefficient C_D is constant over one cycle of vibration, and that the displacement, y_h, is approximated by Eq.(3-38) over one cycle of vibration of cylinder,

$$y_h = \dot{Y}_{hi}.\sin(\omega_n t) \qquad t_i < t < t_i + T \qquad (3\text{-}38)$$

where $\dot{Y}_{hi}$ = the value of y_h at $t = t_i$ (see Fig. 3.2)

By substituting Eq.(3-38) into Eq.(3-37), κ is defined as

$$\kappa = \frac{8}{3\pi} \qquad (3\text{-}39)$$

By substituting this α into Eq.(3-34), the fluid damping factor ζ_{fi} is given as

$$\zeta_{fi} = \frac{2\rho D\, Y_{hi} \cdot \int_0^d C_D \left(\frac{z}{\ell}\right)^2 z.dz}{3\pi\, M_{mo}} \tag{3-40}$$

Eq.(3-40) shows that the fluid damping factor, ζ_{fi}, is a function of the amplitude of the free vibration of the test cylinder in still water, Y_{hi}, and the drag coefficient.

This equation is used in the analysis of the experimental data which was obtained in the experiment on the damping of the test cylinder in still water, described in Chapter 4.

In this case, the unknown value of the drag force coefficient is estimated with several methods.

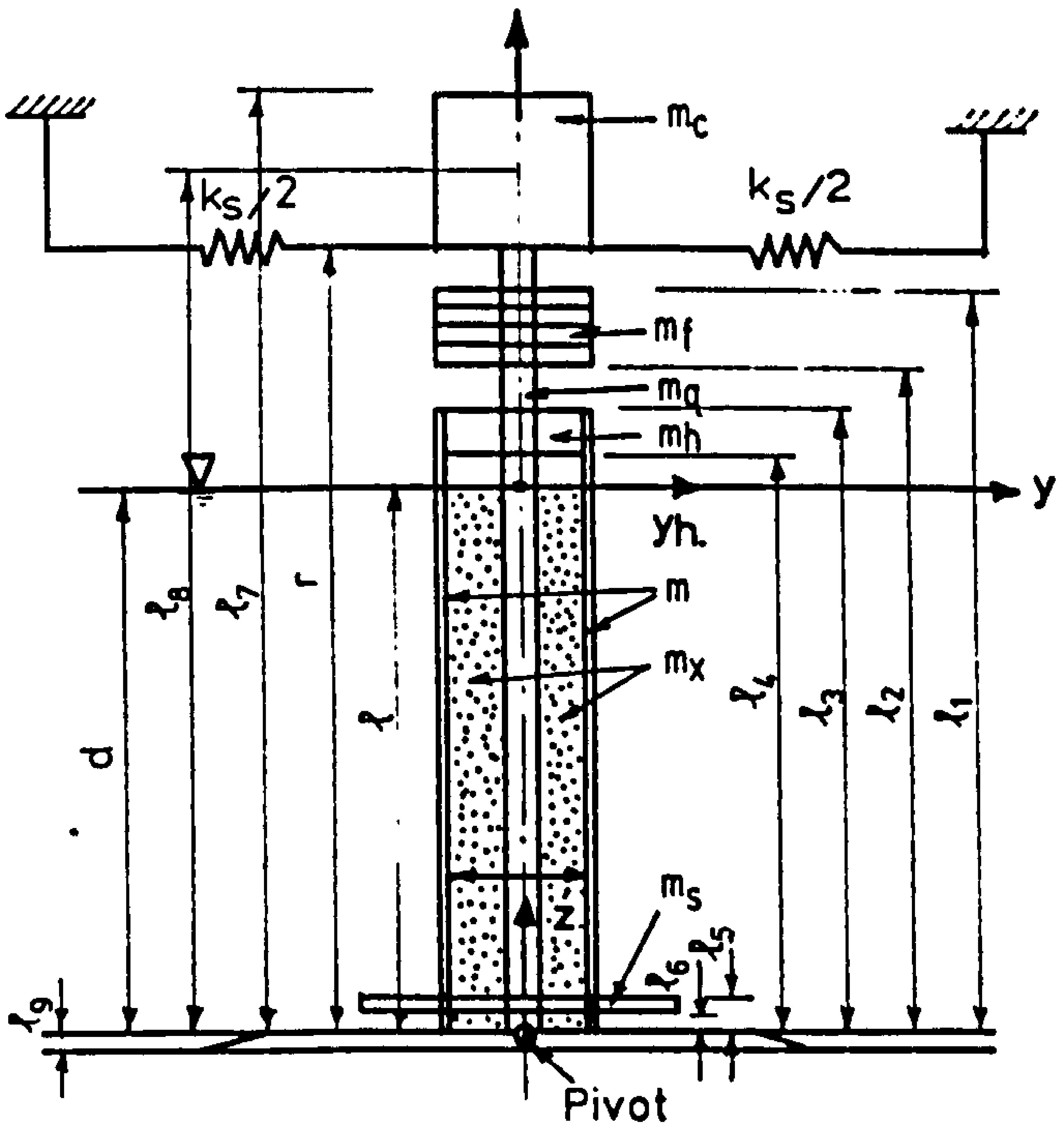

m_c = conducting plate mass/unit length

m_q = core cylinder mass/unit length

m = test cylinder mass/unit length

m_f = flange weight mass/unit length

m_h = holder flange mass/unit length

m_s = support plate and holder flange of bottom mass/unit length

m_i = water mass inside of the test cylinder/unit length

m_a = added mass of water/unit length

d = still water depth

r = distance from pivot to spring

ℓ_1 = distance from pivot to top of flange weight

ℓ_2 = distance from pivot to bottom of flange weight

ℓ_3 = distance from pivot to top of holder flange and test cylinder

ℓ_4 = distance from pivot to bottom of holder flange

ℓ_5 = distance from pivot to top of support plate

ℓ_6 = distance from pivot to bottom of support plate

ℓ_7 = distance from pivot to top of conducting plate

ℓ_8 = distance from pivot to electro-magnetic damping

ℓ = distance from pivot to surface of still water $d = 80$cm

ℓ_q = distance from pivot to bottom of frame.

Fig. 3.1 Definition Sketch of the Test Cylinder

PAGE NUMBERS CUT OFF IN ORIGINAL

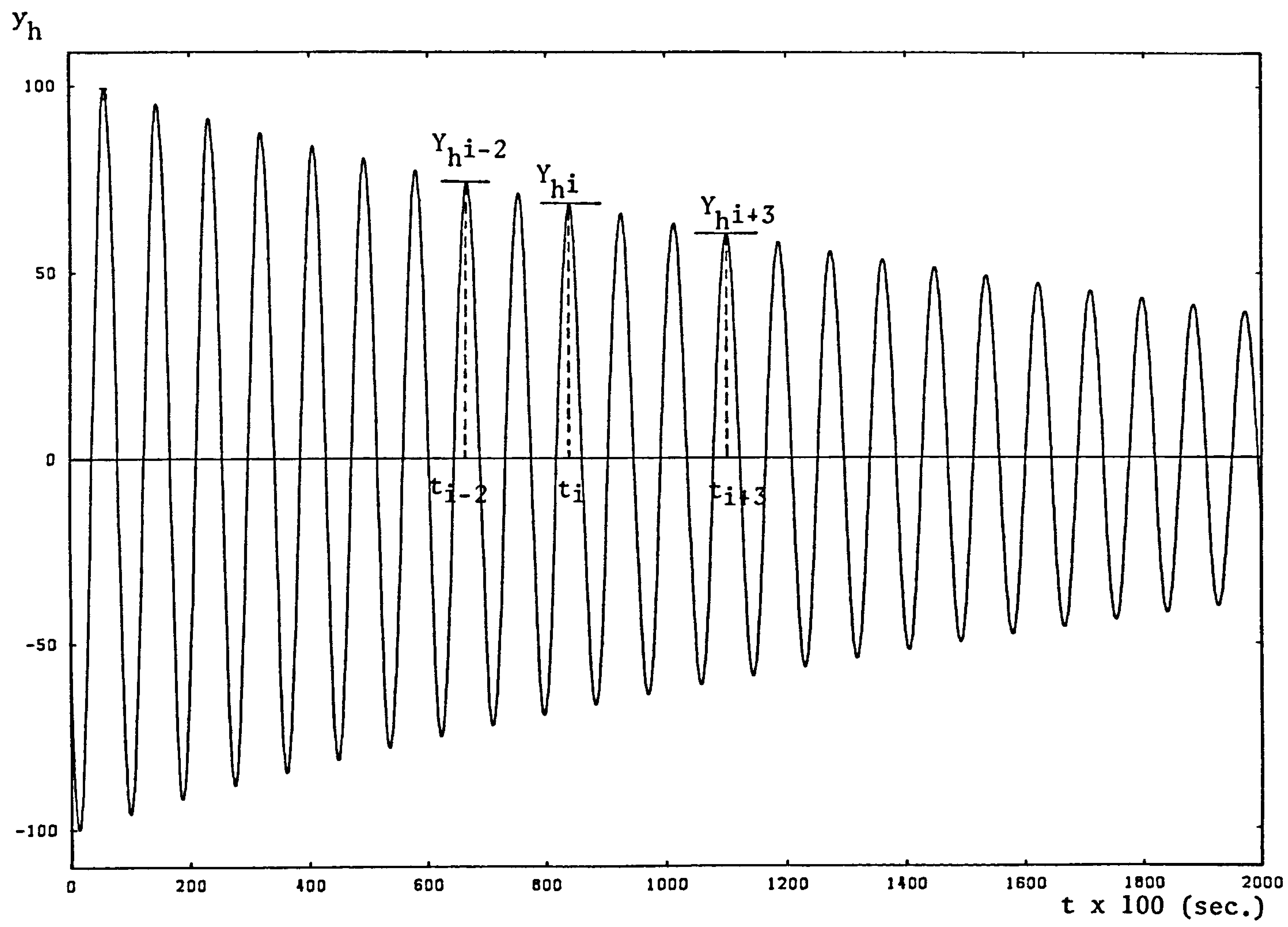

Fig. 3.2 Decay of Free Vibration of the Test Cylinder

CHAPTER 4

EXPERIMENTAL PROCEDURE

4-1 Introduction

This chapter aims to describe the experimental work of the present study. The following experiments were carried out to study the vortex-excited vibration of cylinders in waves.

(1) An experiment on the vortex-excited vibration of the test cylinder in regular waves.

(2) An experiment on the lift force acting on the stable test cylinder in regular waves.

(3) An experiment on the damping of the test cylinder in still water.

A rigid cylinder, which was vertically pivoted on the bottom of the flume, was used in the experiments listed above. The pivoted cylinder has an advantage in its simple mode shape of vibration which could be easily analysed. As described in Chapter 3 (Eq.(3-23) and Eq.(3-26)), the vortex-excited vibration of the test cylinder in regular waves may be controlled by the following parameters: the life force, the ratio of wave frequency to natural frequency, the Keulegan-Carpenter number, the wave depth parameter (wave number), damping coefficient, and a cylinder mass parameter (mass ratio). The relationship between the vortex-excited vibration of the test cylinder and these parameters was examined in the experiment (1). The damping factor of the test cylinder was adjusted by using the electro-magnetic damper in this experiment.

The purpose of the experiment (2) was to obtain a reference value of the lift force which was used in the estimation of the amplification of the lift force acting on the vortex-excited vibrating cylinder. In order to obtain an estimate of the unknown damping force in waves, the fluid damping of the test cylinder vibrating in various depths of still water has been measured in experiment (3).

4-2 The Wave Flume and Wave Gauge

The experiments were carried out in a wave flume in the Department of Civil Engineering at Liverpool University. This flume is glass-sided, and is 18.0m long and 0.75m wide with a maximum working depth of 1.0m. The piston-type wave generator is fixed to one end of the flume and it is servo-controlled. A long beach with a slope of 1:6.4 is installed at the other end to absorb the wave energy. The surface of the long beach is covered with porous matting. The general layout of the wave flume is shown in Fig. 4.1.

The wave gauge was mounted just beside the test cylinder (see Fig. 4.1 and Fig. 4.2) to record the water surface elevation, from which the wave height, H, and the wave period (T) were obtained. The wave gauge used was of the resistance type, and its output signal was amplified by using the wave gauge amplifier before recording.

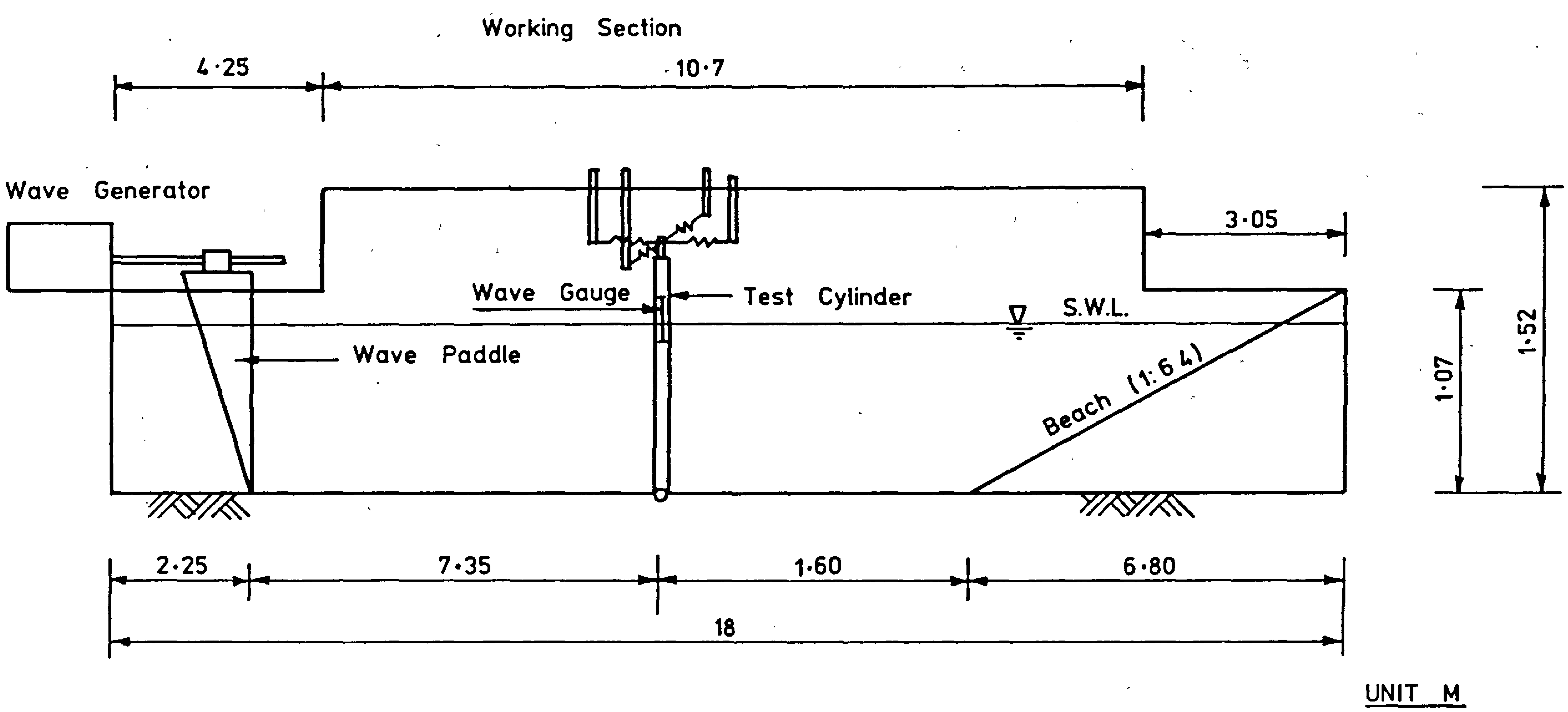

Figure 4.1. Wave Flume.

4-3 The Arrangement of the Test Cylinder

The test cylinder was positioned in the working section of the wave flume, 7.2m from the paddle, as shown in Figure 4.1. The general arrangement of the test cylinder is shown in Figure 4.2. A stainless steel hollow cylinder (outside diameter D = 17.05mm, wall thickness = 0.536mm and length = 985mm) was used. Both ends of the test cylinder were connected to the core cylinder (diameter DC = 10mm and length = 1105mm) by using a holder flange (see Fig. 4.3 and Fig. 4.4). The end flange of diameter = 120mm was attached to the bottom side of the test cylinder to eliminate end effects. The flange weights were attached to the core cylinder above the test cylinder to adjust its equivalent mass, m_e. The natural frequency of the test cylinder was adjusted independently of each equivalent mass, m_e, by changing the stiffness, k_s, of the springs.

The vibration of the cylinder was studied for two cases. In one case, the cylinder was left free to vibrate only in the transverse direction. In the other case, the cylinder was left free to vibrate in any direction. The first arrangement was used for the majority of the experiments. In this case, the support plate was attached on the holder flange at the bottom end of the test cylinder, and it was pivoted on the bottom of the flume to restrict the vibration in the inline direction (see Fig. 4.2 and Fig. 4.3). Two flange weights were attached to the core cylinder. The top end of the core cylinder was mounted with springs only in the transverse direction. Each spring was connected to a support strip (see Fig. 4.4). Two strain gauges were fixed on each support strip to measure its bending moment and thus the force acting on end of it. These strain gauges were connected into a wheatstone bridge circuit in the Bridge Conditioner to produce the output signal corresponding to the displacement of the top end of the core cylinder in the transverse direction.

In the case of the second experiment, the test cylinder was arranged as follows.

(1) Both the support plate and the conducting plate were removed, and the bottom of the core cylinder was pivoted on the support cylinder (see Fig. 4.3).

(2) The top end of the core cylinder was mounted with springs in the inline direction and in the transverse direction.

(3) Three flange weights were attached to the core cylinder.

The displacements of the core cylinder in both directions were also measured by the gauges on the four support strips as described above.

When the top end of the cylinder was mounted with strings replacing the springs in the transverse direction, the stiffness of the support strips was large enough to restrict the top end displacement of the core cylinder. Therefore, the output signals of the gauges corresponded to the bending moment on the cylinder (at the pivot) in the transverse direction.

The general view of the test cylinder arrangement is shown in Plate 1. The views of the lower and upper parts of the test cylinder are shown in Plate 2.

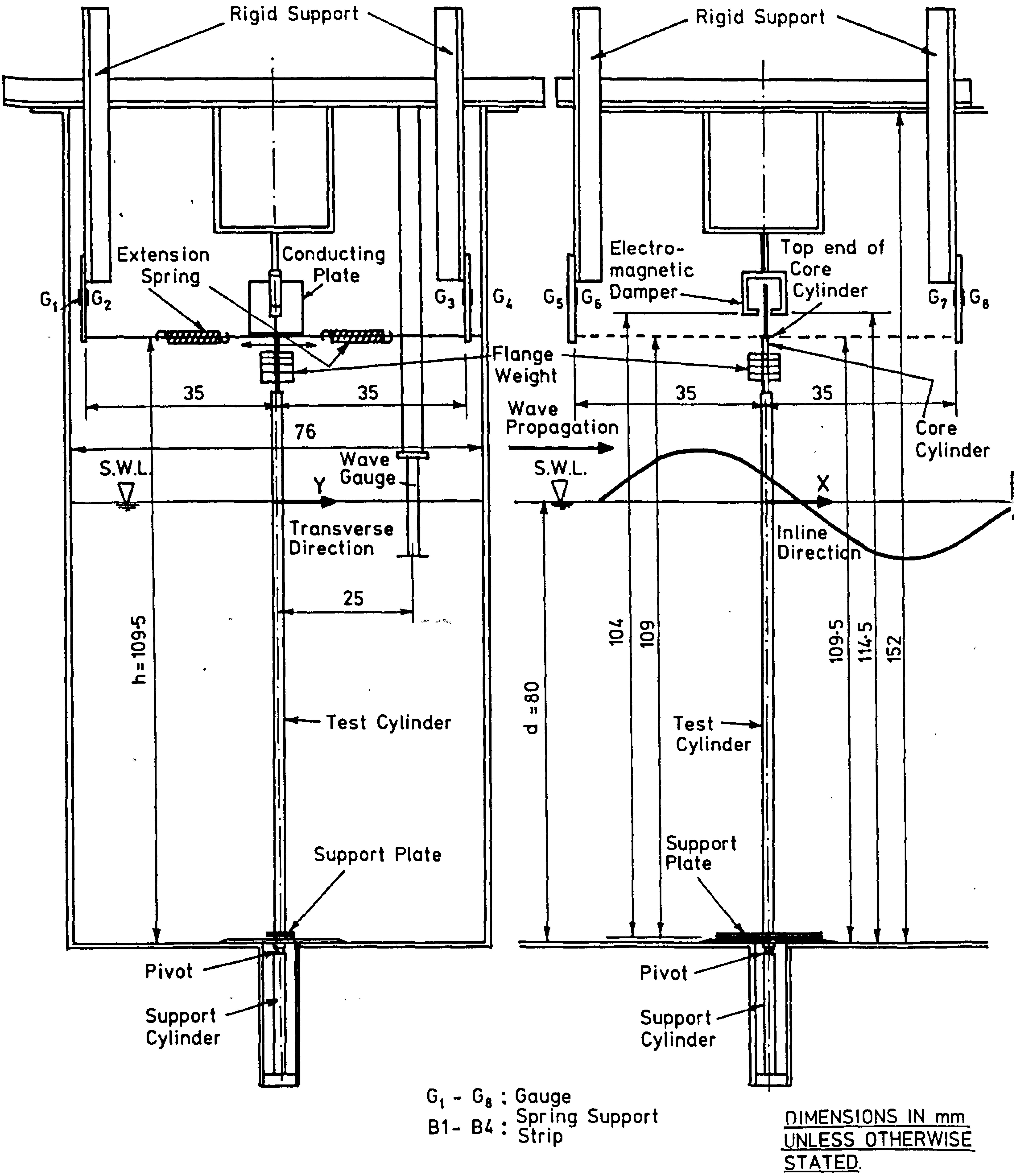

Fig. 4.2 General Arrangement of the Cylinder

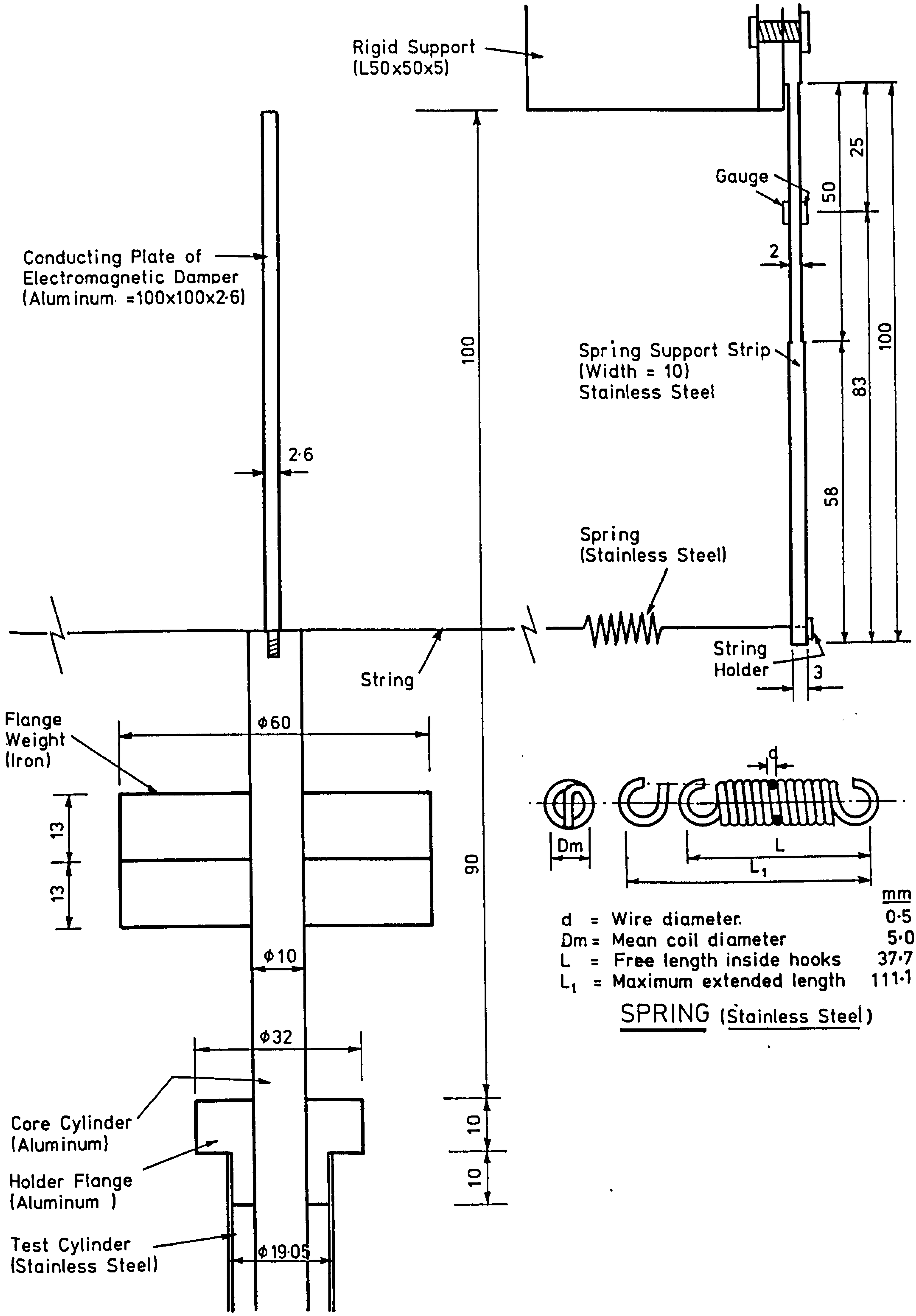

Fig. 4.3 Arrangement of the Top Part of the Test Cylinder

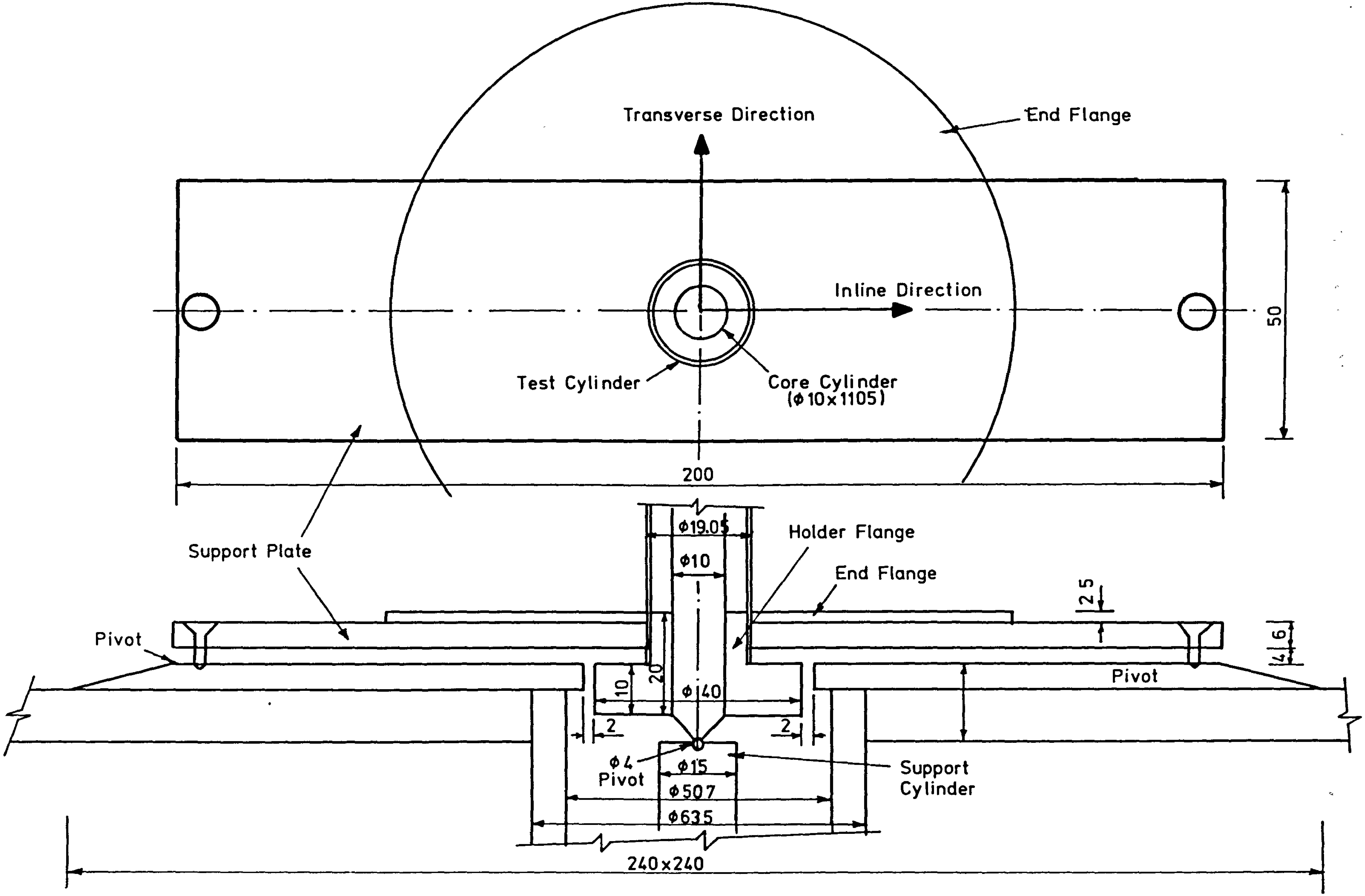

Fig. 4.4 Arrangement of the Low Part of the Test Cylinder

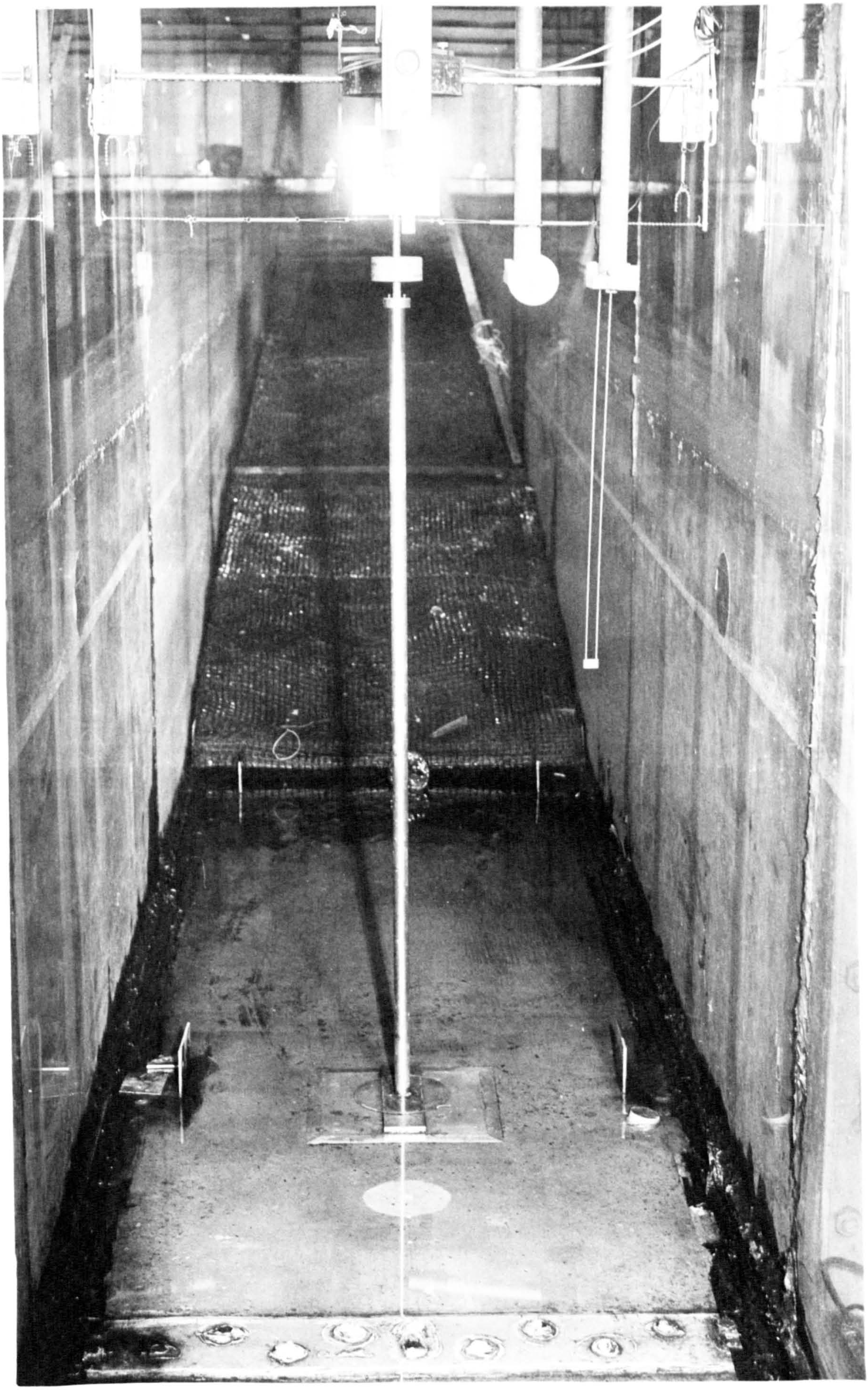

Plate 1 General View of Test Cylinder Arrangement Support

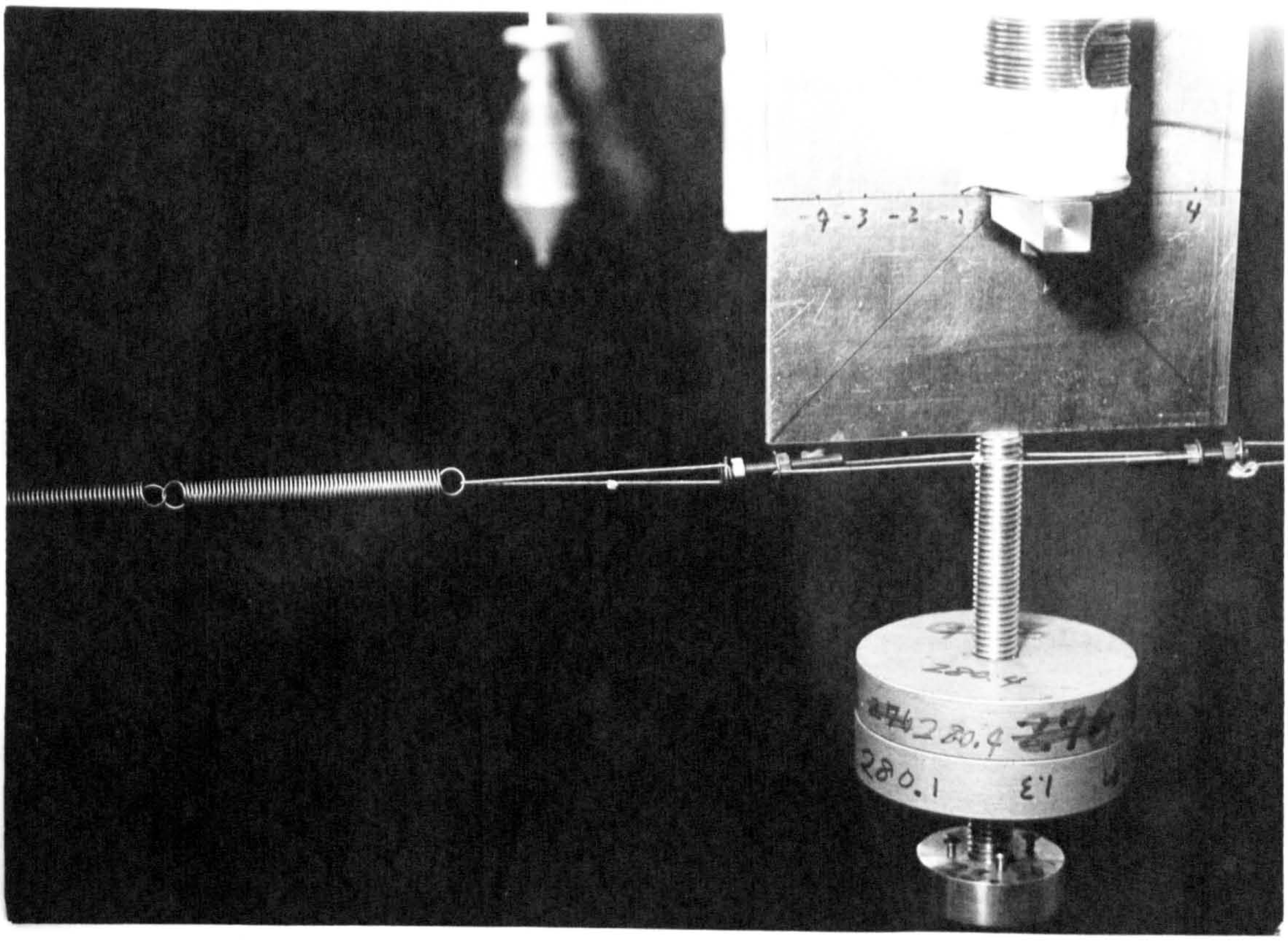

(a) Upper Part

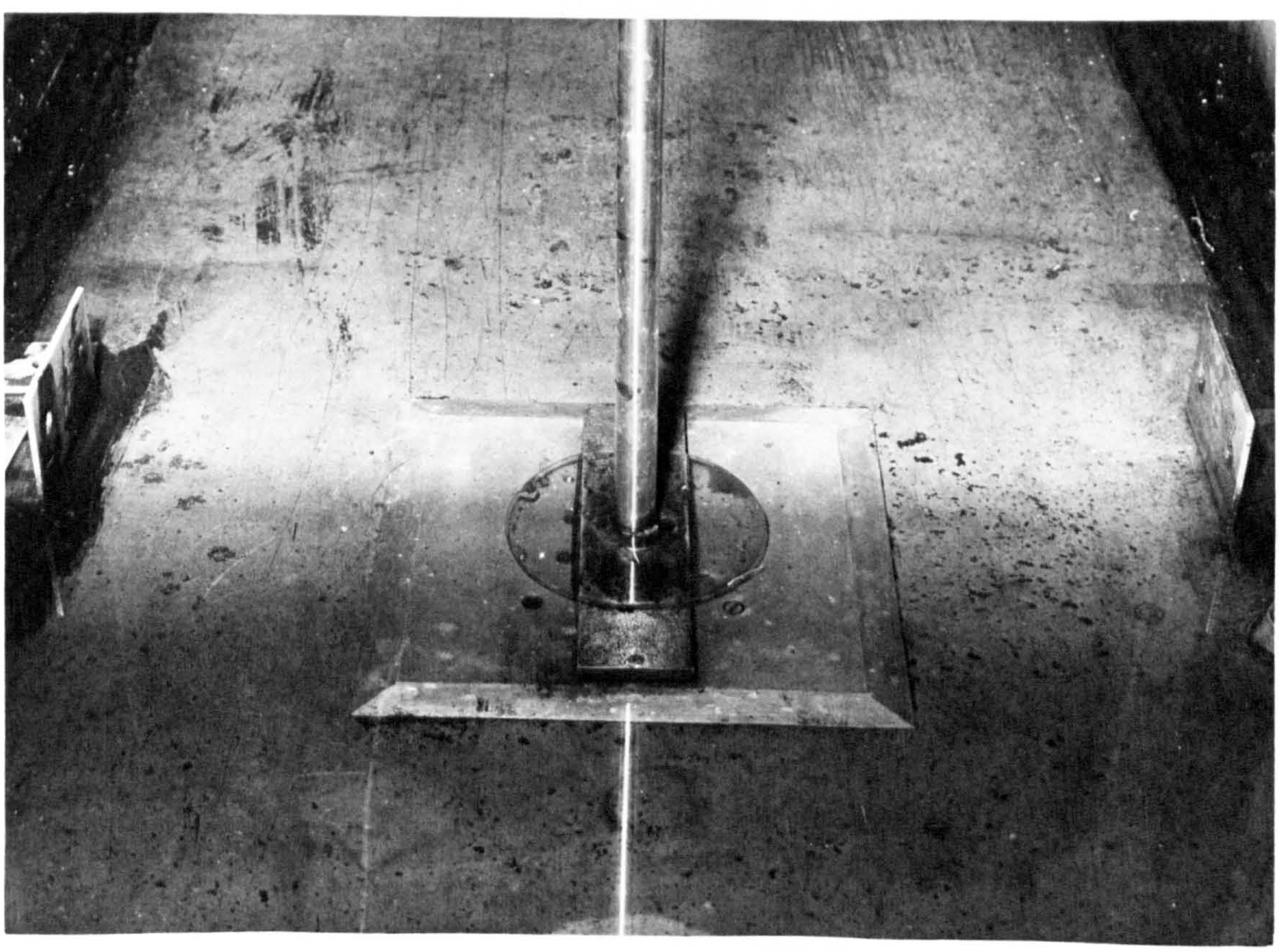

(b) Lower Part

Plate 2 View of Upper and Lower Part of the Test Cylinder

4-4 The Electro-Magnetic Damper

In order to adjust the damping of the test cylinder, an electro-magnetic damper was used. The position and details of this electro-magnetic damper are shown in Fig. 4.2 and Fig. 4.5. It is composed of an electro-magnet and a conducting plate. The electro-magnet is made of a coil and soft iron (see Fig. 4.5). Soft iron is used to minimise the residual magnetism (remanence). The conducting plate is made of aluminium (see Fig. 4.5). The principle of the electro-magnetic damper is as follows (Drysdale and Jolley, 1952).

Suppose the conducting plate is moving across a magnet pole with a velocity, U_c, then an electro-magnetic potential, V_{emf}, is induced in the conducting plate. Then, a belt of eddy current flowing in the direction of arrow, shown in Fig. 4.5, is produced in the conducting plate. V_{emf} is calculated by Eq.(4-1).

$$V_{emf} = b_1.B.U_c \quad [V] \qquad (4\text{-}1)$$

where B is the magnetic flux density (W_b/m^2) in the area b_1 by b_2. Magnetic flux density, B, is calculated as follows.

$$B = \mu_e \frac{N_e.I_e}{\ell_e} \quad [W_b/m^2] \qquad (4\text{-}2)$$

where μ_e = magnetic permeability [Henry/m]

N_e = number of turns of the coil

ℓ_e = length of the coil [m]

I_e = current [A]

If the resistance of the eddy current circuit in the conducting plate is given by, R_c, the eddy current, I_c, passing through the area b_2 over the thickness of the conducting plate is calculated as follows.

$$I_c = \frac{V_{emf}}{R_c} = \frac{b_1.B.U_c}{R_c} \quad [A] \qquad (4\text{-}3)$$

Then, a force, F_c, is produced on the conducting plate by the reaction of this current and it is calculated as follows.

$$F_c = b_1.I_c.B = \frac{b_1^2.B^2.U_c}{R_c} \quad [N] \qquad (4\text{-}4)$$

Eq.(4-4) shows that the force, F_c, is proportional to the velocity of the conducting plate, U_c. This force, F_c, is a viscous type damping force acting on the test cylinder. It will be referred to as the damping force of electro-magnetic damper.

In the experiment, an alternating current, I_e, was used to prevent the generation of residual magnetism (remanence) in the conducting plate. The movement of the test cylinder was restricted to the transverse direction, when the electro-magnetic damper was used. The view of the electro-magnetic damper is shown in Plate 3.

4-5 The Collection of Experimental Data

The block diagram of the measuring system is shown in Fig. 4.6(a). When the test cylinder was mounted with four springs, both in the inline direction and in the transverse direction, the gauges on the four support strips were correspondingly used as the four resistances in two full bridge circuits to respond independently to the top end

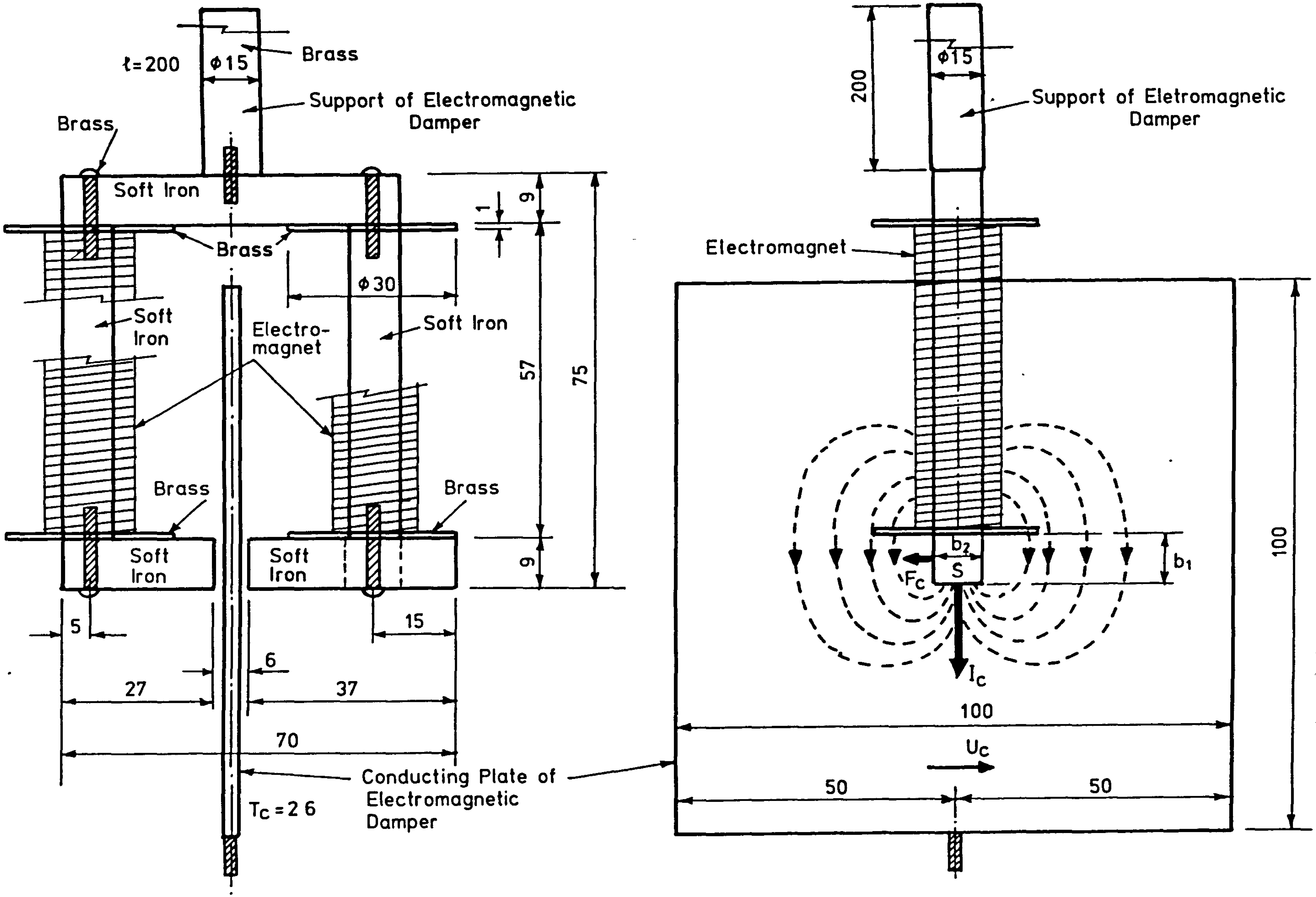

Fig. 4.5 Set Up of the Electro-magnetic Damper

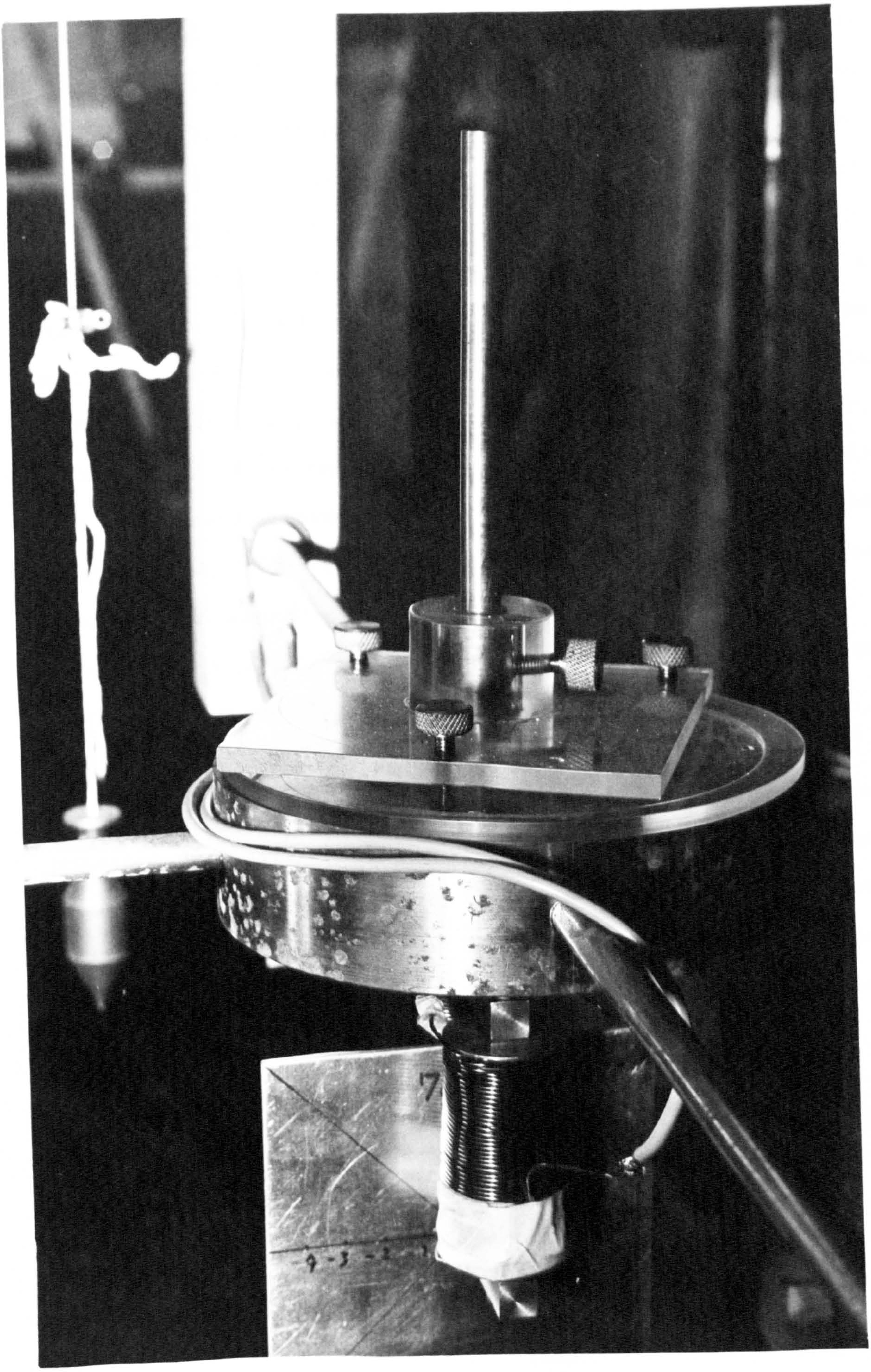

Plate 3 View of Electro-magnetic Damper

displacements of the core cylinder in the inline direction and in the transverse direction. The location of the strain gauges and their bridge connections are shown in Fig. 4.6(b). The output signal of each bridge circuit was amplified through a D.C. amplifier (Universal Amplifier EE-351-UA, FYLDE), and recorded on an Ultra Violet Light Oscillograph (U-V), (Oscillograph M10-120, ELCOMATIC) and on magnetic disk, using a mini computer (Eclipse 140, Data General) by using a standard data collecting program. The output signals of the amplifiers were also connected to low pass filters, [four pole (24PB/OCT) Low Pass, Butterworth, (EE-299-DF&SF Acting Filter, FYLDE)], to eliminate mechanical and electrical noise. These signals were also recorded using the computer. The output signal of the Wave-gauge Amplifier (Wave Monitor Module, CHURCHILL) was also recorded simultaneously with the signals from the strain gauges. These output signals were inspected by using a Monitor Oscilloscope (Digital Storage Oscilloscope OS 400, GOULD) during measurement.

The experimental data stored on disk by the computer was later processed off line. The plotting of experimental data and computational results was done by using the computer plotter (Miplot, WATANABE). The general view of the electronic equipment described above is shown in Plate 4. The general view of the Eclipse computer system is shown in Plate 5.

4-6 Procedure

4-6-1 Calibration of the strain gauges and the wave gauge

In order to obtain meaningful output voltage signals, it was necessary to equate the physical values measured by the test equipment to the output voltage signals by suitable calibration factor. The following calibrations were carried out.

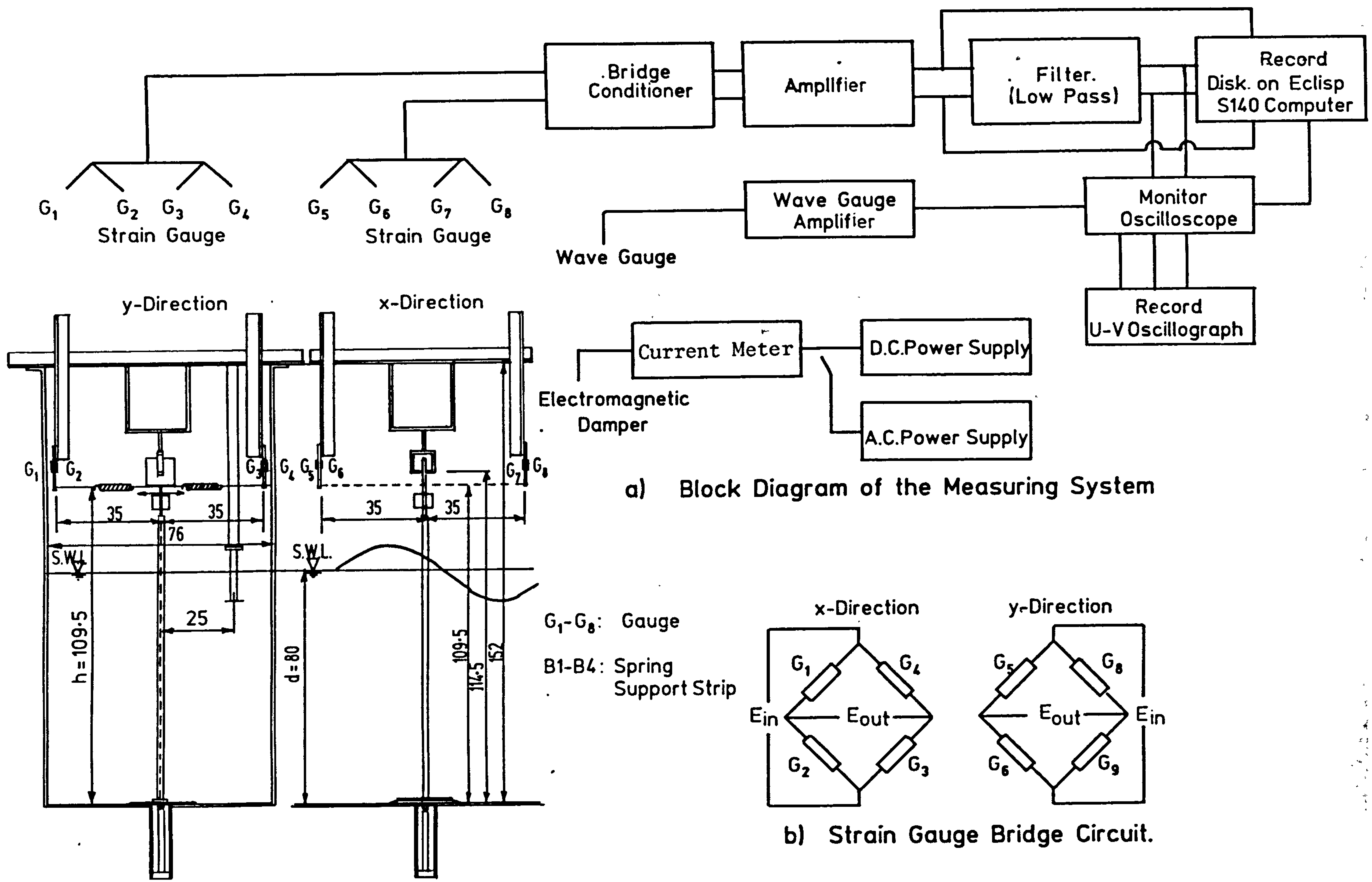

a) Block Diagram of the Measuring System

b) Strain Gauge Bridge Circuit.

c) Location of Strain Gauge & Wave Gauge.

Fig. 4.6 Schematic of Measuring System

Plate 4 General View of the Electronic Equipment

Plate 5 General View of the Eclipse Computer System

(1) Calibration of the strain gauges

To obtain the relationship between the output voltage signals from each bridge circuit and the displacements of the top end of the core cylinder, known loads were applied horizontally to the top end of the core cylinder by weights hung over a pully. The top end displacement of the core cylinder was measured on a vernier scale. The bending moment at the pivot was equal to the product of the load and the distance from the pivot to the top end of the core cylinder. Therefore, the relationship between the output voltage signal and the bending moment at the pivot was obtained. When the test cylinder was mounted with strings (and springs) in the inline and the transverse direction, the sensitivity to direction of these gauges was inspected by loading the weights in the inline and transverse direction independently.

(2) Calibration of the wave gauge

The relationship between the output voltage of the wave gauge and the water surface elevation was obtained by raising and lowering the probe in still water and recording the output voltages. The displacement of the probe was measured using a vernier scale.

4-6-2 Determination of basic parameters

In order to estimate the mass matrix, M_{mt}, damping matrix, C_{mt}, and stiffness matrix, K_{mt}, which control the vibration of the test cylinder, the following measurements were done in both arrangements of the test cylinder described in 4.3.

(1) The relationship between the displacement of the test cylinder and the bending moment at the pivot was determined by loading the top end of the core cylinder horizontally.

(2) The damping factor of the test cylinder and the natural frequency of the test cylinder were measured by plucking its top end and recording amplitude decay of the transient vibration of the cylinder.

The measurements above were done for the following two cases in one case the cylinder was mounted in air, and in the other case the cylinder was mounted in still water (water depth, d = 80cm).

From the first measurement, the stiffness of the test cylinder both in air, K_{mta}, and in water, K_{mtw}, was determined as follows.

$$K_{mta} = \frac{\text{Bending moment at pivot}}{\text{Displacement of the test cylinder at the position 80cm from the flume bottom}} \tag{4-5}$$

$$K_{mtw} = \frac{\text{Bending moment at pivot}}{\text{Displacement of the test cylinder at still water level (d = 80cm)}} \tag{4-6}$$

From the second measurement, the natural frequency of the test cylinder both in air, f_{na}, and in water, f_{nw}, and the total damping factor both in air, ζ_{ta}, and in water, ζ_{tw}, were evaluated. The mass matrix of both in air, M_{mta}, and in water, M_{mtw}, were determined as follows, using the above measurements.

$$M_{mta} = \frac{k_{mta}}{(2\pi\, f_{na})^2} \tag{4-7}$$

$$M_{mtw} = \frac{k_{mtw}}{(2\pi\ f_{nw})^2} \tag{4-8}$$

The damping matrix both in air, C_{mta}, and in water, C_{mtw}, were also determined from the above values by using Eq.(3-22).

$$C_{mta} = 2\zeta ta\ \sqrt{M_{mta} \cdot k_{mta}} \tag{4-9}$$

$$C_{mtw} = 2\zeta tw\ \sqrt{M_{mtw} \cdot k_{mtw}} \tag{4-10}$$

4-6-3 Calibration of the electro-magnetic damper

In order to obtain the relationship between the A.C. currents used in the electro-magnetic damper and the damping factors, ζ_m, produced by those currents, (defined Eq.(3-22-A)), the total damping factor of the test cylinder was measured for the following two cases: in one case the cylinder was mounted in air, and in the other case the cylinder was mounted in still water (water depth d = 80cm). A.C. currents were changed as follows.

$$I_c = 0,\ 0.5,\ 1.0,\ 1.5,\ 2.0,\ 2.5,\ 3,\ 4,\ 5,\ 6,\ 7A$$

These measurements were done whilst allowing the test cylinder to move in the transverse direction only.

4-6-4 Measurement of the change of the damping coefficient with water depth

In order to inspect the change in the fluid damping factor, ζ_f, of the test cylinder with water depth, the total damping factor of the test cylinder was measured for the following water depth, d,

$$d = 0, 10, 20, 30, 40, 50, 60, 70, 80, 90\text{cm}.$$

The initial displacement of the test cylinder at the still water surface was more than one diameter of the test cylinder. The digitising frequency of the signal of gauges corresponding to the vibration of the test cylinder was 100Hz. These measurements were also done whilst allowing the test cylinder to move in the transverse direction.

4-6-5 The vortex-excited vibration of the test cylinder in waves

The experimental conditions used in the experiments on the vortex-excited vibration of the test cylinder are shown in Table 1.

The water depth, d, was kept constant at 80cm and regular waves were used throughout the experiments. The effective mass, m_e, which is used in the calculation of the mass ratio, $m_e/\rho D^2$, and normalised damping, $\delta_r = 2m_e(2\zeta_{ta})/\rho D^2$, is calculated as follows.

$$m_e = \frac{M_{mtw}}{\int_0^d (\frac{z}{\ell}).z.dz} = \frac{3M_{tw}}{d^2} \quad (\because d \simeq \ell) \qquad (4\text{-}11)$$

Where M_{mtw} is the mass matrix in water which was obtained in the measurement (4-6-2) above. It should be noted that ζ_{ta} is the damping factor of the test cylinder in air and it includes only ζ_s and ζ_m.

The natural frequency both in air, f_{na}, and in water, f_{nw}, and the damping factor both in air, ζ_{ta}, and in water, ζ_{tw}, are the values which were obtained in the measurement (4-6-2) above.

The depth parameter, kd, was calculated by using linear wave theory.

Case A, Case AB and Case AC were run to study the vortex-excited vibration of the test cylinder, which was left free to vibrate only in the transverse direction. The relationship between the vortex-excited vibration of the test cylinder and the frequency ratio, f_w/f_{nw}, was measured in the Case A1 and Case A2. The surface KC number, SKC, was fixed at about 12 in Case A1, and it was fixed at about 20 in Case A2. In order to study the multi-appearance of the resonant frequency ratio, (f_w/f_{nw} = 1, 1/2, 1/3 ---) which was pointed out by Sawaragi, Nakamura and Miki (1977) and Isaacson and Maull (1981) as described in Chapter 2, the frequency ratio, f_w/f_{nw}, was changed widely from 0.237 to 1.07 in the Case A1, and it was changed from 0.166 to 0.577 in the Case A2, by changing the wave frequency.

The relationship between the vortex-excited vibration of the test cylinder and the surface KC value, SKC, was measured in Case A3-A11. In each of these cases, the frequency ratio, f_w/f_{nw}, was fixed at around one of the values of the resonance frequency ratios (f_w/f_{na} = 1, 1/2, 1/3 ---).

In order to study the influence of the damping factor on the vortex-excited vibration of the test cylinder, the same kind of measurements as for Case A were done for Case AB, but the damping factor in air, ζ_{ta}, was changed from 0.001 to 0.021 by using the electro-magnetic damper.

The influence of the damping factor on the vortex-excited vibration of the test cylinder, in the particular wave conditions, in which perfect resonance nearly occurred, was measured in Case AC. In this case, the damping factor in air, ζ_{ta}, was changed from 0.001 to 0.0267 by using the electro-magnetic damper.

Case AS was run to study the lift force acting on the test cylinder, which was mounted stiffly as described in (4-3-2). In order to estimate the amplification of the lift force acting on the test cylinder, which was vibrating in the vortex-excited condition, the same waves as those used in Case A were used here.

Case B was run to study the vortex-excited vibration of the test cylinder, which was left free to vibrate in any direction. In order to study the difference between this case and the vortex-excited vibration of the test cylinder, when free to vibrate only in the transverse direction to the wave fronts, the waves were the same as those used in Case A. However, it may be difficult to carry out a strict comparison between the two cases, because the natural frequency, f_{nw}, the damping factor, ζ_{ta} and ζ_{tw}, and mass ratio, $m_e/\rho D^2$, are different for Case A and Case B.

The voltage signal corresponding to the vibration of the test cylinder and the lift force acting to the stable test cylinder was recorded simultaneously with the signals from the wave gauge to study the time lag between the two signals. The digitising frequency of these signals was 50Hz and 100/3Hz in the rest, depending on the period of the incident waves and the period of the vortex-excited vibration of the test cylinder.

In order to study the irregularity of the vortex-excited vibration of the test cylinder (and the lift force acting on the stable test cylinder), the signals were stored on disk on the computer for 30-100 wave periods and were recorded on the U-V recorder over 100-200 wave periods.

A 20Hz low pass filter was used for the measurement of the vortex-excited vibration of the test cylinder, and a 5Hz low pass filter was used for the measurements of the lift force acting to the stable cylinder.

Table 1 Experimental Condition

Case	Mass Ratio	f_{na}	f_{nw}	SKC	f_n/f_{nw}	kd	ζ_{ta}	ζ_{tw}	Reduced Damping (δ_r)
	$m_e/\rho D^2$								$2m_e(2\pi\ \zeta_{ta})/\rho D^2$
A-1	15.7	1.52	1.46	12 $^{+1.07}_{-2.1}$	0.237 ~ 1.07	0.67 ~ 7.98	0.001	0.004	0.20
A-2	15.7	1.52	1.46	20 $^{+4.7}_{-3}$	0.766 ~ 0.577	0.85 ~ 2.33	0.001	0.004	0.20
A-3	15.7	1.52	1.46	6.9 ~ 50.5	0.251	0.71	0.001	0.004	0.20
A-4	15.7	1.52	1.46	18.8 ~ 55.0	0.260	0.73	0.001	0.004	0.20
A-5	15.7	1.52	1.46	9.0 ~ 40.0	0.335	1.01	0.001	0.004	0.20
A-6	15.7	1.52	1.46	11.7 ~ 40.7	0.350	1.07	0.001	0.004	0.20
A-7	15.7	1.52	1.46	4.8 ~ 39.0	0.495	1.98	0.001	0.004	0.20
A-8	15.7	1.52	1.46	3.5 ~ 40.0	0.500	1.81	0.001	0.004	0.20
A-9	15.7	1.52	1.46	4.4 ~ 32.0	0.503	1.83	0.001	0.004	0.20
A-10	15.7	1.52	1.46	5.4 ~ 36.4	0.508	1.88	0.001	0.004	0.20
A-11	15.7	1.52	1.46	4.1 ~ 38.6	0.525	1.97	0.001	0.004	0.20

Continued ...

Table 1 (Continued)

Case	Mass Ratio $m_e/\rho D^2$	f_{na}	f_{nw}	SKC	f_n/f_{nw}	kd	ζ_{ta}	ζ_{tw}	Reduced Damping (δ_r) $2m_e(2\pi\,\zeta_{ta})/\rho D^2$
AB-1	15.7	1.52	1.46	$12\ {}^{+2.1}_{-5.6}$	0.315 ~ 1.05	0.93 ~ 7.64	0.021	0.023	4.14
AB-2	15.7	1.52	1.46	$20\ {}^{+2.8}_{-1}$	0.308 ~ 0.54	0.91 ~ 2.08	0.021	0.023	4.14
AB-3	15.7	1.52	1.46	7.2 ~ 32.5	0.333	1.0	0.021	0.023	4.14
AB-4	15.7	1.52	1.46	8.9 ~ 32.3	0.335	1.01	0.021	0.023	4.14
AB-5	15.7	1.52	1.46	5.6 ~ 32.8	0.503	1.83	0.021	0.023	4.14
AC-1	15.7	1.52	1.46	6.2	0.506	1.85	0.001 ~ 0.0267	0.004 ~ 0.0284	0.20 ~ 5.27
AC-2	15.7	1.52	1.46	8.7	0.508	1.88	0.001 ~ 0.0267	0.004 ~ 0.0284	0.20 ~ 5.27
AC-3	15.7	1.52	1.46	12	0.503	1.83	0.001 ~ 0.0267	0.004 ~ 0.0284	0.20 ~ 5.27
AC-4	15.7	1.52	1.46	20	0.503	1.83	0.001 ~ 0.0267	0.004 ~ 0.0284	0.20 ~ 5.27
AC-5	15.7	1.52	1.46	20	0.336	1.01	0.001 ~ 0.0267	0.004 ~ 0.0284	0.20 ~ 5.27

Continued ...

Table 1 (Continued)

Case	Mass Ratio $m_e/\rho D^2$	f_{na}	f_{nw}	SKC	f_n/f_{nw}	kd	ζ_{ta}	ζ_{tw}	Reduced Damping (δ_r) $2m_e(2\pi\ \zeta_{ta})/\rho D^2$
AS-1	15.7	12.5	12.0	$12^{+3.2}_{-1.3}$	0.025 ~ 0.066	0.57 ~ 2.09			
AS-2	15.7	12.5	12.0	$20^{+3.5}_{-0.7}$	0.039 ~ 0.065	0.95 ~ 2.05			
AS-3	15.7	12.5	12.0	18.5 ~ 34.9	0.031	$0.735^{+0.25}_{-0.25}$			
AS-4	15.7	12.5	12.0	6.9 ~ 37	0.041	1.01			
AS-5	15.7	12.5	12.0	9.3 ~ 34.3	0.06	1.79			
B-1	19.6	1.22	1.203	$12^{+4}_{-0.3}$	0.193 ~ 1.035	0.43 ~ 5.0	0.008 ($Y_{hi}/D=0.4$)	0.0125 ($Y_{hi}/D=0.4$)	1.97
B-2	19.6	1.22	1.203	$20^{+3.8}_{-5}$	0.174 ~ 1.065	0.38 ~ 5.3	0.008 ($Y_{hi}/D=0.4$)	0.0125 ($Y_{hi}/D=0.4$)	1.97
B-3	19.6	1.22	1.203	9.3 ~ 34	0.250	0.57	0.008 ($Y_{hi}/D=0.4$)	0.0125 ($Y_{hi}/D=0.4$)	1.97
B-4	19.6	1.22	1.203	15.2 ~ 47	0.336	0.80	0.008 ($Y_{hi}/D=0.4$)	0.0125 ($Y_{hi}/D=0.4$)	1.97
B-5	19.6	1.22	1.203	3.9 ~ 28.6	0.506	1.36	0.008 ($Y_{hi}/D=0.4$)	0.0125 ($Y_{hi}/D=0.4$)	1.97

CHAPTER 5

RESULTS AND DISCUSSION

5-1 Introduction

This chapter aims to describe and discuss the experimental results of the present study. It will be divided into the following three sections.

In the first section, the characteristics of the damping of the test cylinder in air and in still water will be described. The values of the damping at small amplitude in still water will be explained theoretically by using the equation which was introduced to explain the viscous effect of cylinders at low Keulegan-Carpenter number by Stokes (1901) and Wang (1968). The results obtained in this section will be used to estimate the unknown damping force of the vortex-excited cylinder in waves.

In the second section, the characteristics of the lift force acting on the stiffly mounted test cylinder will be described. These results will be used as reference values of the lift force to be used in the estimation of the amplification of the lift force acting on the vortex-excited test cylinder.

In the third section, the following main characteristics of the vortex-excited vibration of the test cylinder in waves will be described:

(1) The relationship between the vortex-excited vibrations of the test cylinder and the important parameters, which were identified in the linearised model for the vortex-excited vibration of the cylinder in waves described in Chapter 3.

(2) The characteristics of the lift force acting on the vortex-excited test cylinder in waves. The lift force will be evaluated by substituting the values both of the amplitude of the vibration of the cylinder and the unknown damping factor of the cylinder in the vortex-excited condition into the Eq.(3-29). In this case, the unknown value of damping factor will be estimated from the measured value of the damping factors in air and in still water described above.

5-2 The Damping of the Test Cylinder in Air and in Still Water

5-2-1 Calibration of electro-magnetic damper

The relationship between the damping factor, ζ_{tai}, and the non-dimensional test cylinder displacement, Y_{hi}/D, as a function of the AC current, I_e, is shown in Fig. 5.2.1. The value of $Y_{hi}(i=1,2,3...)$ is the amplitude at the i-th oscillation of the test cylinder at the still water level (80cm above the bed). ζ_{tai} is a total damping coefficient of the test cylinder in air calculated for each amplitude of the test cylinder Y_{hi}/D by Eq.(5-2-1).

$$\zeta_{tai} = \frac{1}{2\pi.5}\,\ell n\,\frac{Y_{hi-2}}{Y_{hi+3}} \qquad (5\text{-}2\text{-}1)$$

where Y_{hi-2} = the amplitude of the test cylinder at the (i-2)-th period

Y_{hi+3} = the amplitude of the test cylinder at the (i+3)-th period

Here the value of ζ_{tai} at I_e = 0 shows the structural material damping factor of the test cylinder. It increases slightly with increased amplitude. This may be due to the non-linear characteristics of the structural (material) damping of the test cylinder. (The damping due to air can be expected to make a negligible contribution in this case).

The relationship between ζ_{tai} and I_e for Y_{hi}/D=0.2, 0.6 and 1.0 is shown in Fig. 5.2.2. As shown by Eq.(4-2) and Eq.(4-4), the damping force produced by the electro-magnetic damper is proportional to the square of I_e. This relationship cannot be found in Fig. 5.2.2 because of the saturation of magnetization in soft ironore, Drysdale et al. (1952).

The relationship between the total damping factor of the test cylinder in still water, ζ_{twi}, and Y_{hi}/D as a function of I_e is shown in Fig. 5.2.3. ζ_{twi} is calculated by Eq.(5-2-1) as before. This figure shows that ζ_{twi} is independent of the amplitude effect only for low values of Y_{hi}/D and it becomes amplitude dependent at higher values of Y_{hi}/D. The result of ζ_{tai} at I_e = 0A plotted in Fig. 5.2.1 is also shown in this figure. Subtracting ζ_{tai} at I_e = 0A from ζ_{twi} at I_e = 0A leaves the fluid damping factor ζ_{fi}.

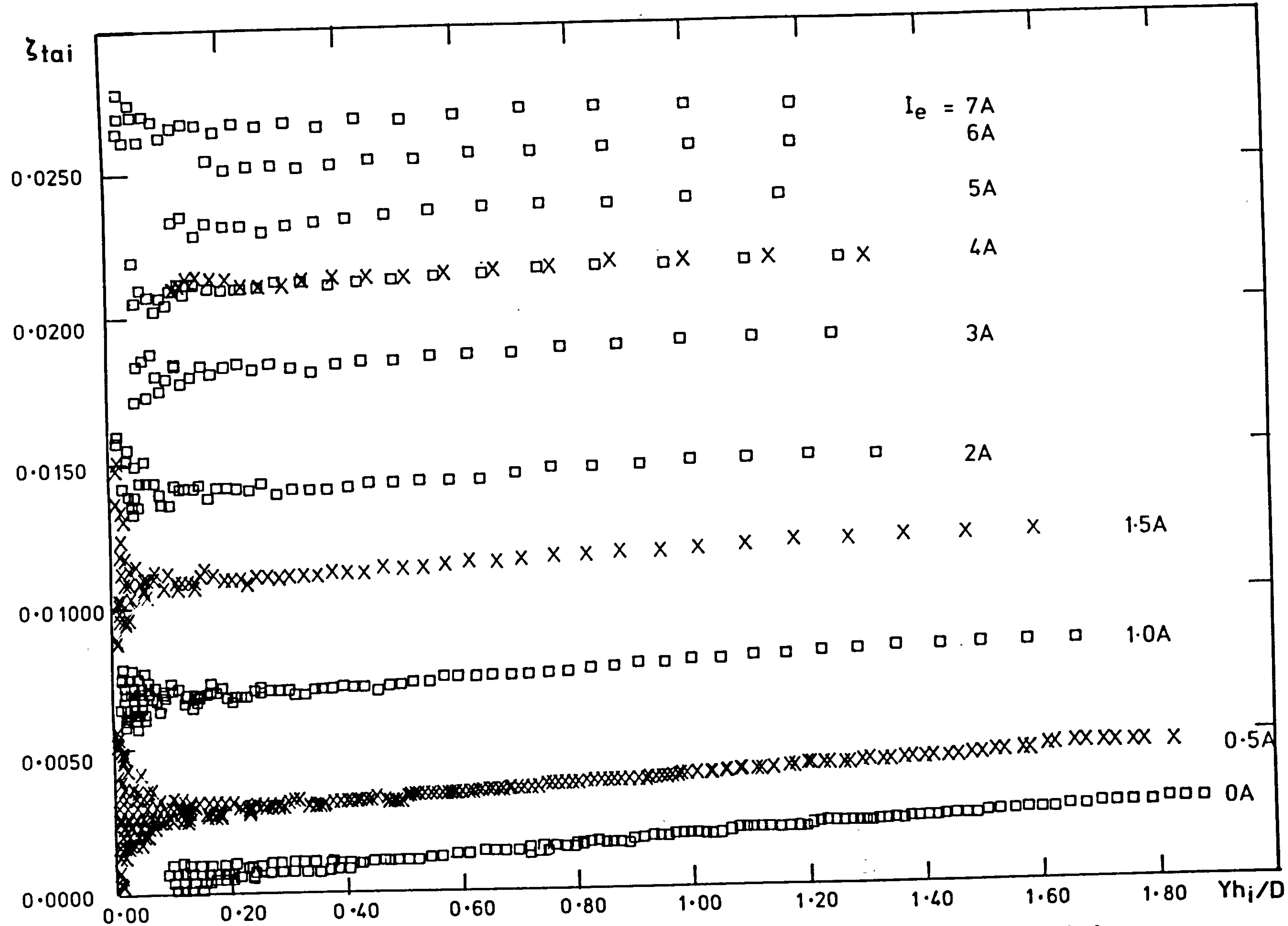

Fig. 5.2.1 The Damping Coefficient(ζ_{tai}) vs. Dimensionless Test Cylinder Displacement(Y_{hi}/D) as a Function of the Current(Ie)

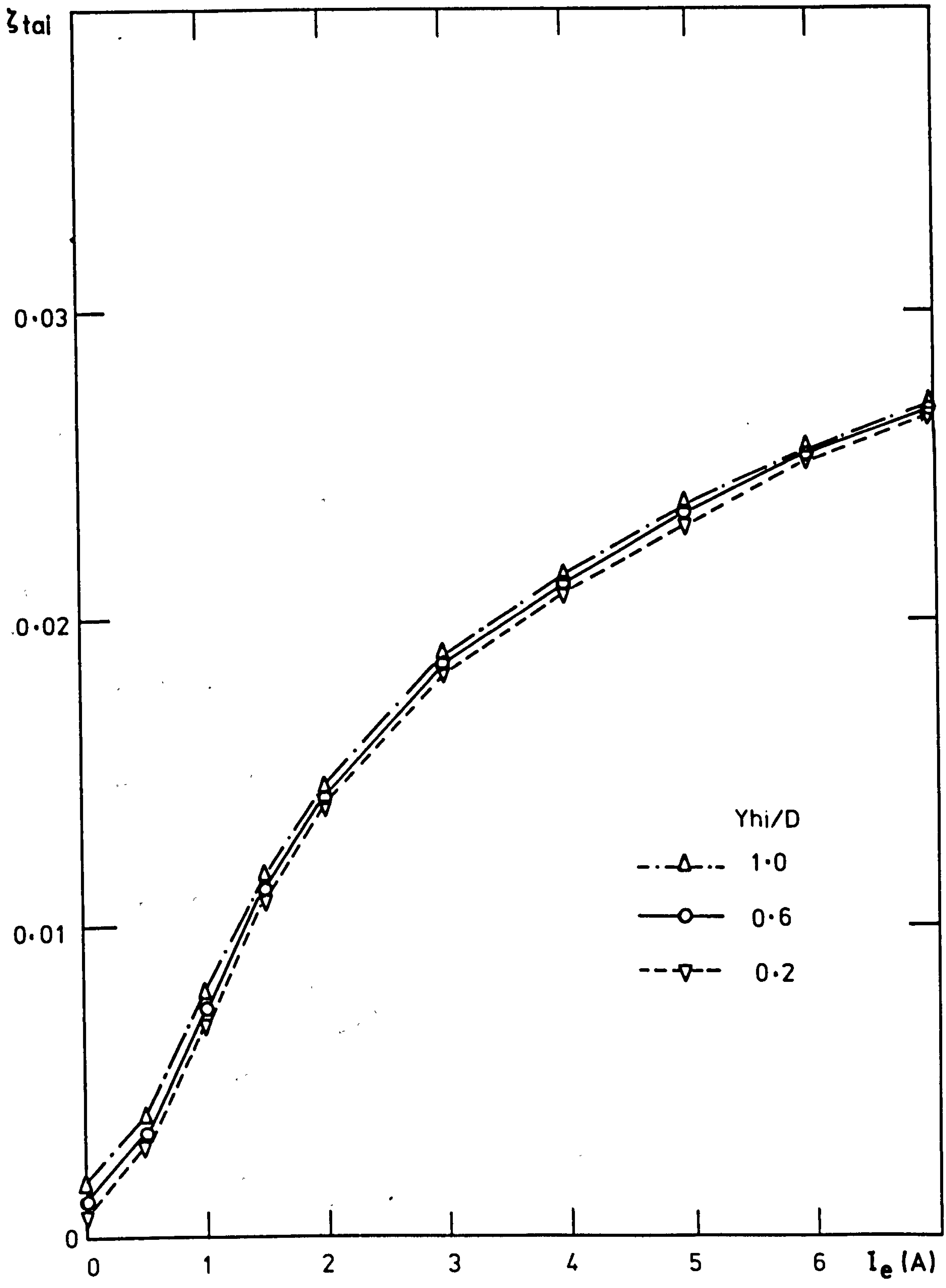

Fig. 5.2.2 The Relationship between the Damping Factor(ζ_{tai}) and the Current(Ie) for Y_{hi}/D=0.2, 0.6 and 1.0

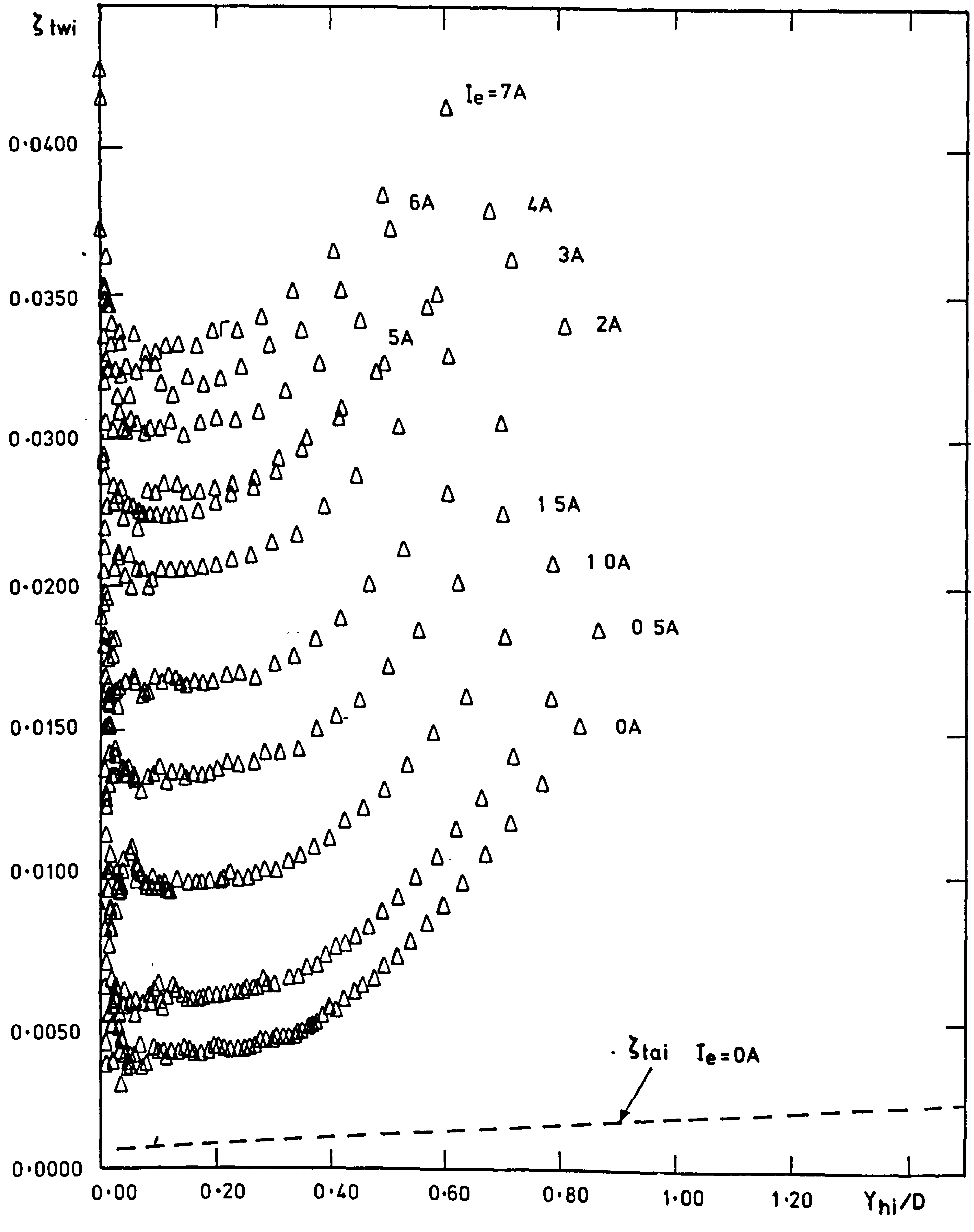

Fig. 5.2.3 The Relationship between the Damping Factor(ζ_{twi}) and Y_{hi}/D as a function of the Current(Ic)

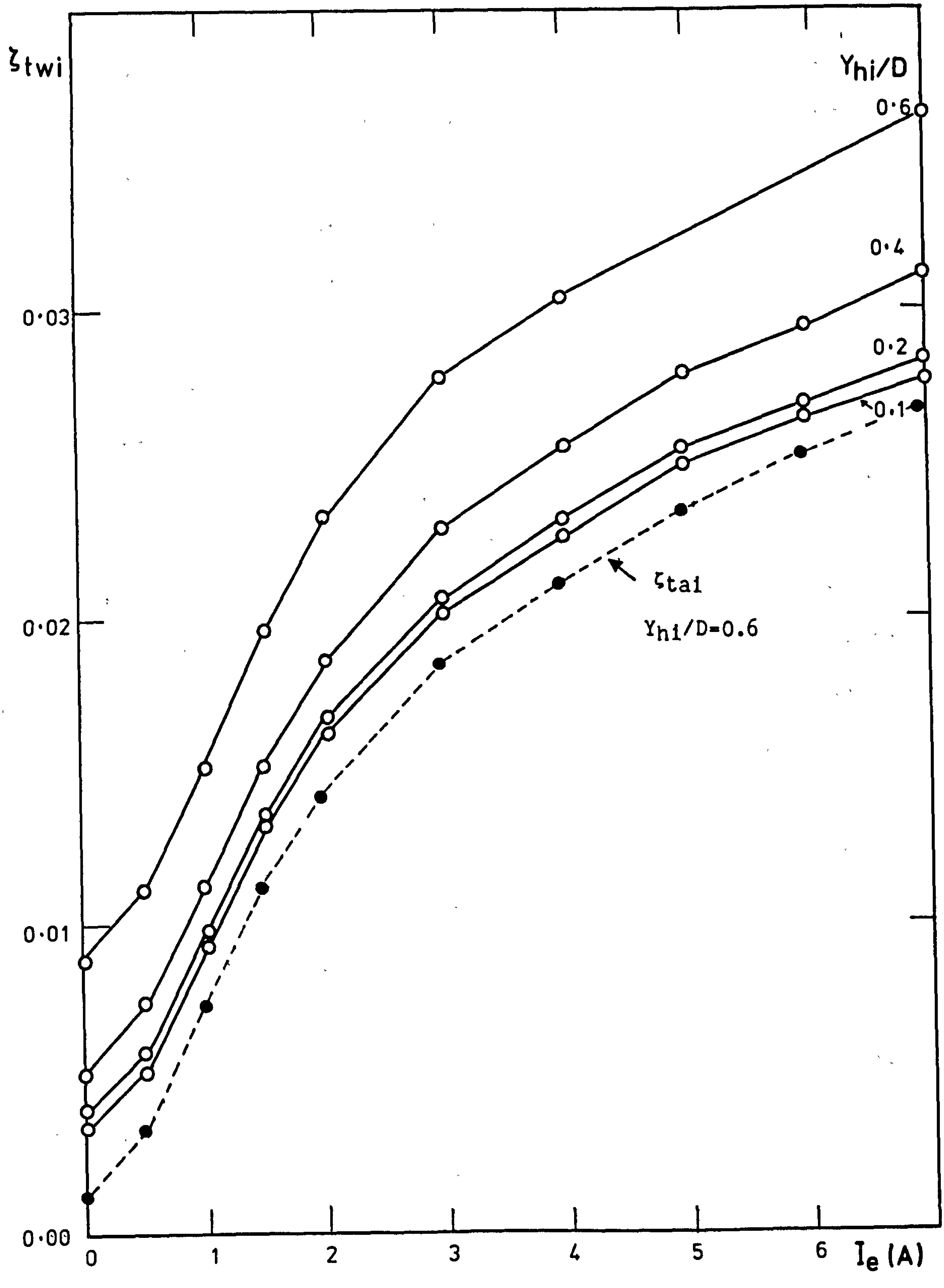

Fig. 5.2.4 The Relationship between the Damping Factor(ζ_{twi}) and the Current(Ie) for Y_{hi}/D=0.1, 0.2,0.4 and 0.6

The relationship between ζ_{twi} and I_e for $Y_{hi}/D=0.1$, 0.2, 0.4 and 0.6 is shown in Fig. 5.2.4. The value of ζ_{tai} at $Y_{hi}/D=0.6$ is also shown in this figure.

In the case of ζ_{tai}, the influence of Y_{hi}/D is very small as shown in Fig. 5.2.2. On the other hand, in the case of ζ_{twi}, the damping depends on the value of Y_{hi}/D owing to the characteristics of the fluid damping. However, the increase in damping due to fluid damping at each value of Y_{hi}/D is nearly independent of I_e.

5.2.2 The change of damping with water depth

The relationship between the total damping factor, ζ_{twi}, in water and Y_{hi}/D for different water depths, d, is shown in Fig. 5.2.5. The purpose of this experiment is to inspect the influence of the end flange (see Fig. 4.4) on the total damping of the test cylinder in water and to obtain the value of ζ_{twi} at small SKC for comparison with theoretical results. This figure shows that as the water depth increases, ζ_{twi} increases and becomes amplitude dependent with the increase of Y_{hi}/D. As shown in this figure, the difference between ζ_{twi} at d=0 and ζ_{twi} at d=20cm is very small. Therefore it can be concluded that the effect of the end flange on the total damping of the test cylinder at large water depths is negligible. The increase of ζ_{twi} at each water depth from its value at water depth d=0 equivalent to ζ_{tai}, depends on the appearance of the fluid damping. Therefore, the fluid damping factor at each water depth can be estimated by subtracting the value of ζ_{twi} at d=0 from the value of ζ_{twi} at each water depth.

The relationship between the fluid damping, ζ_{fi}, and Y_{hi}/D as a function of water depth, d, is shown in Fig. 5.2.6. This figure shows that ζ_{fi} has a constant value in the range of low values of Y_{hi}/D and increases with Y_{hi}/D.

In order to understand the mechanism of fluid damping, it may be useful to express ζ_{fi}, in terms of a drag coefficient, C_D. If the drag coefficient is constant over one cycle of vibration, and is constant along the axis of the test cylinder, Eq.(3-40), showing the relationship between ζ_{fi} and C_D, can be written:

$$\zeta_{fi} = \frac{2\rho.D.Y_{hi}.C_D \int_0^d (\frac{z}{\ell})^2\ z.dz}{3\pi\ M_{mo}}$$

$$= \frac{\rho D^2.(\frac{Y_{hi}}{D}).C_D.d^4}{6\ \ell^2}$$

$$= \frac{\rho D^2.SKC.d^3}{12\pi^2.M_{mo}.\ell} C_D \tag{5-2-2}$$

rearranging Eq.(5-2-2)

$$C_D = \frac{6\pi.M_{mo}.\ell^2}{\rho.D^2.d^4.(\frac{Y_{hi}}{D})} \zeta_{fi}$$

$$= \frac{12\pi^2.M_{mo}.\ell}{\pi.D^2.SKC.d^3} \zeta_{fi} \tag{5-2-3}$$

where SKC is the surface Keulegan-Carpenter number at each water depth d and is shown as

$$SKC = \left(\frac{Y_{hi}}{D}\right) \frac{2\pi d}{\ell} \qquad (5\text{-}2\text{-}4)$$

and the mass matrix M_{mo} is shown as

$$M_{mo} = \Big[\int_0^{\ell_3} m.\left(\frac{z}{\ell}\right).z.dz + \int_0^{r} m_q.\left(\frac{z}{\ell}\right).z.dz + \int_r^{\ell_7} m_c.\left(\frac{z}{\ell}\right).z.dz$$

$$+ \int_{\ell_2}^{\ell_1} m_f.\left(\frac{z}{\ell}\right).z.dz + \int_{\ell_4}^{\ell_3} m_n.\left(\frac{z}{\ell}\right).z.dz + \int_{\ell_5}^{\ell_6} m_s.\left(\frac{z}{\ell}\right).z.dz$$

$$+ \int_0^{d} m_I.\left(\frac{z}{\ell}\right).z.dz + \int_0^{d+\eta} m_a.\left(\frac{z}{\ell}\right).z.dz \Big] \qquad (5\text{-}2\text{-}5)$$

By substituting the fluid damping factor, ζ_{fi}, Y_{hi}/D and the mass matrix M_{mo} into Eq.(5-2-3) and Eq.(5-2-4), the relationship between the drag coefficient C_D and SKC as a function of water depth, d, is obtained. The plot of this value of C_D against SKC is shown in Fig. 5.2.7.

The theoretical variation of C_D with KC is also shown in Fig. 5.2.7. This is calculated by Eq.(5-2-6), which is derived from Wang's (1968) theory for the forces on a fixed cylinder in oscillating flow (Bearman et al., 1984). The first term is identical to that given by Stokes (1901) for the case of spherical and cylindrical pendulum bobs oscillating at low Keulegan-Carpenter number.

$$C_D = \frac{3.\pi^{5/2}}{2.KC.\sqrt{\beta}} + (\frac{3.\pi^2}{2.KC.\beta}) - (\frac{3.\pi^{3/2}}{8.\beta}) \quad (5\text{-}2\text{-}6)$$

where β is defined as

$$\beta = \frac{R_e}{KC} = \frac{D^2.f_{nw}}{\nu} \quad (5\text{-}2\text{-}7)$$

and ν ($= \frac{u}{\rho}$) is the kinematic viscosity.

Measurements by Sarpkaya (1976) and by Bearman et al. (1981) are also plotted in Fig. 5.2.7. Their results were obtained by measuring the in-line force acting on a stiffly mounted circular cylinder in harmonic flow.

This figure shows the following:

(1) The relationship between C_D and SKC is independent of water depth.

(2) The value of C_D decreases with increasing SKC, in the range of SKC < 2, and is approximated with the theoretical curve of Eq.(5-2-6).

(3) Beyond SKC $\cong$ 2, the value of C_D increases with increasing SKC.

The present data of C_D is larger than the theoretical value. This may be due to the fact that the variation of C_D along the axis of the test cylinder is not considered in the estimation of the present data of C_D as shown in Eq.(5-2-3) also that the flow is not truly two-dimensional. The increase of C_D of the present data beyond SKC $\approx$ 2 may be due to the appearance of boundary layer separation and vortex-shedding. The start of the boundary layer separation from a circular cylinder in harmonic flow or in waves, at about SKC = 2-3, has been observed by Bidde (1971), Isaacson et al. (1976), Sawaragi et al. (1979), and Sawamoto et al. (1980).

Fig. 5.2.7 shows that when the test cylinder is vibrating with small amplitude in still water, the fluid damping is produced by a viscous shearing force between the surface of the cylinder and the water, expressed by Eq.(5-2-6). Therefore, when the test cylinder is vibrating with small amplitude, the fluid damping factor, ζ_{fi}, can be estimated by assuming

(1) C_D is constant over one cycle of vibration.

(2) C_D is constant along the axis of the cylinder.

(3) C_D is a function of surface Keulegan-Carpenter number, SKC, and is expressed in Eq.(5-2-6).

The fluid damping factor, ζ_{fi}, can be written as follows by substituting Eq.(5-2-6) into Eq.(3-40).

$$\zeta_{fi} = \frac{\rho.D^2.SKC.d^3}{12\pi^2.M_{mo}.\ell} \quad \frac{3.\pi^{5/2}}{2.SKC.\sqrt{\beta}}$$

$$= \frac{\rho.D^2.\pi^{1/2}.d^3}{8.M_{mo}\ell.\sqrt{\beta}} \qquad (5\text{-}2\text{-}8)$$

where

$$\beta = \frac{D^2 f_{nw}}{\nu} \tag{5-2-9}$$

In the case above, the variation of C_D along the axis of the cylinder is not considered. In order to take account of this effect, it can be assumed alternatively:

(1) C_D is constant over one cycle of vibration.

(2) C_D is not constant along the axis of the cylinder, but is a function of the Keulegan-Carpenter number, KC, at each point and is expressed as Eq.(5-2-6).

Then, the fluid damping factor, ζ_{fi}, can be written as follows by substituting Eq.(5-2-6) into Eq.(3-40).

$$\zeta_{fi} = \frac{2\rho D\, Y_{hi} \int_0^d \frac{3.\pi^{5/2}}{2.KC.\sqrt{\beta}} (\frac{z}{\ell})^2.z.dz}{3\pi\, M_{mo}}$$

$$= \frac{\rho.D^2\pi^{1/2}.d^3}{6.M_{mo}.\ell.\sqrt{\beta}} \tag{5-2-10}$$

where

$$\beta = \frac{D^2.f_{nw}}{\nu} \tag{5-2-11}$$

It should be noted that both fluid damping factor, ζ_{fi}, defined by Eq.(5-2-8) and Eq.(5-2-10) are independent of the amplitude of vibration of the cylinder. Theoretical values of ζ_{fi} estimated by

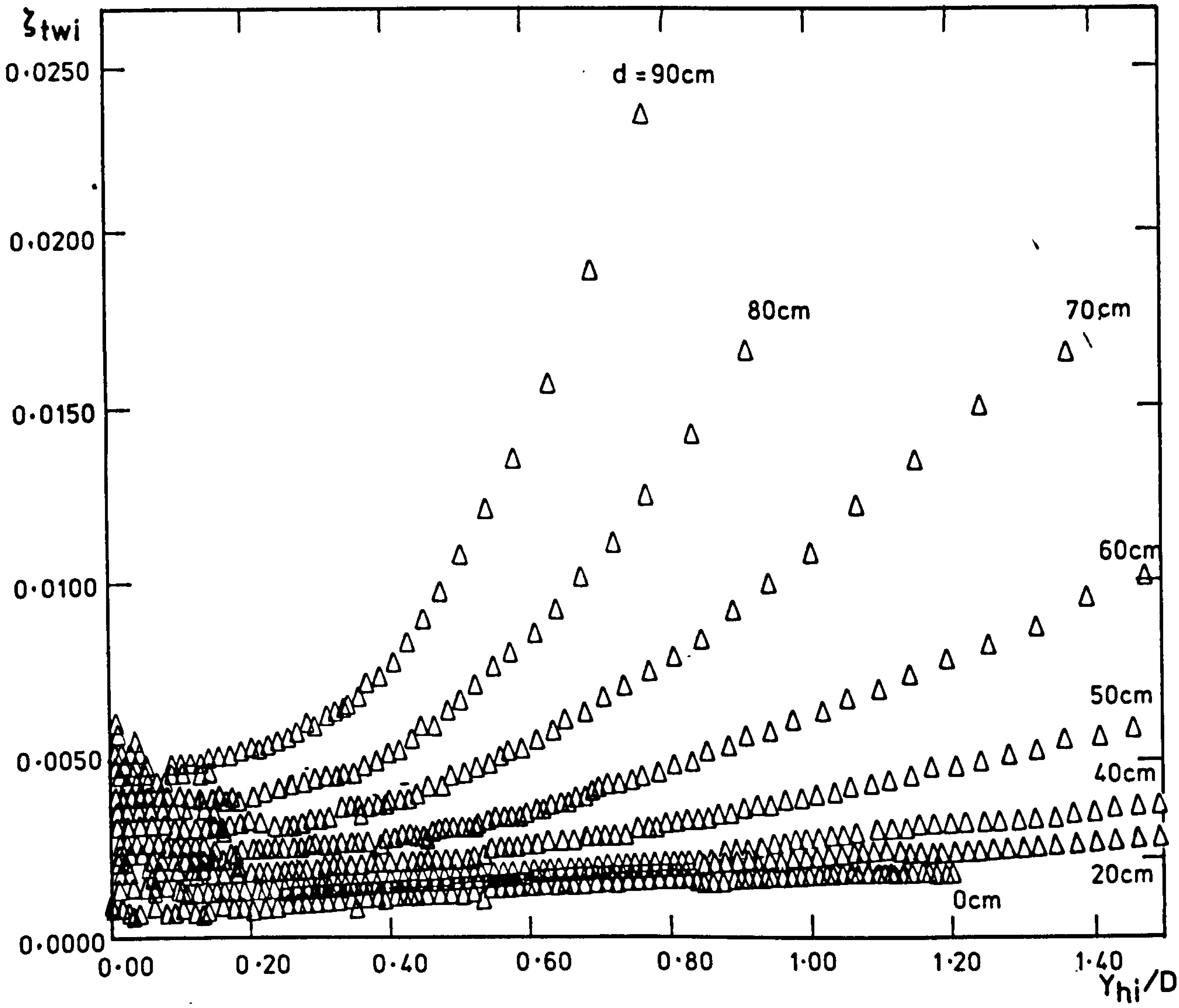

Fig. 5.2.5 The Relationship between the Damping Factor(ζ_{twi}) and Y_{hi}/D for different Water Depth(d)

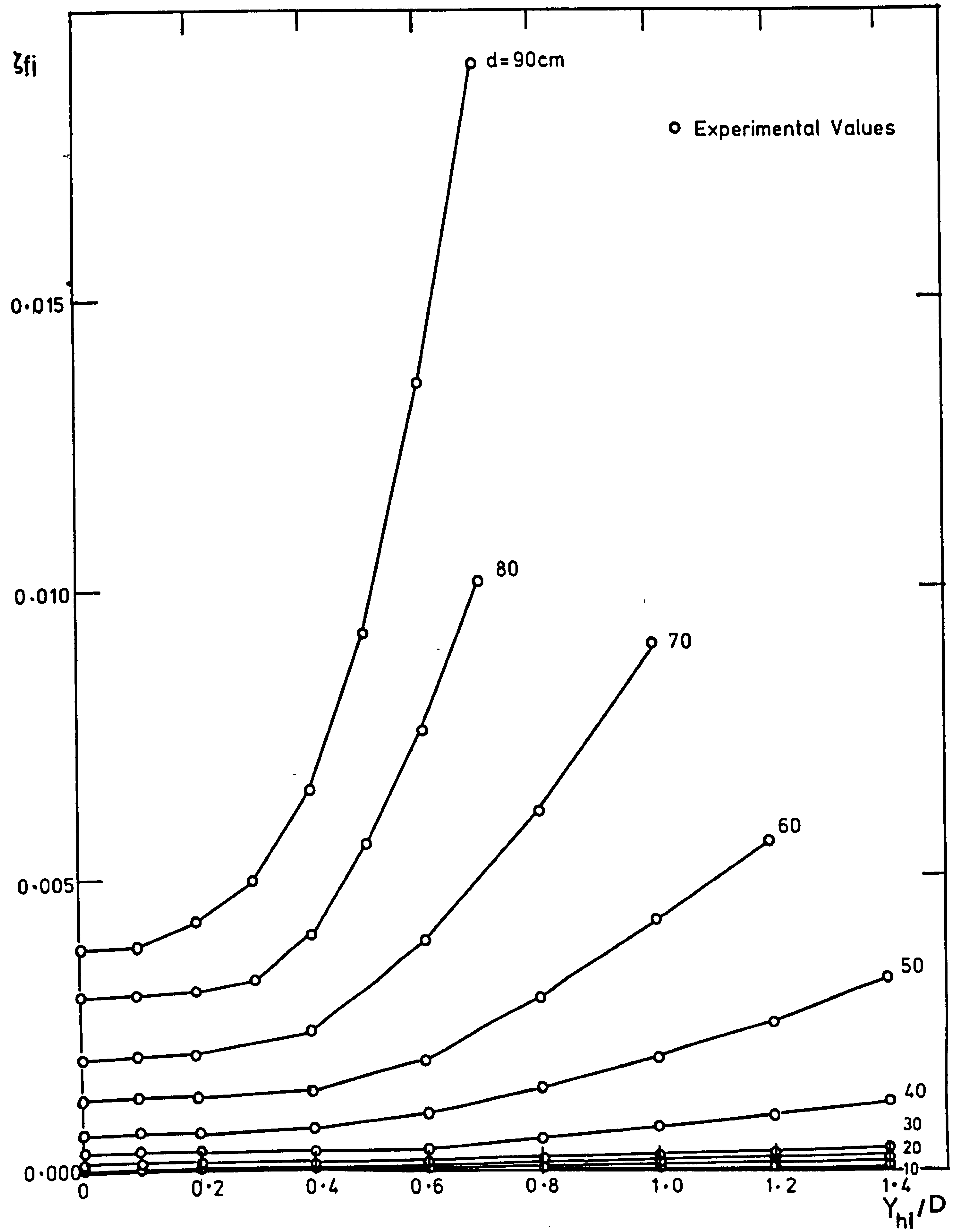

Fig.5.2.6 The Fluid Damping(ζ_{fi}) vs. Y_{hi}/D as a Function of Water Depth(d)

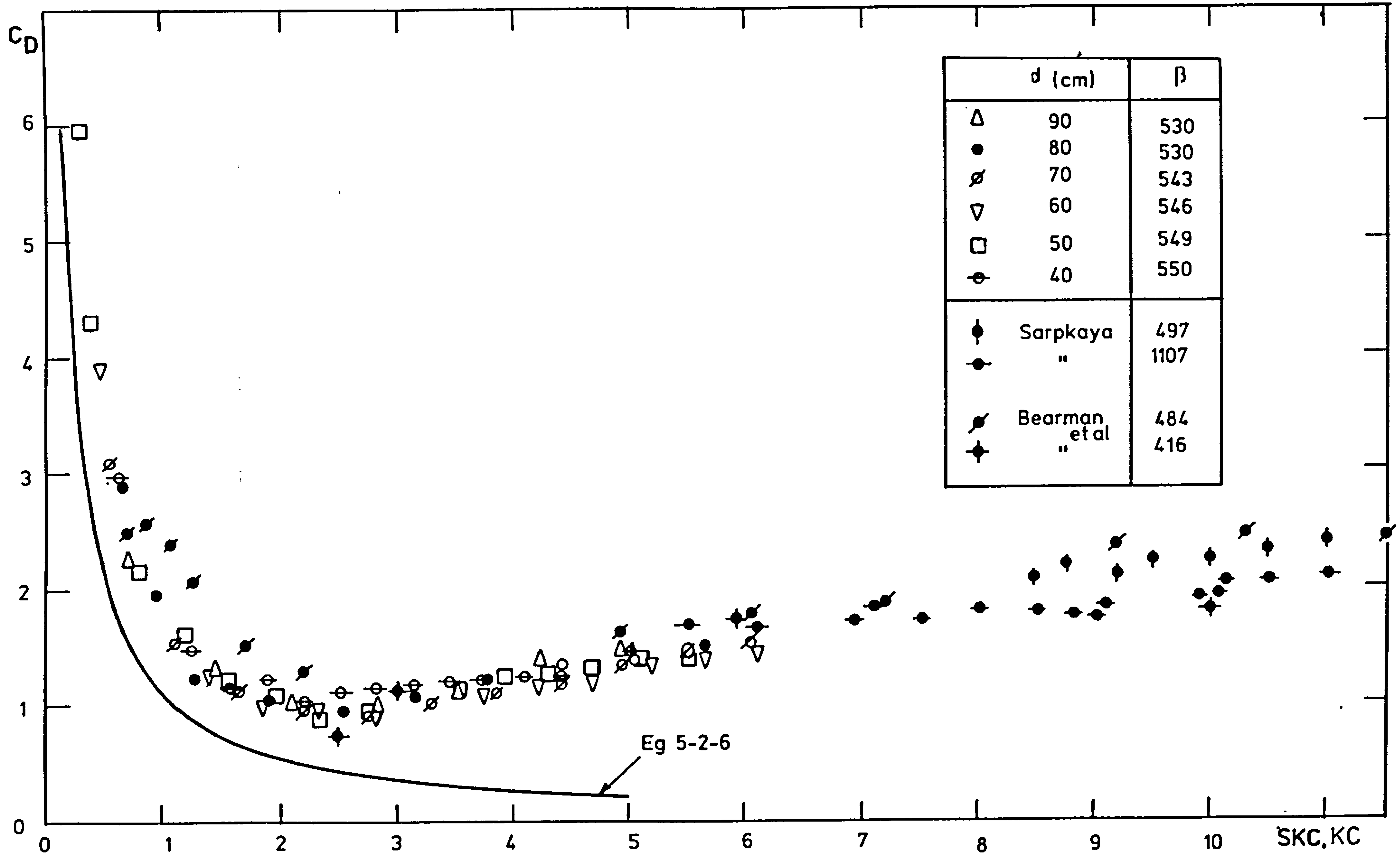

Fig. 5.2.7 The Drag Coefficient(C_D) vs. Surface Keulegan-Carpenter Number(SKC) and Keulegan-Carpenter Number(KC)

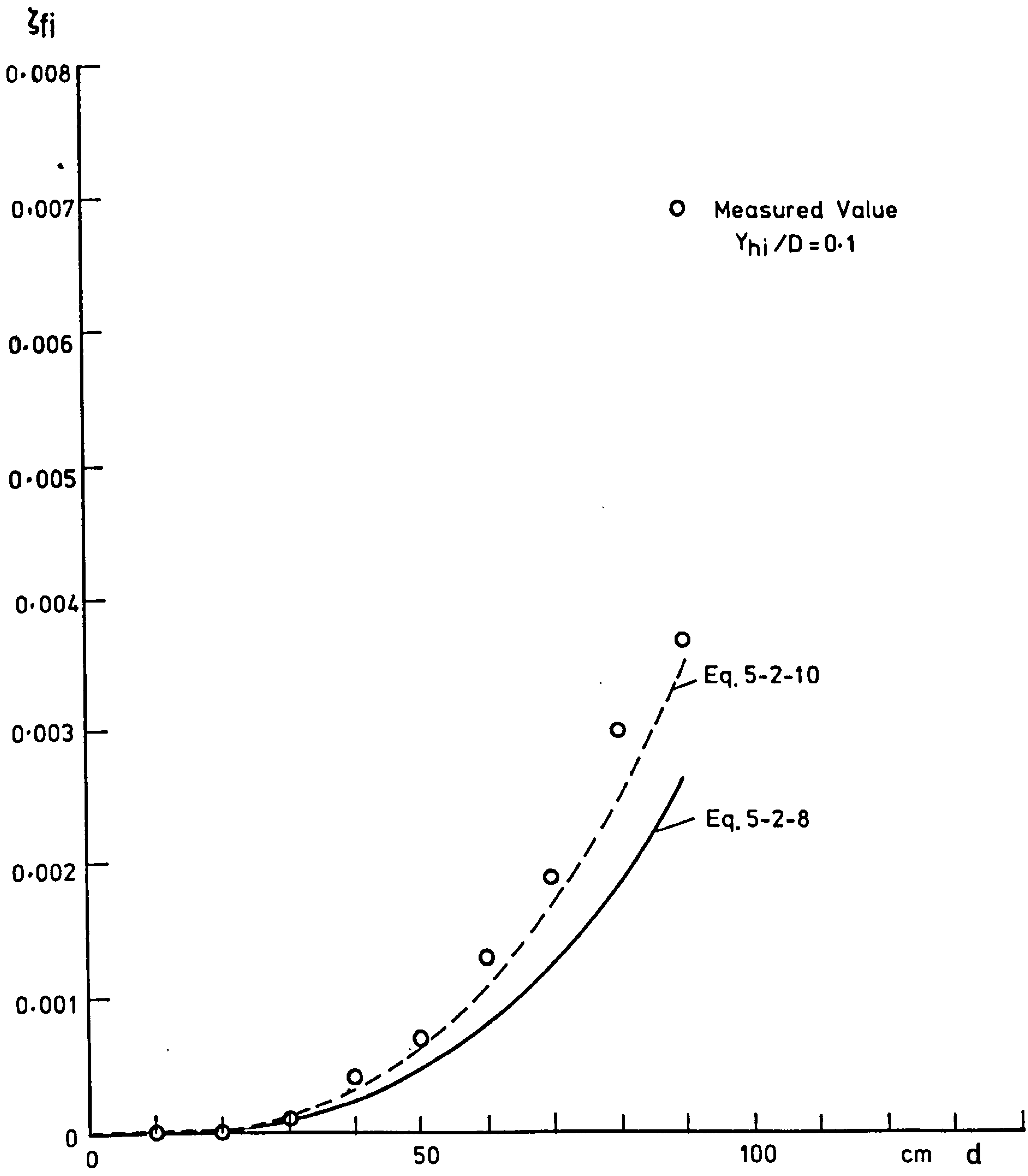

Fig. 5.2.8 The Fluid Damping(ζ_{fi} at $Y_{hi}/D=0.1$) vs. Water Depth(d) for Measured Value and Theoretical Value

Table 5.1 Result of Damping Factor

Water Depth	Natural Frequency		Mass Matrix	Stiffness Matrix	Measured Value	Theoretical Value	Theoretical Value
d (cm)	f_{nw} (Hz)	β $(D^2 f_{nw}/\nu)$	M_{mo} $(g\ s^2)$	k_{mo} g	ζ_{fi} $(Y_{hi}/D=0.1)$	ζ_{fi} (Eq. 5-2-8)	ζ_{fi} (Eq. 5-2-10)
0	1.522	552	112.3	10268	0	0	0
10	1.522	552	113.6		0	0.000004	0.000005
20	1.519	551	114.9		0	0.000030	0.000040
30	1.517	550	116.0		0.0001	0.000101	0.000135
40	1.515	550	117.3		0.0004	0.000239	0.000318
50	1.512	549	118.6		0.0007	0.000461	0.000615
60	1.505	546	119.9		0.0013	0.000791	0.001054
70	1.497	543	121.2		0.0019	0.001245	0.001661
80	1.461	530	122.4	10312	0.0030	0.001863	0.002484
90	1.460	530	123.7		0.0037	0.002624	0.003499

Eq.(5-2-8) and Eq.(5-2-10) at each water depth are shown with the measured value of ζ_{fi} at $Y_{hi}/D = 0.1$ in Table 5.1 and in Fig. 5.2.8. The measured value of ζ_{fi} corresponds well with the theoretical value defined by Eq.(5-2-10) rather than the theoretical value defined by Eq.(5-2-8). This shows that including the variation of C_D along the cylinder axis produces better agreements with observed values.

5-3 The Lift Force Acting on a Stiffly Mounted Test Cylinder in Waves

5-3-1 Method of data analysis

As described in Chapter 2, the time history of lift force acting on a cylinder stiffly mounted in waves, has irregular characteristics. Taking this point into consideration, the following three kinds of effective lift coefficient are defined in the analysis of the total bending moment, $F_{m\ell}$, over 30-100 wave periods.

(1) The maximum effective lift coefficient, C_{Lemax}

C_{Lemax} = (the maximum value of the half peak-to-peak amplitude

$$\text{of } F_{m\ell})/\int_0^{d+H/2} \frac{1}{2}\,\rho.D.U_m{}^2.z.dz \qquad (5\text{-}3\text{-}1)$$

(2) The mean effective lift coefficient, $\overline{C}_{Le}$

$\overline{C}_{Le}$ = (the mean value of the amplitude of the half peak-to-peak

$$\text{amplitude of } F_{m\ell}/\int_0^{d+H/2} \frac{1}{2}\,\rho.D.U_m{}^2.z.dz \qquad (5\text{-}3\text{-}2)$$

(3) The effective lift coefficient for the n-th harmonic, $C_{Le}(n)$

$$C_{Le}(n) = F_{m\ell}(n) / \int_0^{d+H/2} \frac{1}{2}\,\rho.D.U_m{}^2.z.dz \qquad (5\text{-}3\text{-}3)$$

where $F_{m\ell}(n)$ is the total bending moment for the n-th harmonic and is calculated as follows

$$F_{m\ell}(n) = [\{\frac{1}{N.T} \int_0^{N.T} F_{m\ell}(t).\cos(2\pi.n.f_W.t)\}^2$$

$$+ \{\frac{1}{N.T} \int_0^{N.T} F_{m\ell}(t).\sin(2\pi.n.f_W.t)\}^2]^{1/2} \qquad (5\text{-}3\text{-}4)$$

and f_W = cycle of wave frequency

N = number of waves

This effective lift coefficient for the n-th harmonic, $C_{Le}(n)$, can be used to determine the dominant frequency of $F_{m\ell}$.

In order to evaluate quantitatively the variation of the amplitude of $F_{m\ell}$ over many wave periods, the coefficient of variation, C_{VL}, of $F_{m\ell}$ is obtained as follows

C_{VL} = (the standard deviation of the half peak-to-peak amplitude of $F_{m\ell}$)/(the mean value of the amplitude of $F_{m\ell}$) (5-3-5)

5-3-2 The frequency components $C_{Le}(n)$

The relationship between the effective lift coefficient for the first four harmonics ($C_{Le}(n)$, n=1,2,3,4) and the surface Keulegan-Carpenter number, SKC, for three values of kd, (i.e. 0.735 for CASE AS-3, 1.03 for CASE AS-4, 1.79 for CASE AS-5, as shown in Table 1), are shown in Fig. 5.3.1 (a), (b) and (c) respectively. Also the second and third components obtained by Isaacson et al. (1976) for $0.755 < kd < 0.789$ are shown in Fig. 5.3.1(a) to compare with the present data.

The following relationships between the n-th harmonic component of lift coefficient and the KC number have been reported in studies on lift forces acting on a stiffly mounted cylinder in waves and in harmonic flows by Isaacson et al. (1976), Sawaragi et al. (1977), Charkrabarti et al. (1976), Sawamoto et al (1980) and Cotter et al. (1984):

(1) The first harmonic component of lift coefficient dominates for KC number less than about 7.

(2) The second harmonic component dominates for the range of KC number between 7 to 20.

(3) The third harmonic component dominates for the range of KC number between 16 to 25.

The following results can be seen in Fig. 5.3.1:

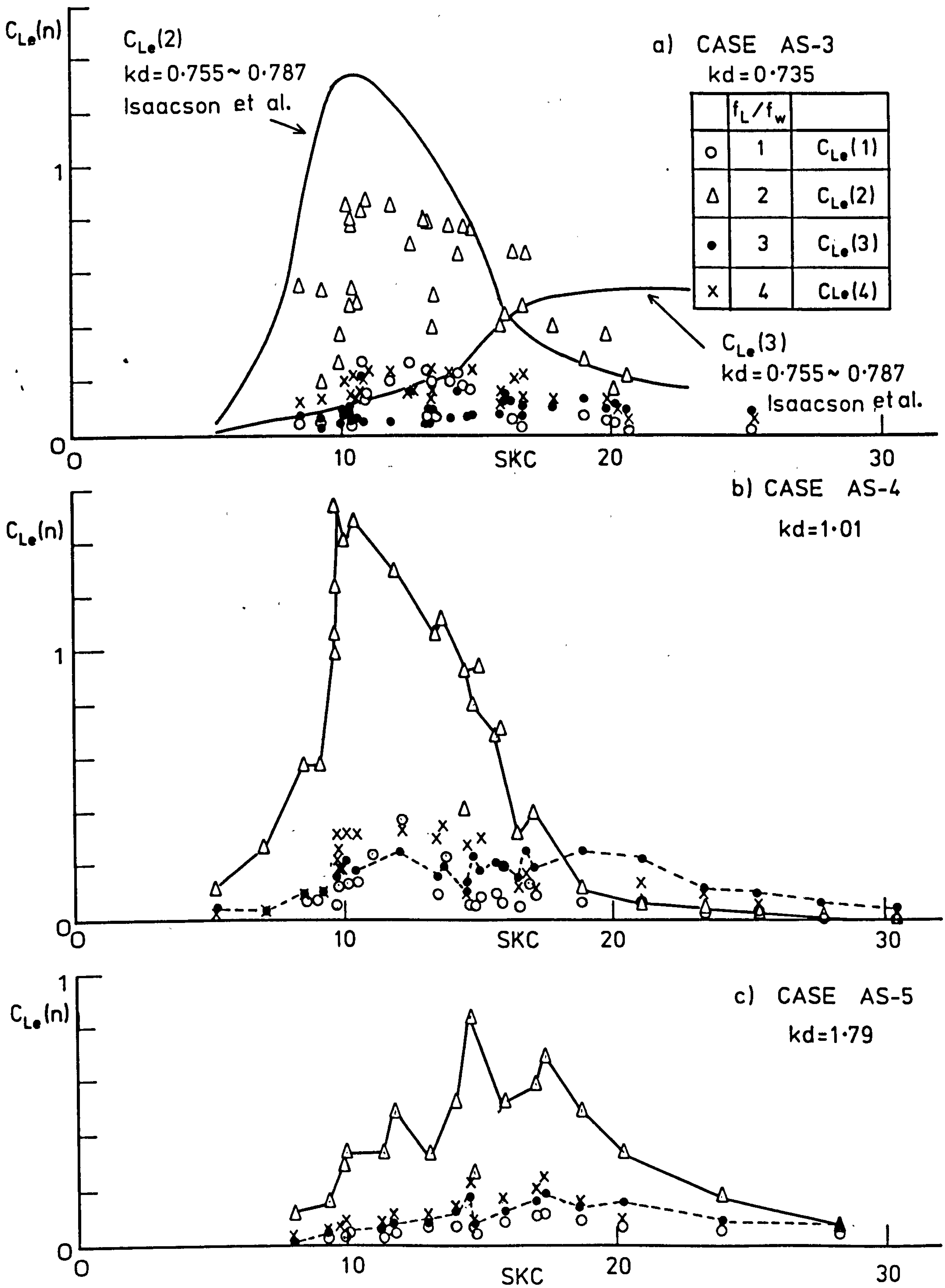

Fig. 5.3.1 The Lift Coefficients for First Four Harmonic($C_{Le}(n)$. n=1,2,3,4) vs. the Surface Keulegan-Carpenter Number(SKC) as a Function of the Wave Depth Parameter(kd)

(1) In the case of kd = 0.735, $C_{Le}(2)$ dominates for the range of SKC between 8 and 10, and it takes a maximum value at SKC between 10 to 15. However, even at higher SKC values it remains greater than $C_{Le}(3)$.

(2) In the case of kd = 1.01, $C_{Le}(2)$ dominates for the range of SKC between 5 to 18 and it takes a peak value at about SKC = 10. The third harmonic component, $C_{Le}(3)$, dominates for the range of SKC between 18 to 28.

(3) In the case of kd = 1.79, $C_{Le}(2)$ dominates for the range of SKC between 8 to 28 and it takes peak value at around SKC = 15.

It is interesting to note as shown in Fig. 5.3.1 that the relative magnitudes of the frequency components of $C_{Le}(n)$ are influenced by kd.

The magnitude of the horizontal water particle velocity, u, decreases rapidly with increasing water depth in the case of large kd and decreases only slowly in the case of small kd. But in the latter case, the waves are more non-linear, having relatively large higher frequency components.

5-3-3 The result of C_{Lemax} C_{Le} and C_{VL}

The relationship between C_{Lemax} and C_{Le}, and SKC for the three values of kd are shown in Fig. 5.3.2 and Fig. 5.3.3, respectively. The root-mean-square values of the lift coefficient, rms.C_L, for several values of kd, which have been obtained by Isaacson et al. (1976), are also shown in Fig. 5.3.3.

In the case of harmonic flow, it has been reported by Sarpkaya (1975), Maull et al. (1978) and Sawamoto et al. (1980) that the lift coefficient plotted against KC number shows two remarkable peak values at KC number of about 10 and about 18. In addition to them, the appearance of two further peaks, at about KC = 26 and about KC = 32, have been reported by Ikeda et al. (1981) and Bearman et al. (1981).

In the present data derived from tests in waves, there is no appearance of several peaks in C_{Lemax} and C_{Le}. Only one peak of C_{Lemax} and of C_{Le} appears at about SKC = 10-15 for kd = 0.735, at about SKC = 10-12 for kd = 1.01 and SKC = 12-16 for kd = 1.79. The magnitude of the peak values of C_{Lemax} and of C_{Le} are also influenced by kd.

The relationship between the coefficient of variation, C_{VL}, and SKC for three values of kd are shown in Fig. 5.3.4 (a), (b) and (c) respectively. This figure shows that small value of C_{VL} occur for kd = 0.735 and kd = 1.01 in the range of SKC between 10 to 16, whereas these small values of C_{VL} do not occur for kd = 1.79. When C_{VL} is less than 0.1, the record of $F_{m\ell}$ on the U-V recorder shows that the time history of $F_{m\ell}$ is very stable and that the amplitude is not intermittent and does not modulate.

It is interesting to note that C_{VL} takes a minimum value of about 0.03 at around SKC = 11, where the peaks of both C_{Lemax} and C_{Le} occur, (see Fig. 5.3.2).

The relationship between C_{Lemax}, C_{Le} and C_{VL}, and the wave depth parameter, kd, are shown in Fig. 5.3.5 (a), (b) and (c) respectively, where the range of SKC is between 10.7 to 15. Several rms. C_L values for SKC = 11, obtained by Isaacson et al. (1976), are also plotted in Fig. 5.3.5(b).

These figures show more clearly the dependence of the characteristics of lift forces to the kd value. Both C_{Lemax} and C_{Le} plotted against kd have three peaks at about kd = 0.8, 1.25, and 1.6. C_{VL} plotted against kd shows that C_{VL} is less than 0.15 in the range of kd < 1.1.

The relationship between C_{VL}, and both SKC and kd is shown in Fig. 5.3.6, where C_{VL} is divided into three ranges and the occurrence of values in each range is related to the corresponding kd and SKC values. As described previously, when C_{VL} is less than 0.1, the variation of $F_{m\ell}$ with time is very stable. The quantity of present data is not sufficient to describe exactly the region where the stable lift force occurs. However, it may be possible to describe roughly that the stable lift force occurs in the range of SKC between about 10 to 15, for values of kd less than about 1.1.

In the case of harmonic flow, the appearance of stable lift forces have been reported by Maull et al. (1978) and Ikeda et al. (1981). The result of Ikeda et al. shows that the stable lift forces appeared in the range of KC between 10 to 14 and in this range of KC, the vortex shedding was stable and regular.

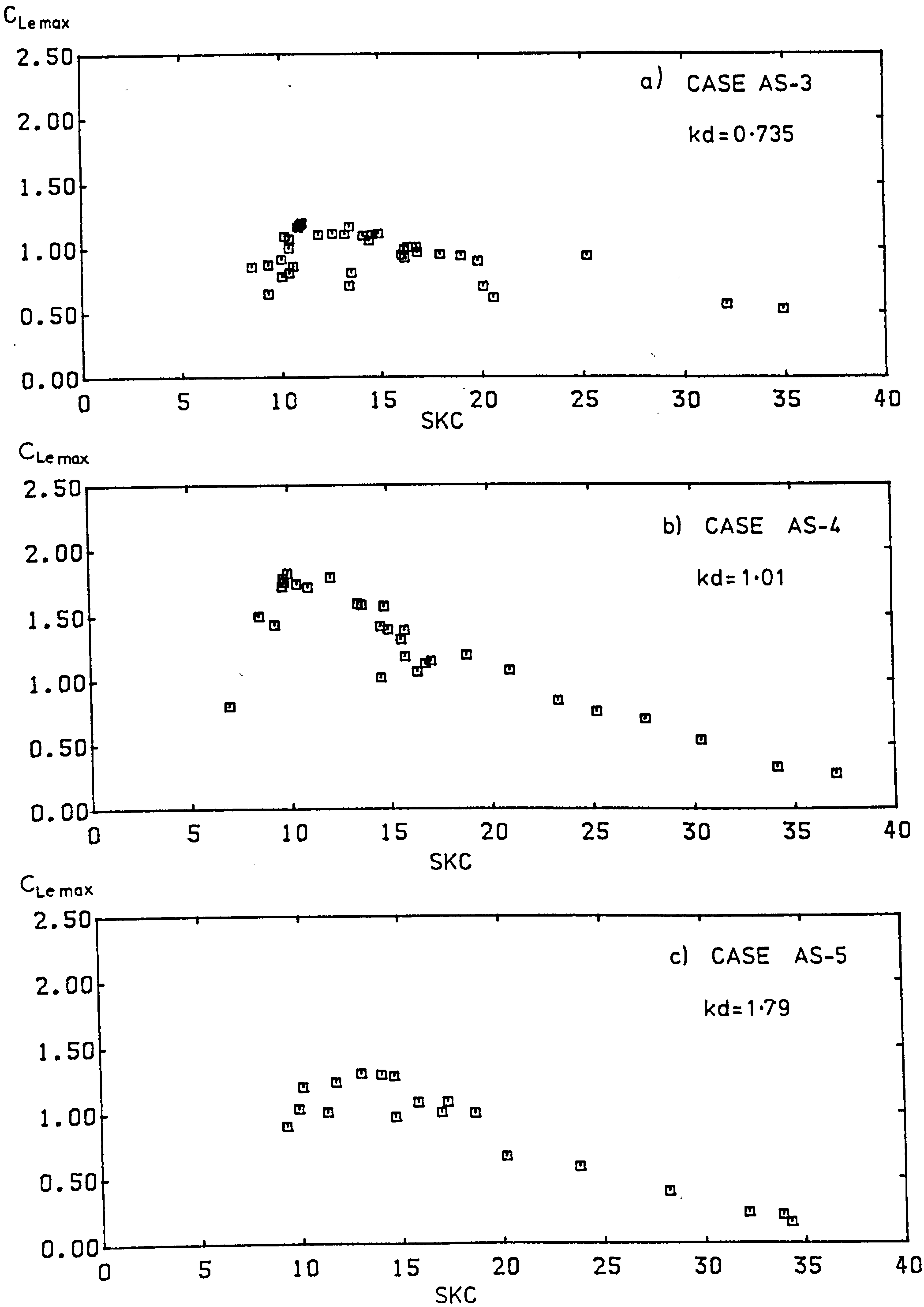

Fig. 5.3.2 The Lift Coefficient(C_{Lemax}) vs. the Surface Keulegan-Carpenter Number(SKC) for Three Wave Depth Parameters

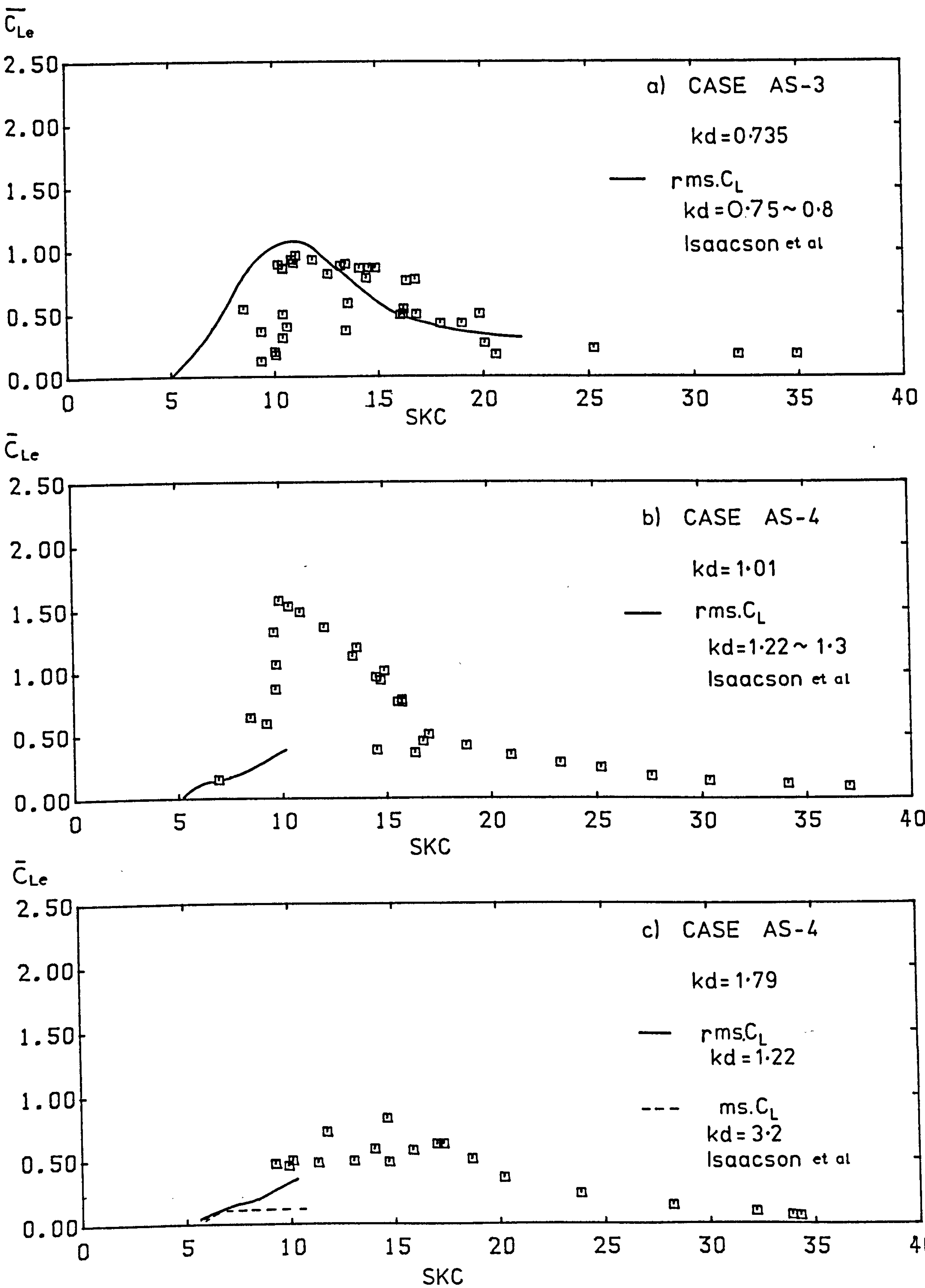

Fig. 5.3.3 The Lift Coefficient($\overline{C_{Le}}$) vs. Surface Keulegan-Carpenter Number(SKC) for Three Wave Depth Parameters(kd=0.735, 1.01 and 1.79)

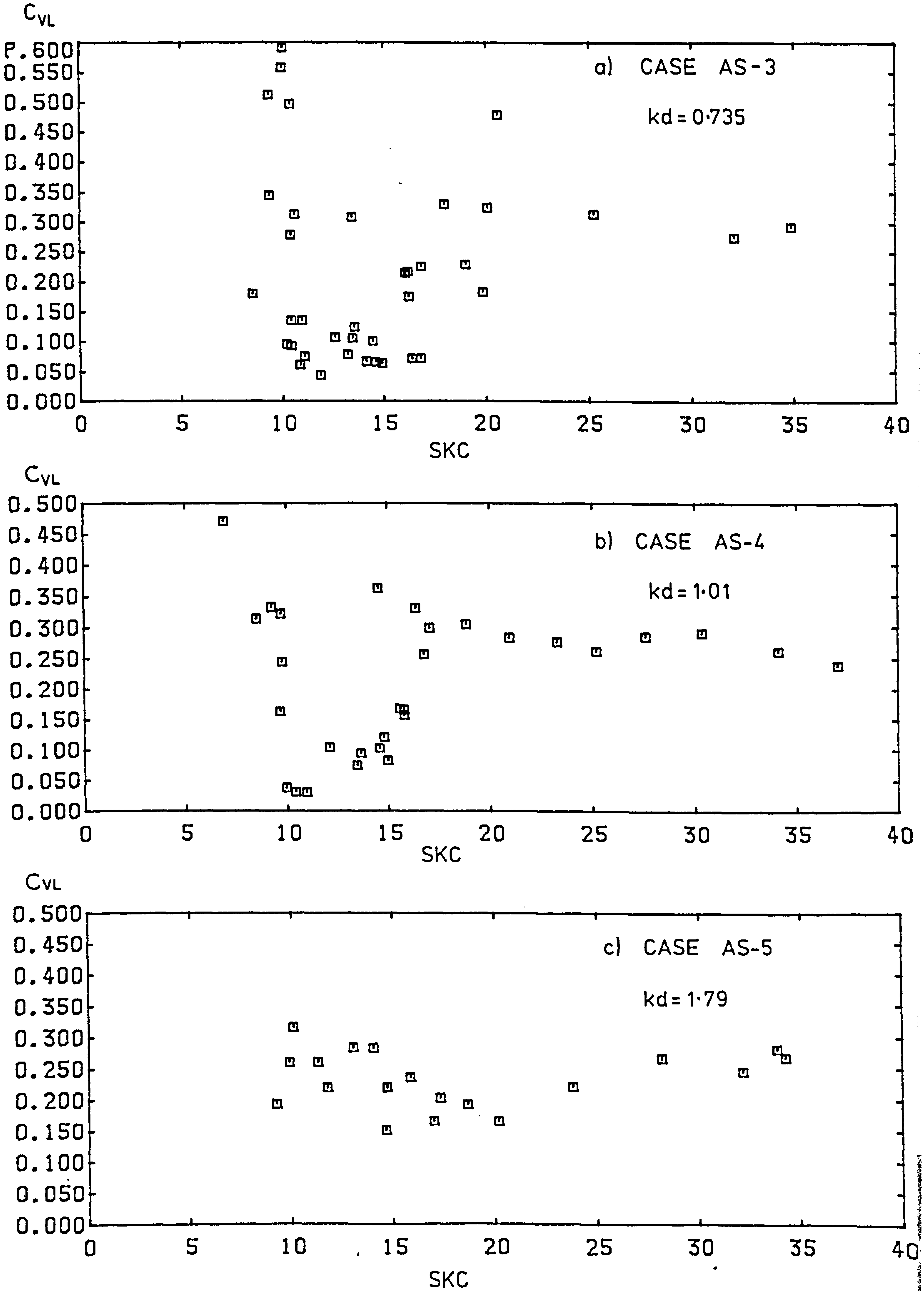

Fig. 5.3.4 The Coefficient of Variation(C_{VL}) vs. Surface Keulegan-Carpenter Number(SKC) for Three Wave Depth Parameters

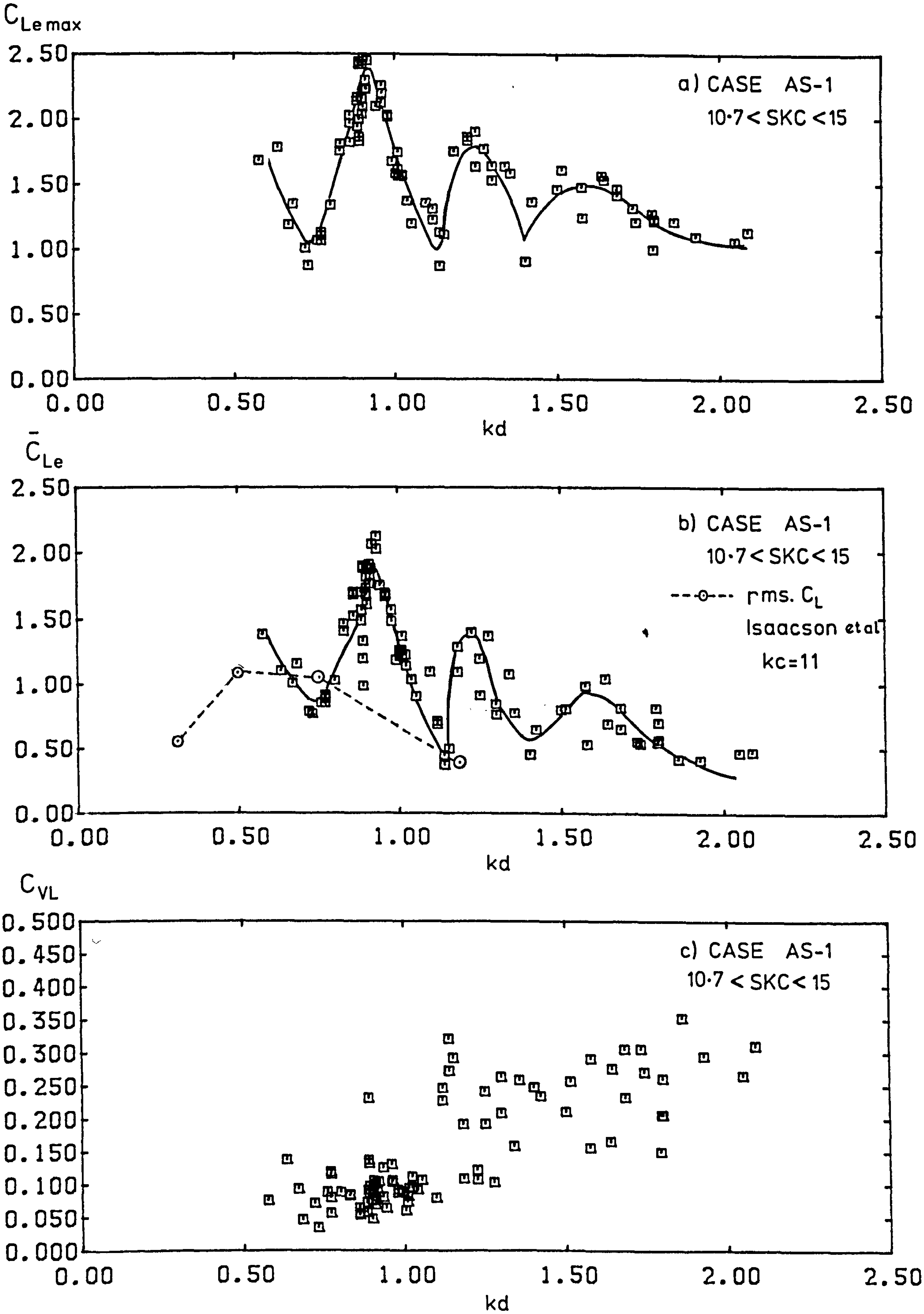

Fig. 5.3.5 The Three Lift Coefficients(C_{Lemax}, $\overline{C_{Le}}$ and C_{VL}) vs. Water Depth Parameter(kd)

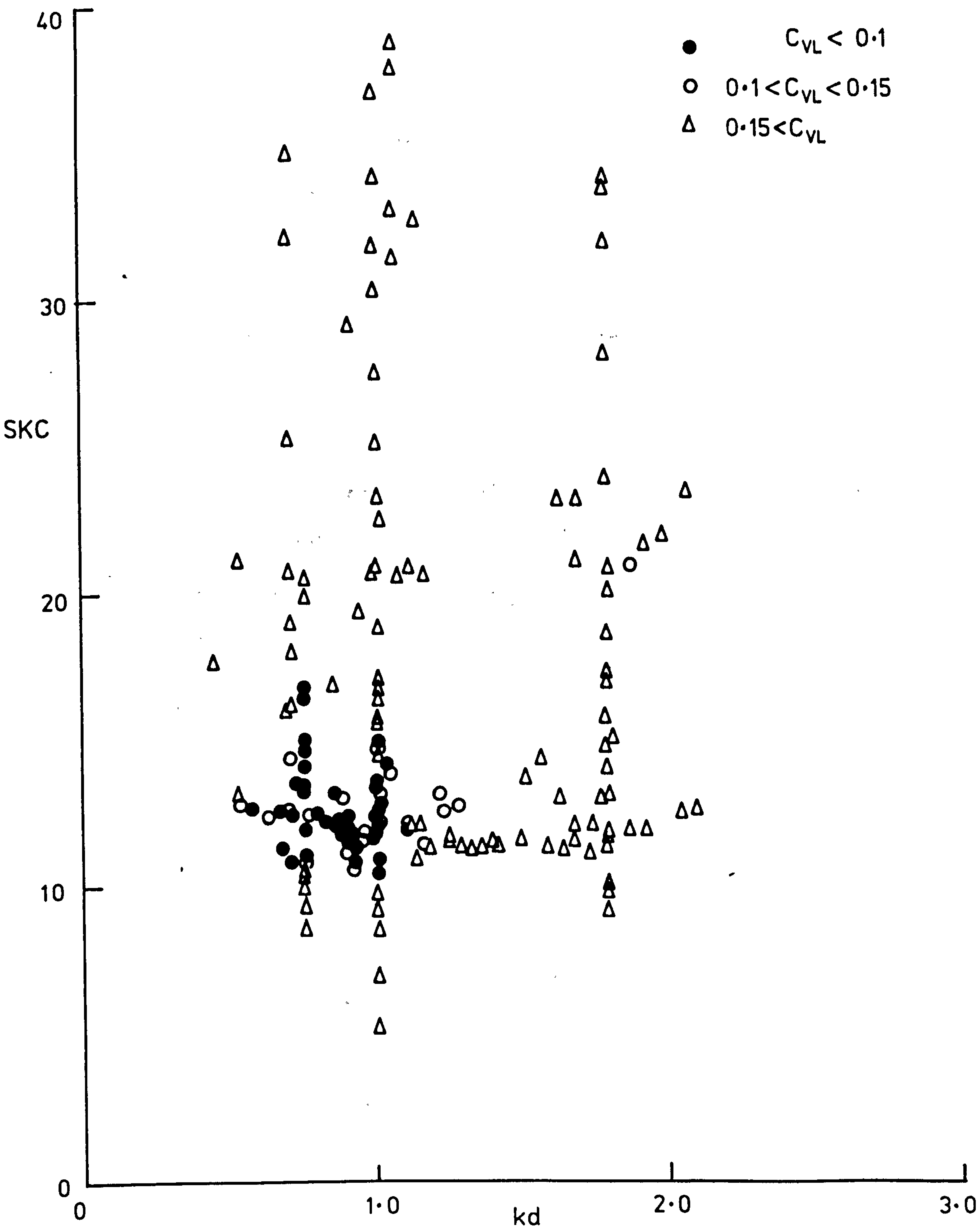

Fig. 5.3.6 The Diagram for the Coefficient of Variation(C_{VL}) Plotted against SKC and kd

Therefore, the appearance of stable lift force may be also due to the appearance of the stable vortex shedding along the cylinder axis because the variation of horizontal water particle velocity in wave, u, with water depth is small in the range of kd ≈ 1.1.

The high value of C_{VL} in the range of kd > 1.2 (see Fig. 5.3.5 and Fig. 5.3.6) shows that the stable lift force does not appear in this range. This result may be due to the fact that the stable vortex shedding is not formed along the axis of test cylinder because the variation of u along the cylinder axis increases with the increase of kd.

5-4 The Vortex-Excited Vibration of the Test Cylinder in Waves

5-4-1 A general description of amplitude and frequency of vortex-excited vibration as a function of frequency ratio f_w/f_{nw}

The following statistical values are obtained in order to study the characteristics of the vortex-excited vibration of the test cylinder in waves because the envelope of its amplitude is irregular.

(1) The mean value of the half peak-to-peak amplitude of the vortex-excited vibration at mean water level (80cm above the bed, see Fig. 3.1) - (Y_{hm}).

(2) The mean value of the frequency of the vortex-excited vibration (f_{ym}).

(3) The coefficient of variation of the half peak-to-peak amplitude of the vortex-excited vibration defined as C_{VY} = (the standard deviation of the half peak-to-peak amplitude of the vortex-excited vibration)/(2.Y_{hm}).

In order to show how the amplitude, Y_{hm}, and the frequency, f_{ym}, vary with f_w/f_{nw},

(1) the relationship between the value of Y_{hm}/D and the frequency ratio f_w/f_{nw} for CASE A-1, CASE A-2, CASE AB-1, CASE AB-2, CASE B-1 and CASE B-2 are shown in Fig. 5.4.1 through Fig. 5.4.6 respectively; and

(2) the relationship between the frequency ratio f_{ym}/f_{nw}, and f_w/f_{nw}, and C_{VY} and f_w/f_{nw} for the same cases as above are shown in Fig. 5.4.7 through Fig. 5.4.12.

The experimental conditions of these test cases are shown in Table 1 and are explained in section 4-6-5. The test cylinder was free to vibrate only in the transverse direction in the runs of CASE A and CASE AB, while in those of CASE B it was free to vibrate in any direction.

In CASE A-1 and CASE A-2, the damping factor of the test cylinder in air, ζ_{ta}, was 0.001. However, in CASE AB-1 and CASE AB-2, ζ_{ta} was changed from 0.001 to 0.021 by using the electro-magnetic damper in order to study the influence of the damping factor on the vortex-excited vibration of the test cylinder in waves. The surface KC number was fixed at about 12 for CASE A-1, CASE AB-1 and CASE B-1, and it was fixed at about 20 for CASE A-2, CASE AB-2 and CASE B-2.

The frequency ratio f_w/f_{nw} was varied by varying the wave frequency, f_w. The value of SKC, $m_e/\rho D^2$, ζ_{ta}, and the reduced damping $2m_e(2\pi\zeta_{ta})/\rho D^2$ are shown in these figures.

The purpose of these figures is to show the character of the vortex-excited vibration of the test cylinder in waves for each of the test cases described above. The detailed features of the vortex-excited vibration of the test cylinder around $f_w/f_{nw} = 1/3$ and 1/2 will be described later. The following main characteristics for each test case are shown in Fig. 5.4.1 through Fig. 5.4.12.

(a) CASE A-1, (SKC $\cong$ 12, $m_e/\rho D^2 = 15.7$, $\zeta_{ta} = 0.001$)

When the frequency ratio approaches the values of $f_w/f_{nw} \cong 1/2$, 1/3 and 1/4,:

(1) The value of Y_{hm}/D has a peak value,

(2) The value of f_{ym} is equal to f_{nw}, and

(3) The value of C_{VY} has a very small value as shown in Fig. 5.4.1 and Fig. 5.4.7.

When the value of C_{VY} is less than 0.01, the time history of the vortex-excited vibration of the test cylinder, y_h, recorded on the U-V recorder, is very regular. It also shows that the amplitude of the vibration is not intermittent and is not modulated. We refer to these phenomena perfect resonant vibration. The appearance of these peak values of Y_{hm}/D may be due to the following.

(1) the resonance between the frequency of the harmonic component of the lift force and the natural frequency of the test cylinder, and

(2) the amplification of each harmonic component of the lift force by means of the increased vortex strength and the correlation in the phase of vortex shedding along the cylinder's axis.

The maximum peak value of Y_{hm}/D occurs at $f_w/f_{nw} \cong 1/2$. This may be due to the domination of the second harmonic component of the effective lift coefficient, $C_{Le}(2)$, at around SKC = 12 observed for the stiff cylinder (see Fig. 5.3.1). The peak value of Y_{hm}/D at $f_w/f_{nw} \cong 1/4$ is small compared with that at $f_w/f_{nw} \cong 1/2$. This may be due to the lower value of $C_{Le}(4)$ and that the amplification of $C_{Le}(4)$ was suppressed by the existence of the larger value of $C_{Le}(2)$.

(b) CASE A-2 (SKC $\cong$ 20, $m_e/\rho D^2$ = 15.7. ζ_{ta} = 0.001)

The perfect resonant vibration described above at $f_w/f_{nw} \cong 1/2$, 1/3, 1/4, 1/5, 1/6 are shown in Fig. 5.4.2 and Fig. 5.4.8. These phenomena may be also associated with the same factors as described above. In this case, the maximum peak value of Y_{hm}/D occurs at $f_w/f_{nw} \cong 1/3$. However, the difference between this maximum peak value and the other peak values is small, compared with that in CASE A-1. This may be due to the small difference between each harmonic component of the lift forces observed for the stiff cylinder.

(c) CASE AB-1 (SKC $\doteqdot$ 12, $m_e/\rho D^2$ = 15.7, ζta = 0.021)

The appearance of resonant vibration at $f_w/f_{nw} \doteqdot$ 1/2, 1/3 is shown in Fig. 5.4.3 and Fig. 5.4.8. In this case, the maximum peak values of Y_{hm}/D are smaller, compared with those of CASE A-1, and the peak value of Y_{hm}/D at $f_w/f_{nw} \doteqdot$ 1/3 is not so clear as that in CASE A-1. This is probably due to the increased damping.

(d) CASE AB-2 (SKC $\doteqdot$ 20, $m_e/\rho D^2$ = 15.7. ζta = 0.021)

The appearance of resonant vibration at $f_w/f_{nw} \doteqdot$ 1/2 and 1/3 is shown in Fig. 5.4.4 and Fig. 5.4.9. Both peak values of Y_{hm}/D at $f_w/f_{nw} \doteqdot$ 1/2 and 1/3 are smaller, compared with those of CASE A-2 because of the increased damping.

(e) CASE B-1 (SKC $\doteqdot$ 12, $m_e/\rho D^2$ = 19.6, ζta = 0.008)

The clear perfect resonant vibration appears at $f_w/f_{nw} \doteqdot$ 1/2. However, the appearance of perfect resonant vibration at f_w/f_{nw} $\doteqdot$ 1, 1/3, 1/4 and 1/5 are not clear as shown in Fig. 5.4.5 and Fig. 5.4.10.

(f) CASE B-2 (SKC $\doteqdot$ 20, $m_e/\rho D^2$ = 19.6, ζta = 0.008)

The appearance of the perfect resonant vibration at $f_w/f_{nw} \doteqdot$ 1, 1/2, 1/3, 1/4 and 1/5 is shown in Fig. 5.4.6 and Fig. 5.4.12. The phenomena of resonant vibrations at $f_w/f_{nw} \doteqdot$ 1/2 and 1/3 are nearly similar to those of CASE A-2.

Fig. 5.4.1 Dimensionless Cylinder Displacement(Y_{hm}/D) vs. Frequency Ratio(f_w/f_{nw}) for CASE A-1

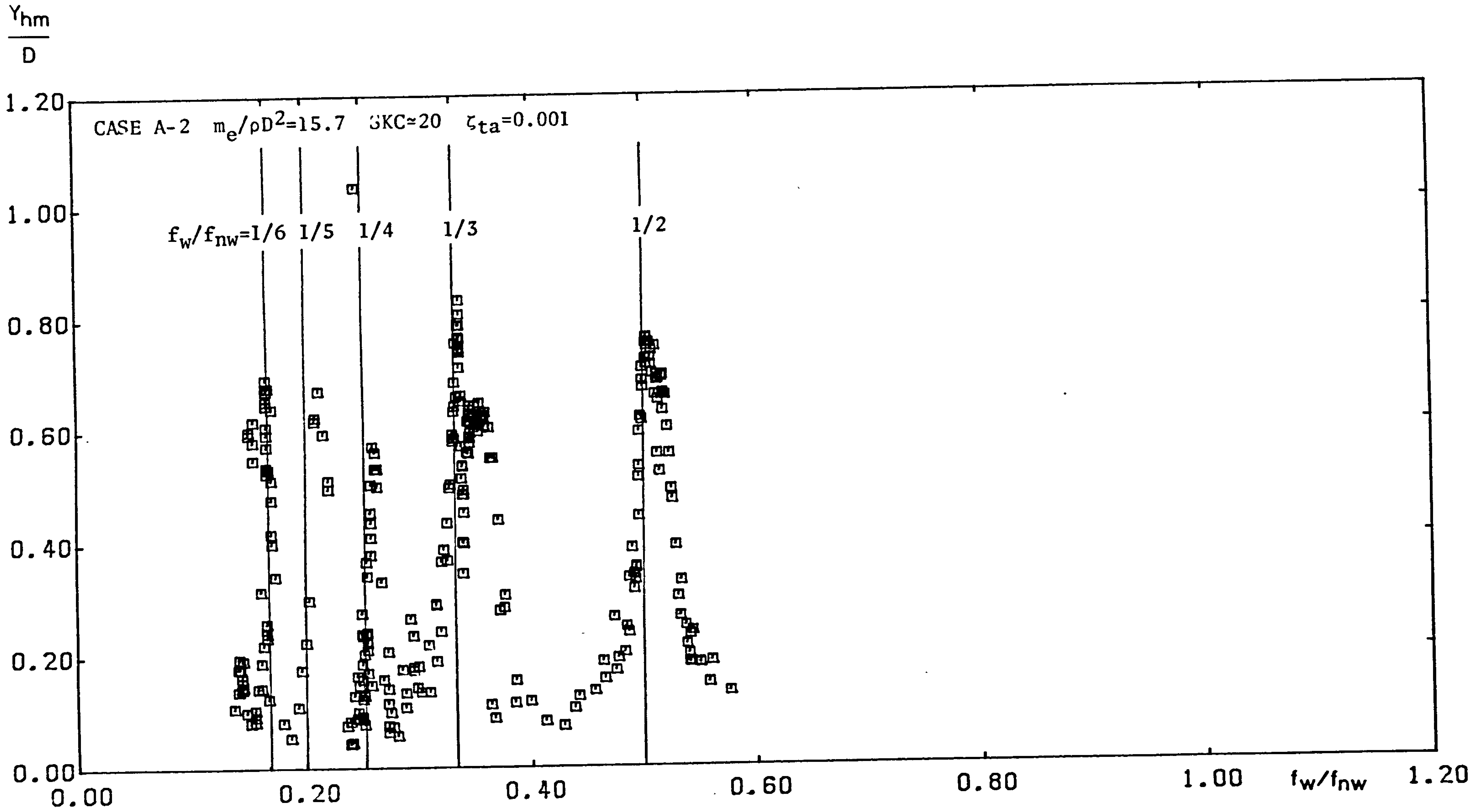

Fig. 5.4.2 Dimensionless Cylinder Displacement(Y_{hm}/D) vs. Frequency Ratio(f_w/f_{nw}) for CASE A-2

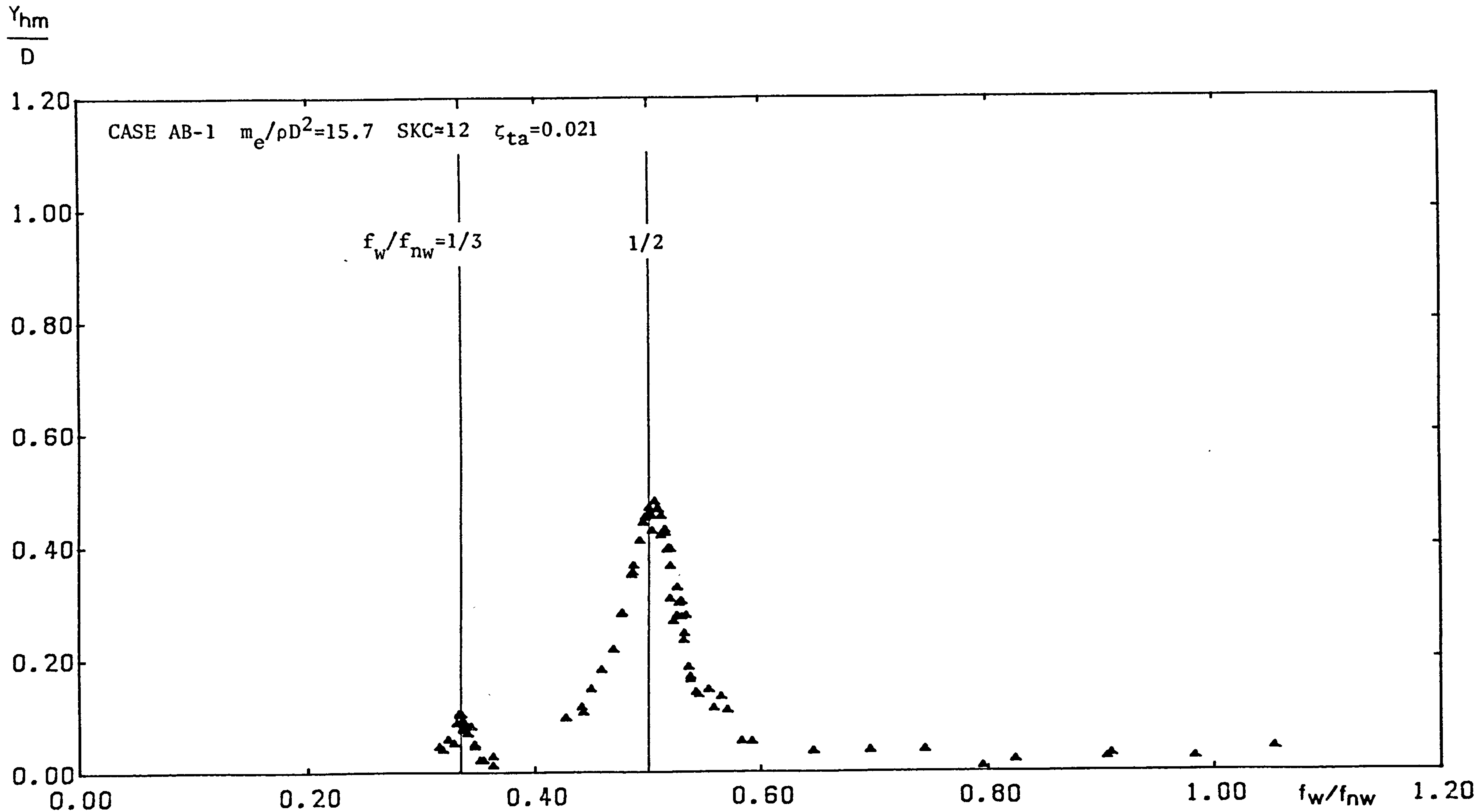

Fig. 5.4.3 Dimensionless Cylinder Displacement(Y_{hm}/D) vs. Frequency Ratio(f_w/f_{nw}) for CASE AB-1

Fig. 5.4.4 Dimensionless Cylinder Displacement(Y_{hm}/D) vs. Frequency Ratio(f_w/f_{nw}) for CASE AB-2

Fig. 5.4.5 Dimensionless Cylinder Displacement(Y_{hm}/D) vs. Frequency Ratio(f_w/f_{nw}) for CASE B-1

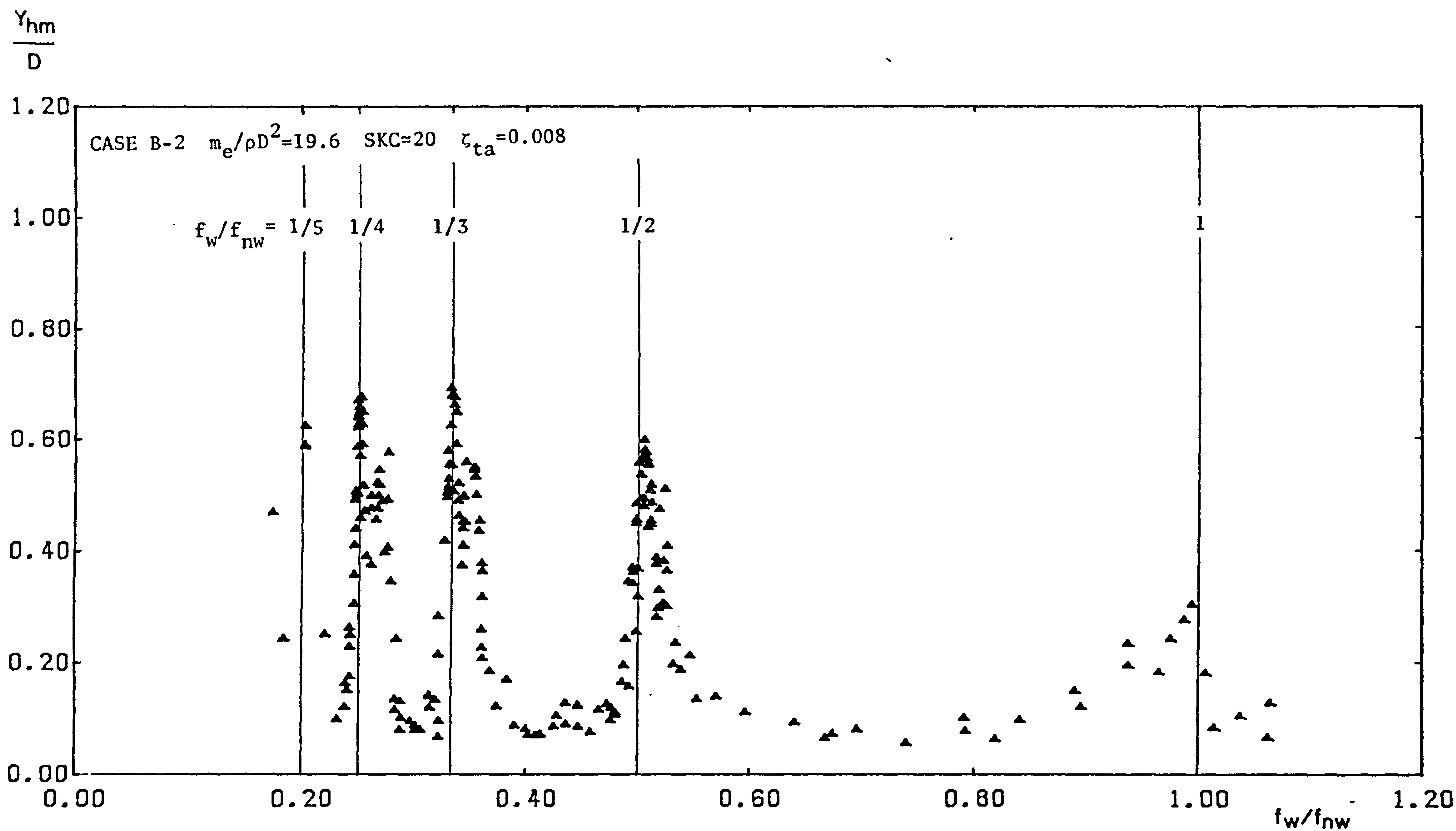

Fig. 5.4.6 Dimensionless Cylinder Displacement(Y_{hm}/D) vs. Frequency Ratio(f_w/f_{nw}) for CASE B-2

Fig. 5.4.7 The Plots of f_{ym}/f_{nw} and C_{VY} against of f_w/f_{nw} for CASE A-1

Fig. 5.4.8 The Plots of f_{ym}/f_{nw} and C_{VY} against of f_w/f_{nw} for CASE A-2

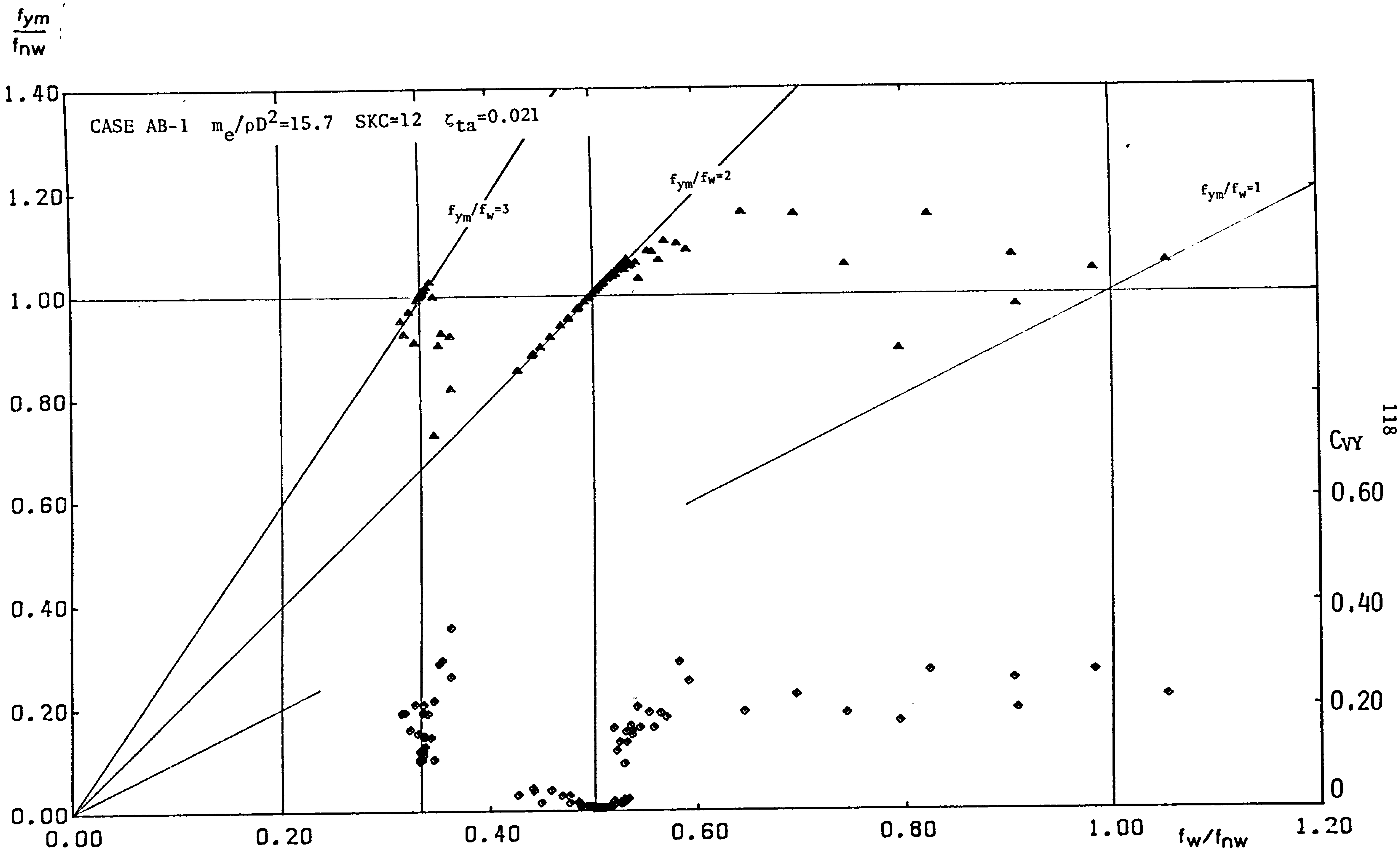

Fig. 5.4.9 The Plots of f_{ym}/f_{nw} and C_{VY} against of f_w/f_{nw} for CASE AB-1

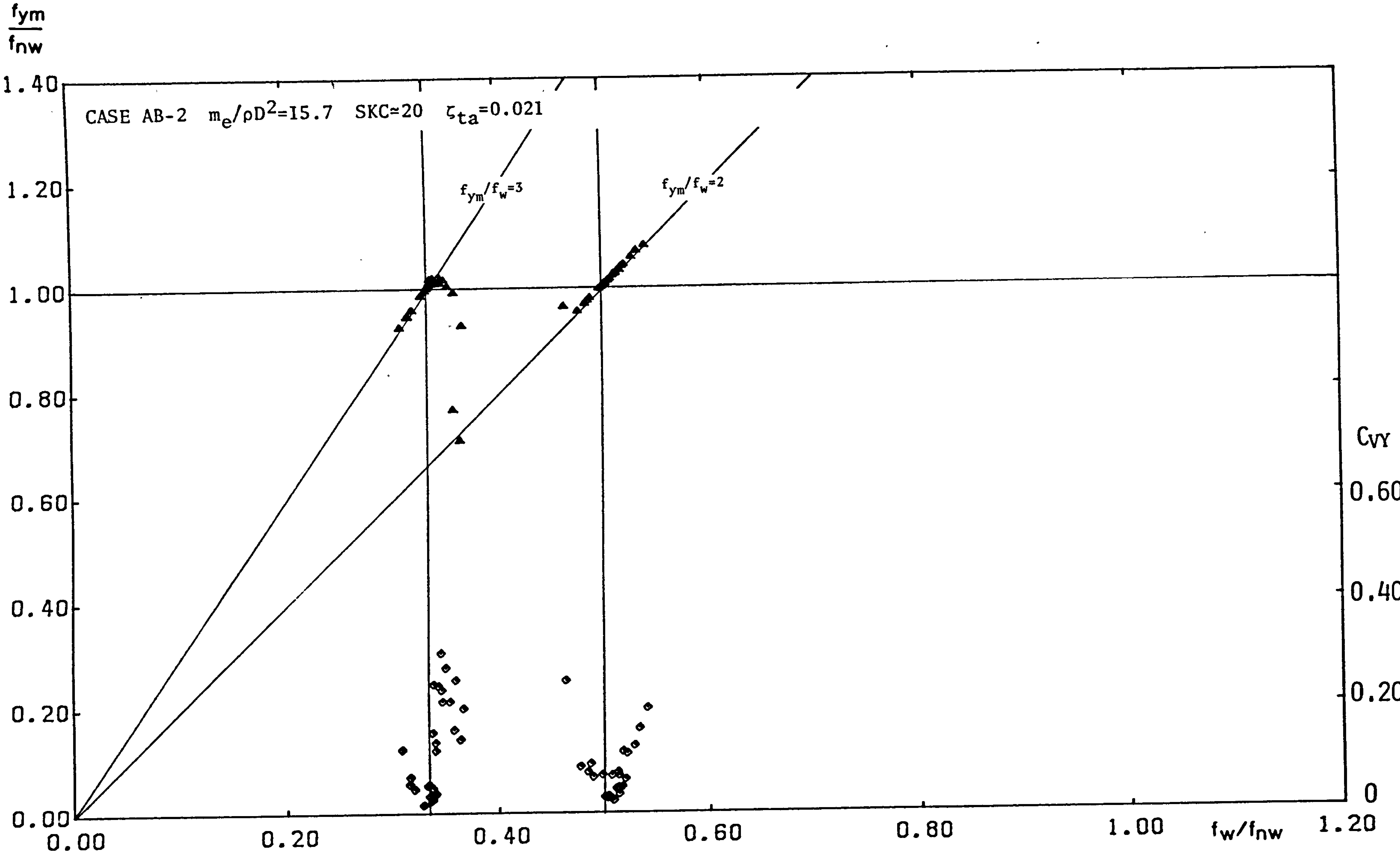

Fig. 5.4.10 The Plots of f_{ym}/f_{nw} and C_{VY} against of f_w/f_{nw} for CASE AB-2

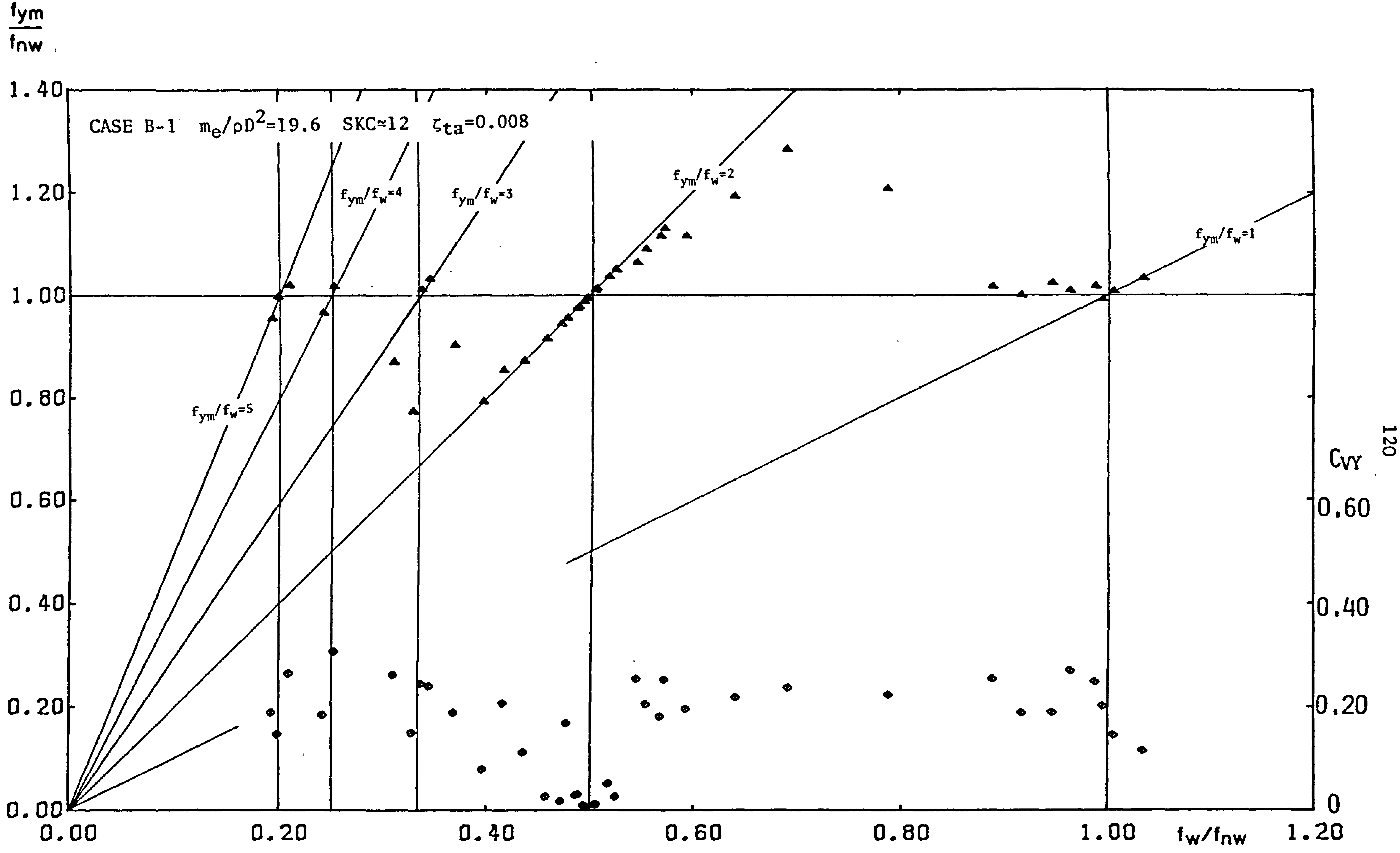

Fig. 5.4.11 The Plots of f_{ym}/f_{nw} and C_{VY} against of f_w/f_{nw} for CASE B-1

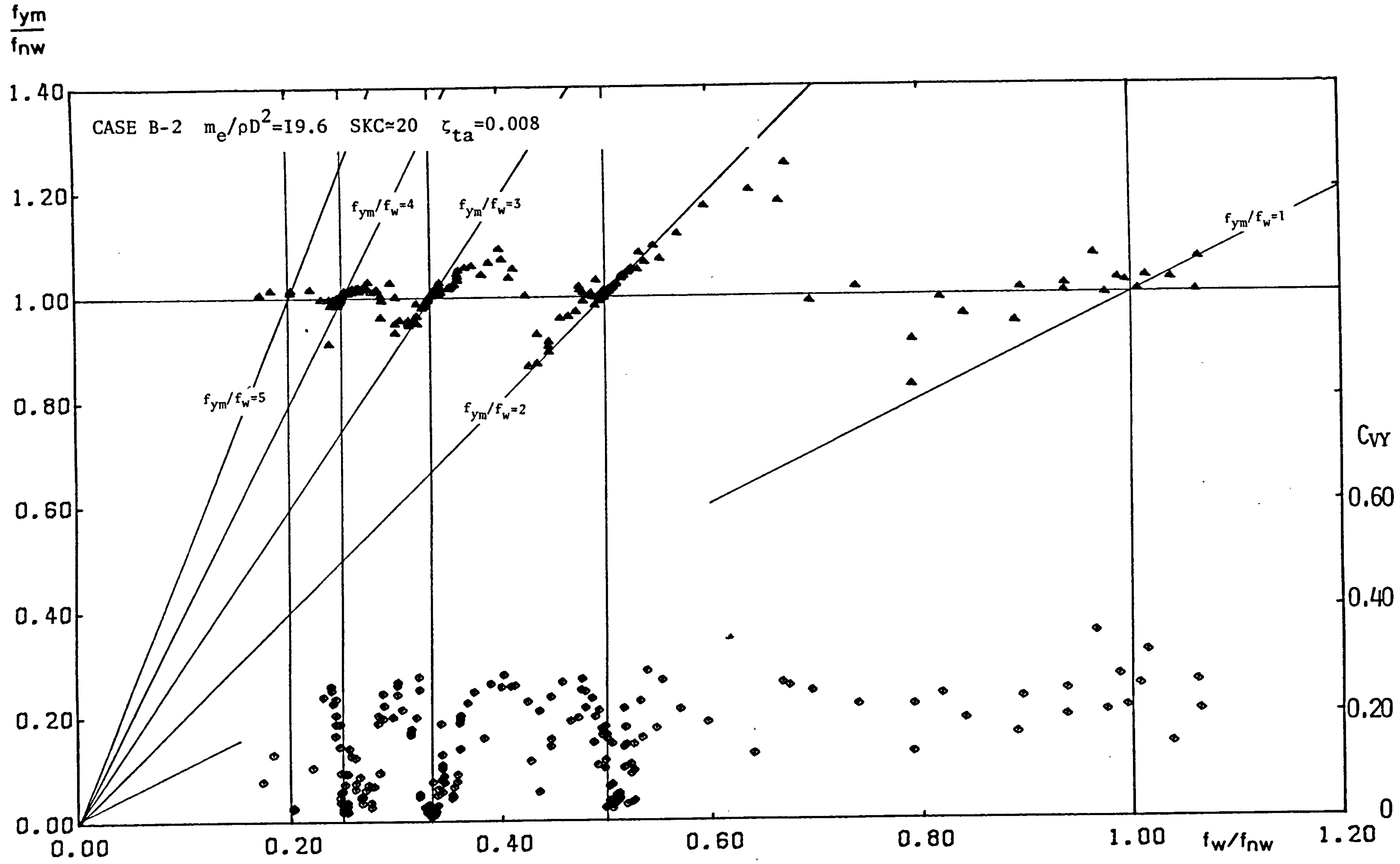

Fig. 5.4.12 The Plots of f_{ym}/f_{nw} and C_{VY} against of f_w/f_{nw} for CASE B-2

As described above, the variation of the vortex-excited vibration of the test cylinder with f_w/f_{nw} depends on the value of SKC and the value of ζ_{ta}. The difference between the vortex-excited vibration of the test cylinder which was left free to vibrate in any direction and the vortex-excited vibration of the test cylinder which was left free to vibrate only in the transverse direction, is not clear in the present study.

The appearances of the perfect resonant vibration at $f_w/f_{nw} \doteq 1/2$ and 1/3, in the range of rms KC value 10 to 15, were reported by Sawaragi et al. (1977) and Isaacson et al. (1981). However, the appearance of the resonant vibration at $f_w/f_{nw} \doteq 1/4$, 1/5 and 1/6 at SKC $\doteq$ 20, have apparently never been previously reported. These multi-appearances of the resonant vibration should be noted as a significant feature of the response of a flexibly supported cylinder in waves.

5.4.2 <u>Detailed description of the vortex-excited vibration with f_w/f_{nw}</u>

In order to study the details of the phenomena of the vortex-excited vibration of the test cylinder at $f_w/f_{nw} \doteq 1/2$ (for SKC $\doteq$ 12) and 1/3 (for SKC $\doteq$ 20), the relationships between f_w/f_{nw} and Y_{hm}/D, f_{ym}/f_{nw} and C_{YY}, for CASE A-1, CASE A-2, CASE AB-1, CASE AB-2 and CASE B are shown respectively in Fig. 5.4.13 (a), (b) and (c) through Fig. 5.4.17 (a), (b) and (c).

In order to show the characteristics of the variation with time of the amplitude of the test cylinder, several examples of the record of y_h on the U-V recorder for CASE A-1, for f_w/f_{nw} in the range between 0.485 to 0.543, are shown with those of CASE AS-1 in Fig. 5.4.18. The experimental conditions and the resulting analysis are shown in Table 5.2. As shown in Table 5.2, the experimental wave conditions of each run of CASE A-1 and CASE AS-1 were the same. Therefore, the results of CASE A-1 are classed with the notation (a) and those of CASE AS-1 are classed with the notation (b) in Fig. 5.4.18.

(a) CASE A-1 (SKC $\doteqdot$ 12, $m_e/\rho D^2$ = 15.7, ζta = 0.001; see Fig. 5.4.13)

As the frequency ratio, f_w/f_{nw}, increases from 0.45 to 0.503, the value of Y_{hm}/D increases smoothly except for some small scatter around f_w/f_{nw} = 0.493. It takes the peak value of 0.74 at f_w/f_{nw} = 0.504. The frequency ratio f_{ym}/f_{nw} in this range of f_w/f_{nw} is also plotted from the relationship

$$\frac{f_{ym}}{f_{nw}} = 2\,\frac{f_w}{f_{nw}} \qquad (5\text{-}4\text{-}2)$$

The value of C_{VY} has a small value in this range of f_w/f_{nw} except for the appearance of large values around f_w/f_{nw} = 0.493. The small value of C_{VY} indicates the regularity of the time history of the vortex-excited vibration of the test cylinder as shown in Fig. 5.4.18. The large value of C_{VY} shows the irregularity of the time history of the vortex-excited vibration of the test cylinder. In this case as shown in Fig. 5.4.18 runs 622w3(a) and 622w3(4), the amplitude is intermittent and modulated.

The peak value of Y_{hm}/D appears at $f_w/f_{nw} \doteq 0.503$ and not at $f_w/f_{nw} = 0.500$ as might be expected. The time-history of the vibration of the test cylinder, y_h, is very regular as shown in Fig. 5.4.18 (run No. 622w9(a)). The detail of this record is shown in Fig. 5.4.19 with the record of the displacement of the water surface elevation, η. The frequency of the vibration of the test cylinder, f_{ym}, is just two times the wave frequency, f_w, as shown in this figure. The appearance of the peak value of Y_{hm}/D at $f_w/f_{nw} \doteq 0.503$ (not at $f_w/f_{nw} = 1/2$) may be due to an increase in the natural frequency of the test cylinder in the vortex-excited condition from the natural frequency of the test cylinder in the condition of free vibrations in still water. This increase of the natural frequency may be caused by the variation of the water surface elevation in the waves and the variation of the added mass coefficient in the vortex-excited condition. If we assume that it is due only to the latter, the added mass coefficient at perfect resonance C_{ar} can be estimated by using Eq.(3-3), Eq.(3-4) and Eq.(4-8) as

$$C_{ar} = 0.79$$

The added mass coefficient in the condition of free vibration in still water, C_{as}, is also estimated from measurements by using the equations above as

$$C_{as} = 1.04$$

The theoretical value of C_{as} is 1.098 calculated by using Eq.(5-4-2) (Bearman et al. 1984) for $\beta = 530$.

$$C_{as} = 1 + \frac{4}{\sqrt{\pi\beta}} + (\pi\beta)^{-3/2} \qquad (5\text{-}4\text{-}2')$$

This equation was defined from Wang's (1968). Its second term was given by Stokes (1901) for the case of spherical and cylindrical pendulum bobs oscillating at low KC number. (Note that, when a circular cylinder is fixed in oscillating flow, the first term of Eq.(5-4-2') is 2, and when a circular cylinder is vibrating in still water the first term of this equation is 1.) The difference between the experimental value of C_{as} = 1.04 and theoretical value of C_{as} = 1.10 may be due to the appearnce of boundary layer separation and vortex-shedding at SKC value above 2, also the three-dimensional effect of the flow. It is worth noting that experimental results of Sarpkaya (1978) show the decrease of the added mass coefficient of a cylinder undergoing forced transverse oscillations in a uniform flow, for the perfect resonant condition. However, King (1971) reported that the added mass coefficient of a cylinder vibrating in the in-line direction with vortex-excited condition in steady current flow is not affected by streaming flow and vortex-shedding.

Returning to Fig. 5.4.13, in the range of f_w/f_{nw} between 0.503 to 0.515, the value of Y_{hm}/D decreases smoothly with increasing f_w/f_{nw}. The value of f_{ym}/f_{nw} still agrees with Eq.(5-4-2) indicating that the oscillation is coupled to the wave frequency, referred to as "wave coupling".

The value of C_{VY} is small because the amplitude of y_{hm} is regular as shown in Fig. 5.4.18 (622w10(a) through 622w13(a)).

In the range of f_w/f_{nw} between 0.515 to 0.519, the value of Y_{hm}/D decreases with increasing f_w/f_{nw} and has a trough value of about 0.41 at $f_w/f_{nw} \approx 0.519$. The value of f_{ym}/f_{nw} deviates downwards from the calculated value of Eq.(5-4-2) as shown in this figure. The value of C_{VY} becomes large because the amplitude of y_h is intermittent and modulates as shown in Fig. 5.4.18 (622w16 and 622w15).

In the range of f_w/f_{nw} between 0.519 to 0.523, the value of Y_{hm}/D increases rapidly from the trough value of $Y_{hm}/D \approx 0.41$ and reaches around $Y_{hm}/D = 0.55$. The corresponding values of f_{ym}/f_{nw} are around $f_{ym}/f_{nw} \cong 1.018$. The value of C_{VY} is small, but it is not so small as the value of C_{VY} in the range of f_w/f_{nw} between 0.49 to 0.514 because the amplitude of y_h modulates without intermittency in the amplitude of y_h as shown in Fig. 5.4.18 (622w16(a)).

The detail of the variation of y_h and η with time, t, for the data of run No. 622w16(a) are shown in Fig. 5.4.20. The variation of the phase angle between y_h and η can be found in this figure. This is due to the difference between the values of f_{ym} and $2f_w$ (see Fig. 5.4.18). The appearance of modulation of the amplitude y_h may be due to the variation of the vortex-shedding strength which is caused by the variation of phase angle above. Now we call this phenomenon "vortex coupling" because Y_{hm}/D increases, and the value of f_{ym} is restricted to a constant which is between the natural frequency of the test cylinder and the vortex-shedding frequency expressed by Eq.(5-4-2) in this case.

At f_w/f_{nw} greater than about 0.523, some points are grouped around a constant value of Y_{hm}/D and the others decrease smoothly with increasing f_w/f_{nw}. When Y_{hm}/D is around 0.55, the value of f_{ym}/f_{nw} is around 1.018 and C_{VY} has a small value at about 0.05. When Y_{hm}/D decreases with increasing f_w/f_{nw}, the value of f_w/f_{nw} is scattered between 1.018 and the calculated value from Eq.(5-4-2). In this case, the value of C_{VY} is between 0.2 and 0.35 because the amplitude of y_h is intermittent and modulates as shown in Fig. 5.4.18 (622w19(a) through 622w22).

However, for the vortex-excited vibration of the test cylinder in the range of f_w/f_{nw} between 0.31 to 0.34, this "vortex coupling" does not appear. The peak value of Y_{hm}/D appears around f_w/f_{nw} = 1/3 and the value of f_{ym}/f_{nw} follows the calculated line from Eq.(5-4-3).

$$\frac{f_{ym}}{f_{nw}} = 3\,\frac{f_w}{f_{nw}} \tag{5-4-3}$$

The value of C_{VY} becomes less than 0.01 just around f_w/f_{nw} = 1/3.

(b) CASE A-2 (SKC ≈ 20, $m_e/\rho D^2$ = 15.7, ζta = 0.001; see Fig. 5.4.14)

In the range of f_w/f_{nw} between 0.32 and 0.336, the value of Y_{hm}/D increases smoothly with increasing f_w/f_{nw}. The peak value of Y_{hm}/D appears at $f_w/f_{nw} \approx 0.336$. In this range of f_w/f_{nw}, the value of f_{ym}/f_{nw} follows the calculated line from Eq.(5-4-3). The value of C_{VY} is less than 0.05.

In the range of f_w/f_{nw} between 0.336 and 0.34, Y_{hm}/D decreases rapidly with increasing f_w/f_{nw} and it takes a trough value at $f_w/f_{nw} \approx 0.34$. The value of f_{ym}/f_{nw} follows Eq.(4-5-3), but it deviates downward at around $f_w/f_{nw} = 0.34$. The value of C_{VY} is less than 0.05, but it takes a large value around $f_w/f_{nw} =$ 0.34.

In the range of f_w/f_{nw} between 0.34 to 0.364, the value of Y_{hm}/D increases rapidly from the trough value and reaches approximately $Y_{hm}/D = 0.65$. The value of f_{ym}/f_{nw} is plotted around $f_{ym}/f_{nw} = 1.01$ and C_{VY} is less than 0.05. These results suggest that vortex coupling is occurring.

In the range of f_w/f_{nw} between 0.36 to 0.38, the value of Y_{hm}/D decreases smoothly with increasing f_w/f_{nw}.

The vortex-excited vibration described above is similar to that of CASE A-1 (the range of f_w/f_{nw} between 0.45 to 0.55). There is clear evidence of vortex coupling found in this case and the range of f_w/f_{nw} over which it occurs is wider than that of CASE A-1.

The appearance of the two peak value of Y_{hm}/D is also shown in the vortex-excited vibration for the range of f_w/f_{nw} between 0.48 to 0.55. However, the deviation of f_{ym}/f_{nw} from the calculation line of Eq.(5-4-2) does not appear, suggesting that the oscillations are mainly wave coupling in this range.

(c) CASE AB-1 (SKC ≅ 12, $m_e/\rho D^2$ = 15.7, ζ_{ta} = 0.021; see Fig. 5.4.15)

CASE AB-2 (SKC ≅ 20, $m_e/\rho D^2$ = 15.7, ζ_{ta} = 0.021; see Fig. 5.4.16)

The appearance of vortex coupling can not be found for these two cases. Therefore, the dynamic response curves of Y_{hm}/D with f_w/f_{nw} are simpler compared with those of CASE A-1 and CASE A-2. The value of f_{ym}/f_w around f_w/f_{nw} = 1/2 or 1/3 agree well with the calculated line from Eq.(5-4-2) or Eq.(5-4-3). Obviously the absence of vortex coupling for these two cases is due to the higher damping. The absence of lock-on for the dynamic response of a cylinder with high damping in steady flow has been reported by Unemara (1971).

(d) CASE B-2 (SKC ≅ 20, $m_e/\rho D^2$ = 19.6, ζ_{ta} = 0.008; see Fig. 5.4.17)

The features of the vortex-excited vibration are quite similar to those for CASE A-2. The appearance of vortex coupling is also found in the vortex-excited vibration for the range of f_w/f_{nw} between 0.23 to 0.28.

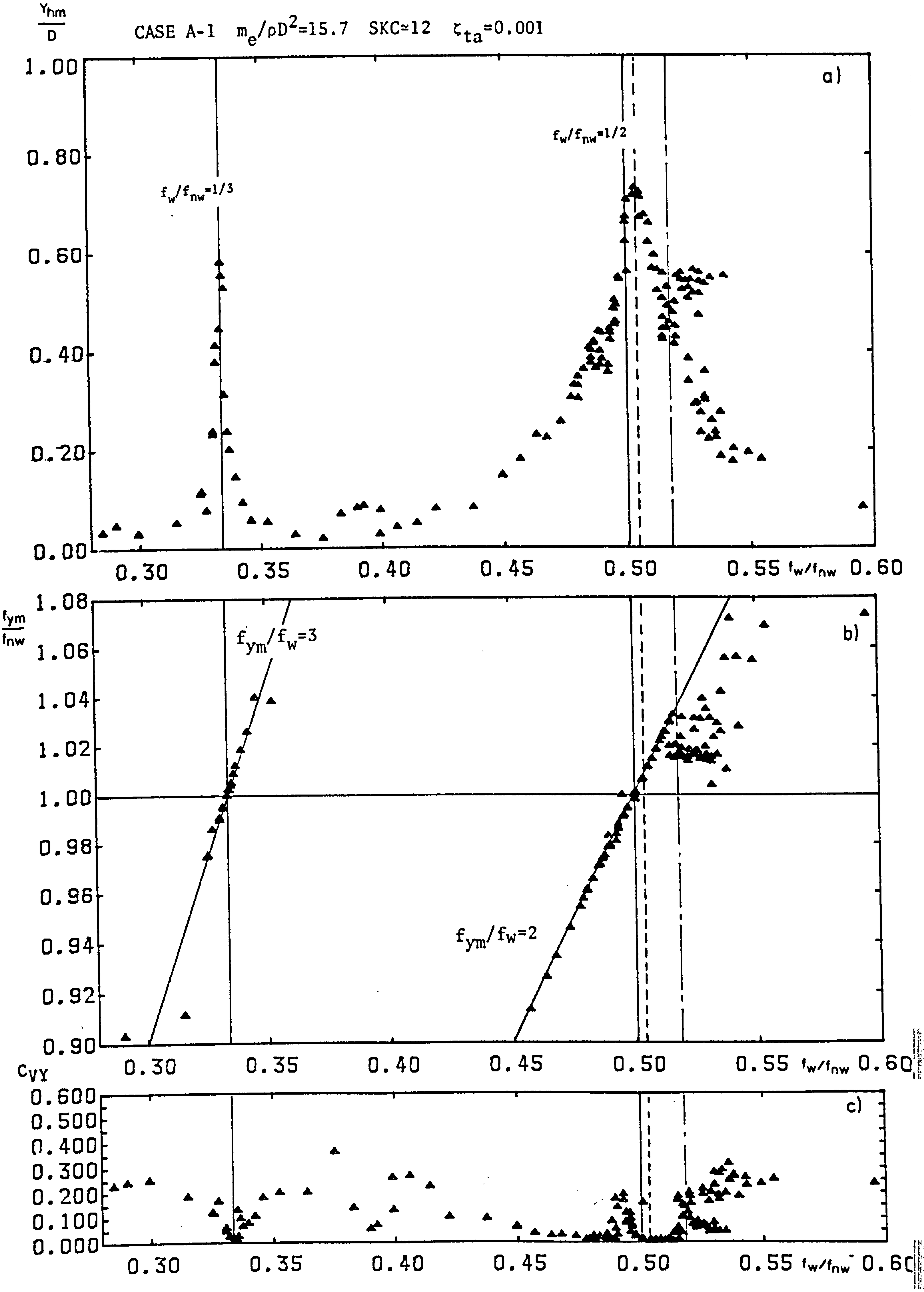

Fig. 5.4.13 The Plots of Y_{hm}/D, f_{ym}/f_{nw} and C_{VY} against f_w/f_{nw} for CASE A-1

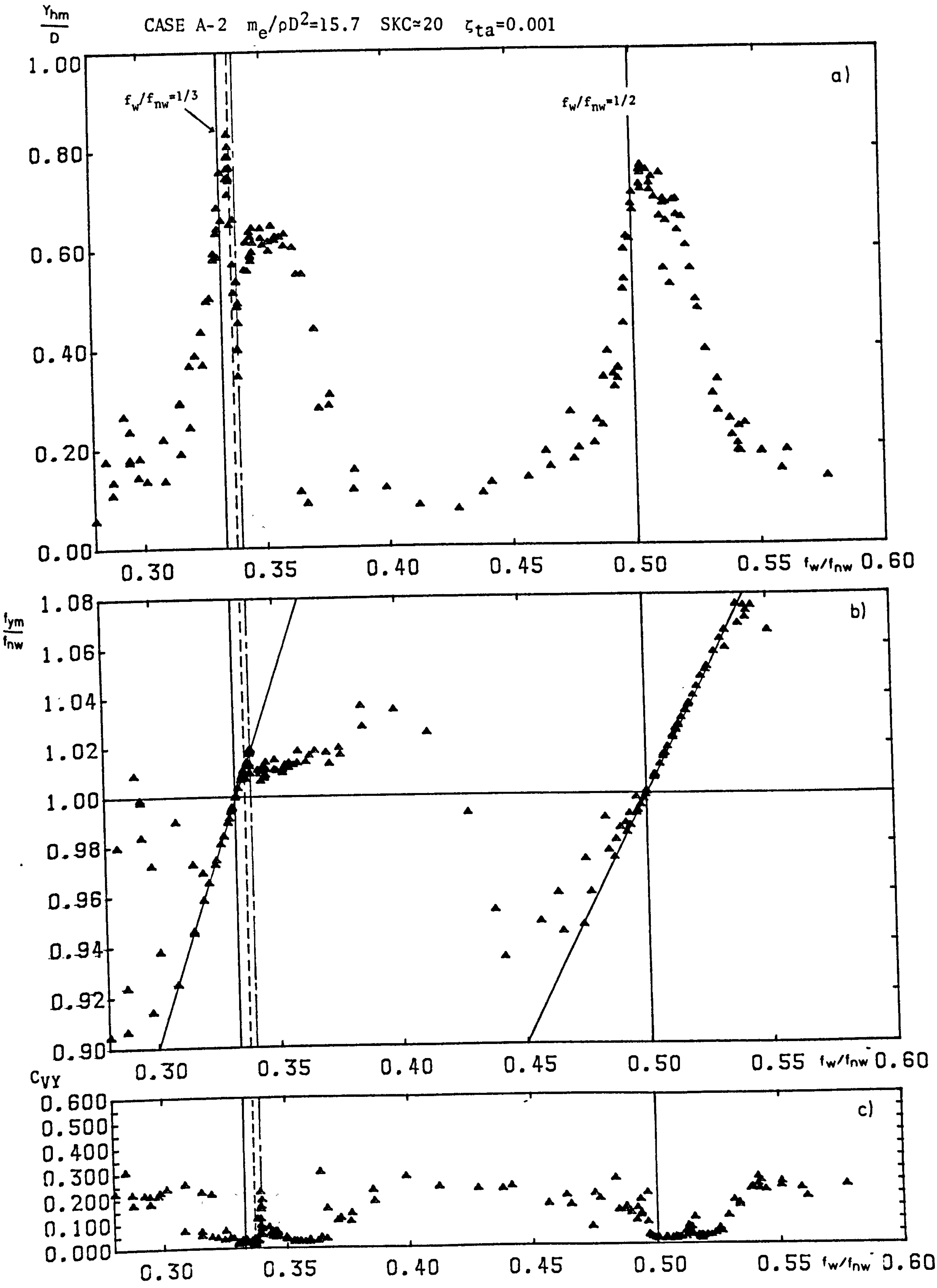

Fig. 5.4.14 The Plots of Y_{hm}/D, f_{ym}/f_{nw} and C_{VY} against f_w/f_{nw} for CASE A-2

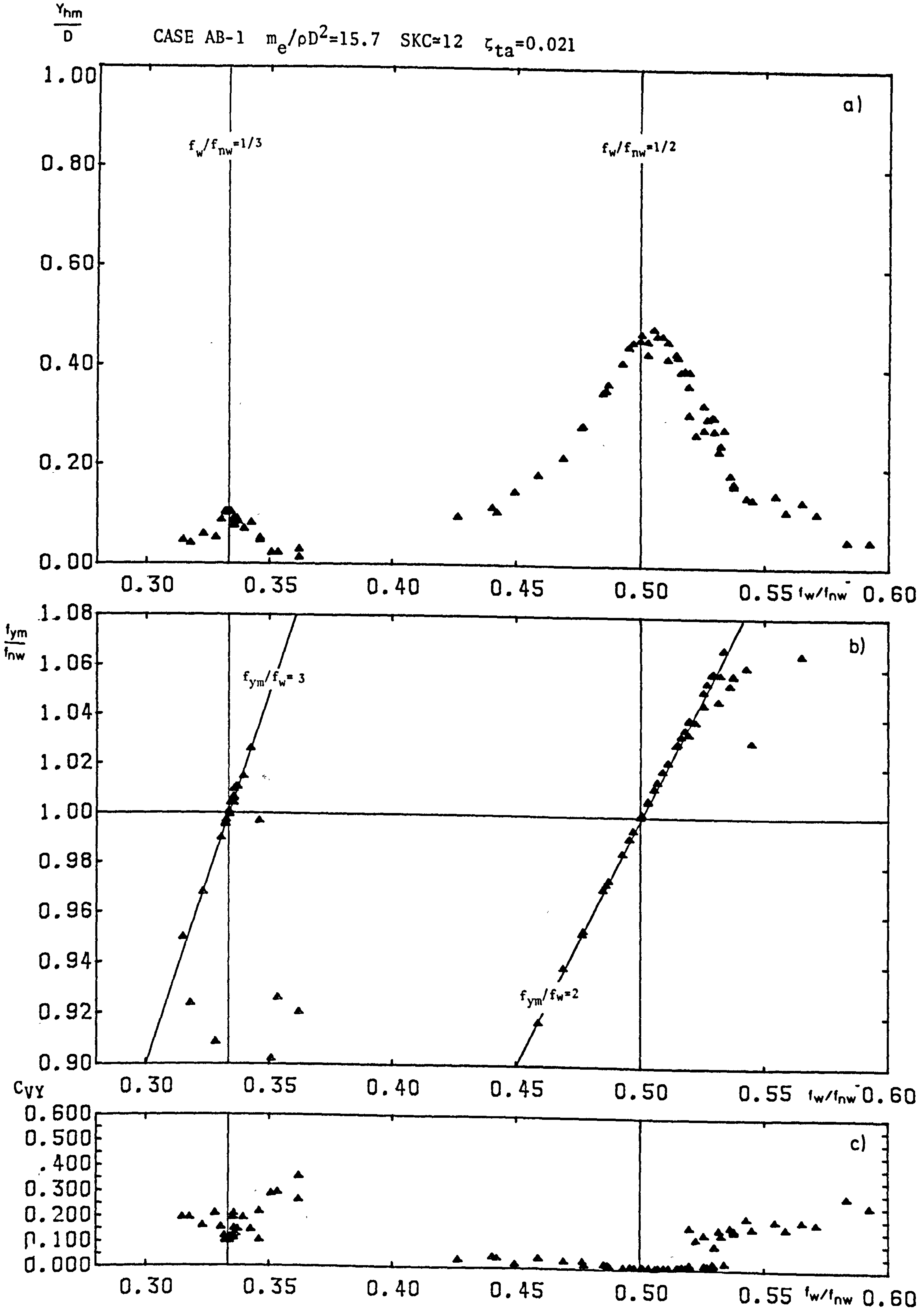

Fig. 5.4.15 The Plots of Y_{hm}/D, f_{ym}/f_{nw} and C_{VY} against f_w/f_{nw} for CASE AB-1

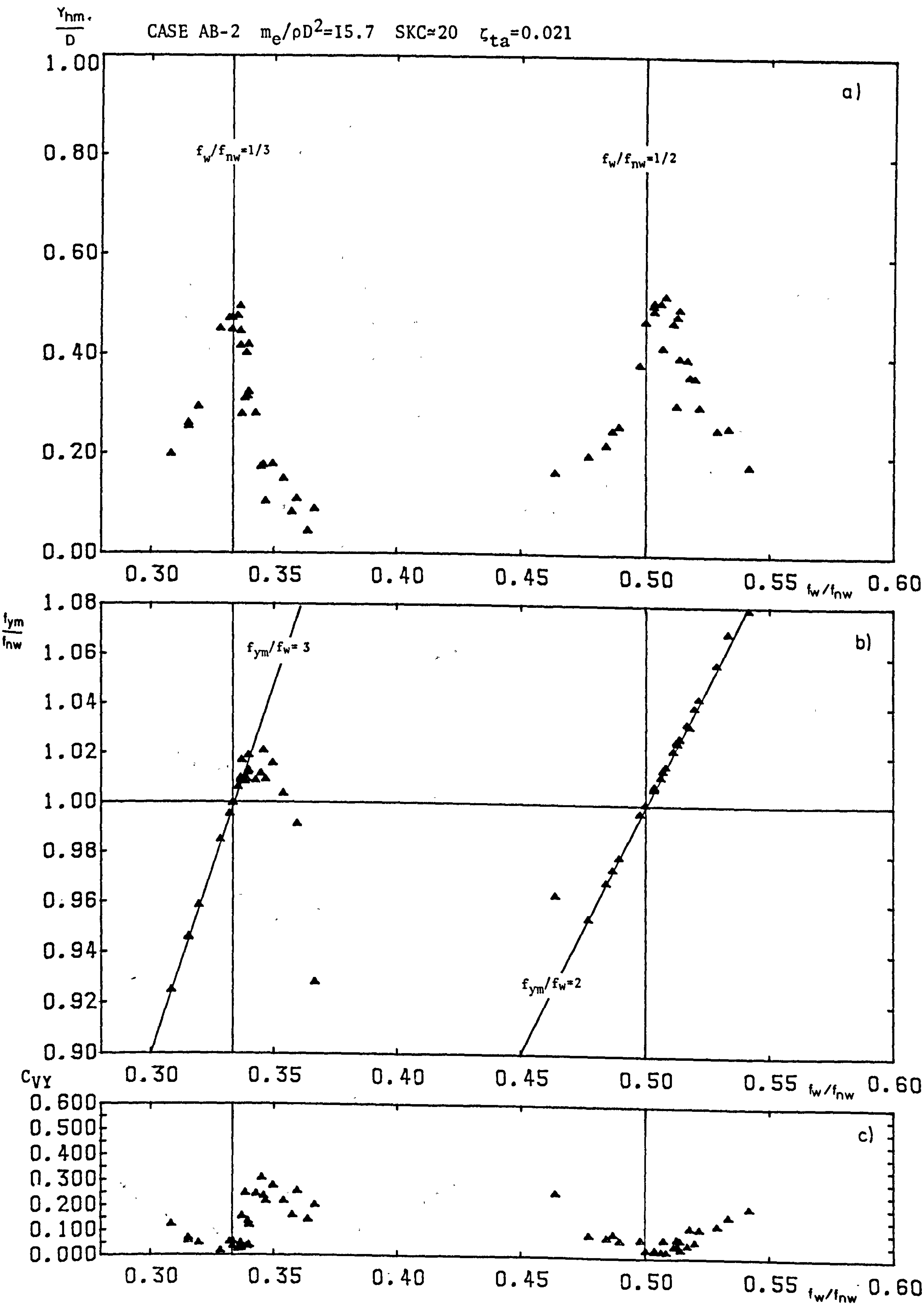

Fig. 5.4.16 The Plots of Y_{hm}/D, f_{ym}/f_{nw} and C_{VY} against f_w/f_{nw} for CASE AB-2

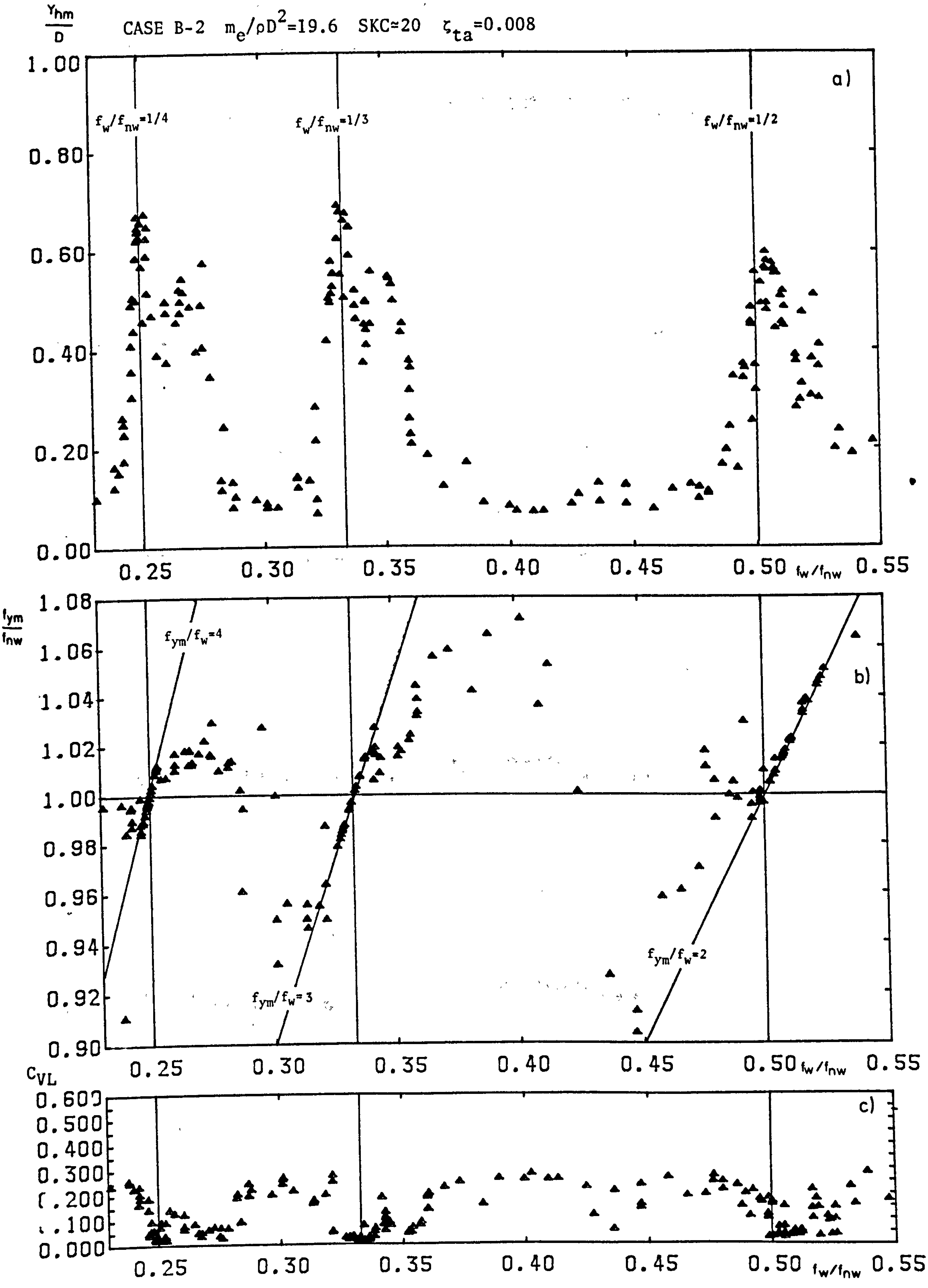

Fig. 5.4.17 The Plots of Y_{hm}/D, f_{ym}/f_{nw} and C_{VY} against f_w/f_{nw} for CASE B-2

(a)--CASE A-1 $\zeta_{ta}=0{\cdot}001$ $f_n=f_{nw}=1{\cdot}461Hz.$

(b)--CASE AS-I $\zeta_{ta}=0{\cdot}021$ $f_n=f_{nw}=1{\cdot}461Hz$

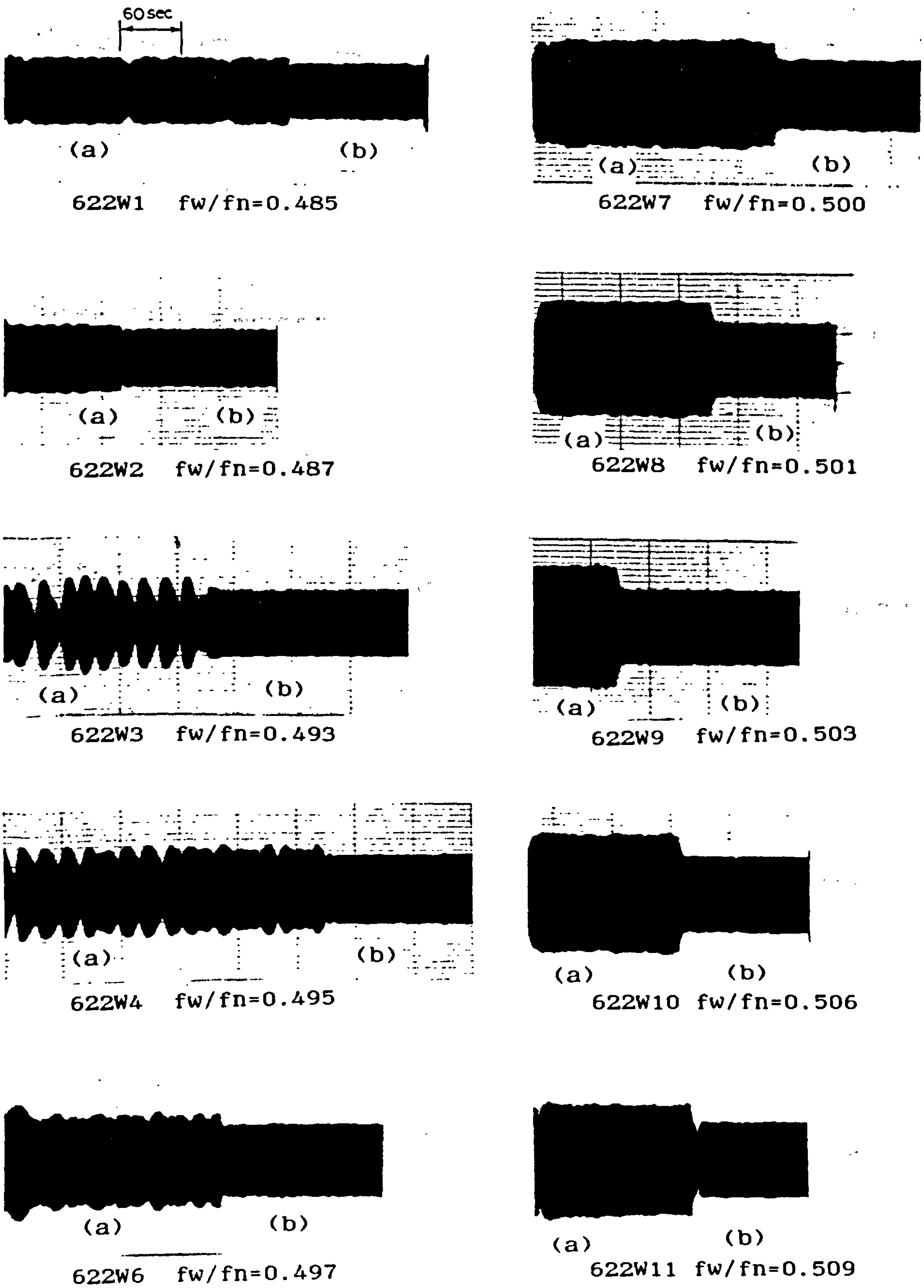

Fig. 5.4.18 The Variation of the Amplitude of the Cylinder with Time(t) for CASE A-1 and CASE AS-1 for f_w/f_{nw} in the Range of between 0.485 to 0.543

(a)--CASE A-1 $\zeta_{ta} = 0.001$ $f_n = f_{nw} = 1.461$Hz

(b)--CASE AS-1 $\zeta_{ta} = 0.021$ $f_n = f_{nw} = 1.461$Hz

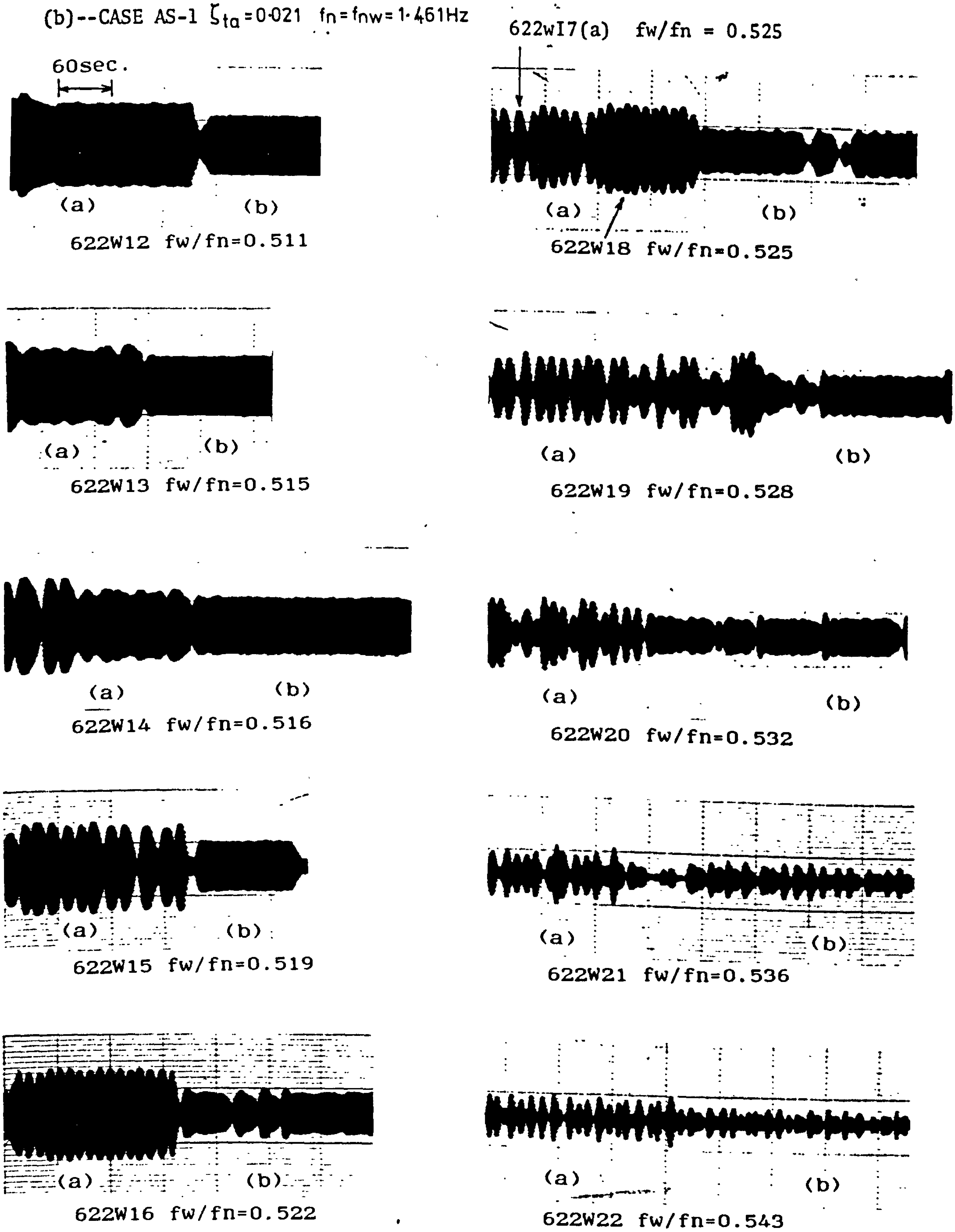

Fig. 5.4.18 (continued)

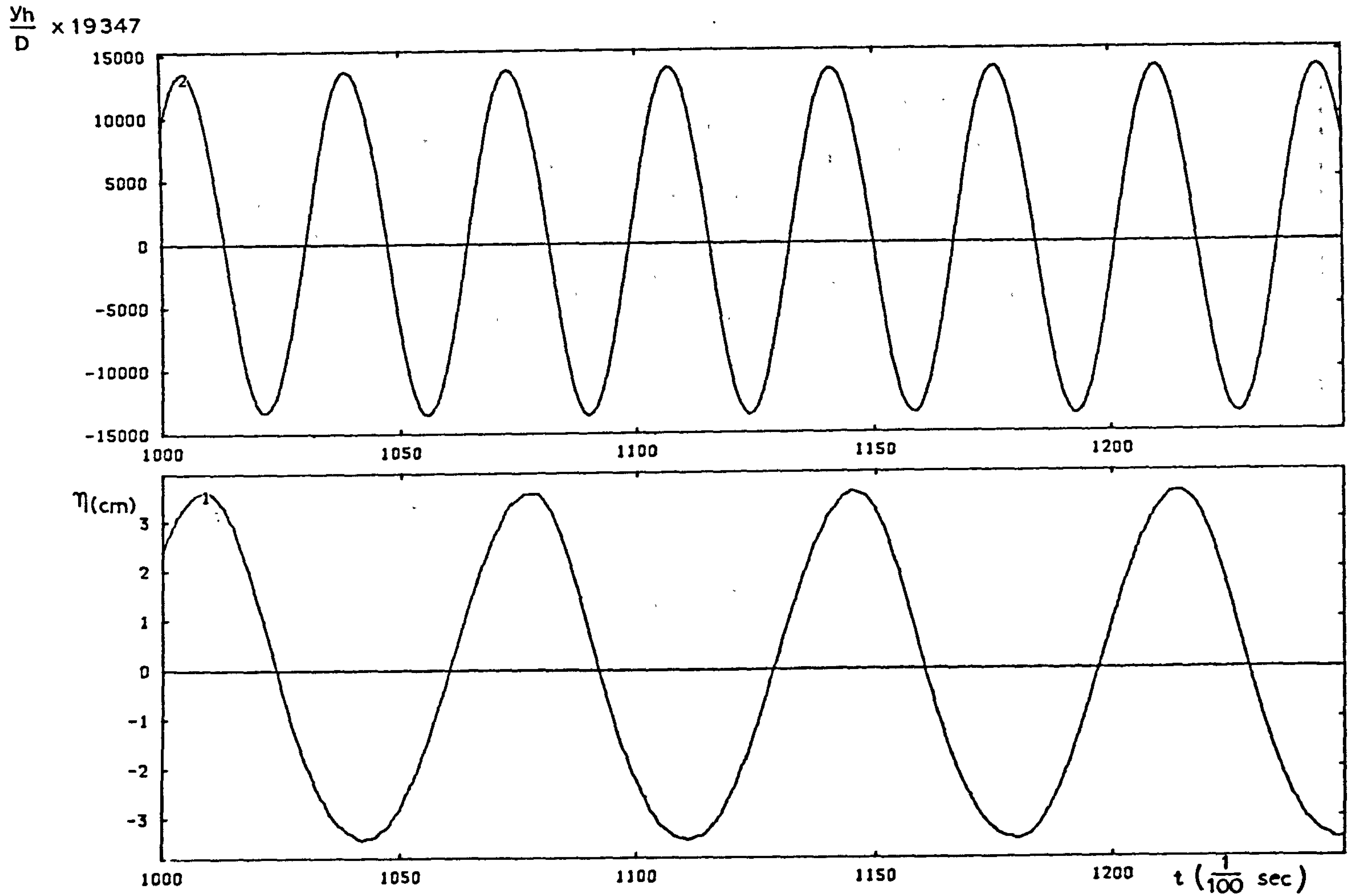

Fig. 5.4.19 The Variation of y_h/D and Water Surface Elevation(η) with Time(t) for the Data of Run No. 622w9(a)

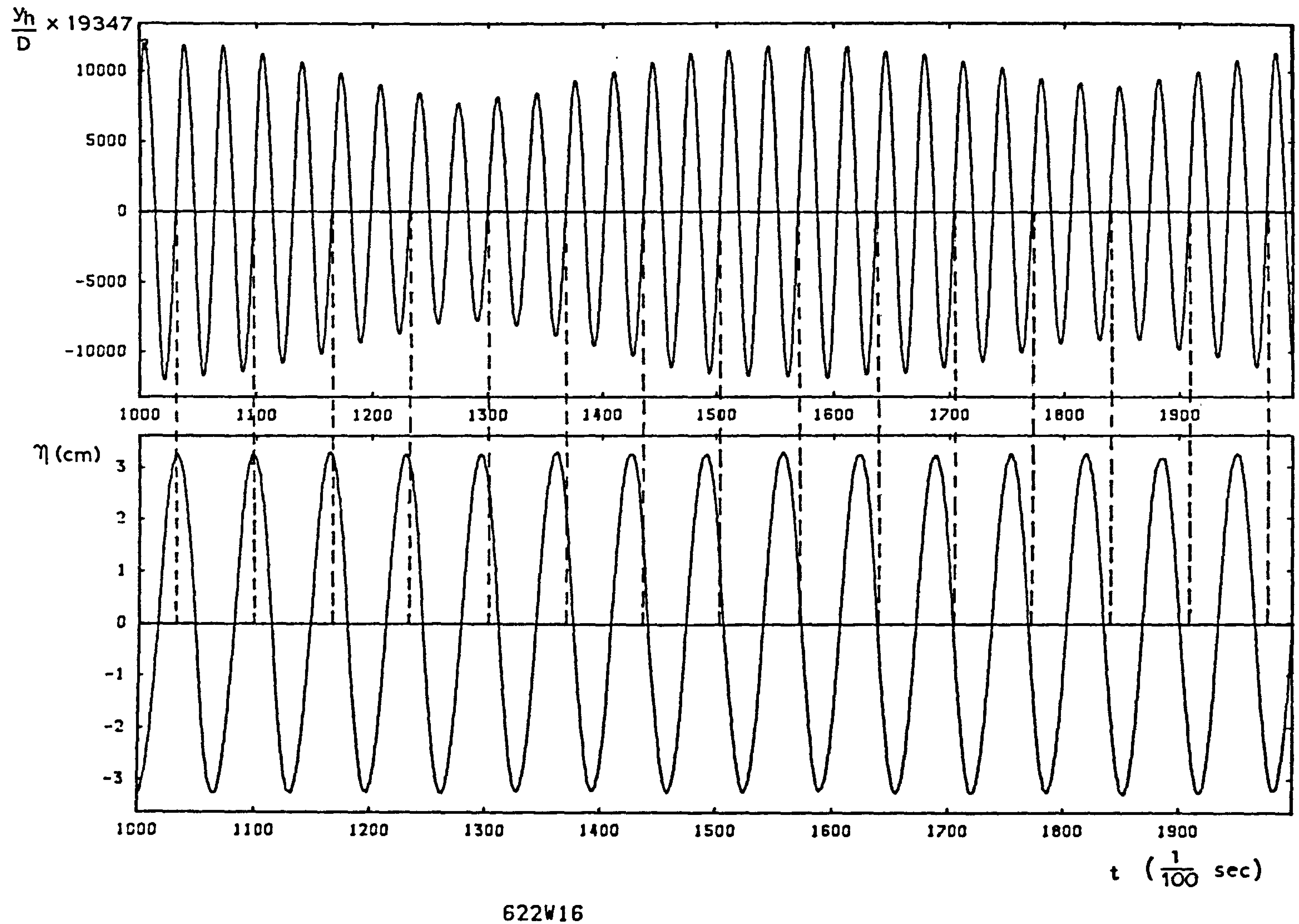

Fig. 5.4.20 The Variation of y_h/D and Water Surface Elevation (η) with Time(t) for the Data of Run No. 622w16(a)

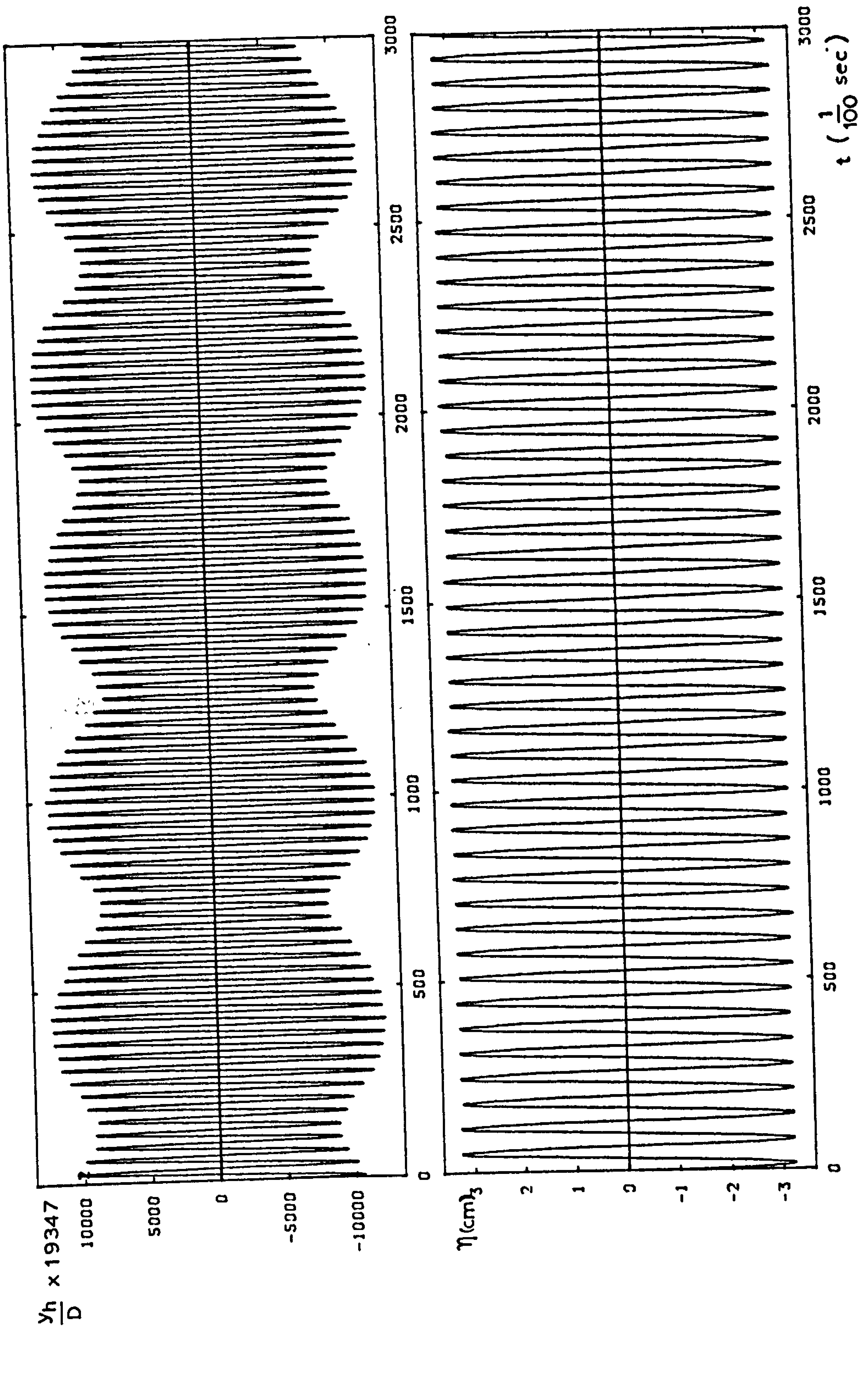

622W16

Fig. 5.4.20 (continued)

Table 5.2 Summary of Experimental Conditions and Results of Several Examples for CASE A-1 and CASE AB-1

(a) CASE A-1 $\zeta_{ta} = 0.001$, $\zeta_{tw} = 0.004$, $m_e/\rho D^2 = 15.7$, $f_{nw} = 1.46/Hz$

(b) CASE AB-1 $\zeta_{ta} = 0.021$, $\zeta_{tw} = 0.023$, $m_e/\rho D^2 = 15.7$, $f_{nw} = 1.46/Hz$

Run No.	SKC	SR_e	f_w/f_{nw}	kd	(a) CASE A-1				(b) CASE AB-1			
					f_{ym}/f_{nw}	Y_{hm}/D	C_{VY}	$\phi_A(2)$	f_{ym}/f_{nw}	Y_{hm}/D	C_{VY}	$\phi_A(2)$
622W1	12.99	3341	0.485	1.72	0.971	0.407	0.018	11°	0.970	0.349	0.017	30°
622W2	11.93	3081	0.487	1.74	0.974	0.419	0.016	12	0.974	0.366	0.010	35
622W3	11.67	3047	0.493	1.77	0.984	0.371	0.192	-2	0.985	0.411	0.007	33
622W4	12.00	3152	0.495	1.79	0.991	0.454	0.094	15	0.991	0.442	0.008	44
622W5	11.98	3147	0.495	1.79	0.991	0.503	0.042	18				
622W6	11.85	3124	0.497	1.80	0.995	0.545	0.030	26	0.994	0.451	0.007	50
622W7	11.63	3081	0.500	1.81	1.000	0.663	0.010	42	1.000	0.456	0.008	60
622W8	12.18	3233	0.501	1.82	1.001	0.708	0.009	47	1.001	0.468	0.006	61
622W9	11.29	3012	0.503	1.83	1.006	0.717	0.005	68	1.006	0.454	0.006	69
622W10	12.38	3317	0.506	1.85	1.011	0.723	0.007	92	1.011	0.479	0.005	74
622W11	12.39	3345	0.509	1.87	1.019	0.661	0.005	120	1.019	0.465	0.006	89
622W12	11.15	3019	0.511	1.88	1.022	0.569	0.010	135	1.022	0.419	0.006	97
622W13	12.13	3311	0.515	1.91	1.030	0.507	0.040	142	1.030	0.424	0.007	107
622W14	12.05	3299	0.516	1.92	1.033	0.447	0.035	141	1.033	0.394	0.009	114
622W15	12.05	3318	0.519	1.94	1.023	0.415	0.199	176	1.034	0.307	0.161	149
622W16	11.15	3085	0.522	1.95	1.014	0.545	0.061	172	1.039	0.267	0.117	98
622W17	12.29	3421	0.525	1.97	1.027	0.585	0.190		1.046	0.277	0.134	153
622W18	12.39	3451	0.525	1.97	1.018	0.529	0.069	178	1.051	0.327	0.016	136
622W19	12.31	3450	0.528	1.99	1.039	0.295	0.199		1.058	0.303	0.022	135
622W20	12.43	3502	0.532	2.01	1.031	0.308	0.187		1.047	0.234	0.154	215
622W21	11.41	3243	0.536	2.04	1.042	0.224	0.284		1.054	0.186	0.166	195
622W22	11.48	3302	0.543	2.09	1.056	0.175	0.258		1.061	0.141	0.202	192

The most remarkable result described above is the appearance of the two peaks of Y_h/D, produced by the perfect resonance coupled with wave and vortex coupling. The perfect resonance appears in the range of lock-on in the case of steady flow, but in waves, it appears only near to f_w/f_{nw} = 1/2, 1/3, 1/4 ... as described above, elsewhere vortex coupling may occur as described above.

The appearance of two peaks of response in waves has been reported by Zedan et al. (1980). However, it is not clear whether their results were due to the same mechanism.

5-4-3 The variation of Y_{hm}/D with SKC

In order to show how the value of Y_{hm}/D varies with SKC, the relationships between Y_{hm}/D and SKC for each CASE A-3, A-4, A-5, A-6, A-7, A-8, A-9, A-11, CASE AB-4, AB-5, and CASE B-3, B-4, B-5 are shown in Fig. 5.4.21 through Fig. 5.4.24. In each of these test cases, the frequency ratio f_w/f_{nw} was fixed at one value around the perfect resonant frequencies, f_w/f_{nw} = 1/2, 1/3 or 1/4. Therefore, using a constant water depth, the value of f_w/f_{nw} is determined by kd in the present data. The value of kd corresponding to each value of f_w/f_{nw} is also shown in these figures. The experimental conditions of these test cases are shown in Table 1 and explained in section 4-6-5. In the runs of CASE A and CASE AB, the test cylinder was free to vibrate only in the transverse direction, while in those of CASE B it was free to vibrate in any direction. In the runs of CASE A, the damping factor of the test cylinder in air, ζ_{ta}, was 0.001. On the other hand, in the runs of CASE AB, ζ_{ta} was changed from 0.001 to 0.021 by using the electro-magnetic damper.

(a) The runs of CASE A ($m_e/\rho D^2$ = 15.7, ζta = 0.001)

The relationship between Y_{hm}/D and SKC for CASE A-11; f_w/f_{nw} = 0.525, CASE A-9; f_w/f_{nw} = 0.503, CASE A-8; f_w/f_{nw} = 0.500, and CASE A-7; f_w/f_{nw} = 0.495 are shown in Fig. 5.4.21.

The similar relationship for CASE A-6 (f_w/f_{nw} = 0.35), CASE A-5 (f_w/f_{nw} = 0.335), CASE A-4 (f_w/f_{nw} = 0.26), and CASE A-3 (f_w/f_{nw} = 0.25) are shown in Fig. 5.4.22.

The value of Y_{hm}/D for CASE A-9 (f_w/f_{nw} = 0.503, kd = 1.83) probably shows the peak value of perfect resonance, which may occur around $f_w/f_{nw} \cong 1/2$ as shown in Fig. 5.4.13 for SKC $\cong$ 12, and Fig. 5.4.14 for SKC $\cong$ 20. This value is large in the range of SKC between 10 to 25. This may be due to the domination of the second harmonic component of the effective lift coefficient, $C_{Le}(2)$, in the range of SKC between 10 to 25, as shown in Fig. 5.3.1(c) for CASE AS-5, kd = 1.79, and the amplification of $C_{Le}(2)$ produced by vortex-excited vibration. This amplification of $C_{Le}(2)$ will be considered later.

The values of Y_{hm}/D for CASE A-7 (f_w/f_{nw} = 0.495, kd = 1.78) and for CASE A-11 (f_w/f_{nw} = 0.525, kd = 1.97) are plotted in order to show the appearance of vortex-coupling. As shown in Fig. 5.4.12 for CASE A-1; SKC = 12 and in Fig. 5.4.13 for CASE A-2; SKC = 20, when vortex-coupling occurs in this case at f_w/f_{nw} = 0.525, the value of Y_{hm}/D is probably larger than that of Y_{hm}/D at f_w/f_{nw} = 0.495.

Although further from resonance, the value of Y_{hm}/D for f_w/f_{nw} = 0.525 is similar to the value of Y_{hm}/D for f_w/f_{nw} = 0.495 over the whole range of SKC. This may be due to the appearance of vortex-coupling. In the range of SKC between 13 and 17, the value of Y_{hm}/D for f_w/f_{nw} = 0.525 seems to be smaller than the value of Y_{hm}/D for f_w/f_{nw} = 0.495. This is probably due to the absence of vortex-coupling or the variation of the range of vortex-coupling for f_w/f_{nw}.

The value of Y_{hm}/D for f_w/f_{nw} = 0.335, kd = 1.01 (see Fig. 5.4.22) probably shows the peak value of perfect resonance close to $f_w/f_{nw} \cong 1/3$ as shown in Fig. 5.4.13 for SKC ≅ 12 and Fig. 5.4.14 for SKC ≅ 20. The appearance of a peak value at SKC ≅ 22 may be due to the domination of the third harmonic component, $C_{Le}(3)$, around SKC ≅ 20 as shown in Fig. 5.3.1(b) for CASE AS-4, kd = 1.01. The convergence of Y_{hm}/D for f_w/f_{nw} = 0.35 to Y_{hm}/D for f_w/f_{nw} = 0.335, in the range of SKC between 15 and 25, may be due to the appearance of vortex-coupling as shown in Fig. 5.4.14 for SKC ≅ 20. It should be noted that although it is further from the response frequency Y_{hm}/D for f_w/f_{nw} = 0.35 is larger than Y_{hm}/D for f_w/f_{nw} = 0.335 for the range of SKC over 26.

The value of Y_{hm}/D for f_w/f_{nw} = 0.251, kd = 0.71 has a peak value around SKC ≅ 32 and is large in the range of SKC between 30 and 36. However, in the range of SKC < 27, it is smaller than Y_{hm}/D for f_w/f_{nw} = 0.26. This may be due to the appearance of a peak value of Y_{hm}/D at $f_w/f_{nw} \cong 0.26$ as shown in Fig. 5.4.2. The value of Y_{hm}/D for f_w/f_{nw} = 0.26 is large over a wider range of SKC, between 20 and 40.

(b) The runs of CASE AB ($m_e/\rho D^2$ = 15.7, ζta = 0.021)

The variation of Y_{hm}/D with SKC for CASE AB-4; f_w/f_{nw} = 0.335, ζta = 0.021 and CASE AB-5; f_w/f_{nw} = 0.503, ζta = 0.021 are shown in Fig. 5.4.23. In order to study the influence of the damping factor on the results, the data of Y_{hm}/D for CASE A-5; f_w/f_{nw} = 0.335, ζta = 0.001 and CASE A-9; f_w/f_{nw} = 0.503, ζta = 0.001 are also plotted in this figure.

In both cases, values of Y_{hm}/D for CASE AB-4 and CASE AB-5 are smaller than those of CASE A-3 and CASE A-9, because of the increased damping. However, the variation of Y_{hm}/D with SKC for CASE AB-3 is similar to that of CASE A-5 and the variation of Y_{hm}/D with SKC for CASE AB-5 is also similar to that of CASE A-9.

(c) Runs of CASE B($m_e/\rho D^2$ = 19.6, ζta = 0.008)

The variation of Y_{hm}/D with SKC for CASE B-3 (f_w/f_{nw} = 0.25, kd = 0.57), CASE B-4 (f_w/f_{nw} = 0.336, kd = 0.8) and CASE B-5 (f_w/f_{nw} = 0.506, kd = 1.36), are shown in Fig. 5.4.24. The phenomena observed for CASE B-5 (f_w/f_{nw} = 0.506) and CASE B-4 (f_w/f_{nw} = 0.336) are similar to those of CASE A-9 (f_w/f_{nw} = 1.83) and CASE A-5 (f_w/f_{nw} = 0.335) respectively. However, the maximum value of Y_{hm}/D of CASE B-3; f_w/f_{nw} = 0.25 appears at around SKC ≅ 25 instead of SKC ≅ 32, for CASE A-3; f_w/f_{nw} = 0.25.

Fig. 5.4.21 The Variation of Y_{hm}/D with SKC for CASE A-7, A-8, A-9 and A-11

Fig. 5.4.22 The Variation of Y_{hm}/D with SKC for CASE A-3. A-4, A-5 and A-6

Fig. 5.4.23 The Variation of Y_{hm}/D with SKC for CASE AB-2, AB-5, A-5 and A-9

Fig. 5.4.24 The Variation of Y_{hm}/D with SKC for CASE B-3, B-4 and B-5

An important and unexpected conclusion from the results described above, is that the variation of Y_{hm}/D with SKC for several values of f_w/f_{nw} has a broad response over a wide range of SKC. This may be also due to the non-linear dynamic amplification of each harmonic component of the lift force by means of the increased vortex strength and correlation in the phase of vortex-shedding along the cylinder axis.

The results of the present study are similar to those of Isaacson et al. (1981) which was restricted to the range of SKC between 5 to 18. The results for SKC over 20 have apparently never been previously reported. The appearance of the large value of Y_{hm}/D for $f_w/f_{nw} \fallingdotseq$ 0.25 over a broad range of SKC should be noted as a significant feature of the response of a flexibly supported cylinder. Although a large response was observed at $f_w/f_{nw} \fallingdotseq 1/5$ and 1/6, not enough data at these frequencies was collected to plot the results as a function of SKC.

5-4-4 The variation of Y_{hm}/D at perfect resonance with normalised damping

In order to study the influence of the damping on the value of Y_{hm}/D at the perfect resonant condition, the relationship between Y_{hm}/D and the normalised damping, $2m_e(2\pi\ \zeta_{ta})/\rho D^2$, for CASE AC-2, CASE AC-3, CASE AC-4 and CASE AC-5, are shown in Fig. 5.4.25 and Fig. 5.4.26. The experimental conditions of these test cases are shown in Table 1. It should be noted that $2m_e(2\pi\ \zeta_{ta})/\rho D^2$ is a function of only ζ_{ta} because the mass ration $m_e/\rho D^2$ is fixed in these test cases. In this case, the test cylinder was free to vibrate only in the transverse direction. In the runs of CASE AC-2, CASE AC-3 and CASE AC-4, the frequency ratio f_w/f_{nw} was fixed at $f_w/f_{nw} = 0.503$ at which the perfect resonance probably occurred as shown in Fig. 5.4.13 for SKC ≈ 12 and Fig. 5.4.14 for SKC ≈ 20. Each value of SKC for these test cases was fixed as follows; CASE AC-2, SKC = 8.7, CASE AC-3, SKC = 12, CASE AC-4, SKC = 20. On the other hand, in the runs of CASE AC-5, the frequency ratio f_w/f_{nw} is fixed at $f_w/f_{nw} = 0.336$ at which the perfect resonance probably occurred as shown in Fig. 5.4.14 and SKC was fixed at 20.

In the case of steady flow, good correlation between the normalised maximum amplitude, A_y/D, in the perfect resonant condition and the normalised damping has been reported by Griffin et al. (1975), and Iwan (1975). Therefore, the data of A_y/D of cylinders pivoted flexibly in steady flow, obtained by Vickery et al. (1962), and Hartlen et al. (1968), after Iwan (1975), are plotted in these figures for comparison with present data.

The data of CASE AC-2; SKC = 8.7, CASE AC-3; SKC = 12 and CASE AC-4; SKC = 20 are shown in Fig. 5.4.25. Each Y_{hm}/D for these test cases increases with decreasing normalised damping and approaches a limiting value. This phenomenon is similar to that of steady flows. However, the limiting values of the present data are smaller compared with that of steady flow. This may be due to the difference of the vortex shedding and vortex-excited vibration for these two cases. Y_{hm}/D for CASE AC-3 and CASE AC-4 are nearly the same as those of steady flow around $2m_e(2\pi\ \zeta_{ta})/\rho D^2 \simeq 5$. (This may show the amplification of lift force).

In order to show the influence of f_w/f_{nw} on the variation of Y_{hm}/D with normalised damping, the results of CASE AC-4; ($f_w/f_{nw} = 0.336$, SKC = 20) and CASE AC-5 ($f_w/f_{nw} = 0.336$, SKC = 20) are shown together in Fig. 5.4.26. The difference between them is negligible in the range of $2m_e(2\pi\ \zeta_{ta})/\rho D^2 < 1.5$. However, Y_{hm}/D of CASE AC-5 is smaller compared with those of CASE AC-4 around $2m_e(2\pi\ \zeta_{ta})/\rho D^2 = 4$.

As shown in Eq.(3-29) on a linearised model, the value of Y_{hm}/D may be expected to be inversely proportional to the normalised damping. However, this relationship is not apparent in Figures 5.4.25 and 5.4.26. This may be due to the variations of the lift force or damping coefficient, probably produced by the vortex-excited vibration.

The appearance of limiting values of Y_{hm}/D for small values of the normalised damping suggests a state of stable equilibrium in which an increase in Y_{hm}/D is associated with an increase in fluid damping (as observed in the case of free vibration in still water, see Fig. 5.2.6).

The number of previous measurements of the response amplitude at perfect response in waves or in harmonic flows is small, as described in Chapter 2. The comparison between Y_{hm}/D for CASE AC-2, CASE AC-3 and CASE AC-4, and Y_{hm}/D or Y_{hmax}/D obtained by Zedan et al. (1980), Isaacson et al. (1981), Angrili et al. (1982), Bullock et al. (1978) and Rajabi (1979) are shown in Fig. 5.4.27. The data of Rajabi (1979) was obtained in harmonic flow. The experimental conditions and symbols in Fig. 5.4.27 for these data are shown in Table 5.3. Y_{hmax} is the maximum amplitude at still water level in waves, and in the case of harmonic flow the maximum amplitude. When cylinder vibrates at nearly perfect resonant condition, the difference between Y_{hm}/D and Y_{hmax} may be small as described previously.

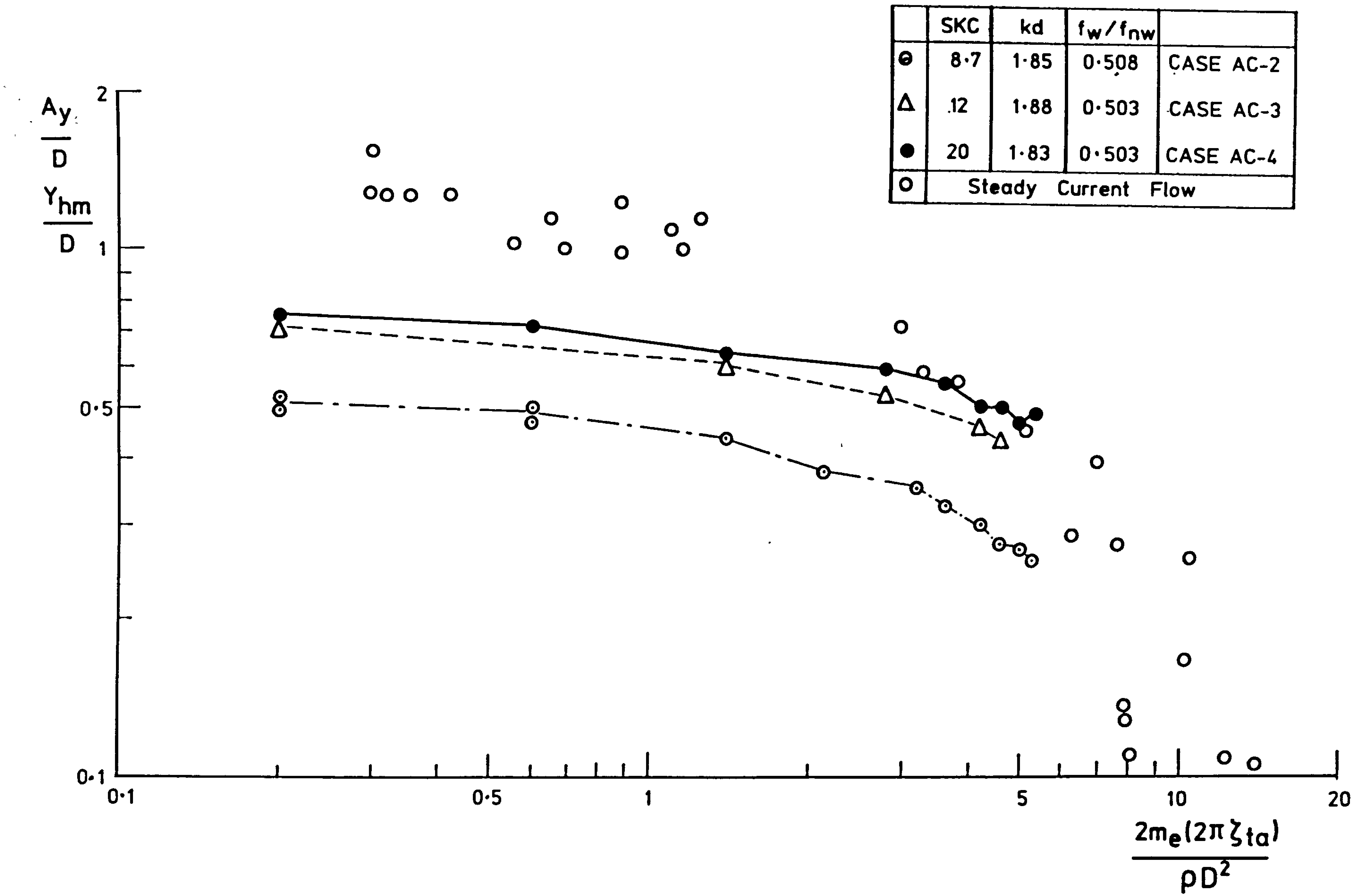

Fig. 5.4.25 Dimensionless Amplitude(Y_{hm}/D for CASE AC-2, AC-3, AC-4 and A_y/D for Steady Flow after Iwan(1975)) vs. Normalised Damping($2m_e(2\pi\zeta_{ta}))/\rho D^2$

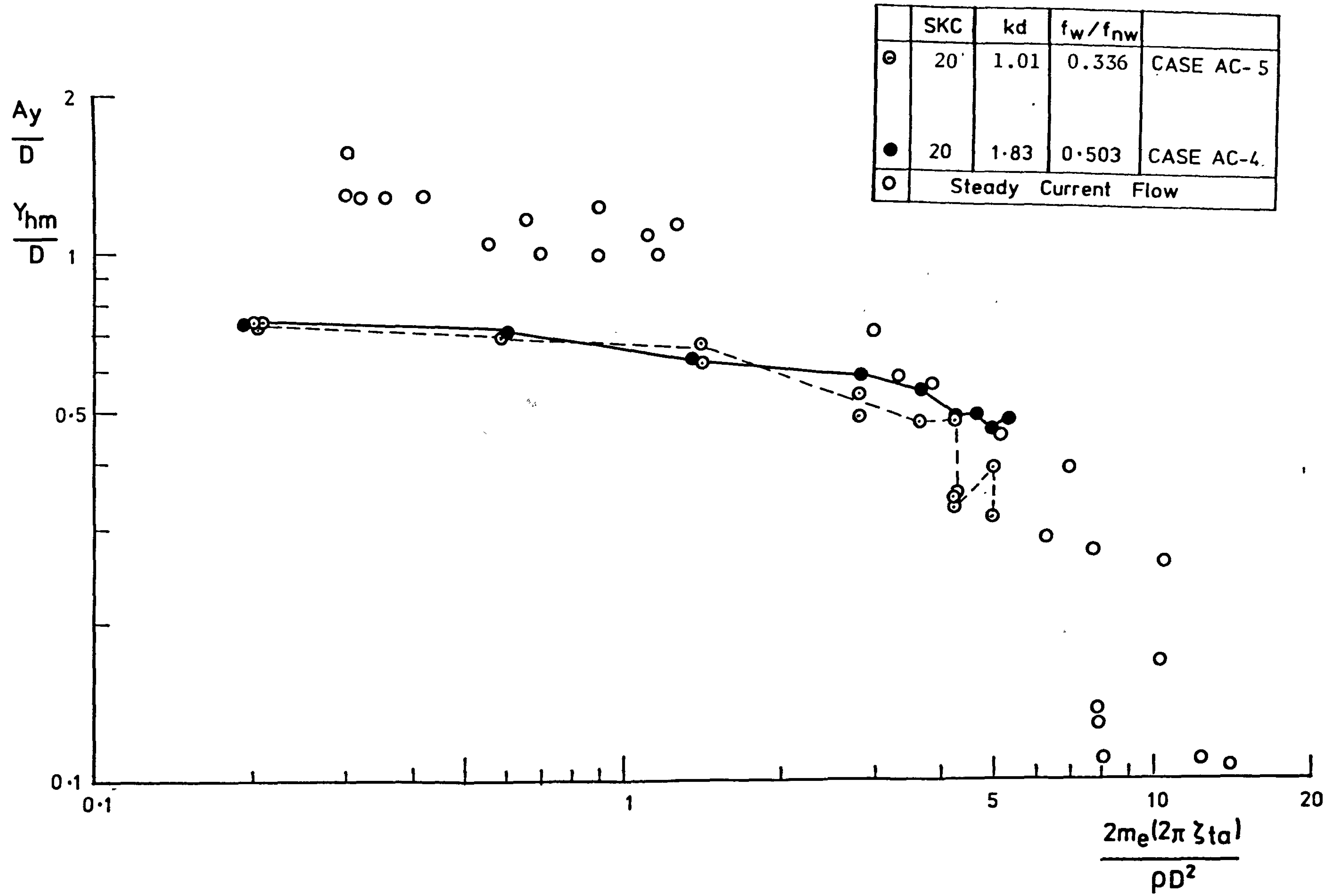

Fig. 5.4.26 Dimensionless Amplitude(Y_{hm}/D for CASE AC-4 and AC-5 and A_y/D for Steady Flow after Iwan(1975)) vs. Normalised Damping$(2m_e(2\pi\zeta_{ta}))/\rho D^2$

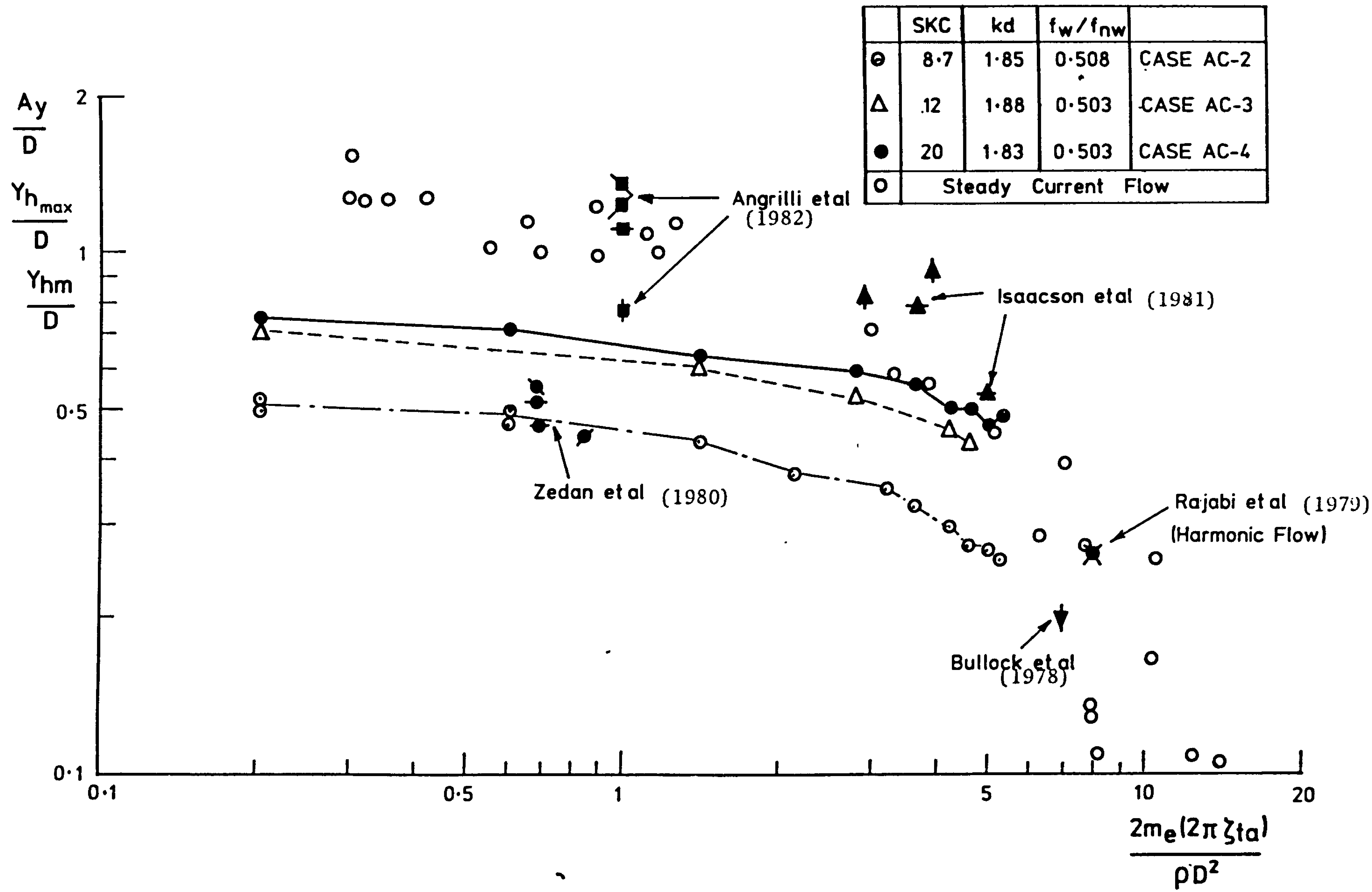

Fig. 5.4.27 Dimensionless Amplitude(Y_{hm}/D for CASE AC-2, AC-3, AC-4 and A_y/D for Steady Flow after Iwan(1975), and Y_{hm}/D and Y_{hmax}/D in Table 5.3) vs. Normalised Damping($2m_e(2\pi\zeta_{ta}))/\rho D^2$

Table 5.3 The Response Amplitude at Perfect Response in Waves and in Harmonic Flow

(Description on the data in Fig. 5.4.27)

Investigator(s)	$m_e/\rho D^2$	$2m_e(2\pi\ \zeta_{ta})/\rho D^2$	f_w/f_{nW}	SKC	kd	Y_{hm}/D	Y_{hmax}/D	Symbol in Fig. 5.4.27	Type of Cylinder
Bullock et al. (1978)	17	6.83	$\simeq 1/4$	23			$\simeq 0.2$		Cantilevered Cylinder in Waves
Zedan et al. (1980)	22.9	0.832	$\simeq 1/2$	11.2	1.63		0.44		Cantilevered Cylinder in Waves
	13.3	0.668	$\simeq 1/2$	12.8	2.60		0.56		
	13.3	0.668	$\simeq 1/2$	11.0	2.60		0.47		
	13.3	0.668	$\simeq 1/2$	11.5	2.60		0.51		
Isaacson et al. (1981)	3.44	3.81	$\simeq 1/2$	15	1.02		0.92		Pivoted Cylinder in Waves
	3.44	4.91	$\simeq 1/2$	10	1.02		0.53		
	6.69	2.82	$\simeq 1/2$	15	1.02		0.82		
	6.69	3.54	$\simeq 1/2$	10	1.02		0.79		
Angrilli et al. (1982)	5.97	0.975	1	17.5	5.65	0.77			Cantilevered Cylinder in Waves
	5.97	0.975	1/2	11.5	1.53	1.11			
	5.97	0.975	1/3	17.8	0.88	1.26			
	5.97	0.975	1/4	35.9	0.62	1.37			
Rajabi (1979)	12	7.84	0.107	55			0.27		Rigid Cylinder Flexibly Supported in Harmonic Flow

The data for cylinders pivoted flexibly in steady flow are also plotted in this figure.

The correlation between the normalised amplitudes Y_{hm}/D or Y_{hmax}/D for perfect resonant conditions, in waves or in harmonic flows, with normalised damping is not as good as that for steady flows.

The present data is consistent with the data obtained by Zedan et al. (1980), Bullock et al. (1978) and Rajabi (1979). The agreement with the results of Isaacson et al. (1981) and Angrili et al. (1982) are poor.

5-4-5 <u>Characteristics of the lift force acting on the vortex-excited test cylinder in waves</u>

As described in (3-2-4), the lift force acting on the observed vortex-excited cylinder can be calculated by using Eq.(3-23) or Eq.(3-29) on the basis of a linear model. Therefore, when the mean value of both Y_{hm}/D and f_{ym}/f_{nw} are measured, the mean value of the effective coefficient of the lift force acting on the observed vortex-excited cylinder, C_{Lm}, may be calculated as follows by modifying Eq.(3-29).

$$C_{Lm} = \frac{8\pi^2 . (\frac{m_e}{\rho D^2}) . \sqrt{\{1 - (\frac{f_{my}}{f_n})^2 + (2\zeta_t . \frac{f_{my}}{f_n})^2}}{3F_S . (kd) . SKC^2 . (\frac{f_w}{f_n})^2} . (\frac{Y_{hm}}{D})$$

(5-4-4)

As described previously, the damping factor in the vortex-excited condition has an unknown value. Therefore, the following three kinds of damping factors, (measured in free vibration tests in air or in still water; see Fig. 5.2.1 through Fig. 5.2.4.), are used to calculate C_{Lm}:

ζ_{ta} = The damping factor in air at $Y_{hi}/D = 0.1$

ζ_{tw} = The damping factor in still water at $Y_{hi} \doteqdot 0.1$

ζ_{tv} = The damping factor in still water at $Y_{hi}/D = Y_{hm}/D$.

(It should be noted that ζ_{tv} is a function of Y_{hi}/D as shown in Fig. 5.2.3.)

Now, we define the lift coefficient calculated by using ζ_{ta} as C_{Lma}, the lift coefficient calculated by using ζ_{tw} as C_{Lmw}, and the lift coefficient calculated by using ζ_{tv} as C_{Lmv}.

5-4-5-1 The variation of lift coefficients C_{Lma}, C_{Lmw} and C_{Lmv} with f_w/f_{nw}

In order to study the variation of the lift force acting on the vortex-excited cylinder with f_w/f_{nw} around $f_w/f_{nw} \doteqdot 1/2$ (kd $\doteqdot$ 1.8), the relationship between f_w/f_{nw}, and Y_{hm}/D and C_{Lma}, C_{Lmw} and C_{Lmv} for CASE AB-1 (SKC $\doteqdot$ 12, ζ_{ta} = 0.021) are shown in Fig. 5.4.28 (a) and (b).

The lift force acting on the test cylinder when mounted stiffly in nearly the same wave conditions as those used in CASE AB-1 were obtained in CASE AS-1 (SKC $\doteqdot$ 12). The relationships between kd and

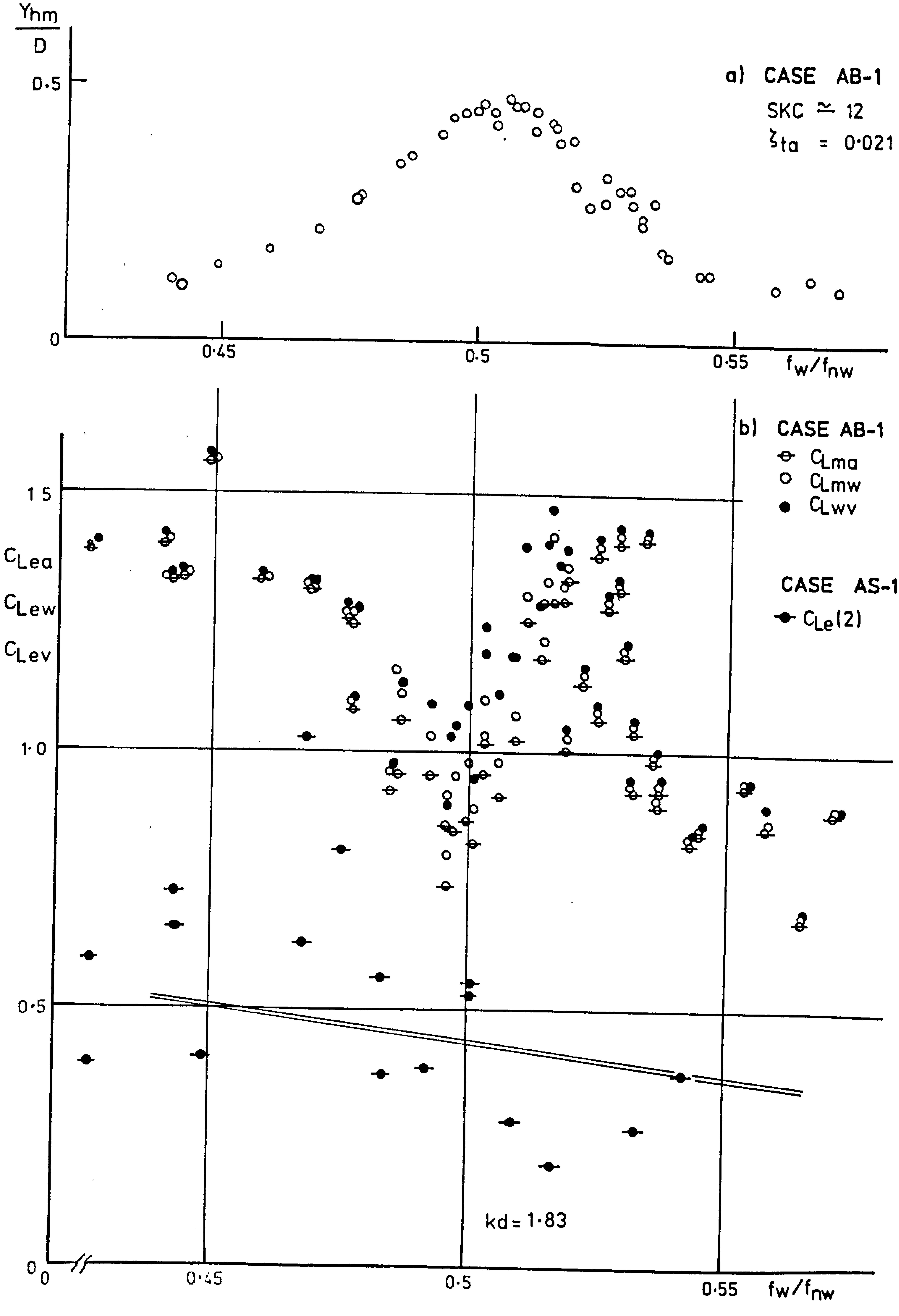

Fig. 5.4.28 The Plot of Y_{hm} and Lift Coefficients(C_{Lma}, C_{Lmw} and C_{Lmv}) against f_w/f_n for CASE AB-1

C_{Lemax}, C_{Le} and C_{VL} for CASE AS-1 were shown previously in Fig. 5.3.5. As shown in this figure, C_{VL} is large around kd ≈ 1.8, indicating that the amplitude of the lift force is unstable.

In order to evaluate the amplification of the lift coefficients, C_{Lma}, C_{Lmw} and C_{Lmv} for CASE AB-1, the second harmonic component of the lift coefficient, $C_{Le}(2)$, for CASE AS-1 is plotted in Fig. 5.4.28. The frequency of this $C_{Le}(2)$ corresponds to f_{ym}, because f_{ym}/f_{nw} for CASE AB-1 follows Eq.(5-4-2) at around $f_w/f_{nw} \approx 1/2$ (kd ≈ 1.8) as shown in Fig. 5.4.15.

The values, C_{Lma}, C_{Lmw} and C_{Lmv} are larger than $C_{Le}(2)$ over the whole range of f_w/f_{nw} in Fig. 5.4.28. This probably shows the amplification of lift force by means of vortex-excited vibration. It is interesting to note that the amplification of these lift coefficients has a minimum value around perfect resonance ($f_w/f_{nw} \approx 1/2$). In this range the vibration is a result of a state of equilibrium between vortex excitation and fluid damping. The minimum value in lift coefficient suggests that for large amplitudes the damping increases disproportionately.

5-4-5-2 The variation of lift coefficient, C_{Lma}, C_{Lmw} and C_{Lmv} with SKC

In order to inspect the variation of the lift force acting on the vortex-excited cylinder with SKC, the relationships between SKC, and Y_{hm}/D and C_{Lm} (C_{Lma}, C_{Lmw}, C_{Lmv}) for CASE A-5, A-9, AB-5 and AB-4 are shown respectively in Fig. 5.4.29 (a) and (b) through Fig. 5.4.32 (a) and (b).

In each of these test cases, the frequency ratio f_w/f_{nw} was fixed at one value around the perfect resonant frequencies; $f_w/f_{nw} \cong 1/2$ for CASE A-9 and AB-5, $f_w/f_{nw} \cong 1/3$ for CASE A-5 CASE AB-4. In the runs of CASE A-9 and A-5, the damping factor in air, ζ_{ta}, was 0.001. On the other hand, in the runs of CASE AB-5 and AB-4, ζ_{ta} was changed from 0.001 to 0.021 by using the electro-magnetic damper.

The lift forces acting on the test cylinder when mounted stiffly in the same wave conditions as those used in CASE A-9 and CASE AB-5 were obtained in the runs of CASE AS-5 (kd = 1.79). The second harmonic component of the lift coefficient, $C_{Le}(2)$ for CASE AS-5 is plotted in Fig. 5.4.29 and Fig. 5.4.30 in order to show the amplification of the lift coefficients C_{Lma}, C_{Lmw} and C_{Lmv} for CASE A-9 (f_w/f_{nw} = 0.503, kd = 1.83, ζ_{ta} = 0.001) and CASE AB-5 (f_w/f_{nw} = 0.503, kd = 1.83, ζ_{ta} = 0.021). The lift force acting on the test cylinder which was mounted stiffly in similar waves as those used in CASE A-5 and CASE AB-4 were obtained in the runs of CASE AS-4 (kd = 1.01). The third harmonic component of lift coefficient, $C_{Le}(3)$ for CASE AS-4 is plotted in Fig. 5.4.31 and Fig. 5.4.32 in order to show the amplification or attenuation of the lift coefficients C_{Lma}, C_{Lmw} and C_{Lmv} for CASE A-5 (f_w/f_{nw} = 0.335, kd = 1.01, ζ_{ta} = 0.001) and CASE AB-4 (f_w/f_{nw} = 0.335, kd = 1.01, ζ_{ta} = 0.021).

(1) Discussion of CASE A-9 (f_w/f_{nw} = 0.503, kd = 1.83, ζ_{ta} = 0.001, ζ_{tw} = 0.004) and CASE AB-5 (f_w/f_{nw} = 0.503, kd = 1.83, ζ_{ta} = 0.021, ζ_{tw} = 0.023)

The variation of each of the coefficients C_{Lma}, C_{Lmw} and C_{Lmv} with SKC for CASE A-9 are shown in Fig. 5.4.29(b). The difference between C_{Lma} and C_{Lmv} is the result of a large difference between ζ_{ta} and ζ_{tv} as shown in Fig. 5.2.23 (I_e = 0A). Each of C_{Lma}, C_{Lmw} and C_{Lmv} has a peak value at SKC ≈ 8. C_{Lma}, C_{Lmw} and C_{Lmv} are larger than $C_{Le}(2)$ in the range of SKC between 5 and 12. This show the amplification of the lift force. On the other hand, they are smaller than $C_{Le}(2)$ in the range of SKC over 15. This shows the attenuation of the lift force.

The variations of each C_{Lma}, C_{Lmw} and C_{Lmv} with SKC for CASE AB-5 are shown in Fig. 5.4.30(b). In this case, the difference between C_{Lma} and C_{Lmv} is smaller than that for CASE A-9 because the difference between ζ_{ta} and ζ_{tw} for CASE AB-5 is small as shown in Fig. 5.2.23 (I_e = 4A).

The lift coefficients C_{Lma}, C_{Lmw} and C_{Lmv} are also larger than $C_{Le}(2)$ in the range SKC between 5 and 15, and each of them has a peak value around SKC ≈ 8 as before. In the range of SKC over 15, each of them is nearly the same as $C_{Le}(2)$.

The values of Y_{hm}/D for CASE AB-5 are smaller than those of CASE A-9 because of the increase in the damping coefficient (ζ_{ta} = 0.021 for CASE AB-5, ζ_{ta} = 0.001 for CASE A-9). However, all three lift coefficients, but particularly C_{Lma}, for CASE AB-5 are larger than those for CASE A-9. These results suggest that the increased structural damping has the effect of reducing the amplitude of oscillation but increasing the lift coefficient. This shows the result of the state of equilibrium between vortex excitation and fluid damping.

(2) Discussion of CASE A-5 (f_w/f_{nw} = 0.335, kd = 1.01, ζ_{ta} = 0.001, ζ_{tw} = 0.004) and CASE AB-4 (f_w/f_{nw} = 0.335, kd = 1.01, ζ_{ta} = 0.021, ζ_{tw} = 0.021)

The variation of C_{Lma}, C_{Lmw} and C_{Lmv} with SKC for CASE A-5 and CASE AB-4 are shown in Fig. 5.4.31 and Fig. 5.4.32 respectively. The difference between C_{Lma} and C_{Lmv} for CASE A-5 is larger than that of CASE AB-4 because of the increase of damping as described above.

In CASE AB-4, C_{Lma}, C_{Lmw} and C_{Lmv} are nearly equal to $C_{Le}(2)$ in the range of SKC lower than 18. On the other hand, in the range of SKC over 18, they are larger than $C_{Le}(3)$, and have peak values around SKC $\approx$ 20. This shows the amplification of lift force in the range of SKC over 18.

In CASE A-5, only C_{Lmv} is larger than $C_{Le}(3)$ in the range of SKC over 18.

The values of Y_{hm}/D for CASE AB-4 are smaller than those for CASE A-5 because of the increased damping. However, the lift coefficients, C_{Lma}, C_{Lmw} and C_{Lmv} for CASE A-5 are larger than those of CASE A-5 in the range of SKC over 18. This phenomenon, strongest for C_{Lma}, again demonstrates the state of equilibrium between vortex excitation and fluid damping as described above (1).

When f_w/f_{nw} is fixed about 1/2, oscillations occur over a wide range of SKC, but the amplification of lift force occurs in the range of SKC between 6-12, as shown in Fig. 5.4.29 and Fig. 5.4.30. It is interesting to note that this range of SKC nearly corresponds to the range of KC, where the vortex-shedding from a stiffly mounted cylinder in waves is induced at twice the frequency of the wave frequency, for example, Chakrabarti et al. (1976), and Rhodes (1980).

Similarly, when f_w/f_{nw} is fixed about 1/3, the range of SKC, where amplification of lift force occurs, nearly corresponds to the range of KC, where the vortex-shedding from a stiffly mounted cylinder in waves is induced at three times the frequency of the wave frequency, Chakrabarti et al. (1976), Rhodes (1980). Therefore it may be estimated that the existence of the amplification of the lift force is a function of f_w/f_{nw} and SKC.

The results for the amplification of the lift force around SKC ≈ 10 ~11.5 for f_w/f_{nw} ≈ 1/2 and around SKC ≈ 18 for f_w/f_{nw} ≈ 1/3 have been reported by Isaacson and Maull (1981), Zedan and Rajabi (1981) Angrilli and Cossalter (1982). The following magnifications factor of lift force, M, (M = the lift coefficient acting on a vortex-excited cylinder/the lift coefficient acting on a stiffly mounted cylinder), have been obtained in their reports:

(1) Isaacson and Maull (1981)

$M = 2.85$ (SKC = 10, $f_w/f_{nw} \approx 1/2$, kd = 1.02, $m_e/\rho D^2 = 6.69$, $\delta_r = 3.54$)

$M = 3.25$ (SKC = 10, $f_w/f_{nw} \approx 1/2$, kd = 2.08, $m_e/\rho D^2 = 6.69$, $\delta_r = 3.59$)

$M = 2.7$ (SKC = 10, $f_w/f_{nw} \approx 1/2$, kd = 3.88, $m_e/\rho D^2 = 6.69$, $\delta_r = 3.54$)

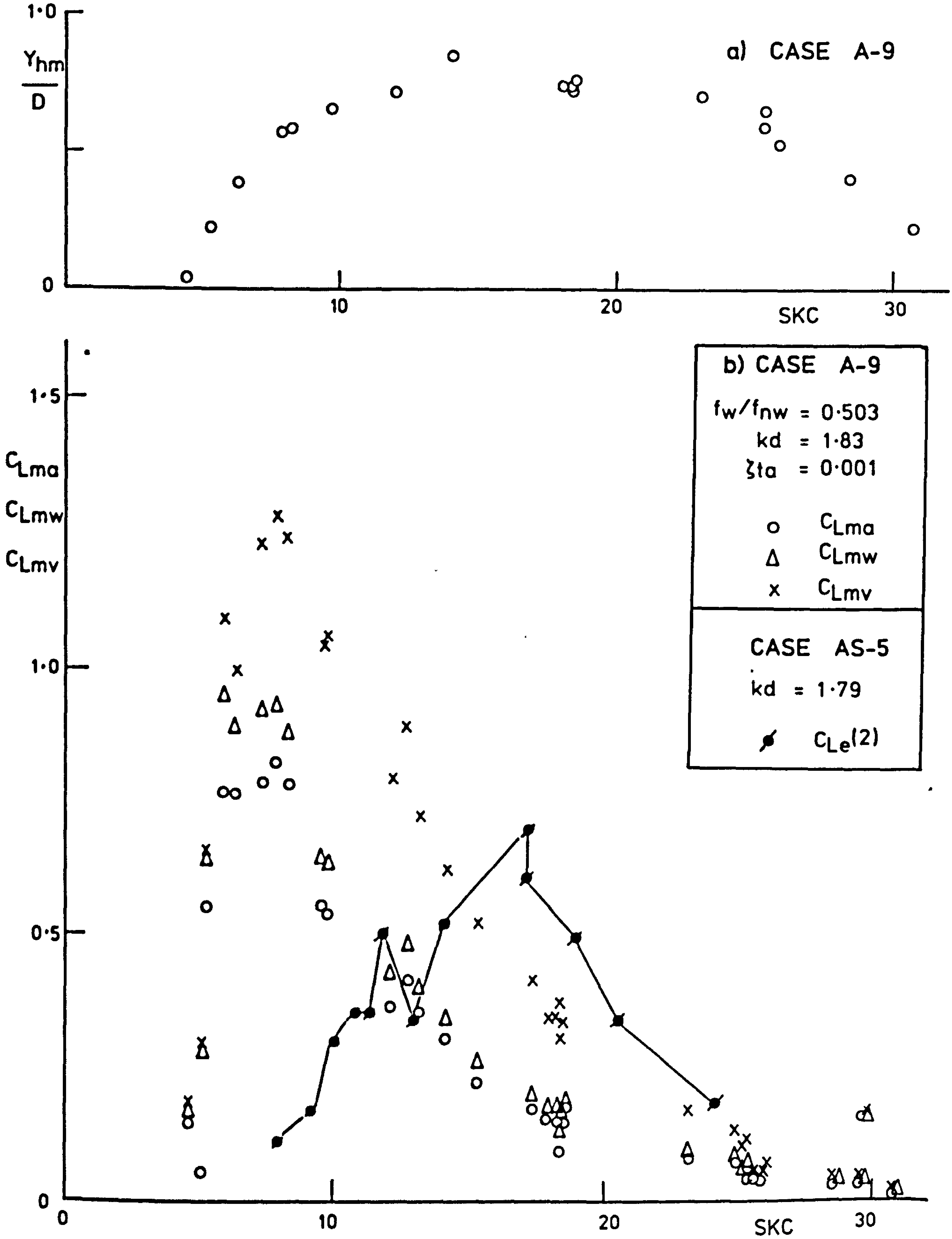

Fig. 5.4.29 The Plot of Y_{hm} and Lift Coefficients(C_{Lma}, C_{Lmw} and C_{Lmv}) against f_w/f_n for CASE A-9

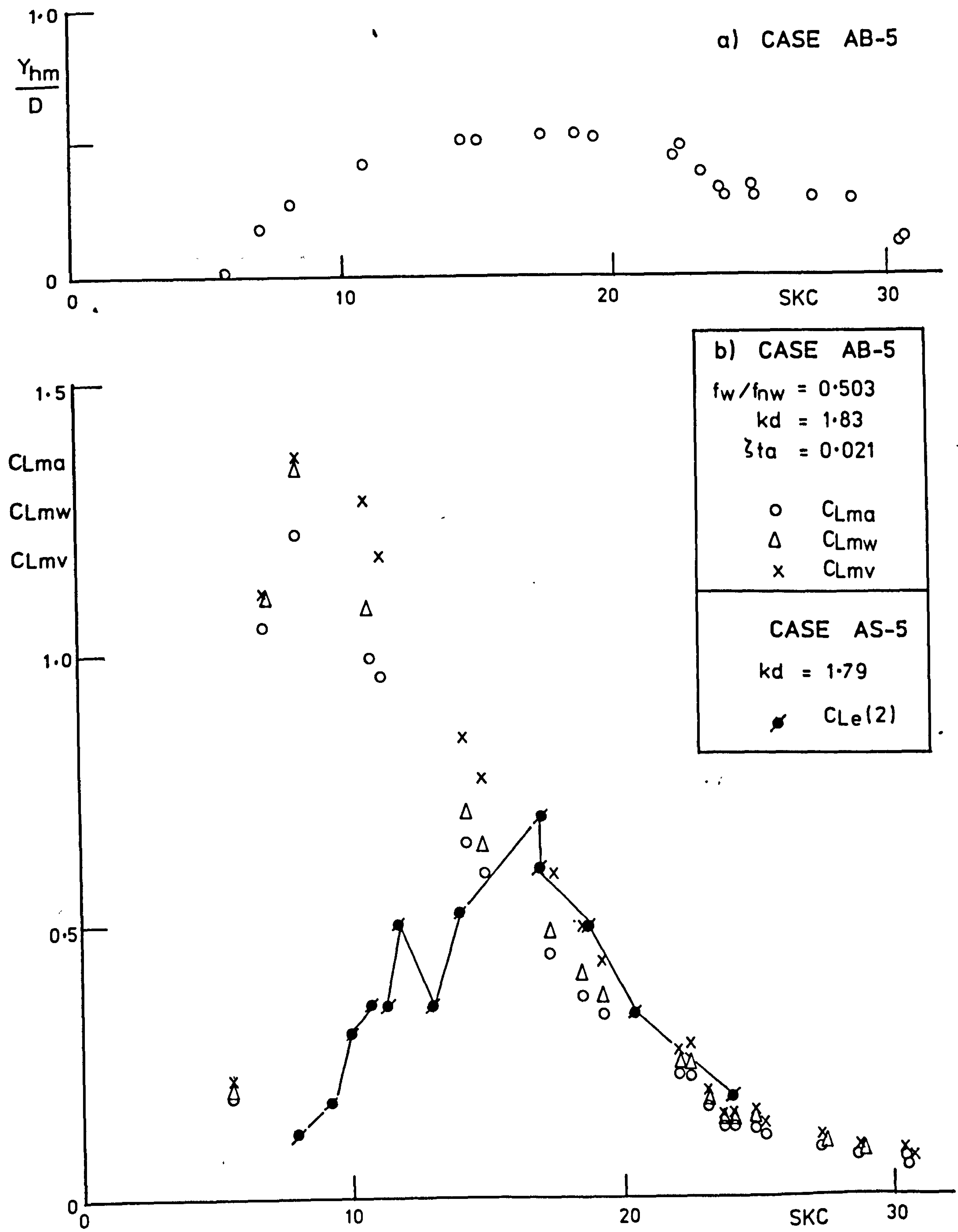

Fig. 5.4.30 The Plot of Y_{hm} and Lift Coefficients(C_{Lma}, C_{Lmw} and C_{Lmv}) against f_w/f_n for CASE AB-5

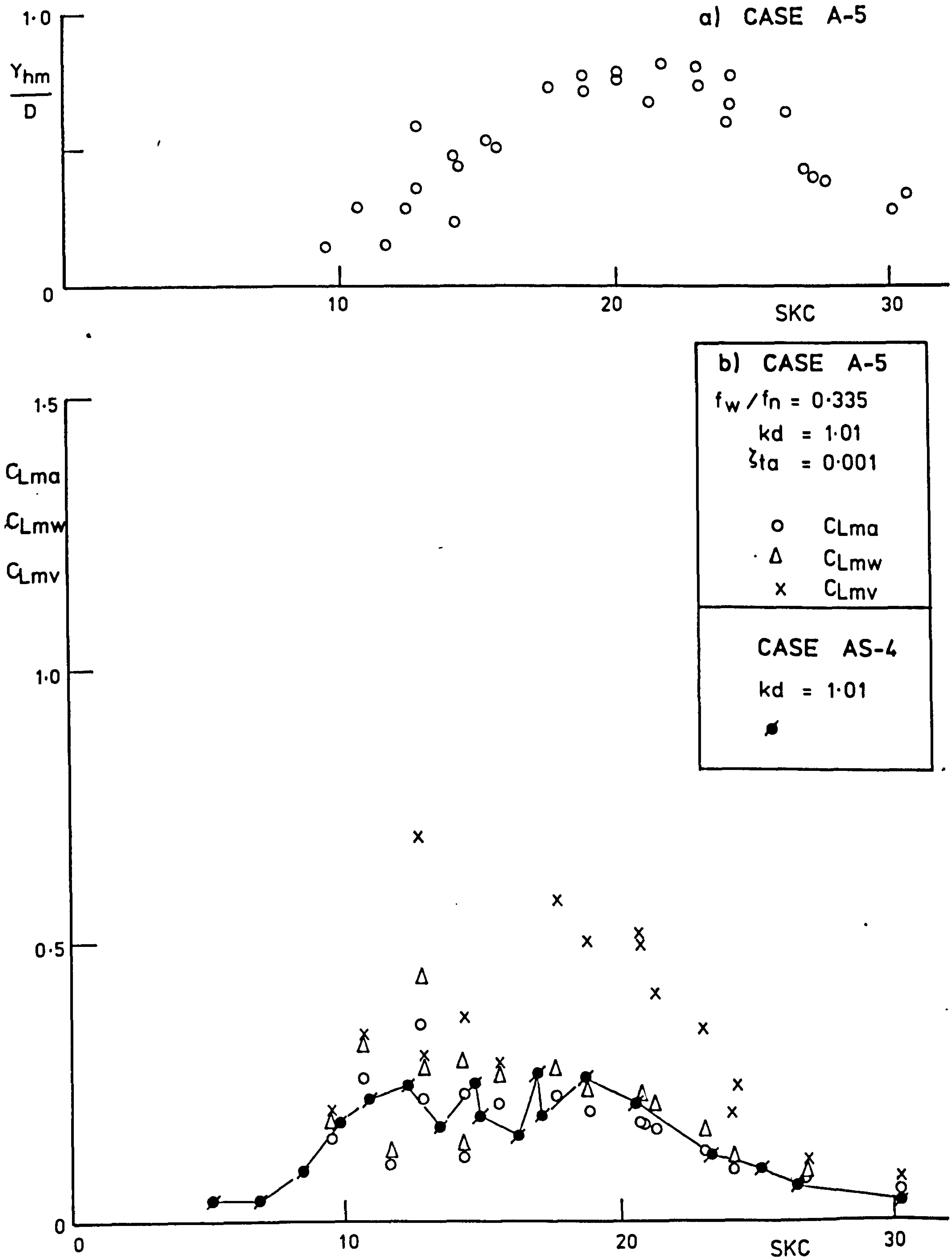

Fig. 5.4.31 The Plot of Y_{hm} and Lift Coefficients(C_{Lma}, C_{Lmw} and C_{Lmv}) against f_w/f_n for CASE A-5

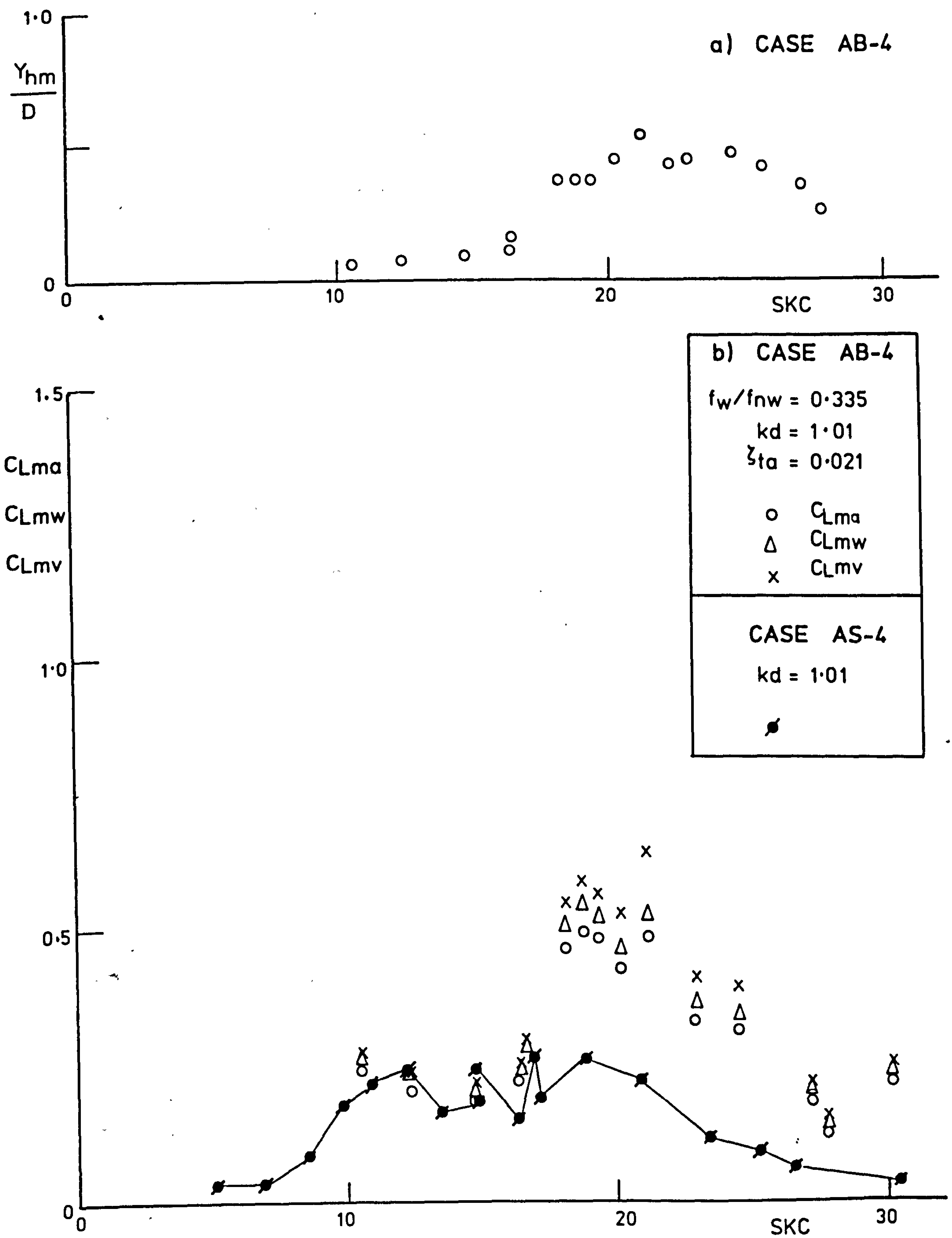

Fig. 5.4.32 The Plot of Y_{hm} and Lift Coefficients(C_{Lma}, C_{Lmw} and C_{Lmv}) against f_w/f_n for CASE AB-4

(2) Zedan and Rajabi (1981)

$M = 3.9$ (SKC = 11.2, $f_w/f_{nw} \cong 1/2$, kd = 1.63, $m_e/\rho D^2 = 22.9$, $\delta_r = 0.832$)

(3) Anglilli and Cossalter (1982)

$M = 1.7$ (SKC = 11.5, $f_w/f_{nw} \cong 1/2$, kd = 1.7, $m_e/\rho D^2 = 5.97$, $\delta_r = 0.975$)

$M = 1.6$ (SKC = 17.8, $f_w/f_{nw} \cong 1/3$, kd = 1.6, $m_e/\rho D^2 = 5.97$, $\delta_r = 0.975$)

Here δ_r is reduced damping ($\delta_r = 2m_e(2\pi\ \zeta_{ta})/\rho D^2$).

5-4-5-3 The variation of the lift coefficients, C_{Lma}, C_{Lmw} and C_{Lmv} with Y_{hm}/D

In order to inspect the variation of the lift force acting on the vortex-excited cylinder with amplitude of the vibration, the relationship between Y_{hm}/D, and the damping coefficient (ζ_{ta}, ζ_{tw}, ζ_{tv}) and the lift coefficient (C_{Lma}, C_{Lmw}, C_{Lmv}) for CASE AC-1, CASE AC-2 and CASE AC-5 are shown in Fig. 5.4.33 (a) and (b) through Fig. 5.4.35 (a) and (b) respectively. The experimental condition of these test cases are shown in Table 1. In each one, the frequency ratio f_w/f_{nw} and SKC were fixed, and the damping factor ζ_{ta} was changed from 0.001 to 0.0226 by using the electro-magnetic damper.

In CASE AC-1 and CASE AC-2, the frequency ratio f_w/f_{nw} was fixed at $f_w/f_{nw} \cong 1/2$ at which the perfect resonance probably occurred and each value of SKC for these cases was fixed as follows: CASE AC-1, SKC = 6.2 and CASE AC-2, SKC = 8.7.

In CASE AC-5, the frequency ratio f_w/f_{nw} was fixed at $f_w/f_{nw} \doteqdot 1/3$ at which the perfect resonance probably occurred as shown in Fig. 5.4.14 and SKC was fixed at 20.

(1) CASE AC-1 (f_w/f_{nw} = 0.503, kd = 1.85, SKC = 6.2)

The data of CASE AC-1 are shown in Fig. 5.4.33. As Y_{hm}/D increases from $Y_{hm}/D \doteqdot 0.2$ to $Y_{hm}/D \doteqdot 0.8$, each lift coefficient increases. In order to show the amplification of these lift coefficients, the values of $C_{Le}(2)$ obtained from the measurement of the lift force acting on the stiffly mounted test cylinder in similar conditions are shown in this figure.

(2) CASE AC-2 (f_w/f_{nw} = 0.503, kd = 1.88, SKC = 12)

The data of CASE AC-2 are shown in Fig. 5.4.34. As Y_{hm}/D increases from $Y_{hm}/D = 0.4$ to $Y_{hm}/D = 0.7$, each lift coefficient decreases. In order to show the amplification of these lift coefficients, the value of $C_{Le}(2)$ obtained from the measurement of the lift force acting on the stiffly mounted test cylinder in similar wave conditions for CASE AC-2, is also shown in this figure. When Y_{hm}/D exceeds about $Y_{hm}/D \doteqdot 0.6$, C_{Lma} and C_{Lmw} are smaller than $C_{Le}(2) = 0.45$ and approaches zero.

(3) CASE AC-5 (f_w/f_{nw} = 0.336, kd = 1.01, SKC = 20)

The data of CASE AC-5 are shown in Fig. 5.4.35. As Y_{hm}/D increases from $Y_{hm}/D \doteqdot 0.3$ to $Y_{hm}/D \doteqdot 0.45$, each lift coefficient increases. Each of these lift coefficients has a maximum value at about $Y_{hm}/D \doteqdot 0.45$. Therefore each lift coefficient decreases with increasing Y_{hm}/D. However, the decrease in C_{Lmv} is not so clear as those in C_{Lma} and C_{Lmw}.

In order to show the amplification of those lift coefficients, the value of $C_{Le}(3)$ obtained from the measurement of the lift force acting on the stiffly mounted test cylinder in similar wave conditions for CASE AC-5 is shown in this figure.

These phenomena clearly show the result of a state of equilibrium existing between vortex excitation and fluid damping and suggest that the maximum limiting value of Y_{hm}/D is independent of structural damping as shown in Fig. 5.4.35(a).

From those figures, the following observations of the lift force acting on the vortex-excited test cylinder in waves may be indicated:

(1) When Y_{hm}/D is lower than about $Y_{hm}/D = 0.45$, the lift force coefficient increases with increasing Y_{hm}/D.

(2) The maximum amplification of the lift coefficient occurs about $Y_{hm}/D = 0.45$.

(3) When Y_{hm}/D rises above $Y_{hm}/D \doteq 0.45$, the lift coefficient begins to decrease.

It is interesting to note that these phenomena are quite similar to those for steady flow. In the case of steady flow, the following phenomena have been reported by Vickery et al. (1962) and Hartlen et al. (1968) after Blevin (1976) and King (1977).

(1) At low amplitudes the lift coefficient increases with increasing amplitude.

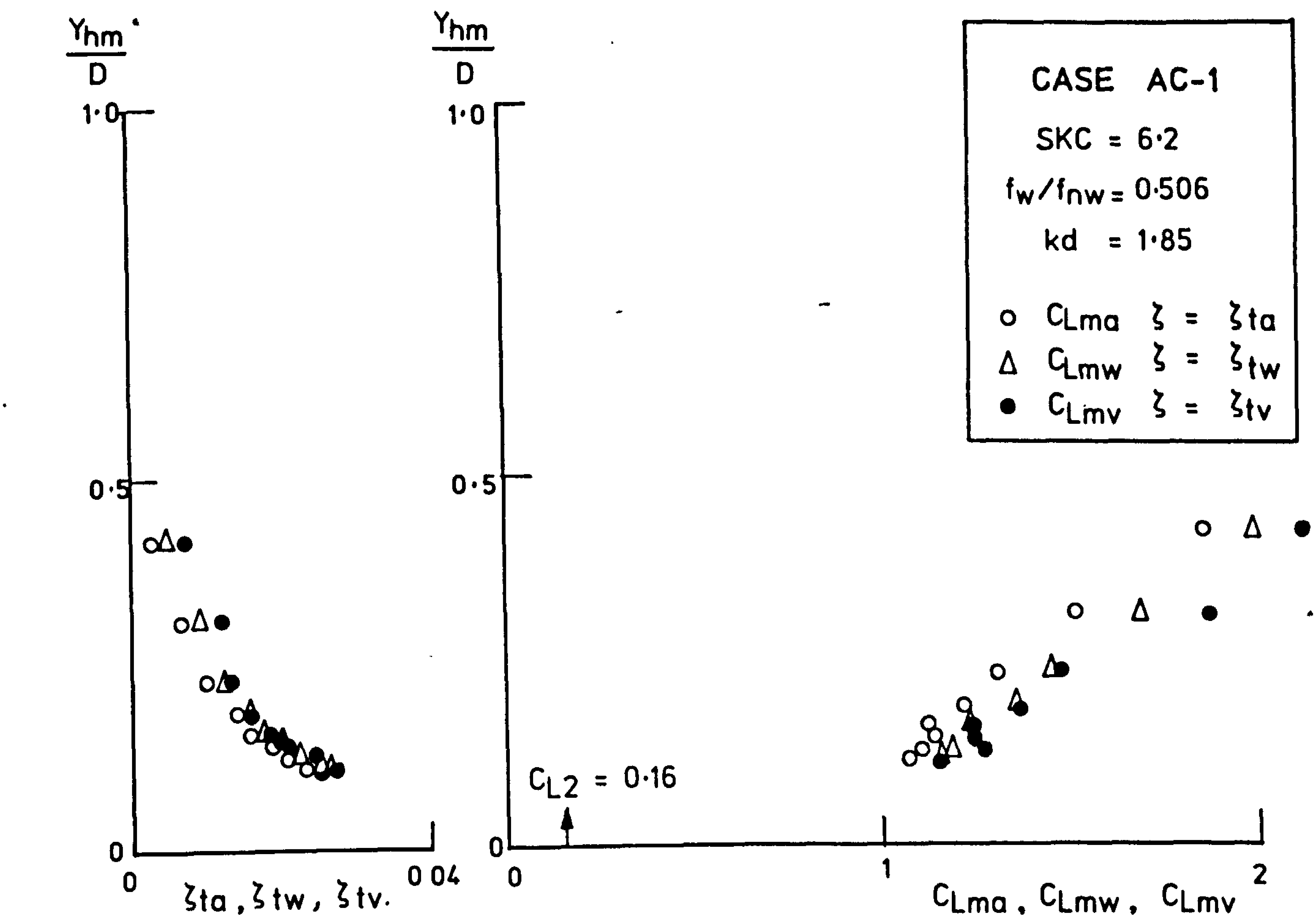

Fig. 5.4.33 The Plot of Y_{hm}/D against Damping Factor(ζ_{ta}, ζtw and ζ_{tv}) and Lift Coefficients(C_{Lma}, C_{Lmw} and C_{Lmv}) for CASE AC-1

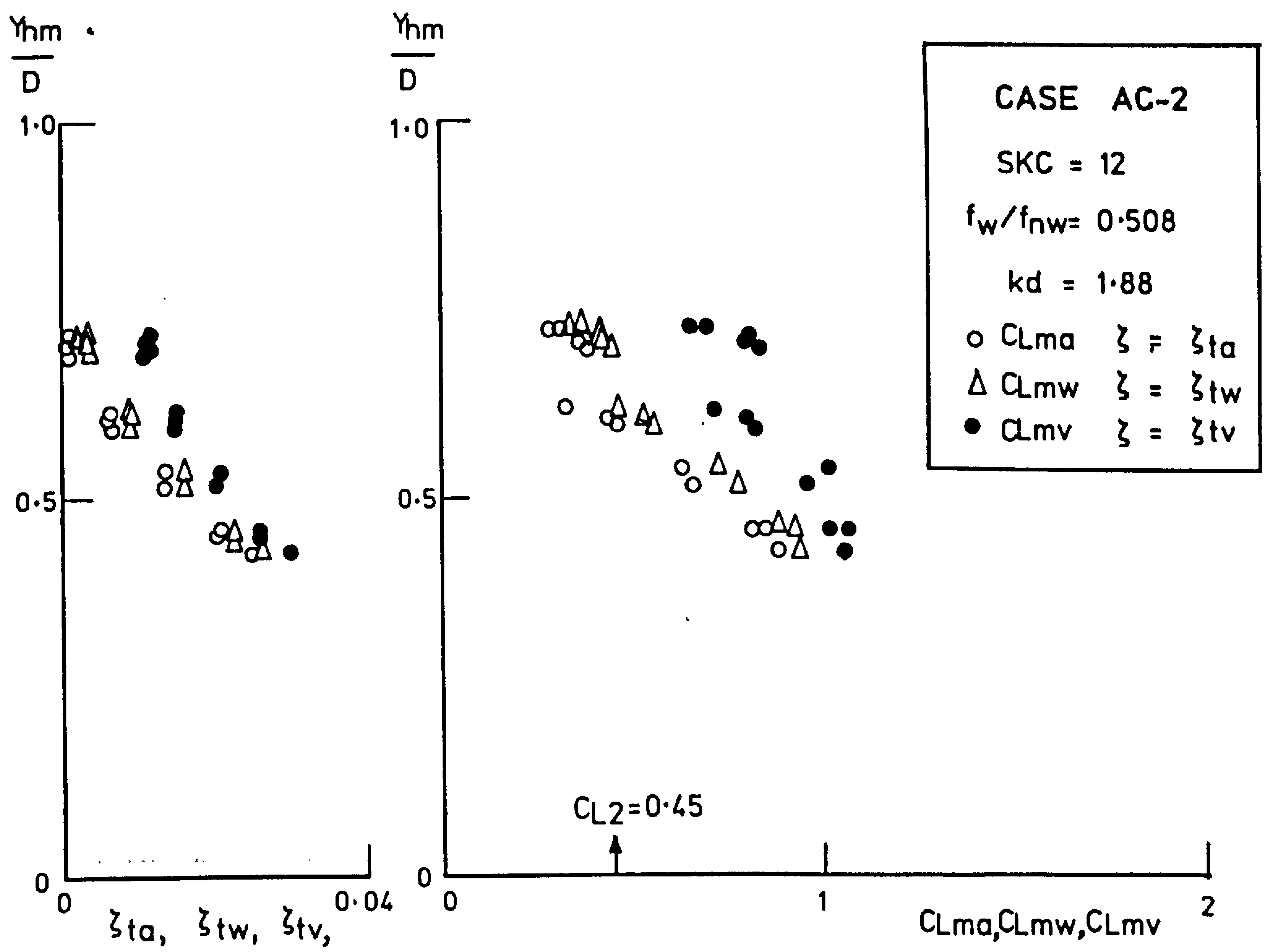

Fig. 5.4.34 The Plot of Y_{hm}/D against Damping Factor(ζ_{ta}, ζ_{tw} and ζ_{tv}) and Lift Coefficients(C_{Lma}, C_{Lmw} and C_{Lmv}) for CASE AC-2

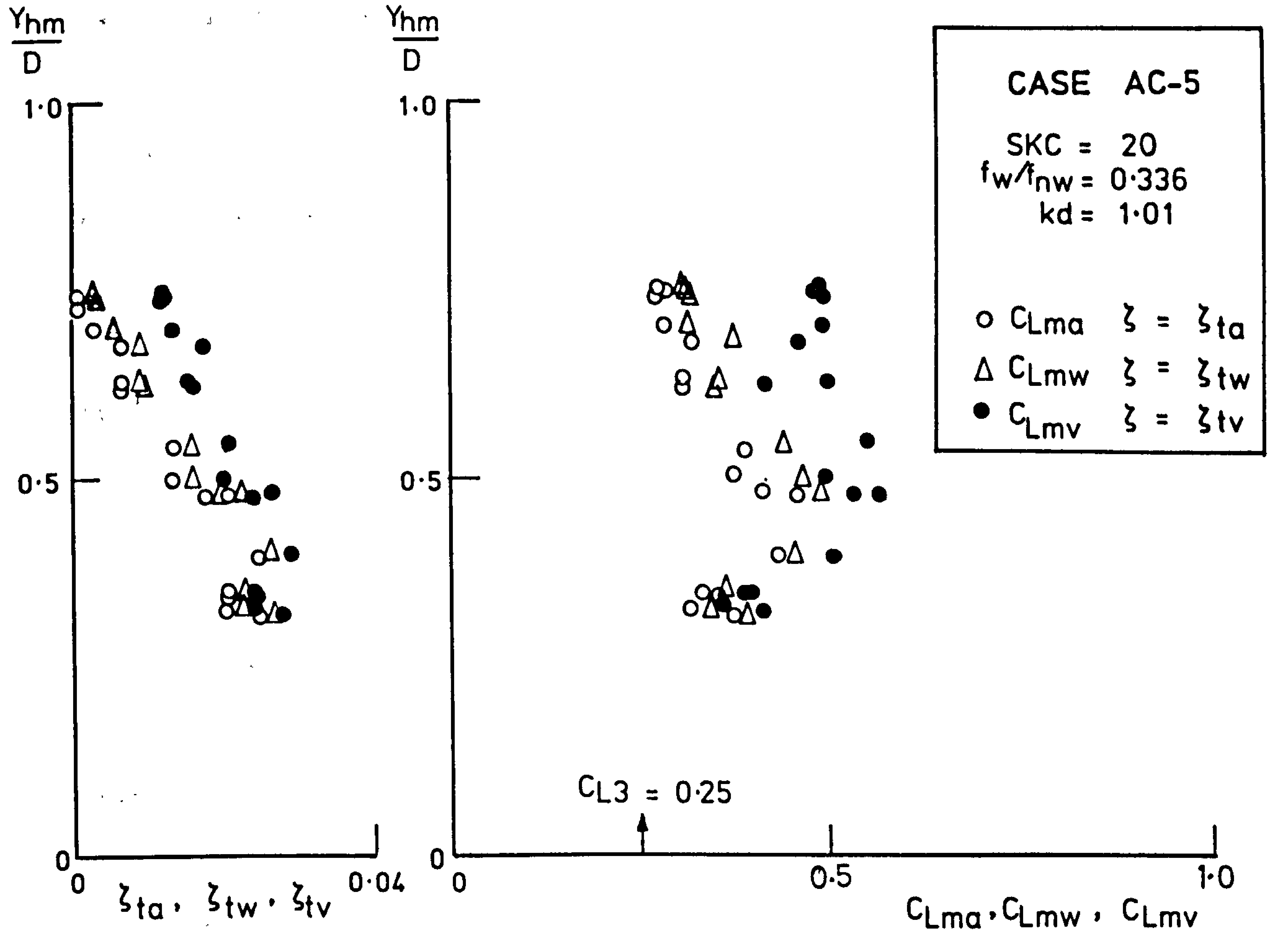

Fig. 5.4.35 The Plot of Y_{hm}/D against Damping Factor(ζ_{ta}, ζ_{tw} and ζ_{tv}) and Lift Coefficients(C_{Lma}, C_{Lmw} and C_{Lmv}) for CASE AC-5

(2) The maximum amplification of the lift coefficient appears in the range of the amplitude between 0.3 diameter and 0.5 diameter.

(3) As the amplitude increases over about 0.5 diameter, the lift coefficient begins to decrease and approaches zero.

5-4-6 The phase angle between the vibration of the cylinder and the water surface elevation

In order to estimate the unknown value of the total damping factor, ζ_{te}, in the vortex-excited condition, the phase angle $\phi_B(n)$ between the displacement of the test cylinder, y_h, and the water surface elevation, η, was obtained. The values of $\phi_B(n)$ are calculated by obtaining the coefficients of the Fourier expansion for the time records of η and y_h.

The relationship between f_w/f_{nw}, and Y_{hm}/D, f_{ym}/f_{nw} and $\phi_B(2)$ for the typical runs of CASE A-1 and CASE AB-1 are shown in Fig. 5.4.36 (a) and (b) and Fig. 5.4.37 (a) and (b). The resulting value of $\phi_B(2)$ are shown in Table 5.2. As shown in Table 1 and Table 5.2, the experimental wave conditions for each run of CASE A-1 and CASE AB-1 were nearly the same. In CASE A-1, the damping factor of the test cylinder in air, ζ_{ta}, was 0.001. On the other hand, in CASE AB-1, ζ_{ta} was changed from 0.001 to 0.021 by using the electro-magnetic damper.

As described in section 5-4-2, around the perfect resonance, the time histories of y_h for the runs of CASE A-1 and CASE AB-1 were very regular and in each case the frequency of vibration is just two times the wave frequency. Therefore it is reasonable to expect that $\phi_B(2)$ for these cases will remain very constant.

The theoretical values of the phase angle, $\phi_A(2)$, between the displacement of the cylinder y_h and the lift force for various values of the damping factor ζ_t are shown in Fig. 5.4.36 (b) and Fig. 5.4.37 (b). The theoretical value of $\phi_A(2)$ is calculated by Eq.(3-26) on the basis of a linear model.

The rate of change of $\phi_B(2)$ with respect to f_w/f_{nw} for CASE A-1 is larger than that for CASE AB-1 because the damping for CASE A-1 is smaller than that for CASE AB-1. In CASE AB-1, the gradient, $\Delta\phi_B(2)/\Delta f_w/f_{nw}$, is nearly equal of the gradient $\Delta\phi_A(2)/\Delta f_w/f_{nw}$, for $\zeta_t = 0.03$ around perfect resonance. The difference between $\phi_B(2)$ and $\phi_A(2)$ for $\zeta_{ta} = 0.03$ may be due to the appearance of the perfect resonance at $f_w/f_{nw} = 0.504$ and the fact that the experimental results is the phase angle between the wave elevation η and the cylinder's displacement y_h. On the other hand, the theoretical phase angle refers to the lift force. It is reasonable to assume, however, that there is not a large change in the phase angle between the wave elevation and the fluid, since the incident flow velocity is in phase with the wave.

The following equation is obtained by differentiating both sides of Eq.(3-26) with respect to f_w/f_{nw},

$$\frac{\partial\phi_A(n)}{\partial f_w/f_n} = \frac{n\{1 + (n\frac{f_w}{f_n})^2\}\sin^2\phi_A(n)}{2\zeta_t(n\frac{f_w}{f_n})^2} \tag{5-4-6}$$

Rearranging Eq.(5-4-6) gives

$$\zeta_t = \frac{n\{1 + (n\frac{f_w}{f_n})^2\}\sin^2\phi_A(n)}{2(n\frac{f_w}{f_n})^2} / (\frac{\partial\phi_A(n)}{\partial f_w/f_n}). \tag{5-4-7}$$

At perfect resonance in the present case with $n = 2$, $\phi_A(n)$ is $\pi/2$. Then Eq.(5-4-7) is expressed as follows

$$\zeta_t = \frac{2}{(\frac{\partial\phi_A(2)}{\partial f_w/f_n})} \tag{5-4-8}$$

Eq.(5-4-8) shows that the total damping coefficient, ζ_t, at perfect resonance is related to the gradient $\partial\phi_A(n)/\partial f_w/f_{nw}$.

By substituting each value of $\partial\phi_B(2)/\partial f_w/f_{nw}$ around perfect resonance for CASE A-1 and CASE AB-1 into Eq.(5-4-8), the following values are derived for the total damping factor, ζ_{te}, in the vortex-excited condition.

ζ_{te} = 0.01 - 0.015 ---- CASE A-1

ζ_{te} = 0.031 - 0.038 ---- CASE AB-1

The values of ζ_{ta}, ζ_{tw} and ζ_{tv} for CASE A-1 and CASE AB-1 are as follows;

$\zeta_{ta} = 0.001$ $\zeta_{tw} = 0.004$ $\zeta_{tv} = 0.012$ ---- CASE A-1

$\zeta_{ta} = 0.021$ $\zeta_{tw} = 0.023$ $\zeta_{tv} = 0.032$ ---- CASE AB-1

ζ_{tv} is the damping factor in still water at $Y_{hi}/D = Y_{hm}/D$. It is interesting to note that ζ_{te} is only slightly larger than ζ_{tv} for each CASE A-1 and CASE AB-1. This suggests that for large amplitudes at perfect resonance the damping is very similar to the damping at the same amplitude in still waters. It may be concluded that the rapid increase in damping, observed in still water test (Fig. 5.2.3), is responsible for the limiting amplitude at perfect response described in section 5-4-2.

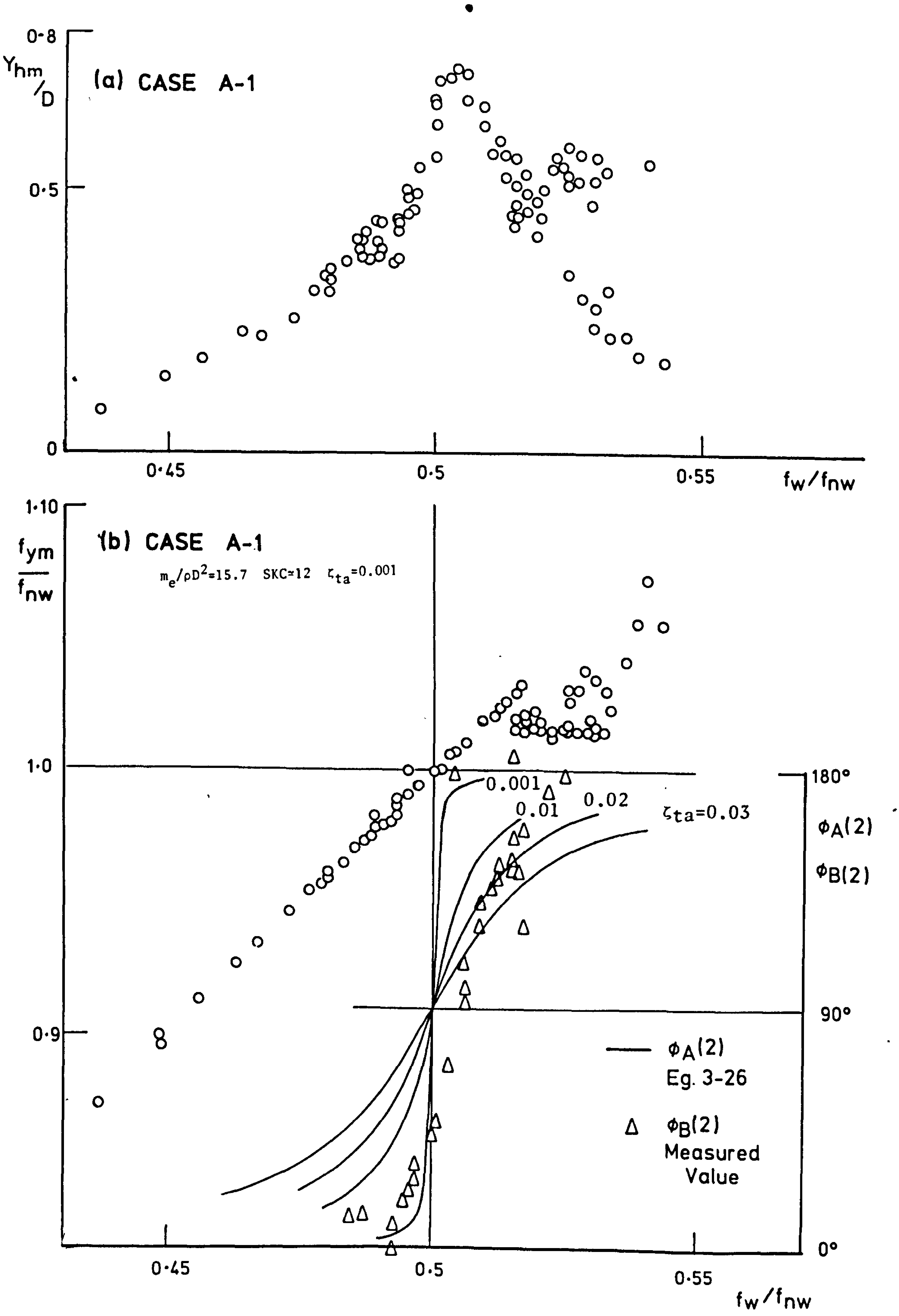

Fig. 5.4.36 The Variation of Y_{hm}/D, f_{ym}/f_{nw} and Phase Angle($\phi_A(2)$ and $\phi_B(2)$) with f_w/f_{nw} for CASE A-1

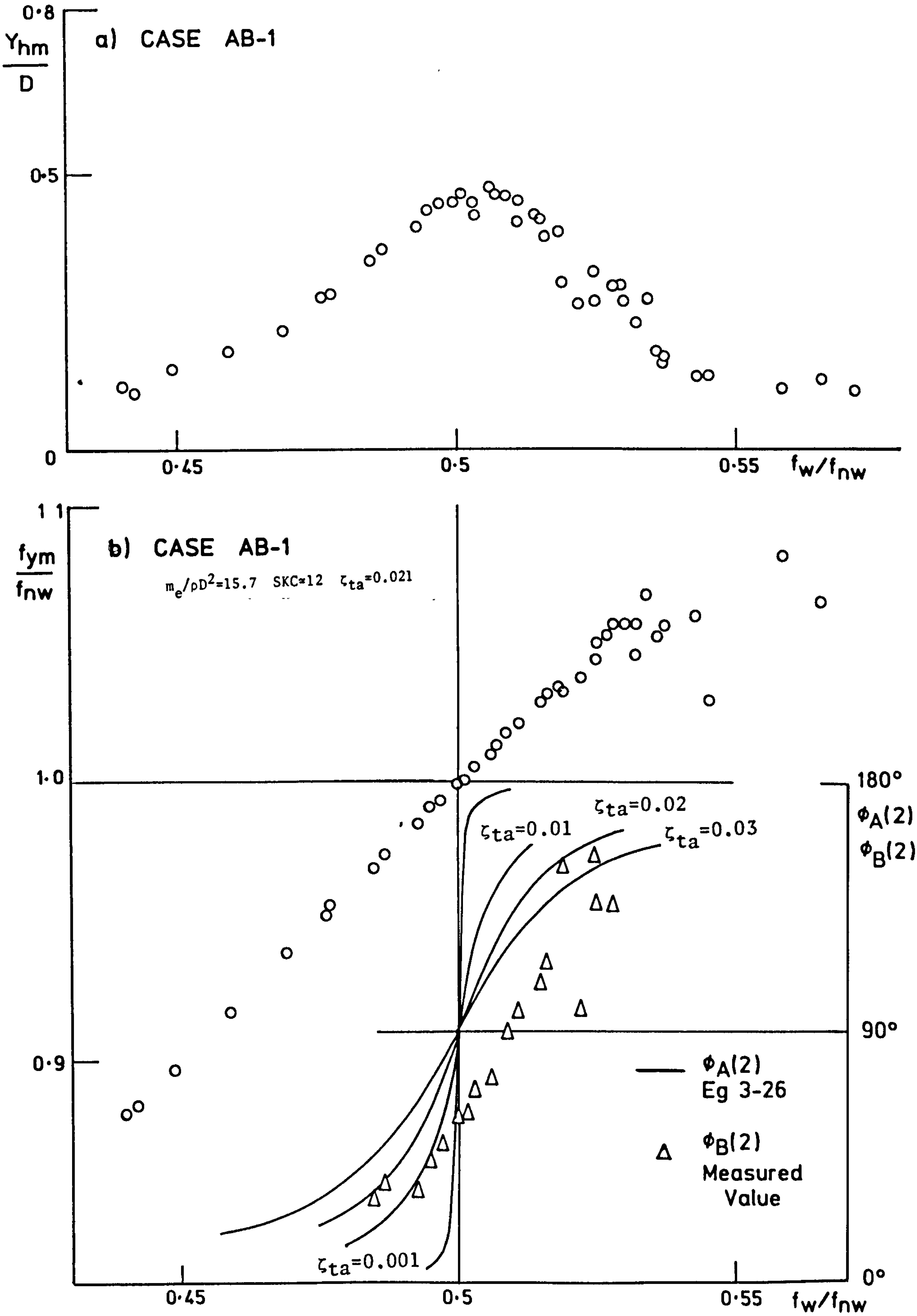

Fig. 5.4.37 The Variation of Y_{hm}/D, f_{ym}/f_{nw} and Phase Angle($\phi_A(2)$ and $\phi_B(2)$) with f_w/f_{nw} for CASE AB-1

CHAPTER 6

THE WAKE OSCILLATOR MODEL FOR VORTEX-EXCITED VIBRATIONS IN WAVES

6-1 Introduction

The non-linear fluid structure interaction of vortex-excited vibrations of the test cylinder in waves have been described in Chapter 5. This non-linear phenomena can not be explained by the linearised model described in Chapter 3. Its characteristics are quite similar to those observed in steady flow in terms of the amplification of the lift force around perfect resonance. The wake oscillator model, Hartlen and Currie (1970), was formulated in order to explain the non-linear fluid structure interactions for steady flow. In this chapter, the application of the wake oscillator model for steady flow to non-linear vortex-excited vibration in waves is considered.

However, there is the following important difference between the vortex-excited vibration in waves and that in steady current flow:

(1) In the case of waves, there are two peaks in the response vibration produced by perfect resonance coupled with waves and by vortex coupling. The maximum response of perfect resonance appears in the range of wave coupling and it appears only near to f_w/f_{nw} = 1/2, 1/3, 1/4 ... as described in 5-4-2.

(2) In the case of steady flow, perfect resonance appears in the range of lock-on between the vortex shedding frequency and the natural frequency of the cylinder.

In the modelling work of the present research, this difference should be considered.

Although several wake oscillator models have been reported, the application of the Hartlen and Currie model (1970) to the vortex-excited vibration in waves is considered in this chapter, because this is a fundamental and simple wake oscillator model for the vortex-excited vibration in steady flow.

6.2 Formulation of the Wake Oscillator Model for the Vortex-Excited Vibration of the Test Cylinder in Waves

We express the total lift force moment matrix of the test cylinder, $F_{m\ell}$, defined in 3-2-1(4) and expressed Eq.(3-14), as follows.

$$F_{m\ell} = \frac{1}{2}\,\rho.D.d^2.F_s(k.d)\;C_{La}\{U_{ms}.\sin(2\pi.f_w.t)\}^2 \tag{6-1}$$

Where C_{La} is a instantaneous effective lift coefficient and is assumed to satisfy the following Van der Pol equation which is based on the wake oscillator model proposed by Hartlen and Currie (1970).

$$\ddot{C}_{La} - \alpha.\omega_0.\left|\sin\left(\frac{\omega_0}{S.SKC}\,\tau\right)\right|.\dot{C}_{La} + \frac{\gamma}{\omega_0}\,\dot{C}_{La}^{\,3}$$

$$+\;\omega_0^{\,2}\,\sin^2\left(\frac{\omega_0}{S.SKC}\,\tau\right).C_{La} = b\dot{y}_r \tag{6-2}$$

In which

$$\tau = 2\pi f_n t$$

$$y_r = y_h/D$$

$$y_r' = dy_r/d\tau$$

$$y_r'' = d^2y_r/d\tau^2$$

$$C_{La}' = d\,C_{La}/d\tau, \quad C_{La}'' = d^2C_{La}/d\tau^2$$

$$\omega_0 = f_{s0}/f_n$$

$$S = \text{Strouhal number} \tag{6-3}$$

Where f_{s0} is the maximum instantaneous vortex-shedding frequency experienced by the test cylinder when stiffly mounted in waves. f_{s0} may be expressed as follows

$$f_{s0} = s\left(\frac{U_{ms}}{D}\right) \tag{6-4}$$

Here U_{ms} is the maximum horizontal particle velocity at still water level, given Eq.(3-15), and f_n is the natural frequency of the cylinder.

The dimensionless parameters α and γ are the Van der Pol coefficients and b is the dimensionless interaction parameter. The implication of these parameters are discussed below and their values are to be found from experimental results.

The expression $\omega_0.\sin(\omega_0.\tau/(S.SKC))$ used in the second and fourth term in Eq.(6-2) can be re-written as follows

$$\omega_o . \sin(\frac{\omega_o}{S.SKC}\tau) = \frac{f_{so}}{f_n} \sin\frac{2\pi t}{T}$$

$$= \frac{S.U_{ms}}{f_n.D} \sin \frac{2\pi t}{T}$$

$$= \frac{S.U}{D}/f_n \qquad (6\text{-}5)$$

This value shows the variation of the instantaneous vortex-shedding frequency ratio with t/T.

Equation (6-2) is slightly different from that of the Hartlen and Currie model for steady current flow. However, the characteristics of the Van der Pol - type equation still may be contained in Eq.(6-2).

In this equation, the first and fourth terms can generate a harmonic oscillation of C_{La} in which the frequency of C_{La} is a function of S and SKC and changes through the wave period in accordance with instantaneous vortex-shedding frequency.

The third and fourth terms in Eq.(6-2) comprise the damping. It has the following characteristics:

(1) When the amplitude of C_{La} is small, it may be amplified with time by the presence of the second term. This may be denoted "Self-excited".

(2) When the amplitude of C_{La} arrives at a large value, this may be restricted by the presence of the third term. This amplitude is then "Self-limited".

The fifth term, $b.\dot{y}_r$, in Eq.(6-2) is the forcing term. This term is introduced to relate the oscillation of C_{La} to the vibration of the test cylinder. When the interaction parameter b is 0, the fluid and structure oscillations are decoupled. The value of y_r is given from the equation of motion of the test cylinder, which is now shown as follows by using Eq.(6-1).

$$M_{Bm}\ddot{y}_r + C_{Bm}.2\zeta t.\dot{y}_r + K_{Bm}\,y_r = F_{m\ell}/(M_{mo}.D.\omega_n^2)$$

$$= F_{m\ell}/(M_{mo}.D.\omega_n^2)$$

$$= \frac{1}{2}\,\rho.D.d^2.F_s(kd)C_{La}\{U_{ms}.\sin(2\pi.f_w.t)\}^2/(M_{mo}.D.\omega_n^2) \qquad (6\text{-}6)$$

where $\ddot{y}_r = d^2y_r/d\tau^2$

The non-linear fluid structure interaction, the interaction between the vibration of the test cylinder and the lift force, may be modelled by solving the simultaneous non-linear differential equations, Eq.(6-2) and Eq.(6-6). The strength of the interaction may be controlled by the value of b.

On the other hand, when the test cylinder is mounted stiffly, the coefficient of the lift force acting on the cylinder may be expressed by the solution of the following equation, which is obtained by putting $y_r = 0$ in Eq.(6-2).

$$\ddot{C}_{La} - \alpha\omega_0\left|\sin\left(\frac{\omega_0}{S.SKC}\,\tau\right)\right|.\dot{C}_{La} + \frac{\gamma}{\omega_0}\,\dot{C}_{La}^{\,3}$$

$$+\ \omega_0^2\,\sin^2\left(\frac{\omega_0}{S.SCK}\,\tau\right).C_{La} = 0 \qquad (6\text{-}7)$$

In this case, although the amplitude of C_{La} is a function of the following: α, β, ω_0, S, and SKC, it may be related mainly by the ratio of α/γ.

6-3 The Solution of the Wake Oscillator Model in Waves

6-3-1 Calculation method

It is difficult to solve analytically the simultaneous common non-linear differential equations, Eq.(6-2) and Eq.(6-6). Therefore they were solved numerically by using a time-stepping linear acceleration method.

As described in 6-2, the main parameters of the frequency of C_{Le} are the Strouhal number and SKC. However, now, Eq.(6-2) is coupled to Eq.(6-6) by means of the forcing term, $b\dot{y}_r$. Therefore, when the amplitude of y_r is large, in which case the frequency of y_r is probably nearly equal to the natural frequency of the test cylinder, f_n, the frequency of C_{La} may be entrapped by this frequency. This phenomenon is similar to the lock-on, between vortex-shedding and vibration frequencies for steady flow. However, as described in 5-4-2, the frequency of the vortex-excited test cylinder in waves was not in general controlled by the natural frequency of the test cylinder. It was controlled rather by the wave frequency in condition of "wave coupling". Therefore, in order to consider this phenomenon in the present model, the Strouhal number S is adjusted to satisfy the following condition in the numerical calculation.

(1) The frequency of C_{La} must be equal to $f_w/2$, $f_w/3$, $f_w/4$ ..., corresponding to the range of SKC.

(2) The phase angle between C_{La} and η is zero.

In a complete model, such relationships would be automatically determined. However these conditions nearly correspond to the observed characteristics of the lift force acting on a stiffly mounted cylinder in waves.

6-3-2 Result of the wake oscillator model

The results of the wake oscillator model in waves for the calculation conditions of CASE W-1 and CASE W-2 are shown in Fig. 6.1 (a) and (b).

In these cases, the wave conditions and the physical parameters of the cylinder are the same. In order to show the effect of the interaction between the vibration of the cylinder and the lift force, the value of α, γ, and b in Eq.(6-2) are selected as follows.

$$\begin{aligned} &\text{CASE W-1 ---} \quad \alpha = 0.2 \quad \gamma = 0.067 \quad b = 0.4 \\ &\text{CASE W-2 ---} \quad \alpha = 0.2 \quad \gamma = 0.067 \quad b = 0.0 \end{aligned} \tag{6-7}$$

Therefore, the fluid structure interaction is not considered in CASE W-2.

The physical parameters of the cylinder are as follows:

$$\begin{aligned} &m_e/\rho D^2 = 30 \\ &2m_e(2\pi\ \zeta_t)/\rho D^2 = 3 \\ &f_n = 1.193 \text{ Hz } (Tn = 0.838 \text{ sec.}) \end{aligned} \tag{6-8}$$

Otherwise, those conditions roughly correspond to the experiments for CASE AB ($m_e/\rho D^2 \cong 15.7$, $2m_e(2\pi\ \zeta ta)/\rho D^2 = 4.14$, $f_w = 1.46$ Hz).

The calculations were carried out in the range of f_w/f_n between 0.436 and 0.55. The wave height H was kept 7cm. The water depth d was kept at 80cm. The wave particle velocity u was calculated by linear wave theory. Therefore, the values of SKC and kd vary as follows:

$$
\begin{aligned}
&f_w/f_n \cong 0.45 \quad && SKC \cong 14 \quad && kd \cong 1.14 \\
&f_w/f_n \cong 0.5 \quad && SKC \cong 13.2 \quad && kd \cong 1.32 \\
&f_w/f_n \cong 0.55 \quad && SKC \cong 12.5 \quad && kd \cong 1.53
\end{aligned} \tag{6-9}
$$

The relationship between f_w/f_{nw} and each amplitude of the dimensionless oscillation Y_r, for CASE W-1 and CASE W-2 are shown in Fig. 6.1(a). The relationship between f_w/f_{nw} and C_{La}, the amplitude of C_{La} and S are shown in Fig. 6.1(b).

In the range of f_w/f_n below about 1/2, the value of Y_r for CASE W-1 is larger than that for CASE W-2. In the range of f_w/f_n above 1.2, Y_r for CASE W-1 is smaller than that for CASE W-2. In the range of f_w/f_{nw} between 0.506 and 0.53, a reasonably stable solution was not obtained. In this area, the frequency of C_{La} is about $3f_{wn}$ and the amplitude of C_{La} modulates without intermittency. The value of Y_r is very small because the frequency of C_{La} is about $3f_w$. It is not clear whether this is due to the calculation method or not, but it is interesting to note that this range of f_w/f_{nw} nearly corresponds to the range of f_w/f_{nw} between 0.52 and 0.53 where the vortex-coupling appears as shown in Fig. 5.4.13.

The maximum value of Y_r for CASE W-1 appears at $f_w/f_{nw} \cong 0.499$. However the experimental result for CASE A-1 (SKC $\cong$ 12, $m_e/\rho D^2$ = 15.7), which roughly corresponds to CASE W-1, shows the appearance of the maximum amplitude at $f_w/f_{nw} \cong 0.504$.

The value of C_{La} for CASE W-2 is clearly larger than that for CASE W-2 in the range of f_w/f_n below 1/2. This shows the amplification of the lift force associated with the oscillation. On the other hand, in the range of f_w/f_{nw} above 1/2, C_{La} for CASE W-1 is smaller than CASE W-2. This shows the attenuation of the lift force.

The experimental results for CASE A-1 showed the amplification the lift force around $f_w/f_{nw} \cong 1/2$ but the attenuation of it at slightly higher values of f_w/f_{nw} did not appear.

The value of C_{La} for CASE W-2 slightly increases with increasing f_w/f_{nw}. This shows that C_{La} for CASE W-2 is a function not only of α and γ but also of SKC, because now SKC is a function of f_w/f_n as described in Eq.(6-9).

The value of S for CASE W-1 is larger than that for CASE W-2 close to $f_w/f_{nw} = 0.5$. The difference between them shows the effect of the adjustment of S, introduced to satisfy the condition of the wave coupling in this model. The variation of S with f_w/f_{nw} for CASE W-2 shows that S is mainly determined by SKC.

This proposed wake oscillator model cannot explain perfectly the general phenomena of the vortex-excited vibration in waves observed in the present experimental work. However, it is interesting to note that the amplification of the lift force around perfect resonance, which may be one of the most important phenomena of the vortex-excited vibration in waves, is roughly reproduced by the present model.

As described previously, the wake oscillator model does not solve the fluid dynamic problem of the vortex-excited vibration, it is only an approximation of the fluid structure interaction. Therefore, in order to make the present model variable, a large amount of experimental data is required to obtain the relationship between the model parameter α, γ, b, and the physical parameters of both cylinders and waves.

The study to find the relationships between the model parameter and the experimental data obtained in the present work will be done.

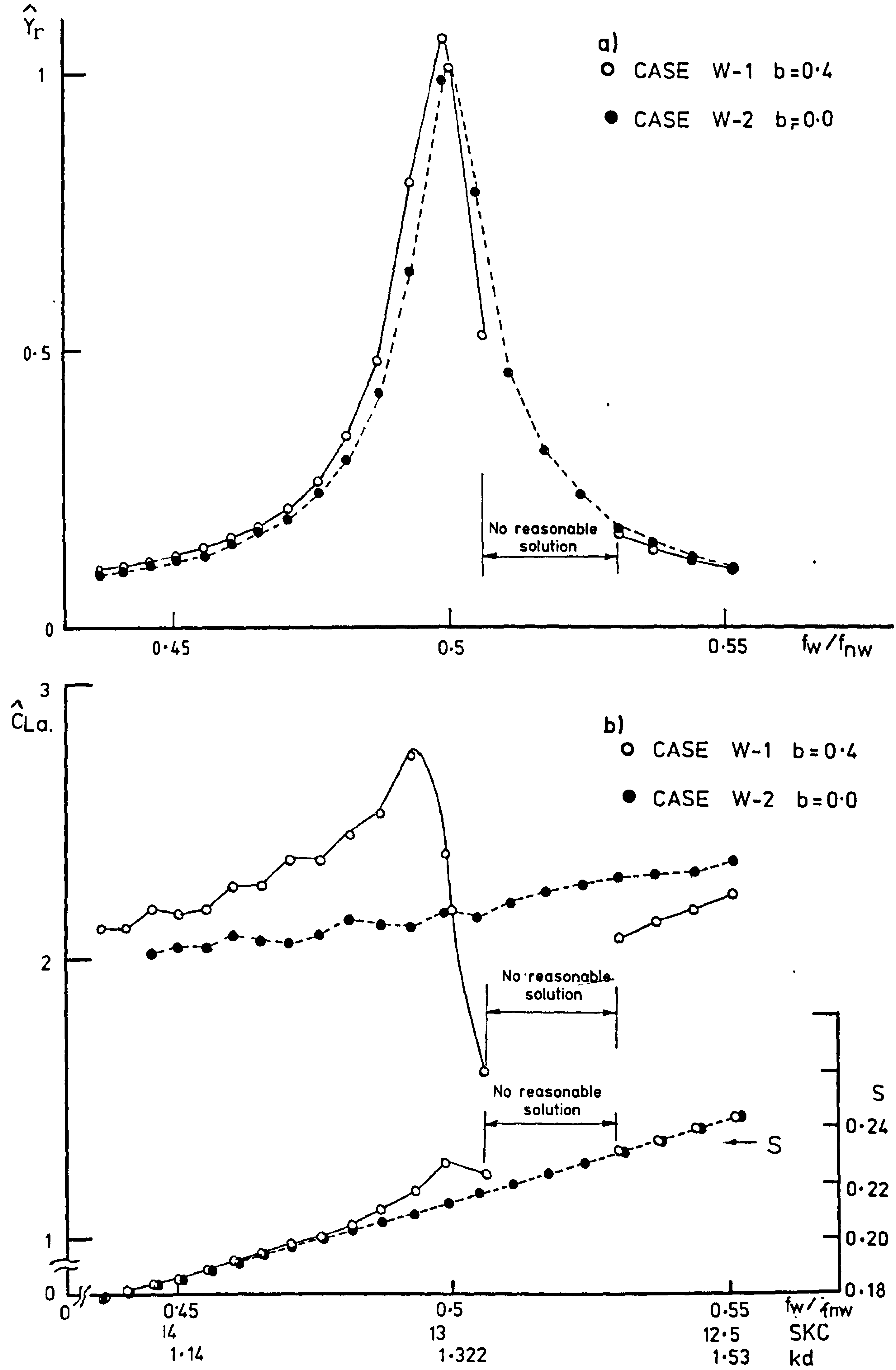

Fig. 6.1 The Results of Wake Oscillator Model in Waves for the Calculation Conditions of CASE W-1 and CASE W-2

CHAPTER 7

CONCLUSION

7-1 General Remarks

The object of the present work was to study the vortex-excited vibration of a cylinder in waves. Laboratory and theoretical investigations have been performed in order to study comprehensively the dynamic transverse response of a vertical cylinder in regular waves. The test cylinder was pivoted at its base and supported flexibly by springs at its top. The movement of the test cylinder and the lift force acting on it when it was stiffly mounted have been measured for surface Keulegan-Carpenter numbers, SKC, in the range 5 to about 40, wave depth parameter, kd, in the range 0.7 to 7.5, and for Reynolds number of about 10^3. The structural damping coefficient of the test cylinder was changed from 0.001 to 0.026 by using an electro-magnetic damper. The purpose of the measurement made on a stiffly mounted cylinder was to obtain a reference value of the lift force to be used in estimating its amplification in conditions of vortex-excited vibrations of the cylinder. In order to obtain an estimate of the unknown damping force of the vortex-excited cylinder in waves, the damping of the test cylinder in free vibrations in various depths of still water was also measured. The major conclusions are as follows.

7-2 Damping in Still Water

The damping factor of the test cylinder in still water was independent of the amplitude of oscillation in the range of low amplitudes. In these conditions the drag coefficient, which is associated with the damping factor by Eq.(3-31), agrees well with the theoretical value of Eq.(5-2-6) which is derived from Wang's (1968) theory for the forces on a fixed cylinder in oscillating flow.

At larger amplitudes the damping factor becomes amplitude dependent. when the surface Keulegan-Carpenter number, SKC, (related to the amplitude of cylinder by Eq.(5-2-4)), is about 2, the drag coefficient deviated from the theoretical value of Eq.(5-2-6) because of the appearance of boundary layer separation and vortex-shedding. Beyond SKC $\approx$ 2, the drag coefficient increases with increasing amplitude and corresponds well with the values obtained by Sarpkaya (1976) and Bearman et al. (1981).

Plots of the damping factor against the amplitude of the cylinder's free oscillation in still water for different water depths show that the variation of the damping factor with water depth can be accounted for by the theory described above (Eq.(5-2-6)).

7-3 The Lift Forces on a Stiffly Mounted Cylinder in Waves

The time history of the lift force acting on a cylinder stiffly mounted in waves has irregular characteristics. Taking this point into consideration, the following statistical values were calculated in the analysis of lift force measurements over 30-100 periods.

(1) The maximum effective lift coefficient (defined by Eq.(5-3-1)).

(2) The mean effective lift coefficient (defined by Eq.(5-3-2)).

(3) The effective lift coefficient for the n-th harmonic (defined by Eq.(5-3-3), n = 1,2,3,4).

(4) The coefficient of variation of the amplitude of the lift force (defined by Eq.(5-3-4)).

The purpose of (4) is to evaluate quantitatively the variation in amplitude of the lift force, over many wave cycles.

The lift for kd = 1.01 is dominated very clearly by the second harmonic $C_{Le}(2)$ in the range of SKC between 9 to 16. The second harmonic $C_{Le}(2)$ was predominant also for kd = 0.735 and 1.79 in the range of SKC between 9 to 18 as reported by other researchers, for example Isaacson and Maull (1976). However, the third harmonic $C_{Le}(3)$, in the present results did not become as important as Isaacson and Maull (1976) reported in the range of SKC between 17 to 24. An increase in $C_{Le}(3)$ shown in the range of SKC between 18 and 25, for kd = 1.01, but $C_{Le}(2)$ remains high, even at high values of SKC for kd = 0.735 and 1.79.

The lift coefficients, C_{Lemax} and $\overline{C}_{Le}$ vary more rapidly with kd than with SKC. Both of them have three peak values at kd = 0.9, 1.25 and 1.6, for the range of SKC between 11 and 15. The maximum value of C_{Lemax} is 2.5 at kd = 0.9 and its minimum value is 1.0 at kd = 1.2 for the range of SKC between 11 and 15. Generally, when lift coefficients are large, the coefficient of variation, C_{VL}, is small indicating the appearance of a stable lift force oscillation.

The amplitude of the lift force has irregular characteristics in most ranges covered in the experiments. However, a stable lift force oscillation appears in the range of SKC between 10 and 15 for the range of kd below 1.1 (see Fig. 5.3.6). In the case of two dimensional harmonic flow, the appearance of stable lift amplitude in the range of 10 and 14 has been reported by Ikeda and Yamanoto (1981).

7-4 The Vortex-Excited Vibration of the Cylinder

The following statistical values were obtained in order to study the characteristics of the vortex-excited vibration of the test cylinder in waves because the envelope of its amplitude was irregular (described in 5-4-1):

(1) The mean value of the amplitude of the vibration --- Y_{hm}

(2) The mean value of the frequency of the cylinder vibration --- f_{ym}

(3) The coefficient of variation of the amplitude of the vibration --- C_{VY}

(4) The mean value of the effective coefficient of the lift force acting on the observed vortex-excited cylinder --- C_{Lm} (defined by Eq.(5-4-4))

(5) The phase angle between the displacement of the test cylinder and the wave surface elevation --- $\phi_B(n)$.

The solution of the linearised model of the vortex-excited vibration of the cylinder in waves shows:

(1) The dimensionless amplitude of the cylinder, Y_{hm}/D, is controlled by the lift coefficient, the ratio of the wave frequency to the natural frequency, f_w/f_n, the surface Keulegan-Carpenter number, SKC the wave depth parameter, kd, damping coefficient, ζ_t, and mass ratio, $m_e/\rho D^2$ (see Eq.(3-23)). In the case of perfect resonance, the damping coefficient and mass ratio are combined in the normalised damping, $2m_e(2\pi\ \zeta t)/\rho D^2$ (see Eq.(3-29)).

(2) The phase angle between the vibration of the cylinder and the lift force acting on it is related to the frequency ratio, $n.f_w/f_n(n = 1,2,3...)$, and damping coefficient (see Eq.(3-26)).

(a) The Variation of the Vortex-excited Vibration with f_w/f_{nw}

The amplitude, Y_{hm}/D, of the vortex-excited vibration of the test cylinder with frequency ratio f_w/f_{nw} (f_{nw} = natural frequency of the test cylinder in still water) depends on the value of SKC and the value of damping coefficient. The most remarkable result is the appearance of two peaks in Y_h/D, produced by perfect resonance coupled with the waves and by vortex-coupling (described in 5-4-2). In the case of steady flow, perfect resonance appears in the range of lock-on, but in waves, it appears only near to f_w/f_{nw} = 1/2, 1/3, 1/4 ... (multi appearance), elsewhere vortex coupling may occur for right damping, in which the oscillation frequency is not simply a multiple of the wave frequency. The multi appearnce of perfect resonance is more clear in cases of higher values of SKC, and lower values of the damping coefficient in air, ζ_{ta}. For SKC $\approx$ 20 and $\zeta_{ta} \approx 0.001$, the perfect resonance occurs at $f_w/f_{nw} \approx 1/2, 1/3, 1/4, 1/5, 1/6$. At perfect resonance, the frequency of the cylinder, f_{ym}, is $2f_w$, $3f_w$, $4f_w$ ... and the vibration of the cylinder is very regular. On the other hand, at vortex coupling, the value of f_{ym} deviates from the curve $f_{ym} = n, f_w$ ($n = 2,3$ ...) and the amplitude of the vibration modulates without intermittency.

The peak value of Y_{hm}/D appears at $f_w/f_{nw} = 0.503$ and not at $f_w/f_{nw} = 0.500$ as might be expected. This may be due to an increase in the natural frequency of the test cylinder in the vortex-excited condition from the natural frequency of the test cylinder in still water. If we assume that it is due only to the variation of the added mass coefficient, C_{as}, in the vortex-excited condition, then C_{as} is found to be 0.79. This value of C_{as} is smaller than the added mass coefficient in conditions of free vibration in still water ($C_{as} = 1.04$) which agree well with the theoretical value.

There were no clear differences in the present study between the vortex-excited vibration of the test cylinder which was left free to vibrate in any direction, and the vortex-excited vibration of the test cylinder when free to vibrate only in the transverse direction.

(b) The Variation of $\dot{Y}_{hm}/D$ with SKC

The variation of the dimensionless amplitude of the cylinder, $\dot{Y}_{hm}/D$, with SKC around $f_w/f_{nw} \approxeq 1/2, 1/3, 1/4$ has a broad response over a wide range of SKC (for example, the value of $\dot{Y}_{hm}/D$ for CASE A-9 ($f_w/f_{nw} = 0.503$) is greater than 0.6 over the whole range of SKC between 10 and 25). This may be due to the non-linear amplification of each harmonic component of the lift force by means of the increased vortex strength and correlation in the phase of vortex-shedding along the cylinder axis.

The results of the present study are similar to those of Isaacson and Maull (1981) which was restricted to the range of SKC between 5 to 18. (The results of effective lift coefficient for SKC over 20 have apparently never been previously reported). The appearance of the large value of $\dot{Y}_{hm}/D$ for $f_w/f_{nw} \approxeq 1/4$ over a broad range of SKC between 20 to 40 should be noted as a significant feature of the response of a flexibly supported cylinder.

(c) The Variation of $\dot{Y}_{hm}/D$ with the Normalised Damping $2m_e(2\pi \zeta_{ta})/\rho D^2$

The value of the normalised amplitude $\dot{Y}_{hm}/D$ for the perfect resonant condition may be expected to be inversely proportional to the normalised damping $2m_e(2\pi \zeta_{ta})/\rho D^2$ as shown in Eq.(3-29). However, this relationship is not apparent in the present study. This may be due to the variations of the lift force or damping coefficient, probably produced by the vortex-excited vibration.

The value of Y_{hm}/D for the perfect resonant condition increases with decreasing normalised damping $2m_e.(2\pi.\zeta_{ta})/\rho D^2$ and approaches a limiting value. This phenomenon is similar to that observed in steady flow. However the limiting value of the present data are smaller compared with those of steady flow (in the case of steady flow, the limiting value of the normalised maximum amplitude, A_y/D is about 1.5 - 1.9. In the case of waves, the limiting value of Y_{hm}/D is about 0.8 for SKC = 20 and 0.5 for SKC = 8.7).

The appearance of limiting values of Y_{hm}/D for small values of the normalised damping suggests a state of a stable equilibrium in which an increase in Y_{hm}/D is associated with an increase in fluid damping.

The present data is consistent with the data obtained by Zedan et al. (1980), Bullock et al. (1978) and Rajabi (1979).

7-5 The Characteristics of the Lift Force Acting on the Vortex-excited Cylinder in Waves

After the mean value of both Y_{hm}/D and f_{ym}/f_{nw} had been measured, the mean value of the effective coefficient, C_{Lm}, of the lift force acting on the observed vortex-excited cylinder was calculated by using Eq.(5-4-4) on the basis of a linear model.

(a) The Variation of C_{Lm} with f_w/f_{nw}

In CASE AS-1 (SKC $\approx$ 12), the values of C_{Lm} are larger than the second harmonic component of the lift coefficient, $C_{Le}(2)$, acting on the stiffly mounted test cylinder in the same wave conditions in the range of f_w/f_{nw} between 0.45 to 0.55 (see Fig. 5.4.15). This shows the amplification of lift force by means of vortex-excited vibration. The amplification of the lift coefficient has a minimum value around perfect resonance ($f_w/f_{nw} \approx 1/2$), because the vibration is a result of a state of equilibrium between vortex excitation and fluid damping in this range.

(b) The Variation of C_{Lm} with SKC

The existence of the amplification of the lift force acting on the vortex-excited cylinder in comparison with the stiffly mounted cylinder is a function of f_w/f_{nw} and SKC. When f_w/f_{nw} is fixed at about 1/2, large amplitudes of oscillation occur over a wide range of SKC, but the amplification of lift force occurs in the range of SKC between 6 to 12 and it varies with SKC. The maximum amplification is about 12 and occurs at SKC $\approx$ 8. It is interesting that this range of SKC nearly corresponds to the range of KC, where the vortex-shedding from a stiffly mounted cylinder in harmonic flow is induced at twice the fundamental frequency, (see Fig. 5.4.29 and Fig. 5.4.30). Similarly, when f_w/f_{nw} is fixed at about 1/3, the range of SKC between 16 to 26, where amplification of lift force occurs, nearly corresponds to the range of KC, where the vortex-shedding from stiffly mounted cylinder in harmonic flow is induced at three times the fundamental frequency. The maximum amplification at $f_w/f_{nw} \approx 1/3$ is about 2 at SKC $\approx$ 20.

(c) The Variation of C_{Lm} with $\dot{Y}_{hm}/D$

The plots of the coefficient C_{Lm} of the lift force acting on the vortex-excited cylinder against the amplitude of the test cylinder $\dot{Y}_{hm}/D$ show the following:

(1) When $\dot{Y}_{hm}/D$ is lower than about $\dot{Y}_{hm}/D = 0.45$, the lift coefficient C_{Lm} increases with increasing $\dot{Y}_{hm}/D$.

(2) The maximum amplification of the lift force occurs at about $\dot{Y}_{hm}/D = 0.45$. In the case of CASE AC-2 (SKC = 6.2, $f_w/f_{nw} \approx 1/2$, kd = 1.85), the amplification of the lift coefficient is about 12 at $\dot{Y}_{hm}/D = 0.45$.

(3) When $\dot{Y}_{hm}/D$ rises above $\dot{Y}_{hm}/D \approx 0.45$, the lift coefficient begins to decrease.

These phenomena are quite similar to those for steady flow, and clearly show the result of a state of equilibrium existing between vortex excitation and fluid damping, and suggest that the maximum limiting value of $\dot{Y}_{hm}/D$ is independent of structural damping (see Fig. 5.4.3 - 5.4.35).

7-6 Phase Angle between the Displacement of the Cylinder and Water Surface Elevation

The plots of the phase angle, $\phi_B(2)$, between the displacement of the test cylinder and water surface elevation against f_w/f_{nw} (around $f_w/f_{nw} = 1/2$) for two values of ζ_{ta} 0.001 and 0.021, SKC $\approx$ 12 show the following.

(1) The rate of change of $\phi_B(2)$ with respect to f_w/f_{nw} for lower damping is larger than that for higher damping.

(2) The total damping coefficient, ζ_{ta}, in the vortex-excited condition, which is obtained by substituting each value of $\Delta\phi_B(2)/\Delta(f_w/f_{nw})$ around perfect resonance for $\zeta_{ta} = 0.001$ and $\zeta_{ta} = 0.021$ into Eq.(5-4-8), is only slightly larger than the damping factor in still water with amplitude equal to that of the vortex-excited vibration of the cylinder. This suggests that for large amplitudes at perfect resonance the damping is very similar to the damping at the same amplitude in still water.

7-7 The Wake Oscillator Model

A wake oscillator model was developed for the unsteady vortex-excited vibration of a cylinder in waves. This has to be time stepped since its solution cannot be integrated analytically. It cannot explain the general phenomena of the vortex-excited vibration in waves observed in the present experimental work. However, the amplification of the lift force around perfect resonance, which is one of the most important phenomena of the vortex-excited vibration, is roughly reproduced by the present model. It is reasonable to expect that with further development related to appropriate experimental measurements a better solution could be obtained.

REFERENCES

Angrilli, F., and Cossalter, V., 1982
'Transverse Oscillations of a Vertical Pile in Waves'. Journal of Fluids Engineering, Vol. 104, pp 46-53.

Bearman, P.W., 1969
'On Vortex Shedding from a Circular Cylinder in the Critical Reynolds Number Regime'. Journal of Fluid Mechanics, Vol. 37, Part 3, pp 577-585.

Bearman, P.W., 1978
'Pressure Fluctuation Measurements on an Oscillating Circular Cylinder'. Imperial College of Science & Technology, London, IC Aero TN 78-109, August 1978. (Bearman, P.W., and Currie, J.M.F.,]979)

Bearman, P.W., Downie, M.J., Graham, J.M.R. and Obasaju, E.D., 1984
'Forces on Cylinders in Viscous Oscillatory Flow at Low Keulegan-Carpenter Numbers'. submitted for publication.

Bearman, P.W., Graham, J.M.R., Naylor, P. and Obasaju, E.D., 1981
'The Role of Vortices in Oscillatory Flow about Bluff Cylinder'. International Symposium on Hydrodynamics in Ocean Engineering, The Norwegian Institute of Technology, pp 621-644.

Bidde, D.B., 1971
'Laboratory Study of Lift Forces on Circular Piles'. Journal of the Waterways, Harbors and Coastal Engineering Division, Proceeding of the American Society of Civil Engineers, pp 595-614.

Birkhoff, G., and Zarantonells, E.H., 1957
'Jets, Wakes and Cavities'. Academic Press, New York.

Bishop, R.E.D., and Hassan, A.Y., 1964
'The Lift and Drag Forces on a Circular Cylinder in a Flowing Liquid'. Proceedings of The Royal Society, A277, pp 32-50.

Bishop, R.E.D., and Hassan, A.Y., 1964
'The Lift and Drag Forces on a Circular Cylinder Oscillating in a Flowing Fluid'. Proceedings of the Royal Society, A277, pp 51-75.

Blevins, R.D., 1977
'Flow-Induced Vibration'. Van Nostrand Reinheld, pp 217.

Blevins, R.D., and Burton, T.E., 1976
'Fluid Forces Induced by Vortex Shedding'. Journal of Fluid Engineering, March, pp 19-26.

Bramley, M.E., 1969
'On the Hydrodynamic Damping of a Circular Cylinder'. M.Sc. Thesis, Dept. of Civil Engineering, Imperial College of Science and Technology, London.

Bullock, G.N., Stansby, P.K. and Warren, J.G., 1978
'Loading and Response of Cylinders in Waves'. Coastal Engineering, pp 2415-2432.

Charkrabarti, S.K., Wolbert, A.L. and William, A.T., 1976
'Wave Forces on Vertical Circular Cylinder'. Proc. ASCE, WW2, pp 203-221.

CIRIA Report UR 8, 1978
'Dynamics of Marine Structures'. CIRIA Report UR 8.

Cotter, D.C., and Charkrabarti, S.K., 1984
'Wave Force Tests on Vertical and Inclined Cylinders'. Proc. ASCE, Vol. 110, No. 1, WW1, pp 1-14.

Di Silvio, G., 1969
'Self-Controlled Vibration of Cylinder in Fluid Stream'. Proceedings of the American Society of Civil Engineers, Journal of Engineering Mechanics 95, pp 347-361.

Drysdale, C.V. and Jolley, A.C., 1952
'Electrical Measuring Instructions - Part One'. Chapman and Hall Ltd., pp 136-139, pp 274-287.

El Baroudi, M.Y., 1960
'Measurement of Two-Point Correlations of Velocity Near a Circular Cylinder Shedding a Karman Vortex Street'. University of Toronto, UTIAS, TN 31.

Feng, C.C., 1968
'The Measurement of Vortex-Induced Effect in Flow Past Stationary and Oscillating Circular and D-Section Cylinders'. M.Sc. Thesis, University of British Columbia, Vancouver.

Ferguson, N. and Parkinson, G.V., 1967
'Surface and Wake Flow Phenomena of the Vortex-Excited Oscillation of a Circular Cylinder'. Journal of Engineering for Industry, November, pp 831-838.

Gerlach, C.R., and Dodge, F.T., 1970
'An Engineering Approach to Tube Flow-Induced Vibrations'. Proc. Conf. on Flow-Induced Vibrations in Reactor System Components, Argonne National Laboratory, pp 205-225.

Gouda, B.H.L., 1975
'Some Measurements of the Phenomena of Vortex Shedding and Induced Vibrations of Circular Cylinders'. Technishe Universitat Berlin Report, DLR-FB 75-01.

Griffin, O.M., 1979
'Vortex-Excited Cross Flow Vibrations of a Single Cylindrical Tube'. The Third National Congress on Pressure Vessel and Piping Technology, San Francisco, California, pp 1-10.

Griffin, O.M., and Koopmann, G.H., 1977
'The Vortex-Excited Lift and Reaction Forces on Resonantly Vibrating Cylinders'. Journal of Sound and Vibration, Vol. 54, pp 435-448.

Griffin, O.M., Skop, R.A. and Koopmann, G.H., 1973
'The Vortex-Excited Resonant Vibrations of Circular Cylinders'. Journal of Sound and Vibration, Vol. 31(2), pp 235-249.

Griffin, O.M., Skop, R.A. and Ramberg, S.E., 1975
'The Resonant, Vortex-Excited Vibrations of Structures and Cable Systems'. OTC Paper No. 2319.

Haberman, 1968
'Vibration Analysis'. Charles E. Merrill Publishing Company, Columbus, Ohio.

Hartlen, R.T., Baines, W.D. and Currie, I.G., 1968
'Vortex-Excited Oscillations of a Circular Cylinder'. University of Toronto Report UTME-TP 6809, November 1968.

Hartlen, R.T., and Currie, I.G., 1970
'Lift-Oscillation Model for Vortex-Induced Vibration'. Proceedings of American Society of Civil Engineers, Journal of Engineering Mechanics, Vol. 96, 1970, pp 577-591.

Holmes, P., 1981
'Fundamental Aspects of Wave Loading and Modelling'. Offshore Structures, The Use of Physical Models in their Design, Edited by G.S.T. Armer and F.K. Faras, The Construction Press, pp 179-199.

Humphreys, J.S., 1960
'On a Circular Cylinder in a Steady Wind at Transition Reynolds Numbers'. Journal of Fluid Mechanics, Vol. 9, pp 603-612.

Ikeda, S. and Yamamoto, Y., 1981
'Lift Force on Cylinders in Oscillatory Flows'. Report of Dept. Found. Eng. and Const. Eng., Saitama Univ., Vol. 10, pp 1-16.

Isaacson, M.Q. and Maull, D.J., 1976
'Transverse Forces on Vertical Cylinders in Waves.' Proc. ASCE, WW1, pp 49-60.

Isaacson, M.Q. and Maull, D.J., 1981
'Dynamic Response of Vertical Piles in Waves'. International Symposium on Hydrodynamics in Ocean Engineering, The Norwegian Institute of Technology, pp 887-904.

Iwan, W.D. and Blevins, R.D., 1974
'A Model for Vortex Induced Oscillation of Structures'. Journal of Applied Mechanics, September, pp 581-586.

Iwan, W.D., 1975
'The Vortex Induced Oscillation of Elastic Structural Elements'. Journal of Engineering for Industry, 97, pp 1378-1382.

Iwan, W.D., and Blevins, R.D., 1975
'A Model for Vortex Induced Oscillation of Structures'. Journal of Applied Mechanics, September, 1974.

Karman, T.H., 1912
'Uber den Mechanismus des Winderstandes den ein bewegter Korper in einen Flussingkeit Erfahrt'. Nachr, Konigl, Gesellschaft.

Keulegan, G.H., and Carpenter, L.H., 1958
'Forces on Cylinders and Plates in an Oscillating Fluid'. Journal of Research, National Bureau of Standards, Vol. 60, 1958, pp 423-440.

King, R., 1971
'The Added Mass of Cylinders'. The British Hydromechanics Research Association, BHRA, Report N-1100.

King, R., 1972
'The Hydrodyanmic Damping of Natural Vibrations of a Cantilevered Cylinder'. The British Hydromechanics Research Association, BHRA, Report RR-1122.

King, R., 1977
'A Review of Vortex Shedding Research and its Application'. Ocean Engng., Vol. 4, pp 141-171.

King, R., Prosser, M.J., and Johns, D.J., 1973
'On Vortex Excitation of Model Piles in Water'. Journal of Sound and Vibration, 29(2), pp 169-188.

Koopmann, G.H., 1967
'The Vortex Wakes of Vibrating Cylinders at Low Reynolds Numbers'. Journal of Fluid Mechanics, Vol. 28, pp 501-512.

Lamb, H., 1975
'Hydrodynamics'. Cambridge University Press, pp 77.

Landweber, L., 1942
'Flow about a Pair of Adjacent, Parallel Cylinders Normal to a Stream, Theoretical Analysis'. Taylor Model Basing Report 485, July.

Leinhard, J.H., 1966
'Synopsis of Lift, Drag, and Vortex Frequency Data for Rigid Circular Cylinders'. Washington State Univ., College of Engineering, Research Division Bulletin 300.

Mair, W.A., and Maull, D.J., 1971
'Bluff Bodies and Vortex Shedding - A Report on Euromech 17'. Journal Fluid Mechanics, Vol. 45, pt. 2, pp 209-224.

Maull, D.J., and Milliner, M.G., 1978
'Sinusoidal Flow Past a Circular Cylinder'. Coastal Engineering, Vol. 2, 1978, pp 149-168.

Meier-Windhorst, A., 1939
'Flatter Schwingungan von Zylindern im Gleichmassigen Flussigkeitsstrom'. Munchen Technishe Hochschule, Hydraulische Institut Mitteilungen Helf 9.

Mercier, J.A., 1973
'Large Amplitude Oscillations of a Circular Cylinder in Low-Speed Stream'. Ph.D. Thesis, Stevens Institute of Technology, Hoboken, New Jersey.

Milen-Thomson, L.E., 1968
'Theoretical Hydrodynamics (5th ed.)'. The MacMillan Press, London, pp 247.

Morison, J.R., et al., 1950
'The Force Exerted by Surface Waves on Piles'. Petroleum Transactions 189, pp 149-157.

Morkovin, M.V., 1964
'Flow around a Circular Cylinder - A Kaleidoscope of Challenging Fluid Phenomena'. Proceedings, Symposium on Fully Separated Flows, American Society of Mechanical Engineers.

Parkinson, G.V., 1974
'Mathematical Models of Flow-Induced Vibrations of Bluff Bodies'. Proceedings of IUTAM-IAHR Symposium on Flow-Induced Structural Vibrations, Karlsruhe, Berlin: Springer Verlag, pp 81-127.

Parkinson, G., Feng, C. and Ferguson, N., 1968
'On the Mechanism of Vortex-Excited Oscillation of Bluff Cylinders'. Symp. on Wind Effects on Building and Structures, Loughborough, (U.K.), paper 27.

Rajabi, F., 1979
'Hydroeleastic Oscillations of Smooth and Rough Cylinders in Harmonic Flow'. Ph.D. Thesis, Naval Postgraduate School, Monterey, CA.

Ramberg, S.E., and Griffin, O.M., 1976
'Velocity Correlation and Vortex Spacing in the Wake of a Vibrating Cable'. Journal of Fluids Engineering, March, pp 10-18.

Rayleigh, L., 1896
'Theory of Sound'. Second Edition, MacMillan, London.

Rhodes, T.C., 1980
'Wave-Induced Loading on a Horizontal Cylinder'. M.Eng. Thesis, Liverpool University.

Roshko, A., 1954
'On the Drag and Shedding Frequency of Two-Dimensional Bluff Bodies'. National Advisory Committee for Aeronautics Report, NACA-TN-3169, July 1954.

Sarpkaya, T., 1975
'Forces on Cylinder and Spheres in a Sinusoidally Oscillating Fluid'. Journal of Fluid Mechanics, Vol. 42, pp 32-37.

Sarpkaya, T., 1976
'Vortex Shedding and Resistance in Harmonic Flow about Smooth and Rough Circular Cylinders at High Reynolds Numbers'. Technical Report No. NPS-59SL76021, Naval Postgraduate School, Monterey, CA.

Sarpkaya, T., 1978
'Fluid Forces on Oscillating Cylinders'. Jour. Waterways etc. Div., ASCE, Vol. 104, No. WW4, pp 275-290.

Sarpkaya, T., 1979
'Vortex Induced Oscillations, A Selective Review'. Journal of Applied Mechanics, ASME, Vol. 46, pp 241-258.

Sarpkaya, T. and Isaacson, M., 1981
'Mechanics of Wave Forces on Offshore Structures'. Van Nostrand Reinhold Company, pp 573

Sarpkaya, T., and Rajabi, F., 1979
'Dynamic Response of Pile to Vortex Shedding in Oscillating Flows'. Offshore Technology Conference Proceeding, OTC Paper No. 3647, Houston, Texas.

Sawamoto, M., Kikuchi, K., Ohba, M. and Kashiwai, J., 1980
'Forces on a Circular Cylinder in an Oscillatory Flow'. Coastal Engineering in Japan, Vol. 23, pp 147-158.

Sawamoto, M., Kikuchi, K. and Yamaji, H., 1979
'Vibration of a Cylinder Induced by Karman-Vortex Shedding'. Proc. 23rd Japanese Conf. on Hydraulics, pp 295-300.

Sawaragi, T., and Nakamura, T., 1975
'Characteristics of Lift Forces on Circular Pile in Waves'. Proc. 22nd Conf. on Coastal Engineering in Japan, JSCE., pp 525-530, (in Japanese).

Sawaragi, T. and Nakamura, T., 1977
'Relations between Wake Vorticies and Acting Forces on a Cylinder in Waves'. Memoirs of the Ehime University, Sect. III (Engineering), Vol. VIII, No. 4.

Sawaragi, T. and Nakamura, T., 1979
'Analytical Study of Wave Force on a Cylinder in Oscillating Flow'. Proceedings of the Specialty Conference on Coastal Structures 79, ASCE, pp 154-173.

Sawaragi, T., Nakamura, T., and Kita, H., 1976
'Characteristics of Lift Forces on a Circular Pile in Waves'. Coastal Engineering in Japan, Vol. 19, 1976, pp 59-71.

Shigemura, T., 1980
'Wave Forces on an Inclined Cylindrical Pile'. Coastal Engineering, pp 1761-1780.

Skop, P.A., and Griffin, O.M., 1973
'A Model for the Vortex-Excited Resonant Response of Bluff Cylinder'. Journal of Sound and Vibration, 27(2), pp 225-233.

Stokes, G.G., 1901
'On the Effects of Internal Friction of Fluid on the Motion of Pendulums'. Mathematical and Physical Papers, Vol. III.

Strouhal, V., 1878
'Uber eine besondere Art der Tonerregung'. Ann. Phys, und Chemie, New Series Vol. 5, pp 216-558.

Surry, D., 1969
'The Effect of High Intensity Turbulence on the Aerodynamics of a Rigid Circular Cylinder at Subcritical Reynolds Number'. University of Toronto Institute for Aerospace Studies, UTIAS Report No. 142.

Toebes, G.H., 1969
'The Unsteady Flow and Wake Near an Oscillating Cylinder'. Journal of Basic Engineering, September, pp 493-505.

Unemara, S., 1971
'On the Vibration of Cylinders caused by Karman Vortex'. J.S.M.E. 14, 75.

Verley, R.L.P., 1978
'An Investigation into the Hydrodynamic Damping of Cylinder Oscillating in Steady Currents of Various Velocities'. River and Harbour Laboratory Report No. STF-60-A78049, Norwegian Institute of Technology, Trondheim-NTH.

Vickery, B.J. and Watkins, R.D., 1962
'Flow-Induced Vibration of Cylindrical Structures'. Proceedings of the First Australian Conference, Held at the University of Western Australia.

Wang, C.Y., 1968
'On High-Frequency Oscillating'. J. Fluid Mech. 32.

Zedan, M.F. and Rajabi, F., 1981
'Lift Forces on Cylinders Undergoing Hydroelastic Oscillations in Waves and Two-Dimensional Harmonic Flow'. International Symposium on Hydrodynamics in Ocean Engineering, The Norwegian Institute of Technology.

Zedan, M.F., Yeng, J.Y., Salane, H.J. and Fischer, F.J., 1980
'Dynamic Response of a Cantilever Pile to Vortex Shedding in Regular Waves'. Offshore Technology Conference Proceedings, OTC Paper No. 3799, pp 45-59.

Zienkiewicz, O.C., and Cheung, Y.K., 1970
'The Finite Element Method in Structural and Continuum Mechanics'. McGraw-Hill Publishing Company Limited.